UNIVERSITY OF KWAZULU-NATAL

QUEUEING THEORY APPROACH TO RAIN FADE ANALYSIS AT MICROWAVE AND MILLIMETER BANDS IN TROPICAL AFRICA

AKINTUNDE A. ALONGE

OCTOBER 2014

QUEUEING THEORY APPROACH TO RAIN FADE ANALYSIS AT MICROWAVE AND MILLIMETER BANDS IN TROPICAL AFRICA

AKINTUNDE AYODEJI ALONGE

In fulfillment of the Degree Of

Doctor of Philosophy in Electronic Engineering.

College of Agriculture, Engineering and Science,

University of KwaZulu-Natal, Durban

OCTOBER 2014

Supervisor:

Professor Thomas J. Afullo

As the candidate's Supervisor, I agree/do not agree to the submission of this thesis

Professor T.J. Afullo   _____

Date   _____

Declaration 1 - Plagiarism

I, ..., with Student Number .... ,
with the thesis entitled *Queueing Theory Approach to Rain Fade Analysis at Microwave And Millimeter Bands in Tropical Africa* hereby declare that:

1. The research reported in this thesis, except where otherwise indicated, is my original research.

2. This thesis has not been submitted for any degree or examination at any other university.

3. This thesis does not contain other persons' data, pictures, graphs or other information, unless specifically acknowledged as being sourced from other persons.

4. This thesis does not contain other persons' writing, unless specifically acknowledged as being sourced from other researchers. Where other written sources have been quoted, then:

    a. Their words have been re-written but the general information attributed to them has been referenced;

    b. Where their exact words have been used, then their writing has been placed inside quotation marks, and referenced.

(v) Where I have reproduced a publication of which I am an author, co-author or editor, I have indicated in detail which part of the publication was actually written by myself alone and have fully referenced such publications.

(vi) This thesis does not contain text, graphics or tables copied and pasted from the Internet, unless specifically acknowledged, and the source being detailed in the thesis and in the References sections.

Signed

……………………………………………………..

Declaration 2 - Publications

DETAILS OF CONTRIBUTION TO PUBLICATIONS that form part and/or include research presented in this thesis (include publications in preparation, submitted, *in press* and published and give details of the contributions of each author to the experimental work and writing of each publication)

JOURNAL PUBLICATIONS

Akintunde A. Alonge and Thomas J. Afullo (2014): 'Rainfall Microstructural Analysis for Microwave Link Networks: Comparison at Equatorial and Subtropical Africa', *Progress in Electromagnetic Research B*, Vol. 59, pp. 45 – 58. [*Published*]

Akintunde A. Alonge and Thomas J. Afullo (2014): 'Characteristics of Rainfall Queues over Radio Links at Subtropical and Equatorial Africa', *Radio Science*, DO1 10.1002/2014rs005424. [*Published*]

A. A. Alonge and T. J. Afullo (2014): 'Fractal Analysis of Rainfall Event Duration for Microwave and Millimetric Networks: Rain Queueing Theory', *IET Microwaves, Antennas and Propagation*. [*In press*]

CONFERENCE PROCEEDINGS

Akintunde A. Alonge and Thomas J. Afullo (2013): 'Temporal Characterization of Rainfall Time Series Analysis for Wireless Networks,' presented at the *GWS Wireless Vitae Conference 2013*, Atlantic City, New Jersey, USA, June 24-27.

Akintunde A. Alonge and Thomas J. Afullo (2013): 'Rainfall Microstructures for Microwave and Millimeter Wave Link Budget at Tropical and Subtropical Sites', presented at the *2013 IEEE AFRICON Conference*, Le Meridien Hotel, Mauritius, September 9-12.

Akintunde A. Alonge and Thomas J. Afullo (2014): 'Rainfall Cell Estimation and Attenuation Studies for Radio links at Subtropical Africa', presented at *South African Telecommunication and Network Application Conference* (SATNAC), Port Elizabeth, August 31- September 3,.

Signed:

………………………………………..

Acknowledgements

Abstract

With an overwhelming demand of larger bandwidth required for high capacity data with content-rich services ranging from high-speed video streaming to multimedia content, there is a continuous need to migrate to higher microwave bands, particularly beyond the regular Ku and Ka bands (between 11 - 40 GHz). The presence of precipitation at these microwave and millimeter bands (3-300 GHz) generally induce rain fade, which is a constraint to network providers intending to achieve optimal service delivery, at acceptable signal to noise ratios (SNRs). In practice, fade countermeasures – static or dynamic – are necessary to combat the consequences of chronic fluctuations of rainfall resulting in signal deterioration and impairment over communication links. However, the implementation of dynamic fade countermeasures is systematically tied upon the available Channel State Information (CSI), which is often time-variant relative to the occurrence of precipitation events. Time-variation of rainfall events are perceptible in measurable rainfall microstructural parameters which vary intensely in space and time. These spatio-temporal variations yield the generation of observable random patterns of signal attenuation during rain events, often in a stochastic manner. To this end, researchers have emphasized on understanding the underlying behaviour of generic rainfall microstructural parameters such as rainfall rate, rainfall Drop Size Distribution (DSD) and radar reflectivity. Therefore, the investigation of these stochastic properties of rainfall processes is primary in the determination of recognisable patterns of rainfall rate and other microstructures. This thesis introduces the queueing theory approach via the Markov Chain technique to investigate the time-varying characteristics of the rainfall process from distrometer data in subtropical and equatorial Africa. Rainfall data obtained from these two climatic locations, at one minute integration time, were processed from sites in Durban, South Africa and Butare, Rwanda, over a specified measurement period. Initial investigation and comparison of rainfall microstructures undertaken at both sites clearly show key differences in their probability distribution profiles at Stratiform-Convective (SC) bounds. The underlying queue discipline of rainfall spikes and their queue metrics are determined and appraised for system performance using rainfall time series database. The results show rain spike generation processes vividly exhibit a First-Come, First-Served (FCFS) semi-Markovian distributed traffic of $M/E_k/s$ discipline, with a varying degree of servers, for different rainfall regimes. Comparison of queue statistics results over different rainfall regimes at the two locations reveal significant differences in their queue metrics and performances. The knowledge obtained from the queue statistics and SC probability analysis are further employed in the determination and classification of rainfall cells, rainfall growth models and path attenuation prediction. The results are compared and validated with data collected from a 6.73km, 19.5 GHz terrestrial link in Durban.

TABLE OF CONTENT

Chapter Three

Analysis of Rainfall Microstructures for Radio Links in Tropical Africa

Chapter Four

Queueing Theory of Rain Spikes over Radio Links

Chapter Five

Comparison of Rainfall Queue Characteristics in Tropical Africa

Chapter Six

Queueing Theory Application in Rainfall Cell Estimation

Chapter Seven

Conclusions and Recommendations

APPENDICES

Appendix A

Appendix B

LIST OF FIGURES

LIST OF TABLES

LIST OF ABBREVIATIONS

BD   Birth-Death

BER   Bit Error Rate

CCDF   Complementary Cumulative Distribution Function

CDF   Cumulative Distribution Function

CV   Coefficient of Variation

DMCP   Discrete Markov Chain Process

DRFM   Dynamic Rain Fade Mitigation

DSD   Drop Size Distribution

DTH   Direct-To-Home

DTMC   Discrete Time Markov Chains

ECS   Extinction Cross Section

FCFS   First-Come, First-Served

FFT   Fast Fourier Transform

FMT   Fade Mitigation Technique

FSL   Free Space Loss

GGD   Generalised Gamma Distribution

IEEE   Institution of Electrical and Electronics Engineers

ITU-R   International Telecommunication Union – Radiocommunication Sector

JW   Joss-Waldvogel

LOS   Line-of-Sight

MC   Markov Chains

ML   Maximum Likelihood

MOM   Method of Moments

NGN   Next Generation Network

PDF   Probability Density Function

RCA   Rain Cell Area

RCD   Rain Cell Diameter

RMSE   Root Mean Square Error

RRF   Radar Reflectivity Factor

RSL   Received Signal Level

SAWS   South African Weather Service

S-C   Stratiform-Convective

SNR   Signal to Noise Ratio

SRFM   Static Rain Fade Mitigation

SST   Synthetic Storm Technique

CHAPTER ONE

General Introduction

*All the mathematical sciences are founded on relations
between physical laws and laws of numbers, so that the aim
of exact science is to reduce the problems of nature to the
determination of quantities by operations with numbers*
– James Clark Maxwell (1831 – 1879)

1.1 Introduction

The subject of electronic communication is full of historical turns and incredible achievements, all within an unbelievable span of over 100 years. At the dawn of this form of communication, when wired system was inspired and birthed, the major concerns involved sending unmodulated signals intelligibly over long distances and expanding local accessibility. Today, communication systems have become more sophisticated and ingeniously complex in design, with major concerns for seamless connectivity at high throughput cum data integrity at the cheapest cost(s). Pragmatically, the objectives of achieving optimal cost-functions tend to be dependent on the multi-lateral delivery of optimal services to end-users of wireless communication technologies. Thus, attention has invariably shifted to the design of high capacity wireless networks with cutting-edge modulation schemes to achieve the near-infinite information transfer speed to low-end customers.

These new developments have pushed the bounds of the traditional framework of communication protocols towards a scenario where satisfactory bandwidth requirements are progressively primary. The outcome of these contemporary developments has lead to reappraisal of microwave and millimeter bands applied in the deployment of radio links for terrestrial and satellite communication. However, the performance of wireless networks deployed at these frequencies become unsatisfactory as transmitted signals suffer from attenuation, scattering and noise coupling leading to varying degrees of signal impairments. These concomitant problems become worse when the propagation medium over the radio link becomes inundated with hydrometeors. Hydrometeors appear in diverse forms some of which include snow, pellets, fog, hail, and lastly, rainfall [*Crane*, 1996; *Hall et al.*, 1996]. Among these listed forms, rainfall is the most ubiquitous phenomenon faced by most wireless networks globally, with the potential capability of disrupting transmissions unexpectedly.

In view of this, this thesis will further the investigation of rainfall attenuation in communication systems operating at microwave and millimeter bands. At these bands, the random and time-scale interactions of independent microstructures such as rainfall rate, rainfall DSD and radar reflectivity cannot be neglected. Thus, the random mechanism behind these microstructures is the topical subject of discussion in this thesis especially from the perspective of time-varying rainfall rate. Each chapter is therefore geared towards a comparative understanding of time dependent rainfall processes in tropical Africa.

1.2 Problem Formulation

In previous research on rainfall in Durban, South Africa, rainfall campaigns spanning almost a decade have provided exciting results on the effects of rainfall attenuation. These research are available in the studies of *Fashuyi et al.* [2006], *Odedina and Afullo* [2008], *Odedina and Afullo* [2010], and more recently, *Owolawi* [2011], *Akuon and Afullo* [2011a], *Afullo* [2011] on rainfall rates mechanics and rainfall drop-size distributions (DSD). More recent studies of rainfall DSD undertaken by *Alonge and Afullo* [2012a] and *Alonge and Afullo* [2012b], have examined the seasonal and regimes effects of rainfall attenuation on microwave networks in Durban. The conclusions on the appropriate model(s) describing the microstructural variability of rainfall parameters have indicated the gamma distribution as most suitable for rainfall rate [*Owolawi*, 2011], and, lognormal distribution for rainfall DSD [*Afullo*, 2011; *Alonge*, 2011]. Invariably, these models particularly the rainfall DSD have been applied in the computations of rainfall specific attenuation. With this, k and α parameters of specific attenuation for the city of Durban have been estimated in *Alonge* [2011] is slightly different from the standards provided in ITU-R P.838-3 [ITU-R Rec P.838-3, 2005]. The availability of frequency dependent parameters, k and α, can in turn be applied to estimate the path attenuation due to rain necessary for microwave link design. For example, *Alonge and Afullo* [2012b] and *Afullo* [2011] used this approach to investigate the seasonal variations in Durban and concluded that intense levels of rainfall attenuation are experienced in summer and autumn seasons. Broadly speaking, past research on the subject of rainfall attenuation in Durban has mainly sought to answer one single question: *what are the most sufficient rain fade margin levels required to compensate for signal degradation in wireless network operating at any microwave or millimeter-wave bands*? Therefore, it is exemplary to know that rainfall attenuation studies in South Africa have therefore mainly converged towards the adoption of "static" decibels of transmission power as a measure of mitigating the effects of rain fade.

Suppression (or cancellation) of rain fade effects, otherwise known as rain *fade mitigation technique* (FMT) should be accompanied by effective power control allocation which could be

static, dynamic, diversity-based or a combination of any of these [*Castanet et al.*, 2003; *Fukuchi and Saito*, 2007; *Sabapathy et al.*, 2011]. The static technique (the scenario undertaken in Durban), often employed in rain attenuation prediction in South Africa as well as in ITU-R publications, has been reported globally as a flawed method of maximizing and optimizing local transmission power in networks [*Castanet*, 2003; *Sabapathy et al.*, 2011]. Besides, this technique may be an insufficient way of matching rainfall microstructural signatures with real-time variation in rain attenuation at the receiver end, leading to under-utilization of spectrum (bandwidth), transmission power, and consequently resulting in network downtime. Therefore, researchers in microwave studies have urged for more unique approach where the real-time influences of rainfall are considered [*Sweeney and Bostian*, 1999; *Shin et al.*, 2002; *Castanet*, 2003; *Sabapathy et al.*, 2011]. In this guise, dynamic and diversity-based techniques suffice as the best methodologies applicable in the suppression or cancellation the effects of rain fade. Thus, an underlying inquiry into the stochastic characteristics of rainfall during rainfall events is overtly important to the subject matter of dynamic fade cancellation. The rainfall probability theory, built on Markov chain properties, offer an interesting insight into the black-box properties of time-variant rainfall rate. While some efforts have been made in this area most especially for rainfall synthesis [*Alasseur et. al*, 2004; *Héder and Bitòs*, 2008; *Maruddani et. al*, 2010; *Das and Maitra*, 2012], the exact nature of the underlying time-varying properties of rainfall events useful for adaptive cancellation of rain fade is yet to be explored. In addition, with the recent knowledge of rainfall cell growth studies in South Africa [*Akuon and Afullo*, 2011a], the time-varying rainfall process can be utilized to optimise the long-distance prediction of rain fade for satellite and terrestrial links operating between 30 GHz - 95 GHz due to emerging bandwidth crises [*Foty et al.*, 2011]. The justification for this proposed research, therefore, lies in not only in counteracting the notorious effects of rain fade at these spectra, but laying the framework for understanding rainfall characteristics required for the allocation of optimal power requirements and radio resources. It is on this basis that effective and power-efficient rains fade suppression algorithms are expected to be developed for future applications in the wireless communication industry.

In this proposed study, a combination of the knowledge of rainfall rates, rainfall DSD, rainfall growth and rainfall cell mechanics will be applied to understand the time-variation of rain rate and hence, rainfall attenuation. The research will investigate the queueing characteristics of rainfall in tropical Africa, with a narrow focus on equatorial and subtropical areas. Broadly speaking, this research seeks to answer the following questions: what are the variations in rainfall microstructural parameters (rainfall rate, rainfall drop-size distribution *e.t.c.*) in tropical Africa? Do rainfall event processes over a radio link qualify as a standard event-based queue

process? What is the nature of the expected queue discipline and performances thereof? What are the benefits of applying the queueing theory approach in rain cell estimation and attenuation prediction over radio links at microwave and millimeter bands? This research will assist in expanding the knowledge of time-domain characteristics of rainfall queues at locations around tropical Africa, as applied in contemporary terrestrial and satellite networks.

1.3 Scope of Work

1. To investigate the variations of rainfall microstructures of rain rate, rainfall DSD and radar reflectivity over subtropical and equatorial Africa.
2. To establish the time-varying characteristics of rainfall events over radio links as a queueing process.
3. To determine empirically the most appropriate queue discipline to describe rainfall process over radio links.
4. To investigate and compare the queueing characteristics of rainfall processes over subtropical and equatorial Africa.
5. To determine from queueing theory approach, the equivalent average rain cell sizes and hence, predict rainfall attenuation and fading effects over subtropical and equatorial Africa.

1.4 Thesis Overview

The overall number of chapters contained in this thesis is seven. Each chapter offers an insight into the contents, objective and the depth of work attained in the course of this research. Therefore, the structure of this thesis begins with the first chapter (Chapter one). This chapter discusses the general introduction into the subject matter of the thesis: the introduction, problem formulation, scope of work, original contribution and publications. Thereafter, the overview of the remaining chapters in this thesis is presented succinctly as follows:

Chapter two is a brief review into propagation losses in wireless communication, the rainfall role in signal attenuation, discussion of rain microstructures and review of time series analysis of rainfall rate over radio links.

Chapter three compares the variation of rainfall microstructural parameters in tropical African locations of Durban and Rwanda with emphasis on their behaviour over stratiform-convective bounds. The probability analysis tool is applied in the investigation of these parameters to understand their behaviours in subtropical and tropical locations. A global comparison of results at the investigated sites is undertaken at the end of this chapter.

Chapter four discusses the investigation and determination of rainfall queueing characteristics in Durban, South Africa. Queue disciplines which give the closest approximations of rainfall traffic conditions are obtained with their appropriate probability distribution models. Performance metrics and other relevant parameters are also obtained in this chapter.

Chapter five examines the rainfall queueing characteristics in tropical African locations of Durban and Rwanda using basic queueing parameters. The information obtained from the queueing results at both sites are compared and evaluated using their performance metrics and steady state behaviour.

Chapter six discusses the application of the rainfall queueing theory in the determination of rainfall cell specifics in Durban and Butare. This has lead to the determination of other parameters relevant to the prediction of rainfall attenuation over radio links at microwave and millimeter bands. The results obtained are validated using terrestrial link measurements at 19.5 GHz.

Chapter seven is the conclusion of the study undertaken in this research. A detailed appraisal of the research contributions (and information) of this thesis are highlighted accordingly with emphasis on possible future research areas.

1.5 Contributions to Knowledge

The contributions of this thesis to the body of exiting knowledge are listed below:

- The comparison of rainfall microstructures in subtropical and equatorial regions of Africa has shown that Stratiform-Convective bounds play a role in the probability distributions profile of the investigated parameters. The characteristics of these parameters tend to vary according to the influence and interactions of the prevailing climatic conditions. It is demonstrated in this work that Stratiform-Convective threshold is a reasonable parameter that presents a larger perspective of differential attenuation conditions around the world.

- Development of queueing theory technique for rainfall rate analysis from distrometer measurements was established in this work. This approach is novel in the understanding of the underlying process of rainfall rate traffic, as they move as rain cells over radio links, at microwave and millimeter bands during rain events. This has led to the determination of the most appropriate queue discipline required to explain the exact nature of time-varying rain rates over different regimes. The findings from this study show that the $M/E_k/3/\infty/FCFS$ queue discipline best describes the rain rate queues in

subtropical and equatorial Africa. The advantage of this technique is applicable in rainfall cell estimation, rainfall growth analysis and channel modelling.

- The formulation of rain growth models and the estimation of rain cell diameters from distrometer measurements in tropical Africa. The queueing theory approach has enabled the analysis of rainfall on a 'singular' spike basis thereby expanding the knowledge of rain attenuation prediction. The quantum understanding of spike service time as a distribution is pivotal to the development of practical channel models for use in radio resource management.

1.6 Publication in Journals and Conference Proceedings

The listed publications below are materials forming part of this thesis with appearances in peer-reviewed and accredited journals, as well as conference proceedings:

1. **Akintunde A. Alonge** and Thomas J. Afullo (2014), "Rainfall Microstructural Analysis for Microwave Link Networks: Comparison at Equatorial and Subtropical Africa" *Progress in Electromagnetic Research B*, Vol. 59, pp. 45 – 58.
   Status: Published

2. **Akintunde A. Alonge** and Thomas J. Afullo (2014), "Characteristics of Rainfall Queues over Radio Links at Subtropical and Equatorial Africa", *Radio Science*, DO1 10.1002/2014rs005424.
   Status: Published

3. **A. A. Alonge** and T. J. Afullo (2014), Fractal Analysis of Rainfall Event Duration for Microwave and Millimetric Networks: Rain Queueing Theory (**Submitted to IET Journals, United Kingdom**)
   Status: In Press

4. **Akintunde A. Alonge** and Thomas J. Afullo (2013), Temporal Characterization of Rainfall Time Series Analysis for Wireless Networks, presented at the *GWS Wireless Vitae Conference 2013*, Atlantic City, New Jersey, USA, June 24-27, 2013.

5. **Akintunde A. Alonge** and Thomas J. Afullo (2013), Rainfall Microstructures for Microwave and Millimeter Wave Link Budget at Tropical and Subtropical Sites, presented at the *2013 IEEE AFRICON Conference*, Le Meridien Hotel, Mauritius, September 9-12, 2013.

6. **Akintunde A. Alonge** and Thomas J. Afullo (2014), Rainfall Cell Estimation and Attenuation Studies for Radio links at Subtropical Africa, Presented at the South African Telecommunication and Network Application Conference (SATNAC), August 31st- September 3rd, 2014.

CHAPTER TWO

Literature Review

2.1 Introduction

There are several attenuation factors that contribute to propagation losses, which generally leads to the impairment and degradation of transmitted signals, over a wireless radio link operating at microwave and millimeter bands. These contributions present diverse forms of interactions with propagated waves along Line-of-Sight (LOS) transmissions through dispersive, absorptive, refractive and diffractive mechanisms [*Banjo et al.*, 1986; *Crane*, 2003]. As a result, the principal attenuation agents responsible for these mechanisms exist in various forms such as vegetation, obstacles like mountains, hills and tall buildings, varying terrain structures, solar flares, ionospheric disturbances and most importantly, precipitation [*Seybold*, 2005; *Ajayi et al.*, 1996]. The various components of precipitation that contribute to signal losses include snow pellets, hail, fog, clouds and rainfall. Rainfall is, perhaps, the most significant (and most meddlesome) of these precipitation forms as it is a global phenomenon affecting communication systems at microwave and millimeter bands. In many tropical areas around the world, the effect of rainfall attenuation is often predominant in communication networks at about 7 GHz and beyond [*Islam et al.*, 1997; *Crane*, 2003]. In temperate regions, these effects may be noticeable from about 10 GHz and beyond [*Green*, 2004]. Therefore, the subject of rainfall is inherently location-specific, and hence, is perhaps one of the important considerations employed in the design of local radio link. Over the years, wireless communication deployed through terrestrial and satellite systems have become sophisticated with increasing need for bandwidth capacity. This has resulted in the deployment of new frequency bands, and thus, the technical migration to higher frequency bands of microwave and millimeter-wave spectrum. These bands are often very susceptible to the effects of rainfall attenuation and are a huge limitation to network performance. Therefore, this chapter will review the progress in the studies of rain attenuation in electromagnetic propagation.

2.2 Frequency Bands in Communication Systems

Practical frequency bands applied in numerous areas of scientific, industrial and commercial applications – often vary from 3 KHz to 3 THz. Between these range, lies the band of interest of this study, the microwave band which ranges from 3-30 GHz and the millimeter-wave band which ranges from 30-300 GHz. These bands support a large array of terrestrial and satellite services such as broadband internet services, Direct-to-Home (DTH), wireless mobile telephone services, marine communication systems, critical military logistics and support, and of recent,

Table 2-1: Frequency band designations according to ITU-R V.431-7 and IEEE 521-2002 standards in communication industry [*ITU-R V.431-7*, 2000; *IEEE 521-2002*, 2002]

GENERIC BAND RANGE	ITU-R V.431-7	IEEE 521-2002	OTHERS
3 – 30 KHz	VLF (Very Low Frequency)		
30 – 300 KHz	LF (Low Fequency)		
0.3 – 3 MHz	MF (Medium Frequency)	MF	
3 – 30 MHz	HF (High Frequency)	HF	
30 – 300 MHz	VHF (Very High Frequency)	VHF	
0.3 – 3 GHz	UHF (Ultra High Frequency)	UHF	
1 – 2 GHz		L band	
2 GHz		S band	
3 GHz	SHF (Super High Frequency)	S band	Microwave band* (**μm** Wave)
4 GHz			
4 – 8 GHz		C band	
8 – 12 GHz		X band	
12 – 18 GHz		Ku band	
18 – 27 GHz		K band	
27		Ka band	
30 GHz	EHF (Extremely High Frequency)	Ka band	
40 GHz			Millimeter wave band (**mm** Wave)
40 – 75 GHz		V band	
75 – 111 GHz		W band	
Above 111 GHz		Millimeter band	
300 GHz			
0.3 – 3 THz	Terahertz Frequency		

*Sometimes, microwave band designation may extend into the upper bound of the EHF segment.

interplanetary communications. Different nomenclatures exist to classify and designate frequency bands, popular among them include the International Telecommunication Union (ITU) and Institution of Electrical and Electronics Engineer (IEEE) nomenclature [*ITU-R V.431-7*, 2000; *IEEE 521-2002*, 2002]. As listed on Table 2-1, these nomenclatures are presented with their respective frequency band in use. Popular bands currently utilized for commercial television broadcast and high speed data services among the microwave range include the C, Ku, K and Ka band. Currently, Next Generation Networks (NGN) technologies

are being deployed on some of these bands as they are easily marketable and scalable platforms for optimal spectrum utilization.

2.3 Sources of Losses in Electromagnetic Propagation

The objective of communication is to ensure – the delivery of intelligible information at the receiver end – as the transmitted signal travel through propagation media. However, the process of transmitting signals over a wireless link is not completely loss-free and error-free as certain attenuation agents impair the quality of transmitted information. Depending on the nature of the radiation pattern of transmitting antennas, the effect of these attenuation agents can be partially or wholly destructive. At microwave and millimeter-wave bands, the preferred mode of signal transmission is often by LOS propagation i.e. the transmitter and the receiver must 'see' each other. A narrow antenna beamwidth is usually required to achieve a stronger and directed energy level in a straight line, within the range of Fresnel design constraint [*Crane*, 2003]. In accordance to link budget designs, many frequent forms of losses are encountered along a typical LOS which ultimately results in signal impairment and noise injection. Among these losses include Free Space Loss (FSL), obstacle/diffraction losses, multipath losses, antenna pointing/misalignment error losses, rain fade loss. Figure 2-1 gives an illustration of typical sources of the mentioned losses for a typical LOS terrestrial link. More details are also given in Table 2-2 about the possible causes of some of the resultant losses accompanying LOS transmission over microwave and millimeter bands.
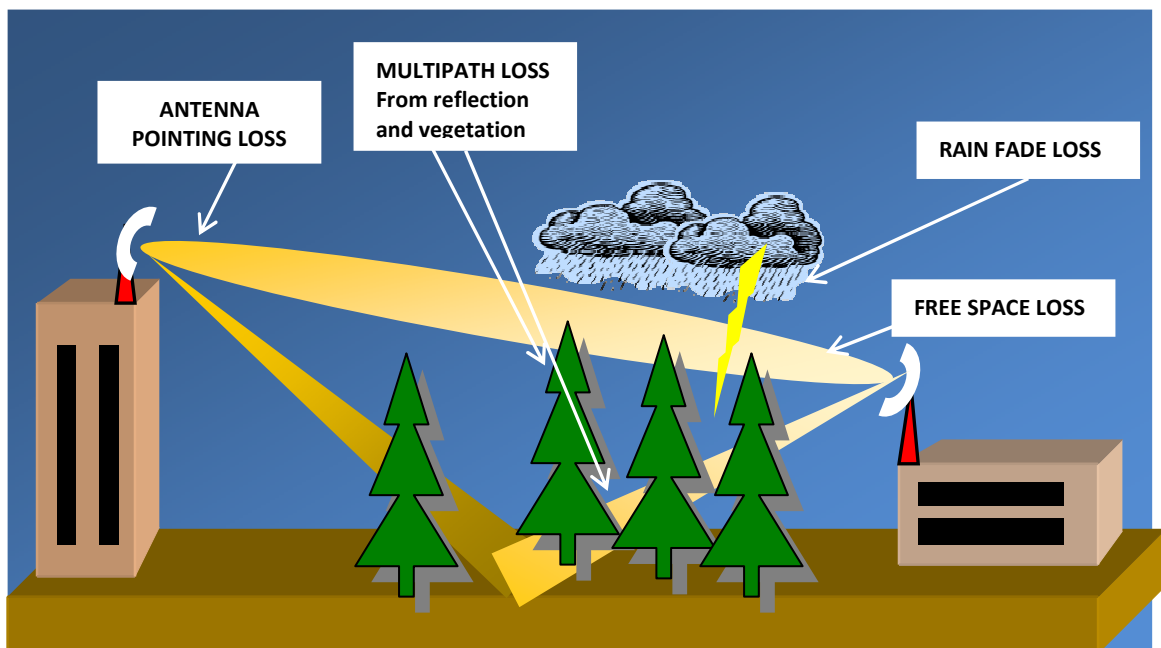
Figure 2-1: Identification of the physical sources of signal loss in LOS terrestrial link

Table 2-2: Frequent sources of signal losses and impairments over LOS radio links

TYPE OF LOSSES	LIKELY CAUSES
FREE SPACE LOSS	Spatial loss due to outward geometric spreading of waves in transmission media
POINTING/MISALIGNMENT ERROR LOSS	Non-precise orientation of transmitter and receiver for LOS communication
RAIN FADE LOSS	Spatial variability of rainfall rates over rainfall cells during signal transmission
MULTIPATH LOSS	Multiple reflections from hard surfaces during propagation
ATMOSPHERIC LOSS	Presence of gaseous constituents in the atmosphere
DIFFRACTION LOSS	The absorption and reflection of transmitted waves around obstacles and apertures

In link budget design, a simple routine of estimation is often employed by engineering practitioners to ensure that signal losses across radio links are minimal. This routine is generic in network design as it ensures that proper and adequate power levels are matched with potential system losses accompanying signal transmission over a radio link. Thus, it is always necessary that any of such proposed links satisfy the link budget equation given by [*Freeman*, 2007; *Mämmela and Kolteba*, 2011]:

$$P_{rx} = P_{tx} + G_{tx} + G_{rx} + G_i - FSL - A_t - A_p \qquad [dBm] \qquad (2.1)$$

where,

P_{tx} is the transmitted power level in dBm

P_{rx} is the received power level in dBm

G_{tx} is the gain of the transmitting antenna in dBi

G_{rx} is the gain of the receiver antenna dBi

FSL is the Free Space Loss in dB

G_i is the summation of gains from other sources in dB

A_t is the summation of path attenuations/losses from other sources in dB

A_p is the path attenuation due to rainfall in dB

Each of parameters seen in (2.1) is an important input to link budget preparation and are further discussed. Firstly, the antenna gain, G, is a parameter related to the antenna aperture size and receiving area. It is often computed as follows:

$$G = 10 \log_{10}\left(\frac{\eta \pi^2 {D_a}^2}{{\lambda_a}^2}\right) \quad [dBi] \tag{2.2}$$

where η is the efficiency of the antenna system usually taken as values between 0.65 and 0.8, D_a is the antenna physical size in metres and λ_a is the wavelength to which the antenna is tuned.

The Free Space Loss (FSL) is a parameter attributed to the geometric spreading of waves as they travel through the propagation medium (free space). This loss increases as frequency and path length of the wireless communication system increases. The FSL of any wireless communication system is given by [*Freeman*, 2007]:

$$FSL = 92.4 + 20 \log_{10} L_{km} + 20 \log_{10} F_{GHz} \; [dB] \tag{2.3}$$

While the rain fade loss, which is computed from the rainfall path attenuation, A_p, is computed from *ITU-R P.530-15* [2013] given as:

$$A_p = A_s \, r L_{km} \; [dB] \tag{2.4}$$

As seen from above, (2.4) is dependent on the rainfall specific attenuation (A_s), length factor (r) and transmission distance between microwave links, (L_{km}). This expression is valid for terrestrial links *i.e.* links where elevation angle is less that 2°. Modification of (2.4) is often required if satellite links are under consideration.

It is interesting to note that apart from rain attenuation and atmospheric attenuation components from (2.4), other parameters that induce signal losses over a LOS radio link are more or less fixed over path lengths and frequency, irrespective of time domain variations.

2.3.1 Contribution of Losses to Signal Impairment

As clearly seen in (2.1), there are other significant losses suffered by electromagnetic wave travelling through a standard propagation medium. Apart from path attenuation due to rainfall, other important path attenuations are due to the presence of atmospheric gases, vegetation, buildings, clouds and fogs. Therefore, it is more pleasant to describe this parameter, A_t, as seen in (2.1) as an algebraic sum of all losses from different components. This is given by:

$$A_t = \sum_i A_i \quad [\text{dB}] \qquad \qquad \text{for } i = 1, 2, 3, \ldots \qquad (2.5)$$

where A_i represents various elements of path attenuation from different sources to be summed accordingly.

The members of A_i are the family of atmospheric gases which are often present in the lower atmospheric layer of the earth surface. Oxygen and water vapour belong to these set of gases which have adverse effect on both Earth-space and terrestrial communication especially at high frequencies. The behaviours of these two gases are not entirely regular as they have sudden peaks as transmission frequency bands increases. From the earliest significant contribution to studies on gaseous attenuation by *Liebe* [1981], *Liebe* [1983], *Liebe and Hufford* [1989], the effects of these gases are obvious with window periods. In these previous studies, the atmosphere is assumed as a non-turbulent propagation medium inundated with gaseous components having absorptive and dispersive properties. These series of studies experimented on the attenuation properties of these gases between microwave frequencies of 1 GHz to 300GHz at ambient temperature close to 300 K. In their report, *atmospheric windows* were reportedly observed for oxygen gas attenuation profiles with attenuation peaks between 50/75 GHz and 100/150 GHz. For water vapour, these peaks were observed between 20/30 GHz, 150/200 GHz and 250/300 GHz. These results are also reported in latter parallel literature [*Ippolito*, 1981; *Crane*, 2003; *Seybold*, 2005;]. The path attenuation losses attributed to water vapour and oxygen up to 300 GHz are presented in Figure 2-2.

Another source is the influence of vegetation such as trees, which often causes scattering of electromagnetic waves along LOS, and hence, path losses. At higher frequencies, the influence of dry and wet weather conditions, seasonal cycles, number and species of trees along the link do vary the effects of vegetation on propagation [*Seybold*, 2005]. The path loss due to this obstacle can be found empirically by using the physical parameters related to the transmission. For this, *Meng et al.* [2009] specified that vegetation losses can be represented by a
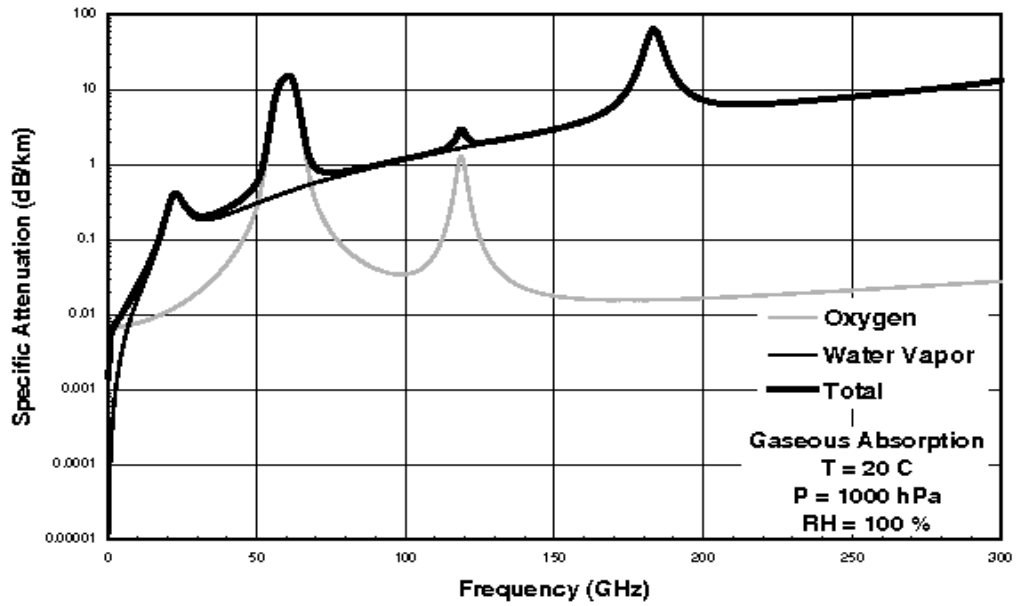
Figure 2-2: Effects of atmospheric attenuation over microwave and millimeter-wave bands [*Crane*, 2003]

mathematical function relating the transmitting frequency and path length. This is given by:

$$L_{atm} = Af^B L_{km}{}^C \quad [dB] \tag{2.6}$$

where constants A, B and C are empirical constants related to the undertaken measurements. The variable *f* is the frequency in GHz and L_{km} is the path length of transmission in *km*.

It should be noted that among all the sources of signal impairment so far mentioned in this section, losses attributed to FSL and rain attenuation appear to be the largest irrespective of the transmission frequency, path length and geographical influences. While FSL is inevitable in any radio link, it is universally accepted to be same everywhere in the world even as it is both frequency and distance dependent. The universality of rainfall attenuation pattern (or rainfall losses) is generally unacceptable as it varies according to geographical and climatic characteristics [*Crane*, 1996]. Besides, the mechanism of this particular attenuation is primarily due to scattering, absorption and depolarization of propagating waves which is often intense in tropical, equatorial and monsoon regions [*Seybold*, 2005]. Therefore, it is pertinent to discuss the subject of rainfall as it is the fulcrum upon which this thesis is based. Discussions related to rainfall and other related topics are hereby highlighted in coming sub-sections of this chapter.

2.4 Rainfall Attenuation over Communication Links

Rainfall is a phenomenon where rainfall droplets produced from cloud formation process, are dispersed into the atmosphere, as a result of natural energy interactions over a large area. The meteorological process of rainfall is a little complicated with high variation in space, duration and frequency of occurrence [*Ajayi et al.*, 1996]. When rainfall is incident over a communication link, part of the propagated energy of the transmitted wave is dissipated and lost due to scattering and absorption. The continuous process of scattering and absorption eventually leads to signal impairment resulting in rainfall attenuation, which gradually transforms into rain fade over specified event duration [*Sinka and Bitó*, 2003]. This process is mainly due to the presence of different sizes of rain droplets along the horizontal profile of the atmosphere, usually below cloud level. The rainfall intensity, otherwise measured as *rainfall rate* is a measurable microstructure related to the distribution of rain droplets over a typical link. Other measurable rain microstructures include rainfall Drop Size Distribution (DSD), radar reflectivity, rain drop-shape and liquid water content [*Seybold*, 2005]

Rainfall characteristics are non-uniform and inhomogeneous over the horizontal region of the atmosphere [*Crane*, 1980]. It has also been shown in the *ITU-R P.837-6* [2012] document that rainfall varies in latitudinal dimension from region to region. Therefore, it is often expected that different areas around the world experience different monthly, seasonal and yearly variations of rainfall patterns. Research has shown that propagation parameters of frequency and radio path length are the main factors affecting the level of rainfall attenuation experienced over a communication link [*ITU-R P.530-15*, 2013]. Generally, rainfall attenuation is known to worsen the signal quality as the frequency and path length of the wireless link increases. It is therefore valid to conclude that high-capacity networks, propagating beyond 10 GHz, evidently suffer more from the effects of rain. Another important parameter affecting signal propagation is the influence of rainfall types, which is often different around the world, as are climatic characteristics. Therefore, the next sub-section will discuss the subject of rainfall types.

2.4.1 Classification of Rainfall Types

There are two major classifications of rainfall types based on their physical characteristics: stratiform and convective rainfall [*Moupfouma*, 1987; *Houze*, 1997; *Tokay et al.*, 1999; *Mandeep and Allnut*, 2007]. These two categories are based on the nature of cloud formation, condensation and strength of the rainfall [*Moupfouma*, 1987; *Houze*, 1997]. Stratiform rainfall is produced from weak nimbostratus clouds which results in light drizzle and widespread rain usually over a large area. They extend up to 1 km across the vertical profile of the isotherm height with rain rates usually less than 10 mm/h [*Ajayi et al.*, 1996]. Convective rainfalls, on the

other hand, are produced from strong cumulonimbus clouds which are often local and reaching up to 100 km/h [*Houze*, 1997]. They are mainly responsible for shower and thunderstorm rainfalls where rainfall rates exceed 10 mm/h [*Houze*, 1997]. *Moupfouma* [1987] and *Ajayi et al.* [1996] in their work indicated that these types of rainfall are typically frequent at equatorial and tropical climates.

However, some researchers apply three rainfall regimes of drizzle, shower and thunderstorm to classify rainfall [*Adimula and Ajayi*, 1996]. In recent rainfall campaigns at Southern African areas, the four regime approach of drizzle (< 5 mm/h), widespread (between 5 and 10 mm/h), shower (between 10 and 40 mm/h) and thunderstorm (> 40 mm/h) have also been applied to classify rainfall [*Afullo*, 2011; *Alonge and Afullo*, 2012c]

2.4.2 Measurement of Rainfall

Rainfall is primarily measured in terms of different microstructural quantities. As a result, a number of microstructures can be successfully measured by ground-based or space–bourne equipments. A combination of ground-based equipments of rain gauge networks, disdrometers and radars are preferable in the measurements of microstructures such as rainfall rate, rainfall DSD and radar reflectivity. Rain gauges and distrometers provide useful information related to the time-varying properties of rainfall over the horizontal profile of rainfall in the troposphere. They are also cheaper, easier to maintain and readily available compared to radars. The distrometer, however, provides more information on the rain droplet distribution present in the atmosphere during rainfall events. Radars are deemed more expensive but provide useful analysis and aerial measurements of rainfall properties over longer distances with significant information on the vertical and horizontal variation [*Ajayi et al.*, 1996; *Green*, 2004; *Tenório et al.*, 2010]. Space-borne measuring equipments for rainfall have the advantage of vertical height position that allows for accurate measurements over large areas. Examples are satellites and weather balloons which are effectively used with onboard equipments such as radars and high-resolution cameras to track and monitor rainfall characteristics. This equipment offer wider coverage areas and can be applied in the precise estimation of rainfall cells and other useful parameters. However, the high cost of installation and system maintenance are often disadvantages in the widespread use of such equipment for research purposes [*Ajayi*, 1996].

2.4.3 Rainfall Rate Distribution

Rainfall rate is a microstructural parameter used to describe the number of rain gauge tips occurring per hour of any rain event. In the real sense, this parameter actually quantifies the rate

(or intensity) at which rainfall water is collected over a conventional measuring system such as a rain gauge.

Rainfall is a natural phenomenon, with systematic variation in space and time over different areas of the world [*Ajayi et al.*, 1996]. This suggests that regional variability of rainfall rate exists on a seasonal and year-to-year basis. The rain rate distribution is an established statistical tool used to distinguish and compare rainfall rate at different areas around the world. The most important statistical parameter for evaluating the influence of rain rate on radio links is the $R_{0.01}$. This parameter is derived from the 0.01% exceedence value of the Complementary Cumulative Distribution Function (CCDF). Mathematically, this parameter can be obtained from the knowledge of the Cumulative Distribution Function (CDF). Therefore, $R_{0.01}$ is exactly the CDF component at 99.99% availability of rainfall rate, which is satisfactory for radio design purposes. Figure 2-3 shows the rain rate distribution profile over Durban over a span of about 24 months between 2009 and 2010. It can be seen that the CCDF varies for each month of the year indicating monthly variability over the same location. This shows that rainfall rate is a highly variable parameter over the yearly span of collected data. On the issue of global variability of rain rate, rain maps have been authored in the studies of *Crane* [1996] and in the recommendations of ITU-R [*ITU-R P.837-6*, 2012]. These maps are used to partition different regions of the world according to their unique CCDFs. The ITU-R map is the most updated map and gives a better statistics on point rainfall rate at 0.01% exceedences around different areas of the world. This map can be found in Appendix A.
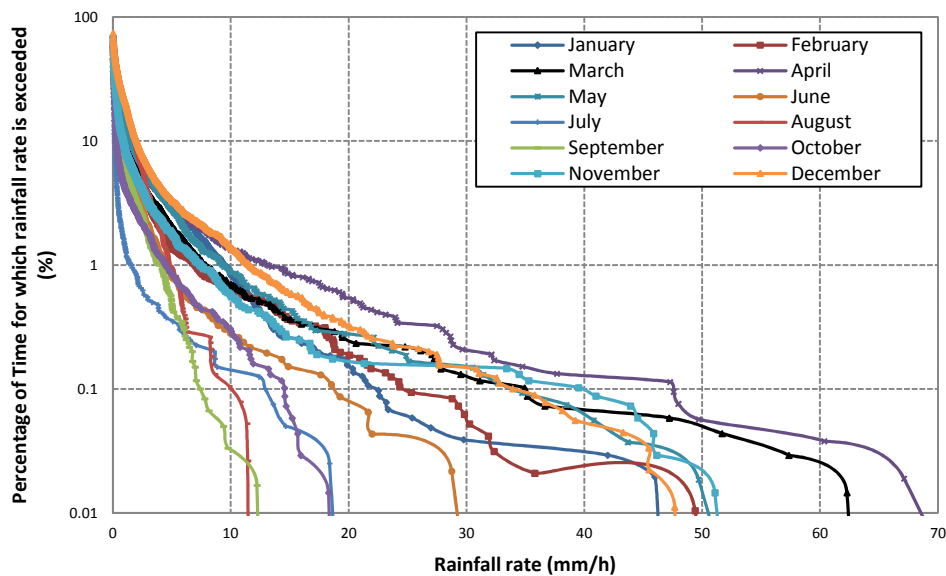
Figure 2-3: Monthly Distribution of Rainfall Rate over Durban between 2009 and 2010 [*Alonge*, 2011]

There have been considerable analytical studies on the subject of rainfall rate worthy of mention. *Moupfouma and Dereffye* [1982], in their work, found that the distribution of any local rainfall rate data exists between gamma and lognormal distributions. Thus, a simple probability function was proposed to simulate the rain rate distribution given by:

$$P\ (R \geq r) = \ a\frac{exp(-ur)}{r^b} \tag{2.7}$$

The parameters *a*, *b* and *u* are constants valid for only when *r* > 2mm/h.

In a follow-up study, *Moupfouma* (1985) extended the definition the constants in (2.7) to cater for global applications by considering data from 15 locations around the world. Thus, these new set of relationships were mainly dependent on the rainfall rate at $R_{0.01}$. There have also been further modifications of these functions to improve the shape of the distribution profile of rainfall rate in tropical and temperate areas of the world by *Moupfouma and Martin* (1993).

2.4.3.1 Rainfall Rate Mathematical Theory

The mathematical theory of rainfall rate usually begins with the description of its relationship with other relevant rainfall parameters. The general assumption is usually with reference to the rain drop shape, which is practically assumed spherical for simplicity. Thus, a rain drop *sphere* with a known diameter, *D*, has a volume, *V(D)*, defined by:

$$V(D) = \ \frac{4\pi}{3}\left(\frac{D}{2}\right)^3 \quad [mm^3] \tag{2.8}$$

The rain drop terminal velocity is an important parameter which tends to vary with the atmospheric pressure, temperature and relative humidity. Hence, there have been a number of popular models representing the terminal velocity of rain drops in air. Among the popular models are those proposed by *Gunn and Kinzer* [1949], *Atlas and Ulbrich* [1977] and *Beard* [1976] model which was modified by *Van Mook* [2002] as reported by *Owolawi* [2010]. *Atlas et al.* [1973] modified the experiments of *Gunn and Kinzer* [1949] to give a simplistic form of terminal velocity given by:

$$v_t(D) = \ 9.65 - 10.30\exp(-0.6D) \quad [m/s] \tag{2.9}$$

while *Atlas and Ulbr*ich [1977] gave their model as:

$$v_t(D) = 17.67 \times (0.1D)^{0.6} \quad [m/s] \tag{2.10}$$

where D is the diameter of the rain drop in both cases of (2.9) and (2.10).

The diameter integral of the product of the rain drop volume, terminal velocity and rainfall DSD from zero to infinity describes the rainfall rate function described in *Sadiku* [2000] as:

$$R(D) = \int_0^\infty v_t(D)N(D)V(D) \, dD \quad [mm/h] \tag{2.11}$$

Modifying (2.11) by substituting for *V*(*D*) from (2.8) yields a generic rain rate function which is related to the third moment of the rainfall DSD and is given by:

$$R(D) = 6\pi \times 10^{-4} \int_0^\infty v_t(D)N(D)D^3 dD \quad [mm/h] \tag{2.12}$$

Therefore, rainfall rate can be estimated given the knowledge of the terminal velocity and rainfall DSD provided the diameter range of rain drops are within satisfactory limits.

2.4.4 Rainfall Drop Size Distribution (DSD)

Rainfall drop size distribution refers to generic description of a scaled probability density function of rain drops of different sizes within a spatially defined area. The spatial variability of rain drop population, in terms of the logical extent and spread, is often used to identify rain cells. The determination of rainfall DSD is also location-specific largely because it is related to another microstructure, rainfall rate, which has also been proven to be location-specific. Research has shown that a wider spectrum of rain drops of different sizes exists as rain rate increases during a typical rain event. In practice, the shape of rain drops is inherently important to the drop size studies. The terminal velocity of a rain drop is often reliant on shape parameters such as diameter as seen in (2.9) and (2.10). On this, *Li et al.* [1995] and *Li et al.* [2000] suggested that rain drop shapes often range from spherical shapes to spheroidal and then, oblate-spheroidal depending on the magnitude of rain rate.

The earliest established study of rain drop sizes is that of *Laws and Parsons* [1943], where the independent parameters of volume fraction percentage and terminal velocity of individual rain drops are used to estimate rain DSD. This study was adopted by the ITU and was largely found to give a good estimation of DSDs in temperate regions [*Owolawi*, 2010]. The description of

rain DSD mathematics has been shown to be strongly related to the Probability Density Function (PDF) of available drop sizes. *Ulbrich* [1983] describes the raindrop mathematical representation for rain drop size theory as:

$$f(D) = \frac{N(D)}{\int_{o}^{\infty} N(D)dD} \quad [mm^{-1}] \quad \text{for } D > 0 \tag{2.13}$$

where $f(D)$ is the PDF of the rain drop sizes, $N(D)$ is the rain DSD function and D is the mid-value diameters of rain droplets usually ranging from 0.2 mm to about 5.5 mm.

From (2.13), it follows that denominator is the rain rate-dependent scaling constant of $f(D)$ known as the drop concentration variable, N_t. Thus, it follows that the drop concentration per unit volume is approximately the *zeroth* moment of the rain drop diameter defined as:

$$N_t = \int_{o}^{\infty} N(D)dD = \sum_{i} N(D_i)\Delta D_i \quad [m^{-3}] \tag{2.14}$$

The moment of rainfall DSD is an important relation with a number of applications in rainfall statistics [*Kozu and Nakamura*, 1991; *Timothy et al.*, 2002]. Mathematically, the DSD moment is defined as:

$$M(n) = \sum_{i=1}^{N} D_i^{n} N(D_i)\Delta D_I \quad [m^{-3}mm^{n}] \tag{2.15}$$

where n is the moment number are often used in the determination of other rainfall microstructures given the knowledge of the rain DSD. For example, setting $n = 0$ (zeroth moment) yields the drop concentration as earlier seen in (2.14). The third, fourth and sixth moments are useful in estimating the rainfall rate or liquid water content, rainfall attenuation and radar reflectivity respectively [*Kozu and Nakamura*, 1991].

The Method of Moment (MOM) parameter estimation technique is the most popular method of computing the unknown parameters of statistical distributions of rainfall DSD [*Ajayi and Olsen*, 1985; *Kozu and Nakamura*, 1991; *Timothy et al.*, 2002]. The description of rainfall DSD patterns can be enhanced by modelling the data using statistical distribution functions. There are four popular statistical model often employed by researchers in DSD modelling: lognormal, modified gamma, Weibull and negative exponential models. The first two models have been

extensively demonstrated to work favourably with data from tropical areas with high rainfall rates [*Awang and Din*, 2004; *Das et al.*, 2010]. The last model, on the other hand, has been proven to be the most preferable for temperate climates [*Law and Parson*, 1943; *Marshall and Palmer*, 1974; *Bhattacharyya et al.*, 2000]. The discussion will focus on lognormal and modified gamma models based on their importance in the evaluation of rainfall drop sizes in tropical areas.

2.4.4.1 Lognormal Rainfall DSD

The lognormal model rainfall DSD model is a three-parameter function defined from *Ajayi and Olsen* [1985] and *Maitra* [2004] as:

$$N(D_i) = \frac{N_T}{\sigma D_i \sqrt{2\pi}} \exp\left[-0.5 \left(\frac{\ln(D_i) - \mu}{\sigma}\right)^2\right] \qquad [m^{-3} mm^{-1}] \qquad (2.16)$$

where N_T is the total number of rain drops per unit volume, μ is the mean of the drop size data and σ is the standard deviation of the drop sizes. These parameters are dependent on the prevailing local rainfall rate, R, given as:

$$N_T = a_o R^{b_o} \qquad (2.17a)$$

$$\mu = A_\mu + B_\mu \ln(R) \qquad (2.17b)$$

$$\sigma^2 = A_\sigma + B_\sigma \ln(R) \qquad (2.17c)$$

where the coefficients, a_o, b_o, A_μ, B_μ, A_σ and B_σ can be obtained through regression analysis.

It is usual that the MOM technique as given in (2.15) is equated to the lognormal moment generator given by [*Kozu and Nakamura*, 1991]:

$$M_n = N_T \exp\left[n\mu + \frac{1}{2}(n\sigma)^2\right] \qquad (2.19)$$

where n is the moment index and other parameters are components of the lognormal distribution. The third, fourth and sixth moments of (2.19) are solved to obtain the input parameters as required. The lognormal DSD model is most preferred model in the descriptive statistics of rainfall DSD in tropical areas around the world because it works well at regions with high rainfall rate occurrence [*Ong and Shan*, 1997; *Awang and Din*, 2004; *Das et al.*, 2010]. Figure 2-4 gives the variation of rainfall DSDs at different tropical locations around the world at 75 mm/h. The locations compared are Singapore [*Ong and Shan*, 1997], Nigeria [*Ajayi*
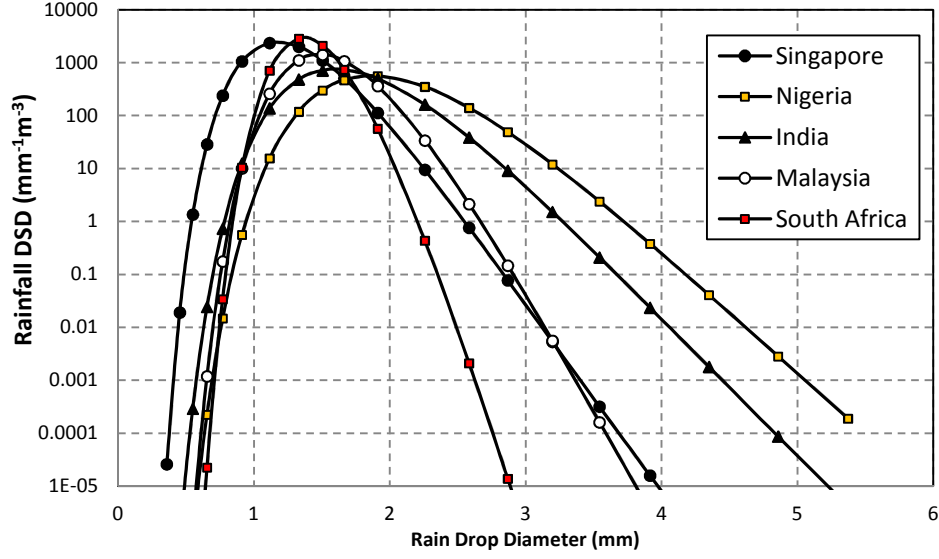
Figure 2-4: Comparison of rainfall DSDs at different part of the world

and Olsen, 1985], India [*Maitra*, 2004], Malaysia [*Tharek and Din*, 1992] and South Africa [*Alonge*, 2011]. At this particular rain rate, the probability of having maximum rain drops beyond 3 mm in Durban is almost zero, compared to results from other locations.

2.4.4.2 Modified Gamma DSD

The modified gamma model is a modification of the classical exponential DSD function proposed by *Marshall and Pal*mer [1974], where D^μ represents the exponential modifier. This distribution is given by *Atlas and Ulbrich* [1974]:

$$N(D_i) = N_o D_i{}^\mu \exp(-\Lambda D_i) \qquad [m^{-3}mm^{-1}] \qquad (2.20)$$

where N_o represents the constant related to number of rainfall drops, μ is the shape parameter and Λ is the slope parameter of the distribution. These parameters are also related to the rainfall rate given by:

$$N_m = a_m R^{b_m} \qquad\qquad (2.21a)$$
$$\Lambda = a_\Lambda R^{b_\Lambda} \qquad\qquad (2.21b)$$

The coefficients in (2.21a) and (2.21b) can be obtained from regression analysis from results of the MOM technique. The modified gamma DSD moment generator is equated to raw moments of the data as given by *Kozu and Nakamura* [1991]:

$$M_n = N_m \frac{\Gamma(\mu + n + 1)}{\Lambda^{\mu+n+1}} \qquad (2.22)$$

The moment generator (2.20) is solved for the third, fourth and sixth moments as (2.19) and the estimators are obtained simultaneously. This model is suitable for rainfall DSDS at both temperate and tropical areas [*Ulbrich*, 1983; *Bhattacharya et al.*, 2000; *Awang and Din*, 2004].

2.4.5 Rainfall Radar Reflectivity

Radar reflectivity refers to the back-scattering characteristics of radar systems when electromagnetic waves are reflected from targeted sources. In radar systems deployed for rainfall studies, a standard measurement indicator called the Radar Reflectivity Factor (RRF) is used to investigate the nature of the back-scattering dynamics. RRF (denoted by *Z*) is described as the integral of the sixth moment of rainfall DSD over the entire diameter of rain drops available within the swept (or scanned) volume of a radar system. RRFs are useful for resolving the characteristics of the target or objects including number densities, scattering properties, attenuating properties and refractive properties. Mathematically, the sixth moment of rain DSD as a continuous function of (2.15) is given by:

$$Z = \int_0^\infty D^6 N(D) dD \quad [mm^6 m^{-3}] \qquad (2.23)$$

where all parameters maintain their usual definitions.

The dependence of *Z* on rainfall DSD makes it a useful parameter in remote sensing of precipitation at microwave bands over large areas [*Kumar et al.*, 2011]. Reflectivity is related to the rainfall rate and this relationship is variable due to dynamics of rainfall microphysics [*Battan*, 1973; *Anagnostou*, 2004]. This relationship has established the understanding of stratiform and convective rainfall systems, and their role in the variations of rainfall attenuation.

2.5 Rainfall Attenuation Prediction

The *ITU-R P.530-15* [2013] in their documents proposed a systematic technique of predicting rainfall path attenuation over terrestrial links at any location around the world. This classical method of computing path attenuation due to rain, A_p, over an effective distance, d_{eff} is given as:

$$A_p = \gamma_r d_{eff} \qquad [dB] \qquad (2.24)$$

where γ_r is the specific attenuation dependent on two power-law parameters, k and α, as obtained in *ITU-R P.838-3* [2005] such that:

$$\gamma_r = kR_{0.01}{}^\alpha \qquad [dB/km] \qquad (2.25)$$

,and, d_{eff} is the effective path length of the communication link given by:

$$d_{eff} = rd \qquad [km] \qquad (2.26)$$

where r is the length factor and d is the actual path length of the communication link. The *length factor* refers to the portion of the path length affected by rainfall which is estimated as thus [*ITU-R P.530-15*, 2013]:

$$r = \frac{1}{0.477d^{0.633}R_{0.01}{}^{0.073\alpha}f^{0.123} - 10.579(1 - exp(-0.024d))} \qquad (2.27)$$

where f is the frequency of transmission in GHz.

2.5.1 The Distance-Loss Concept of Rain Attenuation

The propagation of electromagnetic wave occurs when a energy transference from local antenna system is allowed to travel through free space. Once in free space, the forward travelling component of the electromagnetic wave interacts with different media often consisting of gases, microscopic granules and rainfall. The rainfall media is usually of great concern as it is highly sensitive to the frequency of the travelling wave energy, as well as its amplitude. Thus, in a rainy medium, the attenuated portion of this wave is approximately equal to the exponential factor of distance, l and propagation constant, γ given by *Van de Hulst* [1957]:

$$A_p = e^{-\gamma l} \qquad (2.28)$$

By further simplification in the decibel unit , this becomes:

$$A_p = 4.343\,\gamma l \qquad [dB] \qquad (2.29)$$

If the RHS of (2.29) is given as function of the unit length of km, then it can easily be seen that:

$$A_s = 4.343 \times 10^3\,\gamma \qquad [dB/km] \qquad (2.30)$$

The unit, A_s, is defined as the specific attenuation due to rainfall. *Sadiku* [2000] gave the function, γ, as the product of the rain DSD, $N(D)$ and extinction cross section, Q_{ext}, so that when integrated over an averaged path for an infinite number of rain drop sizes with different diameter, D, it becomes [*Ajayi et al.*, 1996]:

$$\gamma = \int_0^\infty N(D)Q_{ext}(D)\,dD \tag{2.31}$$

When (2.31) is substituted into (2.30), this gives a universally accepted formulation for estimating the specific attenuation of rainfall at any location given by:

$$A_s = 4.343 \times 10^3 \int_0^\infty N(D)Q_{ext}(D)\,dD \quad [dB/km] \tag{2.32}$$

This shows that rainfall specific attenuation is mainly dependent on the diameter of the available distribution rain droplets and the Extinction Cross Section (ECS). The extinction cross section has been investigated using perturbation techniques by *Li et al.* [1995; 2000]. However, the complexities of their computation are not easily implemented in estimating specific attenuation. In the literature, the Mie scattering approach [*Mie*, 1908] is preferred for the estimation of ECS. This approach assumes that the real part of the forward scattering amplitude is evaluated to estimate the relative extinction such that:

$$Q_{ext}(D) = \frac{4\pi}{k^2}\,Re\left\{ \frac{1}{2}\sum_{p=0}^\infty (2p+1)[a_n(m,\alpha) + b_n(m,\alpha)] \right\} \quad [mm^2] \tag{2.33}$$

The coefficients, $a_n(m,\alpha)$ and $b_n(m,\alpha)$, correspond to the Mie scattering coefficients which are dependent on m the complex refractive index of water, and, α which depends on the ambient temperature and droplet frequency. *Sadiku* [2000] and *Mätzler* [2002a, 2002b] gave the solution of these coefficients based on the account of the spherical nature of the raindrops using special spherical Bessel functions for spherical raindrops given by:

$$a_n(m,\alpha) = \frac{m^2 j_n(m\alpha)[\alpha j_n(\alpha)]' - j_n(\alpha)[m\alpha j_n(m\alpha)]'}{m^2 j_n(m\alpha)\left[\alpha h_n^{(1)}(\alpha)\right]' - h_n^{(1)}(\alpha)[m\alpha j_n(m\alpha)]'} \tag{2.34a}$$

$$b_n(m,\alpha) = \frac{j_n(\alpha)[m\alpha j_n(m\alpha)]' - j_n(m\alpha)[\alpha j_n(\alpha)]'}{h_n^{(1)}(\alpha)[m\alpha j_n(m\alpha)]' - j_n(m\alpha)\left[\alpha\,h_n^{(1)}(\alpha)\right]'} \tag{2.34b}$$

where *m* represents the complex refractive index of water at a specified ambient temperature; $j_n(m\alpha)$ and $j_n(\alpha)$ is the spherical Bessel of the first kind with $m\alpha$ and α as their arguments repectively; $h_n^{(1)}(\alpha)$ is the spherical Hankel function of the first kind.

The recent works of *Odedina and Afullo* [2010] and *Alonge and Afullo* [2011] on Mie scattering technique showed that a functional fit relating the ECS to the radius of a rain droplet. This expression is given as:

$$Q_{ext}(R) = k_{ext}\bar{a}^{\varsigma_{ext}} \qquad [mm^2] \qquad\qquad (2.35)$$

Where k_{ext} and ς_{ext} are the power-law coefficients related to the ECS. The results of these coefficients are presented in Appendix C from the studies of *Alonge and Afullo* [2011].

The procedure discussed from (2.32) to (2.35) can easily be implemented if there are readily available rainfall data to compute rain microstructures like rainfall DSD. In the absence of data, the ITU-R method proposed in the publication of *ITU-R P.838-3* [2005] can be useful in estimating specific attenuation due to rainfall. The procedures for this method are given in Appendix B. However, there are concerns about this method as it appears that it leads to the under-estimation of specific attenuation in tropical locations [*Das et al.*, 2010] and over-estimation in subtropical locations [*Alonge and Afullo*, 2012b].

2.5.2 Rain Fade Mitigation Techniques

The mitigation techniques used to suppress the effects of rainfall attenuation and fading are broadly divided into two categories: Static Rain Fade Mitigation (SRFM) and the Dynamic Rain Fade Mitigation (DRFM).

The SRFM is the traditional method of assigning a constant power level, corresponding to the maximum rain attenuation experienced at 99.99% of rainfall occurrence over the year, to the link budget. This principle is derived from the ITU-R requirements in their global recommendations in *ITU-R P.838-3* [2005], *ITU-R P.837-6* [2012] and *ITU-R P.530-15* [2013]. As rainfall rate availability at 99.99% ($R_{0.01}$) varies globally, it is proper to assert that the assignment of power levels will vary globally likewise. The major advantage of this method is its simplicity and quick adaptability to any location around the world. However, this method is not totally economical and effective in the deployment of emerging radio technologies which emphasizes on stringent power management schemes for base station. This is because it fails to employ a *power-level-on-demand* approach to check the effects of rain fade during rain events.

This simply means that SRFM allocates power level to rainfall countermeasure throughout the year, irrespective of the period of dry spell, which dominates the calendar year. In the long run, this technique fails to consider the time domain effects of rain fade which is a great disadvantage.

Other methods such adaptive power control, site diversity, adaptive coding and modulation, and antenna reconfiguration are categorized as DRFM techniques [*Acosta*, 1997; *Castanet et. al*, 2003; *Marayuma*, 2008]. Such dynamic techniques are deemed robust because they approach attenuation mitigation by applying feedback-and-update procedures in the time domain, which require elaborate algorithm routines during rain events. The updated underlying parameters may include among others transmission power levels, frequency modulation schemes, antenna beam-width alterations [*Acosta*, 1997; *Umebayashi et. al*, 2005; *Nakazawa et. al*, 2010]. Usually, the considerations for any of these parameters are dependent on the spatiotemporal and random behaviour of rain rate and rain attenuation. These factors, in turn, vary with rain cell sizes, rain rate, operating frequency of the designed base station and transmitting distance between the transmitter and receiver.

2.6 Rainfall Attenuation and Rain Rate Characteristics in the Time Domain

The time domain properties of rainfall attenuation have been shown to vary randomly as rainfall rates have time signatures that are also randomly varied. Since rainfall rate is related to rainfall attenuation as shown in ITU-R publications, it is considered as an independent variable in attenuation studies [*ITU-R P.838-3*, 2005; *ITU-R P.530-15*, 2013]. Therefore, understanding the time-varying characteristics and stochastic process of rain rate is advantageous to understanding rainfall attenuation. Perhaps, the greatest benefit of understanding the stochastic variation of rainfall in the time domain is in the future development of rainfall time-correlated channel models. There have been a number of attempts at demystifying time series characteristics of rainfall rate and rainfall attenuation. The most dominant approach is the utilization of Markov Chain (MC) probabilities applied in most recent studies [*Van de Kamp*, 2003; *Alasseur et al.*, 2004; *Heder and Bitós*, 2008; *Maruddani et al.*, 2010].

The MC probability theory is an approach for understanding chain-like probability events in which a step-wise jump from one state to another is linked by probabilities. The *Markov chain*, as it is called, first appeared in the works of *Andrey Andreyevich Markov* (1856-1922) in 1906, which was later extended by *Andrey Nikolaevich Kolgomorov* in 1936. MCs are initiated from the popular subject of stochastic Markov processes, which is applied to characterize time-varying phenomena predicated upon the past probabilities of the system [*Dymarski*, 2011]. This

term is more agreeably used to describe statistically dependent and time domain systems, which are often mapped as discrete or finite state spaces, in short and long term predictions. It is applied in a number of real time systems for predictions, projections and evaluation of time-varying systems mainly in life sciences, engineering, financial and business analysis, and, meteorological sciences.

2.6.1 Markov Chain Modelling for Rain events and Rain Attenuation Time Series

The application of MCs in rainfall attenuation studies employs the knowledge of probability theory to establish empirical state transition indices. Primarily, the technique involves the use of rainfall rate or rain attenuation thresholds to determine states within a specified time. Sometimes, other criteria may be added to make the technique robust and practicable; two of such studies are hereby considered. One of such cases is the application of two-level Markov model structure by *Alasseur et al.* [2004] over Spain. In their work, the Markov chain structure generates rain rate samples based on its previous time samples. The first level is usually semi-Markovian and is important in the determination of 'rain and 'no rain' states. The second level employs an *N*-state Markov chain that considers rain rate intensities from previous time samples. To this end, a 42-state Markov chains with Gaussian conditional probability is applied to determine the probability of current rain rates from previous samples. This study showed that a higher number of Markov states produced better resolution especially for higher thresholds of rain rates. The approach gave a good agreement between the experimental data and the simulations.

The second study is that of *Maruddani et al.* [2010] which focused mainly on the application of a variant of the Markov model called the Hidden Markov Model (HMM). In this study of rainfall synthesis, HMM was applied to determine the channel characteristics through the determination of rainfall rate states over Indonesia. In this method, rainfall rate from rain gauge data were categorized into four states and applied to determine HMM parameters some of which include initial matrix, transition matrix and output symbol among others. Their approach was mainly applied in the synthesis of rain rates and the prediction of rain fade for channel modelling, The model assumes that the conditional matrix probability of an output symbol, b^t, given the input symbol, a^t, is given by:

$$\mathrm{P}\{b_i{}^t | a_i{}^t\} = \mathrm{P}\{b_1, a_1\}\,\mathrm{P}\{b_2, a_2\} \dots \mathrm{P}\{b_t, a_t\} = \prod_{i=1}^{t} \mathrm{P}\{b_i | a_i\} \qquad (2.36)$$

The overall system can be represented by embedded elements given by $\{S, A, B, \pi, P\{a\}\}$ where S is the channel space state, A and B are the input and output alphabets respectively, π is the initial state probability and the conditional Markov probability is given by $P\{a\}$ with elements $\Pr\{a, j|i\}$.

2.7 Climatic Characteristics of Study Areas

Throughout this study, the rainfall attenuation studies will comparatively focus on two locations at the tropical sub-Saharan Africa: Durban, South Africa at 29°52'S, 30°58'E and Butare, Rwanda at 2°36'S, 29°44'E. From the location coordinates, both cities tend to lie along similar longiitudinal coordinates, hence, varied forms of tropical climate are experienced at both sub-saharan African locations. Figure 2.5 gives the map of these two areas at their locations on the African continent. Durban being located at the Southern tip of the African continent experiences gentler form of tropical features which is often described as *subtropical*. On the other hand, Butare, being close to the great Equator, predominantly experiences a high-strung form of tropical characteristics classified as *equatorial*. In the proceeding subsections (2.7.1 and 2.7.2), the characteristics and features of these locations are further discussed.

2.7.1 Features of Subtropical Africa: Durban

Durban is a South-Eastern city located along the coastline of South Africa in the KwaZulu-Natal Province. The city is bounded by the Indian Ocean with an average of 28 m above sea level. The annual weather is modulated by warm current of Agulhas throughout the year. It is classified as a subtropical zone, under category *C* (mild mid-latitude climate), sub-category *f* ('feutch' or moist) and hot temperature, *a* (between 23°C and 27.9°C) of the *Köppen-Geiger* climatic classification [*Kotek et al.*, 2006]. Therefore, the complete sub-category profile of Durban is given as humid subtropical class (*Cfa*). This classification inherently describes a location with a hot summer and variable rainfall pattern annually. With an annual rainfall of over 1000 mm and annual temperature of about 20°C, the city is perhaps the warmest in the Southern African clime with four seasonal cycles: summer, autumn, winter and spring [*Fashuyi et al.*, 2006; [1]].

Over the years, the city has been a subject of persistent research in the understanding of rainfall attenuation problems in the South African region. Some of these campaigns are hereby highlighted as follows: *Odedina and Afullo* [2008] and *Odedina and Afullo* [2010] approached their studies by utilizing hourly rainfall data from the South African Weather Services (SAWS). Largely, their studies also focused on the influence of integration times in Durban and the derivation of a similar relationship at other South African cities. Rainfall attenuation modelling

(a)

(b)

Figure 2-5: Maps showing the two locations of study in Sub-Saharan Africa [3] (a) Durban in South Africa (b) Butare in Rwanda

was undertaken using an experimental terrestrial link operating at 19.5 GHz between Howard College campus and Westville campus of the University. These earlier studies were simultaneously complemented by the research of *Owolawi and Afullo* [2007] and Owolawi [2011] for which rain attenuation contour maps were developed for South African cities based on the available five-minute rainfall data from SAWS. An initial investigation into the area of rainfall DSD modelling was considered using the method of Maximum Likelihood (ML) parameter estimation technique. *Afullo* [2011], in a similar guise, applied the Kernel parameter estimation approach to estimate the model parameters of rainfall DSD in Durban. A further research into the development of rainfall DSD models, seasonal variation of rainfall characteristics and estimation of rainfall attenuation in Durban was investigated in the studies of *Alonge and Afullo* [2012b] and *Alonge and Afullo* [2012c]. Furthermore, *Akuon and Afullo* [2011a] and *Akuon and Afullo* [2011b] worked on the development of rain cell models using SAWS rain gauge networks and microwave laboratory disdrometer. This research assisted in the prediction of rainfall path attenuation for terrestrial and satellite links over South Africa. In a much more recent work, *Adetan and Afullo* [2013] and *Adetan and Afullo* [2014] demonstrated using disdrometer data, the proportionate critical diameters essential for the severe influence of rainfall specific attenuation over Durban, South Africa and Butare, Rwanda.

2.7.2 Features of Equatorial Africa: Butare

Butare is a Rwandan city located in South-Western part of Rwanda, which is a central African country. The city is about 2° south of the Equator and hence, is a flourishing equatorial location. On the *Köppen-Geiger* climatic map, the city is assigned with *A* (tropical rain forest) and *w* (wet) characteristics, hence, it is grouped as tropical wet climate (*Aw*). The seasons at this location are mainly divided into four categories: dry and wet seasons occurring twice in a year. The dry seasons occur from June to September and January to March, while the wet seasons occur between mid-March to June, and then, mid-September to December [4]. This is in consonance with observations in tropical locations that dry seasons occur relatively for short periods or may not be present at all [*Green*, 2004].

Like most parts of the country with domineering high altitude almost everywhere, the altitude at Butare reaches as high as 1700m making it a good location for Earth-space communication [*Alonge and Afullo*, 2013b]. Based on the unusual rainfall pattern around the Southwestern region of Rwanda, Butare experiences a high percentage of shower and thunderstorm rainfalls throughout the year. The heavy rainfall patterns are observed in the annual rainfall average of about 1150 mm with annual average temperature not exceeding about 20 °C [5].

This site is to be investigated based on the equatorial rainfall characteristics as compared to the subtropical rainfall pattern in Durban. Therefore, the next chapter focuses on the statistical variation of rainfall microstructures with measurements in Durban, South Africa and Butare, Rwanda. This detailed study will initially form the basis of understanding the spatial properties of these microstructures to be investigated.

CHAPTER THREE

Analysis of Rainfall Microstructures in Tropical Africa

3.1 Introduction

Hybrid networks supported by satellite and terrestrial microwave links require high-speed connection, and hence, higher frequency spectrum operating within the microwave and millimeter band region to deliver sophisticated low-end services to customers. However as earlier discussed in literature review, wireless networks transmitting beyond 10 GHz are often limited by the attenuating characteristics of rainfall. Globally, rainfall attenuation is a subject of interest especially at locations of immense and intense rainfall events. More so, many of these locations at low and mid latitudes around the world, have been of interest to radio engineers as they have unstable levels of rain fade. Rainfall microstructural parameters are very important as they provide information on potential outages and network black-outs due to unstable rain fade levels. The knowledge of the exact nature of the variation of rainfall microstructures in tropical Africa is largely an unexplored area. Therefore, this chapter compares rain microstructures of rainfall rate, rainfall DSD and radar reflectivity at equatorial and subtropical Africa. Rainfall data is obtained from the RD-80 Joss-Waldvogel (JW) distrometer measurements at two sites, Durban, South Africa and Butare, Rwanda. The measurements are taken as a single data - and then processed accordingly to determine their Stratiform-Convective (S-C) thresholds at 38 dBZ. These thresholds, as computed at the two sites, are then applied as theoretical boundaries to separate the rainfall measurements into stratiform and convective regimes. Furthermore, the specific attenuation due to rain at both sites are predicted via the Mie scattering technique and duly compared. Finally, the determination and comparison of S-C thresholds at other global sites are determined at 38 dBZ with other results in tropical Africa.

3.2 Background of Stratiform-Convective Classification

The mechanism of rainfall attenuation is a result of the scattering and absorption of transmitted signal energy by rainfall droplets. This mechanism is dependent on frequency, drop-shape and temperature [*Aydin and Daisley*, 2002; *Das et al.*, 2010]. The amount of energy absorbed or scattered depends on the rain drop-size and rainfall rate, which are often inhomogeneous in space and time during rain events. Thus, for a rain event, it is very likely to experience different attenuation within a swept area, at the same rainfall rate due to the varying number of rain drops of different sizes [*Chen et al.*, 2011].

The obstruction of the strongest signature of Fresnel ellipsoids by dense columns of rain droplets in a swept area can be estimated by quantifying reflectivity via the processing of

electronic data from radar systems or alternative ground measurements. Ground or space-borne radar measurements both estimate reflectivity parameters with background information on rain DSD and droplet densities [*Tenório et al.*, 2010; *Kumar et al.*, 2011]. In the absence of radars, the rainfall distrometer or rain gauge networks can be deployed to provide alternative measurements of rain rate and droplet density. Better still, it can provide information related to rainfall indices such as Liquid Water Content (LWC), rain rate and radar reflectivity [*Bartholomew*, 2009].

Generally, rainfall process during a rainfall event can be considered to have three-stage constituent regimes: stratiform, transitional and convective [*Tokay et al.*, 1999; *Wilson and Tan*, 2001]. Researchers have reported the existence of these regimes in relation to their prevailing cloud types leading to rain events. For instance, *Houze* [1997] reported that stratiform precipitations (~ < 20 mm/h) are usually associated with strong horizontal profile, with widespread and low rain rates over a large cell area. They are formed from nimbostratus clouds and appear as bright bands under radar [*Houze*, 1997]. Convective precipitations (~ > 20 mm/h), on the other hand, are induced from cumulus and cumulonimbus cloud formations. They are reputed to have stronger and columnar vertical profiles with characteristically small rain cells (less than 4 km in diameter) [*Houze*, 1997; *Anagnostou*, 2004]. The transition portion as observed in the studies of *Kumar et. al* [2011], mostly exists as a buffer regime during intense rainfall, between stratiform and convective regimes or vice versa. Generally, the stratiform portion of a rain event is mainly responsible for drizzle and widespread rainfalls, while, the convective portion generates rainfall of showers and thunderstorms. Classifying of precipitation datasets assists in the understanding of cloud physics and rainfall retrieval process from measurements [*Houze*, 1997]. It is also very useful in estimation of rain cell areas for the assignment of advection velocities in radio link designs [*Begum et al.*, 2006]. In recent studies, classification (or discrimination) of S-C threshold can also be applied to determine the vertical extent and precipitation profile in temperate and equatorial climates [*Capsoni et al.*, 2006; *Lam et al.*, 2010]. There are different methods of classifying Stratiform and Convective (S-C) regimes from distrometer and radar measurements [*Houze*, 1973; *Awaka*, 1997]. Some of these methods include the Background-Exceeding Technique (BET) for ground measurements and Precipitation Radar (PR) algorithms for processing radar images. For simplicity, this study employs the reflectivity threshold of 38 dBZ for the S-C classification as proposed by *Gamache and Houze* [1982].

3.3 Measurement and Data Processing

In the absence of conventional radar-derived data, the Joss-Waldvogel (JW) RD-80 distrometer was employed at the sites in Durban, South Africa (29°52′S, 30°58′E) and Butare, Rwanda (2°36′S, 29°44′E) for the measurement of rainfall microstructural parameters. The JW RD-80 impact disdrometer unit is a rainfall data archiving and retrieval system categorically employed in the measurement and monitoring of rainfall microstructural parameters namely rain rate, rainfall drop-size, rain accumulation and rain reflectivity. It is designed and manufactured by Disdromet Ltd, Switzerland [2].

The RD-80 distrometer unit is most recent series sequel to RD-69 unit that operates on the principle of accelerating rain drop impact on its topmost sensitive surface area. This principle is obtained from the studies of *Gunn and Kinzer* [1949] which estimated conveniently the rainfall diameter interval and drop terminal (or fall) velocity. The system consists of two independent units connected to the microcomputer via an RS-232 ethernet cable standard: the outdoor unit and the indoor unit. The circuit structural design of this distrometer is shown in Figure 3-1a, while the system architecture is shown in Figure 3-1b. The outdoor unit consists of a highly-sensitive pressure transducer, which produces low power signal from rain drop impact collected over a sampling area of 0.005 m^2 and at a variable sampling interval between 30 or 60 seconds. The indoor unit is an embedded signal processing system which acts as an interface to the computer archive. The outdoor unit speaks to the indoor unit via the RS-232 communication protocols after which inbuilt algorithms are used to convert the incoming information to rainfall parameters. Usually, the processed data is logged to the computer for future use. The unit has an inbuilt capability of characterizing detected rainfall drops into 20 specified diameter classes (from 0.359 mm to 5.373 mm) at ±5 % accuracy. The diameter range for each class is
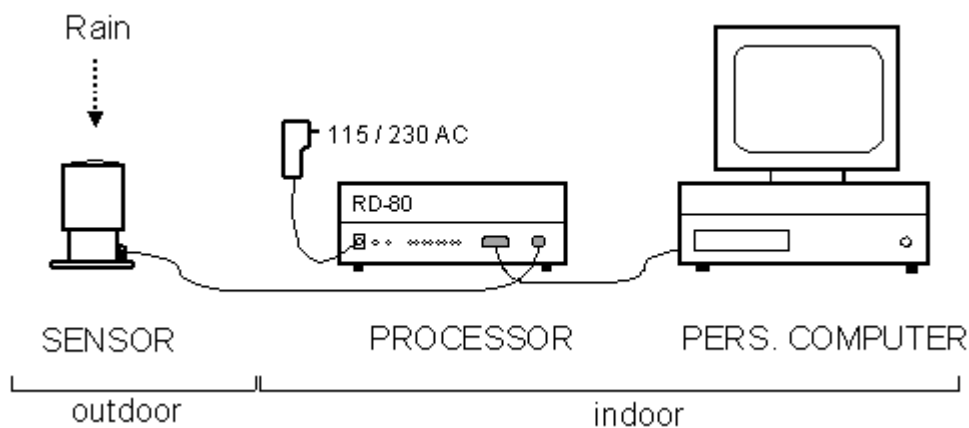
Figure 3-1a: The configuration of the outdoor and indoor units of the Joss-Waldvogel RD-80 impact distrometer system (RD-80 product information: [2])
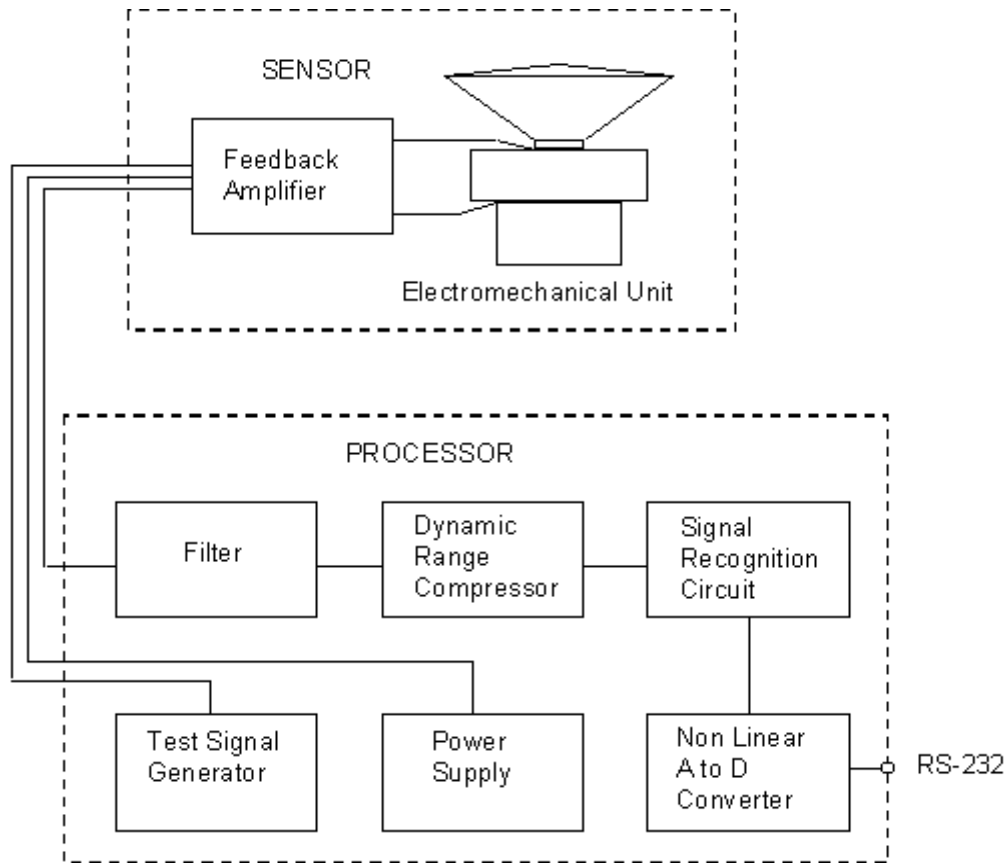
Figure 3-1b: Block diagram for the circuit structure of JW RD-80 distrometer (RD-80 product information: [2])

equivalent to $\left(D \pm \frac{\Delta D}{2}\right)$ mm, so that the minimum bound for any class is $\left(D - \frac{\Delta D}{2}\right)$ mm, while the maximum bound is $\left(D + \frac{\Delta D}{2}\right)$ mm. Information available in Appendix D shows the designation of this distrometer for the available diameter channels for droplet sizes, their fall velocities and equivalent diameter intervals. In Durban, the equipment was installed at the University of KwaZulu-Natal (UKZN), Howard College Campus, Durban, from January 2009 to December 2010. At Butare, the equipment was installed at the National University of Rwanda (NUR), Butare, with a shorter period - between March 2012 and December 2012. The equipment at both locations were configured to generate rainfall data at one minute interval. Hence, the default rainfall integration time used in this thesis is one minute (or 60 seconds). For data processing, rainfall measurements with aggregate number of drops less than 10 were discarded; this is to minimize the underlying effects of dead time errors. Additionally, only rainfall samples exceeding 1 mm/h were considered, so that for Durban and Butare, a total of 8073 and 3659 useful rainy samples were processed respectively. The maximum rainfall rate recorded in Durban and Butare is 117.15 mm/h and 78.52 mm/h respectively. A summary of all the distrometer measurements and other informative details are presented in Table 3-1.

Table 3-1: Site Locations and Measurement Specifics

Location	Total Rainfall (mm)	Lat ^{O}S	Long ^{O}E	No. of Rainy Events	Samples (minutes) Collected	Filtered	Climatic Features
DURBAN	703.34	29°52′	30°58′	242	86470	8073	Subtropical
BUTARE	561.43	2°36′	29°44′	74	19973	3659	Equatorial

At this point, understanding the unique geographic and climatic conditions at the two measurement locations is pertinent to this study. Butare, is located at a South-Western, low-latitude coordinates (close to the Equator) of 2°36′S and 29°44′E of the country of South-Western Rwanda. The equatorial conditions at this location induce the prevalence of super-tropical climate resulting in severe thunderstorms and strongly convective rains. Highland features are prominent with terrain elevation of 1700 m above sea level, hence, mountainous [*Alonge and Afullo*, 2013b]. Unlike the super -tropical climatic features present at Butare, Durban is located at mid-latitude coordinates of 29°52′S and 30°58′E, with an underlying subtropical climate along the East coast of South Africa. The rainfall pattern appears as a combination of temperate and tropical patterns - characterized by a combination of stratiforms and few cases of strong thunderstorms. In addition, Durban possesses a natural coastline with 28 m height above sea level with the climate modulated annually by the easterly Indian and Atlantic Ocean currents. Apart from these features, these locations also have different structures of seasonal cycles with Butare experiencing wet and dry seasons occurring twice in its annual cycle. On the other hand, Durban experiences a four-season annual cycle comprising of summer, autumn, winter and spring.

3.4 Radar Reflectivity Data Classification for the Stratiform-Convective Bounds

The data from the JW distrometer consists of rain drop number statistics and derived rainfall rate. To classify the measurements from the two sites into S-C samples, their radar reflectivity indices are computed using the appropriate algorithm. Therefore, the Radar Reflectivity Factor (RRF) algorithm related to the sixth moment of rainfall DSD is computed. This is given by:

$$z = \sum_{i=1}^{20} N(D_i)D_i{}^6 \Delta D_i \qquad [mm^6 m^{-3}] \qquad (3.1)$$

,and, the reflectivity in dBZ given as:

$$Z = 10\, Log_{10}(z) \quad [dBZ] \qquad (3.2)$$

where $N(D_i)$ is the rainfall DSD of the ith channel computed from the distrometer in (3.1) [*Chen et al.*, 2011]:

$$N(D_i) = \frac{C_i}{A_s \times T \times v(D_i) \times D_i} \quad [mm^{-1}m^{-3}] \tag{3.3}$$

where C_i is the number of drop available at the ith channel, A_s is the sampling area of the distrometer cone set as 0.005 m^2, T is the sampling interval given as 60 seconds, $v(D_i)$ is the terminal velocity of the ith channel and ΔD_i is the diameter interval of the ith channel.

The computed radar RF (Z) as explained by earlier authors can be written as a simple power-law function with rainfall rate (R) [*Marshall and Palmer*, 1948; *Battan*, 1973; *Feingold and Levin*, 1986]. This expression, also known as *Z-R* relationship, proposed by *Marshall and Palmer* [1948] is given as:

$$z = AR^b \quad [mm^6m^{-3}] \tag{3.4}$$

where A and b from numerous studies are coefficients dependent on geographical and climatic factors. The standard *Z-R* expression given in their study was computed as $A = 200$ and $b = 1.6$ from the exponential DSD for European climate. *Battan* [1973], in addition, also produced *Z-R* results for 69 locations around the world.

By combining (3.1) - (3.3), the coefficients A and b for continuous rainfall in Durban and Butare are obtained by regression technique. In Table 3-2, we present results of the monthly rainfall parameters in Durban and Butare. In Durban, peak reflectivities vary over the months annually with the highest value of 55.15 dBZ observed in the month of April. This coincides with the recorded peak rain rate of 117.15 mm/h. The b coefficients of the *Z-R* parameter are seen to be fairly constant (~ 1.55) from December to May which coincides with the period of summer and autumn. Elsewhere, the values are also seen to be close between September and November (~1.65). For the entire year, the averaged peak reflectivity is 48.63 dBZ. At Butare, the monthly peak reflectivity also varies over the year. The highest value is observed in March at 54.42 dBZ and fails to correspond to the peak rainfall rate. The peak reflectivity is also seen to decrease from March to June, with a dry spell in July. Thereafter, the reflectivity remains fairly constant. For the overall datasets in both cases, the overall Z-R coefficients are obtained for Durban ($A = 157.76$, $b = 1.52$) and Butare ($A = 265.6$, $b = 1.45$). The coefficients at Butare are slightly closer to those obtained in the studies of continental and equatorial Africa by

Table 3-2: An Overview of Monthly Rain Statistics in Durban and Butare

Location	Month	Duration (min)	Total Acc. (mm)	Peak Rain Rate (mm/h)	Peak Reflect.(dBZ)	Z-R Function
DURBAN	JAN	1396	88.25	48.93	47.22	$126R^{1.55}$
	FEB	974	56.76	49.38	46.46	$170R^{1.56}$
	MAR	522	42.13	66.25	47.34	$104R^{1.55}$
	APR	630	54.40	117.15	55.15	$147R^{1.58}$
	MAY	651	44.47	76.43	51.54	$602R^{1.24}$
	JUNE	231	3.59	38.61	54.99	$197R^{2.05}$
	JULY	34	3.08	23.36	43.61	$342R^{1.60}$
	AUG	621	23.04	12.59	50.17	$333R^{1.67}$
	SEP	388	16.46	18.57	40.59	$88R^{1.66}$
	OCT	216	15.61	20.37	41.57	$86R^{1.62}$
	NOV	541	39.61	57.67	47.99	$83R^{1.65}$
	DEC	1671	109.13	47.83	56.96	$124R^{1.54}$
BUTARE	MAR	215	26.41	68.33	54.42	$270R^{1.59}$
	APR	1119	90.03	78.52	52.24	$267R^{1.46}$
	MAY	174	34.39	73.99	51.46	$244R^{1.42}$
	JUNE	609	72.13	56.71	50.88	$208R^{1.50}$
	JULY	-NR-	X	X	X	X
	AUG	271	25.79	60.94	51.78	$296R^{1.37}$
	SEP	279	23.60	35.96	47.39	$276R^{1.57}$
	OCT	662	51.70	71.59	51.92	$304R^{1.39}$
	NOV	330	36.2	46.84	50.71	$245R^{1.48}$

Sauvageot and Lacaux [1995] and *Ochou et. al* [2007]. In Durban, however, the coefficients appear closer to the earlier results of *Marshall and Palmer* [1948] with lower value of *A*.

The determination of S-C thresholds for the datasets at the two sites is computed using the 38 dBZ threshold proposed by *Gamache and Houze* [1982]. Equations (3.2) and (3.4) are modified so that the rainfall rate transition threshold, R_{th}, at 38 dBZ is given as:

$$Log_{10}\ (R_{th}) = \frac{3.8 - Log_{10}\ (A)}{b} \qquad (3.5)$$

where R_{th} is the rainfall rate at the S-C threshold in mm/h.

By computation, these thresholds (R_{th}) in Durban and Butare are found to be 11.34 mm/h and 8.84 mm/h respectively from their *Z-R* relationships. This shows that rainfall typically begins an 'early' transition into convective rainfall at Butare, with about 2.5 mm/h lag behind Durban. On obtaining these thresholds, the filtered data at both locations are then reclassified into stratiform and convective rainfall regimes as seen in Figs. 3-2a-d. A summary of the classified data samples for each regime at the sites is presented in Table 3-3. As seen in this table, stratiform rainfalls account for about 95% and 85% of rainfall measurements in Durban and Butare respectively.

Table 3-3: Data Samples of Stratiform and Convective Rains at Butare and Durban

LOCATION	STRATIFORM (R < R_{th})		CONVECTIVE (R > R_{th})	
	Samples	Z-R Fit	Samples	Z-R Fit
DURBAN	7667	$162.31R^{1.48}$	406	$149.67R^{1.59}$
BUTARE	3093	$277.88R^{1.40}$	566	$149.04R^{1.66}$
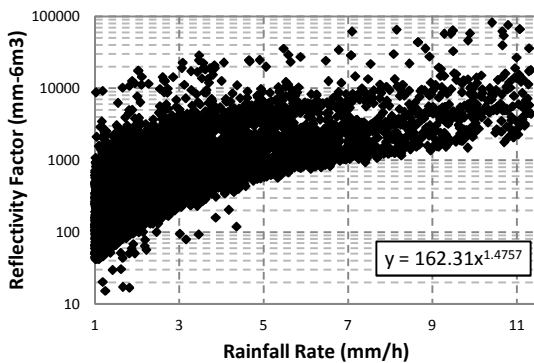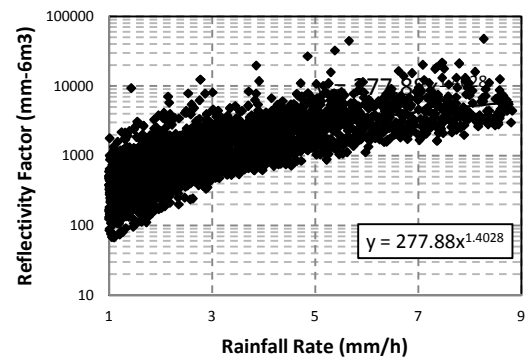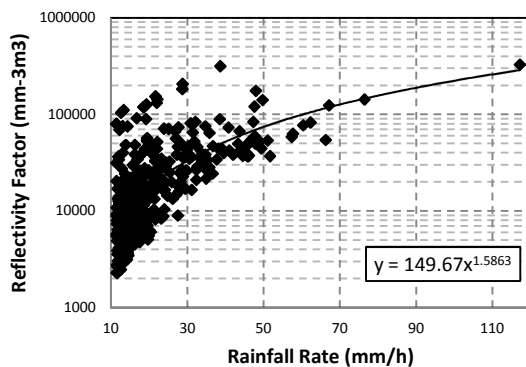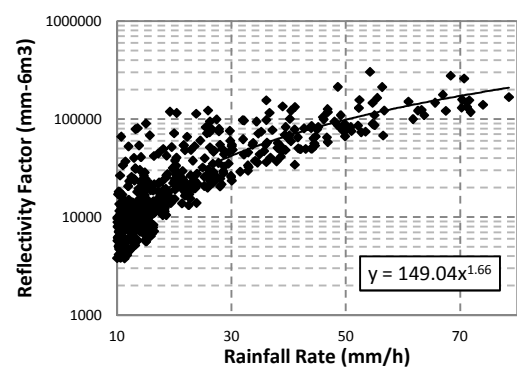
Figure 3-2: The continuous plots of radar reflectivity versus rainfall rate observed at the sites: (a) Durban –Stratiform ($R < 11.34$ mm/h) (b) Durban – Convective ($R > 11.34$ mm/h) (c) Butare–Stratiform ($R < 8.84$ mm/h) (d) Butare–Convective ($R > 8.84$ mm/h)

Thus, about 5% and 15% of the overall classified data are convective samples at both sites. Again, the predominance of stratiform precipitation at the two measurement sites is consistent with observations at mid-latitude areas, especially in tropical regions [*Houze et al.*, 1990; *Nzekou et al.*, 2004; *Tenório et al.*, 2010].

By fitting the reflectivity samples at both sites for stratiform and convective regimes, it is found that *A* coefficients of the Z-R function for former regime are higher than that of the latter regime (see Table 3-3). Conversely, *b* coefficients for convective regime are higher than those observed for stratiform regime. At Butare, *A* coefficients for stratiform are higher than those observed in Durban. On the other hand, *b* coefficients in Durban for convective regime are lower than seen at Butare. A close similarity in the reflectivity coefficients is also observed under the convective regime with Durban (*A* ~ 150, *b* ~ 1.59), and Butare (*A* ~ 149, *b* ~ 1.66). This discovery signifies approximate rainfall structures at both sites for convective precipitation.

3.5 Statistical Comparison of Rain Microstructural Parameters at S-C Bound

The variation of rainfall characteristics at equatorial and subtropical areas depend on the dynamics of the microphysics. Therefore, it is important to understand the differences in stratiform and convective regimes of rainfall microphysics at these sites. To achieve this, the already classified datasets are examined statistically under three microphysical parameters namely: rainfall rate, rainfall DSD and radar reflectivity.

3.5.1 Comparison of Rainfall Rate Distributions at S-C Precipitation Bound

The Complementary Cumulative Distribution Function (CCDF) of the rainfall rate datasets, for both stratiform and convective regimes from both sites are generated as shown in Figure 3-3a and 3-3b. The maximum bound of the stratiform regime at both locations equals to the threshold obtained from (3.5). For the convective regime, the maximum bounds are 120 mm/h and 80 mm/h respectively in Durban and Butare respectively.

From Fig. 3-3a, it is observed that the compared CCDF at Butare slightly exceeds that of Durban for stratiform regimes for the period of comparison. However, the CCDFs intercept at 6.3 mm/h and diverge due to the influence of the gradual breakaway as 38 dBZ thresholds are approached. From Fig. 3-3b, the CCDF in Durban is seen to exceed that of Butare – for rain rates up to about 45 mm/h for the convective regime. However, beyond this rain rate, Butare is seen to increasingly have higher exceedence values of CCDF than Durban until they intercept at around 74 mm/h; and thereafter diverges. Based on the observations from the CCDF comparisons under

convective conditions, it is intuitive to note that Butare experiences higher exceedences than Durban beyond 20 mm/h, until both sites approach the breakpoint at $R_{0.01}$ similar under convective regime. Between the first breakpoint at 45 mm/h and the second at 72 mm/h, the plot indicates higher frequencies of heavy thunderstorms in Butare compared to Durban. However, due to the higher maximum rainfall rate recorded in Durban, rain rates beyond 0.1% of the exceeded time are higher under stratiform regime. Table 3-4 summarizes the rain distribution statistics at both sites exceeded at 0.1%, 0.01%, and 0.001% of the time. Evidently, these percentages are higher in Durban for both regimes as seen from the results.
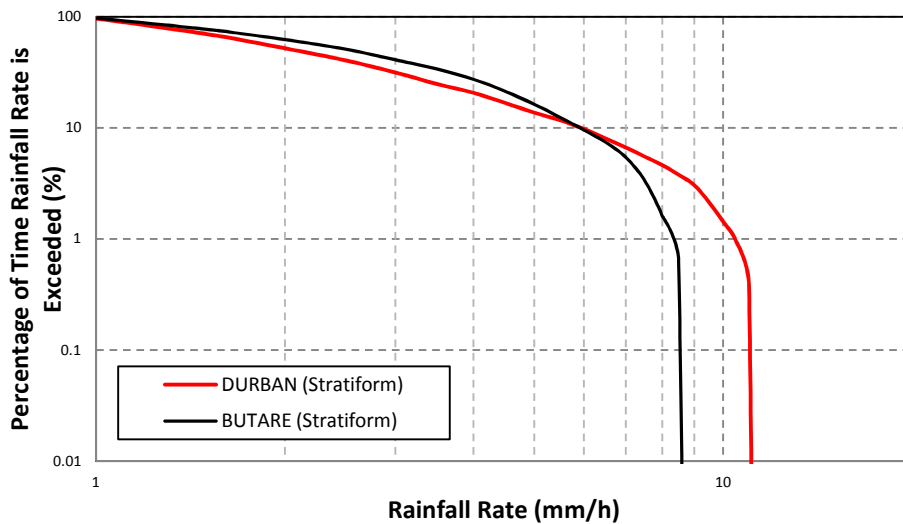
(a)
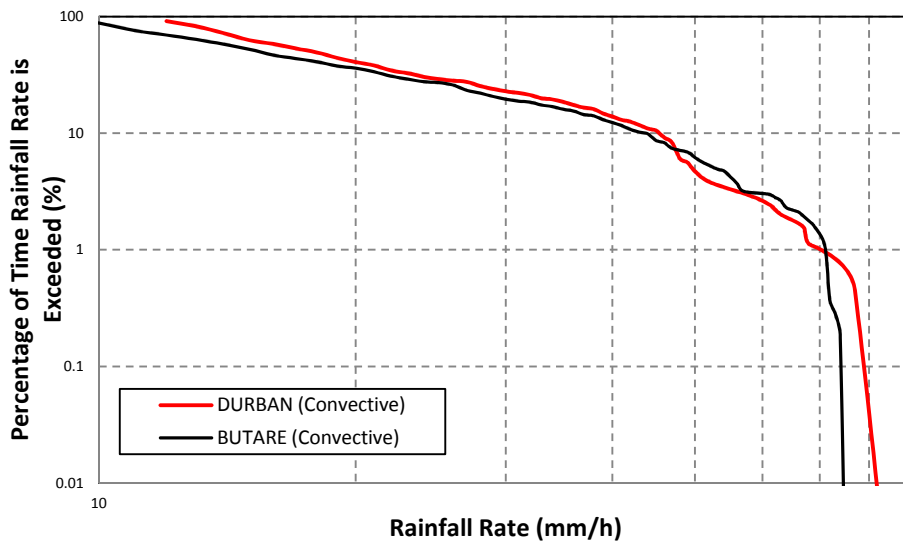
(b)

Figure 3-3: Rainfall Rate Distribution observed in Durban and Butare: (a) Stratiform (b) Convective

Table 3-4: Comparison of rain rate exceedences for measurements in Durban and Butare

Time Percent	STRATIFORM		CONVECTIVE	
(%)	DBN	BTR	DBN	BTR
0.1	11.01	8.55	79.2	72.2
0.01	11.07	8.6	82.3	74.5
0.001	11.28	8.62	85.8	79

3.5.2 Comparison of Rainfall DSDs at S-C Precipitation Bound

The rainfall DSDs at the two sites based on stratiform-convective classes are compared by applying a known statistical distribution model. The preferred model selected for this study is the three-parameter lognormal distribution with three unknown variables. The lognormal model has been proposed in several studies as the foremost model useful for rainfall DSD estimation in tropical and subtropical locations from measurements [*Ajayi et al.*, 1996; *Das et al.*, 2010]. The lognormal distribution for rain droplets is given as:

$$N(D_i) = \frac{N_t}{D_i \sigma \sqrt{2\pi}} \, exp\left[-0.5\left(\frac{\ln(D_i) - \mu}{\sigma}\right)^2\right]$$

$$\text{for } N_t > 0; \; -\infty < \mu < +\infty; \; \sigma > 0 \quad (3.6)$$

where N_t, μ and σ are the unknown variables with the diameter D_i as the only input obtained from measurement.

Using the Method of Moments (MOM) for parameter estimation, the variables corresponding to each rainfall regime at these locations are computed [*Kozu and Nakamura*, 1991]. The 3rd, 4th and 6th moments of the measured rain dropsize data are used to obtain the three unknown lognormal parameters, based on their rainfall relationships [*Kozu and Nakamura*, 1991]. The derived results obtained are given as regression functions dependent on the rainfall rate, *R*. Table 3-5 gives a summary of the functions representing the solutions obtained for the parameters of each regime based on the lognormal DSD. The plots for the lognormal DSD model computed at different rainfall rates across the two investigated regimes are shown in Figure 3-4 (a)-(d). The rainfall rates investigated are at 5 mm/h, 15 mm/h, 40 mm/h and 80 mm/h.

Firstly, it is observed that the distribution of small droplets in Butare decreases rapidly as the rainfall rates increases, while transiting from stratiform to convective regimes. Infact, this anomaly is much more severe for the rain droplets under convective regimes with small rain drop

Table 3-5: Parameters of the Lognormal DSD for Stratiform and Convective Rains

BOUNDS	PARAMETERS	DURBAN	BUTARE
STRATIFORM BOUND	N_T	$300R^{0.0614}$	$101.72R^{0.2463}$
	μ	$-0.3441 + 0.2462 \, \text{Ln} \, (R)$	$-0.0776 + 0.2133 \, \text{Ln}(R)$
	σ^2	$0.075 + 0.0005 \, \text{Ln}(R)$	$0.0818 - 0.005 \, \text{Ln}(R)$
	PARAMETERS	DURBAN	BUTARE
CONVECTIVE BOUND	N_T	$170.39R^{0.2011}$	$161.3R^{0.0805}$
	μ	$-0.1295 + 0.1903 \, \text{Ln} \, (R)$	$-0.1587 + 0.2498 \, \text{Ln}(R)$
	σ^2	$0.0275 + 0.018 \, \text{Ln}(R)$	$0.0439 + 0.0053 \, \text{Ln}(R)$
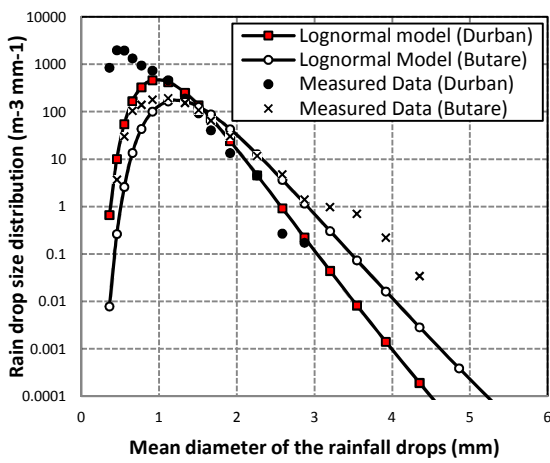
(a)
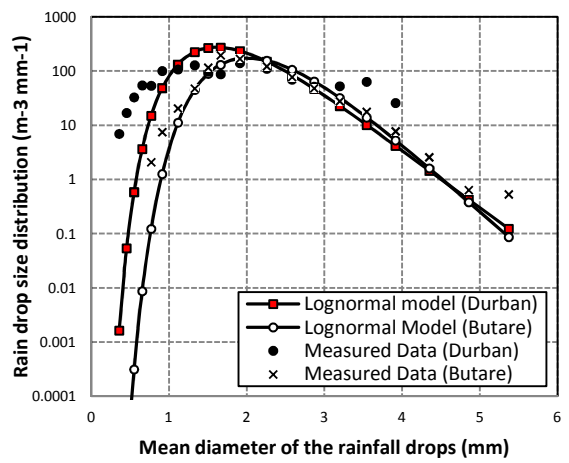
(c)
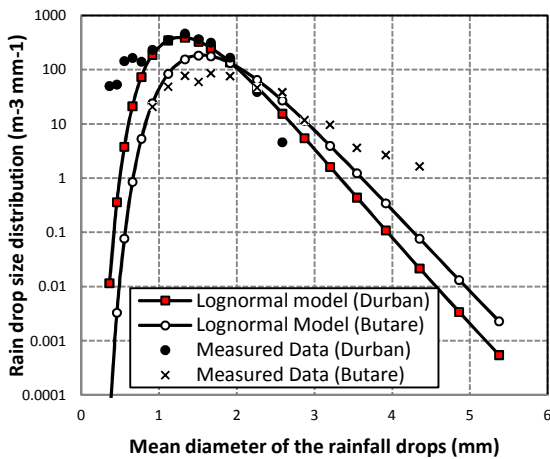
(b)
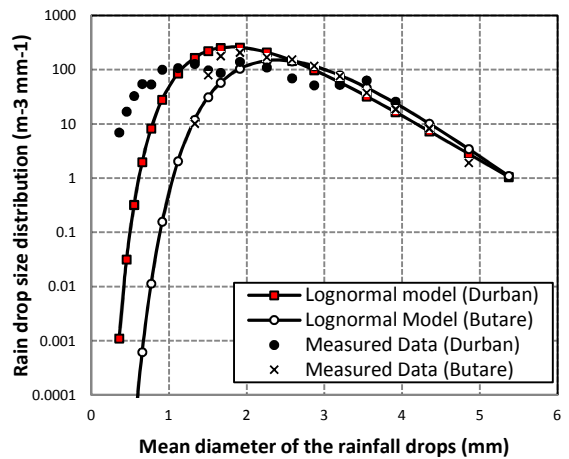
(d)

Figure 3-4: Rainfall DSD variation in Durban and Butare using the S-C Bounds at Different Rain Rates: (a) 5 mm/h (b) 15 mm/h (c) 40 mm/h (d) 80 mm/h

sizes (with diameter less than 0.913 mm) having DSDs less than one and tending to zero. In contrast, Durban is seen to experience higher scales of DSDs for both stratiform and convective regimes. Interestingly, it is also observed that larger rain drop sizes have higher statistical representation at Butare for stratiform regime, than seen in Durban (see Figs. 3-4a and 3-4b). However, for convective regime, the DSDs of large droplets are similar at both Durban and Butare (~ > 2.5 mm). This suggests that the structural distribution profile of large rain droplets at Butare and Durban are slightly similar under convective conditions. However, the near-absence of smaller droplets (~ < 2.5 mm) at the Rwandan site (please see Figs. 3-4c and 3-4d) under convective conditions, may be linked to its equatorial characteristics and its unique height above the sea level (~1.7 km).

From research, it has been documented that areas around tropical regions have reduced population (and smaller probability occurrence) of smaller rain droplets especially at high rainfall rates i.e. convective conditions [*Ulbrich*, 1983; *Sauvageot and Lacaux*, 1995]. Additionally, the intense and 'super-tropical' structure of rainfall at Butare – as with most locations around the equator – validates these observations. It might suffice to add that the integrity of large droplets produced from rain clouds will be much higher at this location. This is partly due to the near-passive nature of droplet disintegration mechanisms like rain height and wind effects during rainfall. The implication of this phenomenon will ultimately affect the contributions of rain droplets in wave scattering and absorption mechanism responsible for rain attenuation as will be later seen.

3.5.3 Comparison of Radar Reflectivity Distribution at S-C Rain Precipitation Bound

The radar reflectivity distributions for stratiform and convective regimes obtained in Durban and Butare are shown in Figures 3-5a and 3-5b. It should be noted that applying the S-C rain rate threshold to the two-regime datasets result in 'smearing' of reflectivity values below and above the 38 dBZ threshold for stratiform and convective regimes as seen in Fig 4a and b. The 'smearing' is attributed to the randomness of the rainfall DSD generation process during rain events. Therefore, it is possible to have rainfall rate samples with values above 38 dBZ under stratiform conditions, and then below 38 dBZ under convective conditions.

In Fig. 3-5a, the stratiform distributions at the two locations are seen as having the same shape profiles with different statistical mean (μ_z) and standard deviation (σ_z). The radar reflectivity distribution in Durban is seen as having higher probabilities of reflectivities less than 28 dBZ, while the converse is obtained at Butare. This variation, we know is also related to the rainfall
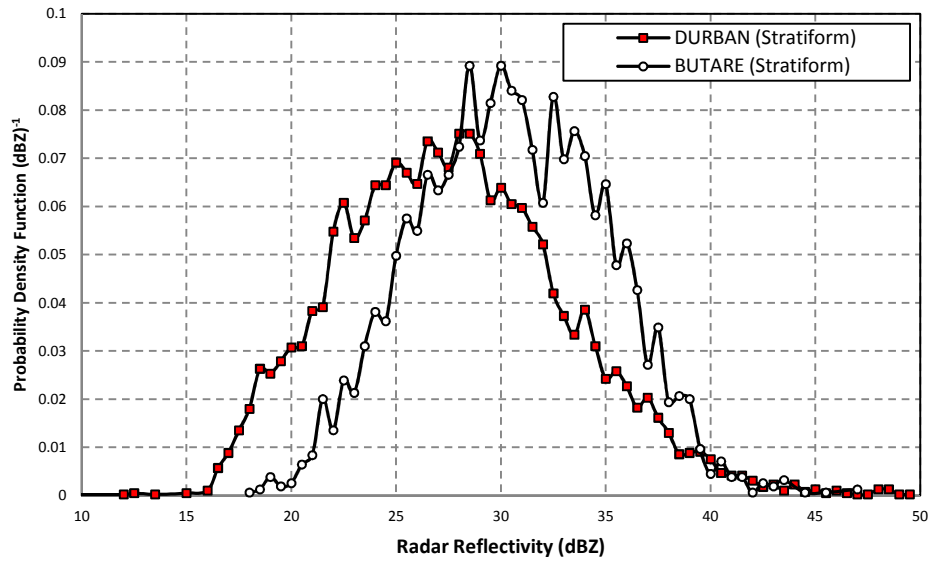
(a)
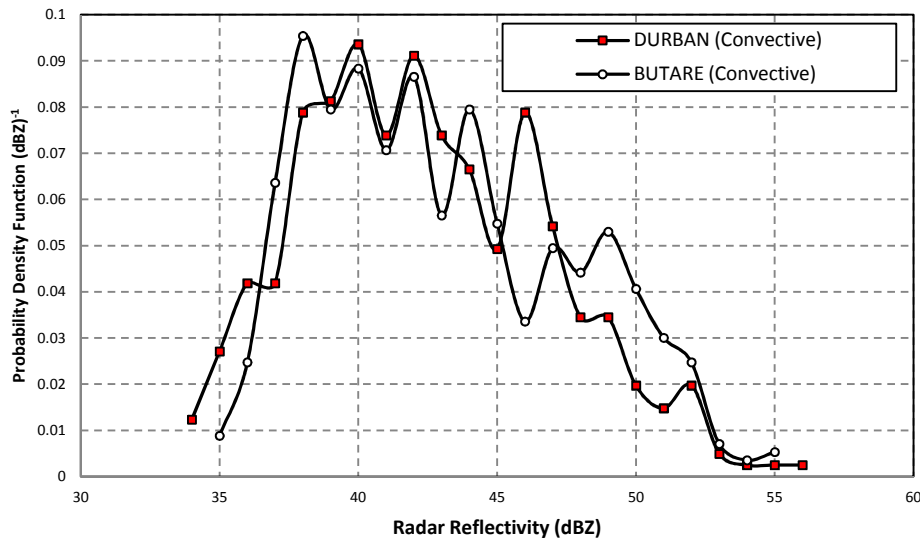
(b)

Figure 3-5: The radar reflectivity distributions for stratiform and convective rainfall bound: (a) Durban (b) Butare

DSD – this translates to variation in the appearance of rain drop sizes. Firstly, it should be noted that under stratiform DSDs, the visible presence of small rain droplets is responsible for the lower values of radar reflectivities less than 18 dBZ, in Durban. In the case of Butare, reflectivity samples greater than 28 dBZ have higher occurrence probability than seen in Durban. This again is due to the obvious presence of large droplets for the stratiform DSD profile as earlier explained (see subsection 3.5.2). For the convective reflectivity distribution profile in Fig. 3-5b, we notice a striking similarity in the shape profile of reflectivity values for samples at both locations. The shape profiles of the radar reflectivity probabilities at both locations are evidently

normally distributed and can be statistically described by a Gaussian distribution function given by:

$$p(Z) = \frac{1}{\sigma_z\sqrt{2\pi}} exp\left[-\frac{1}{2}\left(\frac{Z - \mu_z}{\sigma_z}\right)^2\right] \qquad [dBZ]^{-1} \qquad (3.7)$$

The parameters, μ_z and σ_z, from (3.7) are obtained for the two sites by applying the method of maximum likelihood parameter estimation technique.

The radar reflectivity data are further analysed based on the stratiform and convective regimes. For stratiform class, the set of parameters estimated in Durban (μ_z = 27.42, σ_z = 5.42) and Butare (μ_z = 30.24, σ_z = 4.5) are with Root-Mean Square (RMS) errors of 0.31% and 0.62% respectively. Likewise, the parameters for the convective classes are found accordingly with Durban (μ_z = 41.94, σ_z = 4.41) and Butare (μ_z = 42.54, σ_z = 4.6) having corresponding RMS values of 1.76% and 1.06% respectively. Again, the close values of computed parameters under convective conditions at both locations, indicates a similarity in the rainfall structures for showers and thunderstorms. To confirm this from the earlier results in Table 3-2, the *A* coefficients for convective Z-R relationship at Butare (~149.04) and Durban (~149.67) are also close. Even at that, their *b* coefficients are closer with Butare (~1.66) and Durban (~1.59) – with the former having a higher value. This pattern suggests a sort of similarity in the convective patterns at both locations, with the only noticeable difference being the scale of their Z-R functions. However, these characteristics may not translate into similar specific attenuation index as will be seen later. This is true because the scattering of transmitted signals (forward scattering) required for attenuation is much more related to the transmission frequency and particle size.

3.5.4   Implications of Microphysical Variations on Rain Attenuation

Network engineers are mainly concerned with the performance of radio links as telemetry is varied. Of particular interest is the extent of rainfall effects on link performances, during periods of fluctuating Received Signal Level (RSL). The specific attenuation is an indication of the amount of the projected power losses due to rainfall (or rain fade) per kilometer. For simplification of computing results from rainfall DSD functions, the Mie scattering approach is used to compute these results. The specific attenuation can be computed using the equation given in *Ajayi et al.* [1996] as:

$$A_S(f, R) = 4.343 \times 10^{-3} \sum_{i=1}^{20} N(D_I)Q_{ext}(D_i)\Delta D_i \qquad [dB/km] \qquad (3.8)$$

where $N(D_i)$ is the rain DSD, $Q_{ext}(D_i)$ is the extinction cross section in mm^2 and ΔD_i is the diameter interval.

The extinction cross section is simplified by the Mie scattering expression given as:

$$Q_{ext}(R) = \frac{4\pi}{k^2} Re\{S(0)\} \approx k_{ext}(\bar{a})^{\varsigma_{ext}} \quad [mm^2] \tag{3.9}$$

where $\bar{a}$ is the radius of the rain droplets in *mm*, while, k_{ext} and ς_{ext} are the Mie coefficients obtained from elaborate computations of spherical Bessel functions. These coefficients can be seen in Appendix C.

The computations for Durban at 20°C have been computed from the studies of [*Alonge*, 2011]. At Butare, the same Mie computation procedure for Durban is applied with an assumed temperature of 20°C. At high rainfall rates, rain droplet spectra are mainly oblate-spheroid and spheroidal in shape. Concerning this, *Malinga et al.* [2014] in their recent study showed that ECS computations at high rain rates using Mie technique compared with *Morrison and Cross* [1974] and *Pruppacher and Pitter* [1971] models gave percentage differences up to 30% at 100 GHz. Therefore, specific attenuation values predicted from Mie coefficients is limited in accuracy, especially for rain droplets at high rain rates operating over high microwave frequencies.

By applying the results from Table 3-2, the specific attenuation for stratiform and convective rain regimes at both Durban and Rwanda are computed. The lognormal DSDs from both sites, generated from (3.6), are applied to generate their specific attenuations. As seen from the plots in Figs. 3-6(a) and (b), the specific attenuation at Butare starts diverging from the Durban results at about 40 GHz. The target rainfall rates at 10 mm/h, 25 mm/h and 75 mm/h are also investigated from 4 GHz to 100 GHz as seen in Table 3-6. From Table 3-6, the predicted specific attenuation at Butare starts to decline at 40 GHz for a rain rate of 10 mm/h. At 25 mm/h, the decline is noticeable from 20 GHz; at 80 mm/h, the decline is noticed from 8 GHz. Broadly speaking, there is a rapid decline in the predicted specific attenuation as rainfall transits from stratiform to convective regimes at Butare. For obvious reasons, it seems the decline of specific attenuation over high frequencies and high rain rates, is related to the relatively large population of larger rain droplets. We have earlier noted that the dearth of smaller droplets plays an important role in the DSD and reflectivity profile. Recently, *Adetan and Afullo* [2014] suggested a maximum diameter bound of ≤ 3.5 mm in the percentage of critical diameters of rain drops responsible for specific attenuation at Butare. Furthermore, they reported a decline in the role(s) of these range critical diameters in Butare compared to their observation in Durban. Their findings are observed
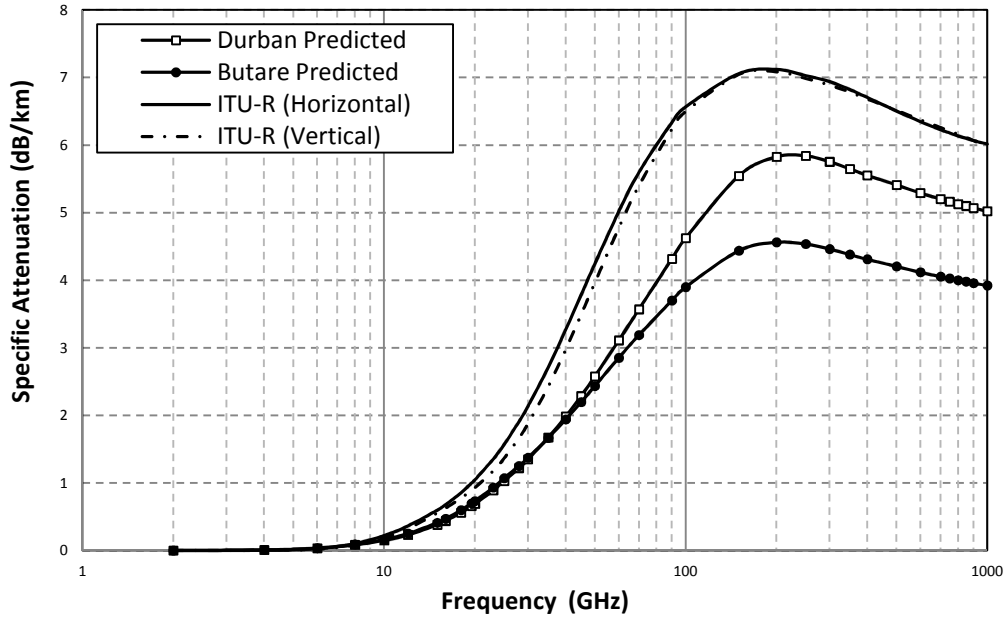
(a)
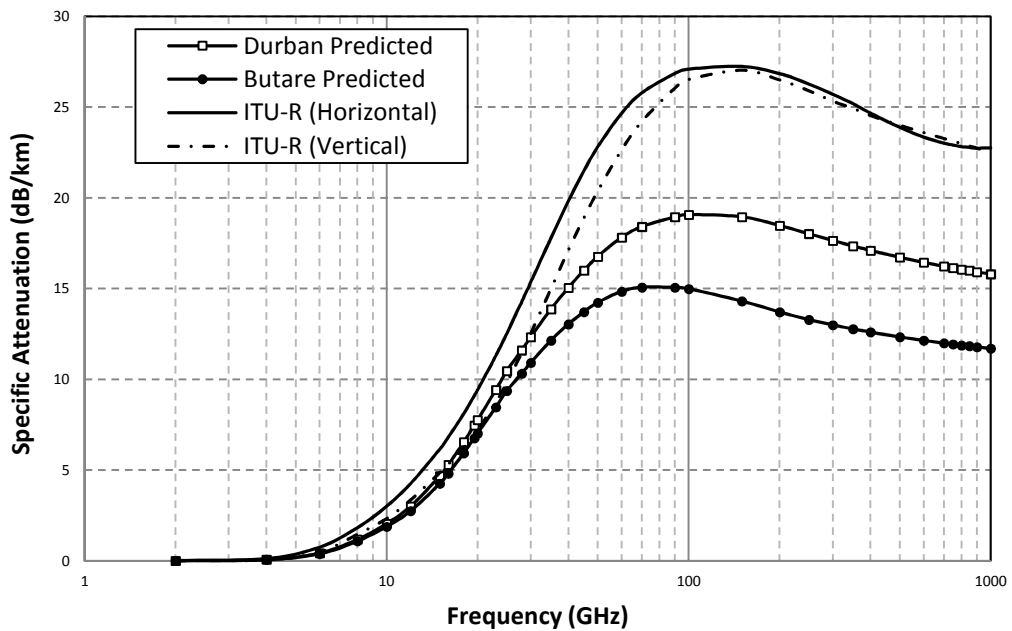
(b)

Figure 3-6: Specific attenuation in Durban and Butare computed with Mie technique at 20°C compared with ITU-R P.838-3 at (*a*) $R = 10$ mm/h (*b*) $R = 80$ mm/h

to be consistent with the findings of this comparative study. Therefore, the predicted specific attenuation is observed to be generally higher in South Africa than Rwanda, from about 30 GHz. However, both sites do have lower specific attenuation than the predicted specific attenuation values from ITU-R P.838-3 [*ITU-R Rec. P.838-3*, 2005].

Table 3-6: Predicted specific attenuation from the lognormal distribution at Butare and Durban

FREQUENCY (GHz)	DURBAN RAIN RATE (mm/h)			BUTARE RAIN RATE (mm/h)		
	10	25	80	10	25	80
4	0.01	0.02	0.07	0.01	0.02	0.07
8	0.08	0.29	1.18	0.09	0.29	1.09
10	0.15	0.51	2.05	0.16	0.51	1.88
15	0.38	1.21	4.68	0.41	1.21	4.26
20	0.69	2.10	7.76	0.73	2.09	7.02
25	1.03	2.98	10.46	1.07	2.93	9.37
30	1.35	3.69	12.33	1.37	3.61	10.91
40	1.98	4.94	15.05	1.94	4.72	13.04
45	2.29	5.46	15.99	2.20	5.17	13.71
50	2.58	5.92	16.76	2.44	5.57	14.23
60	3.11	6.69	17.81	2.85	6.18	14.83
90	4.32	8.09	18.94	3.70	7.17	15.06
100	4.62	8.40	19.07	3.90	7.36	14.98
200	5.83	9.22	18.47	4.56	7.69	13.70
300	5.75	8.95	17.65	4.46	7.41	12.99
400	5.55	8.66	17.10	4.31	7.18	12.60

3.6 Comparison of S-C Rain Rate Thresholds at other Locations

To examine the consistency of the computed results of S-C rain rate thresholds in Durban and Butare, a global comparison is considered. Therefore, Z-R results from other locations with different climato-meteorological scenarios are adequately compared. Some of the African locations are Ile-Ife, Nigeria [*Ajayi and Olsen*, 1985], Benin Republic [*Moumouni et al.*, 2008], Niger Republic [*Ochou*, 2007], Senegal [*Nzekou*, 2004] and Congo [*Sauvageot and Lacaux*, 1995]. The compared locations around the Asian region include Calcutta, India [*Maitra*, 2004], Hassan and Ahmedabad at India [*Das et al.*, 2002] and Singapore [*Kumar et al.*, 2011]. The Oceania areas include Kapingamarangi, Micronesia [*Tokay and Short*, 1996] and Darwin, Australia [*Short et al.*, 1990]. Finally, some locations in the Americas include Canada [*Marshall and Palmer*, 1948], and lastly, Florida and Marshall Islands and Oregon, USA [*Stout and Mueller*, 1968].

Parameters of proposed *Z-R* relationships from studies at some of these locations were applied to initially estimate R_{th}. Locations without available Z-R information were substituted with their equivalent rainfall DSD parameters, either from lognormal distribution or modified gamma distribution. Locations at which DSD functions are applied to obtain *Z-R* results include Ile-Ife,

Table 3-7: Comparison of S-C Thresholds at other Global locations

ZONES	SITES	LOCATION		Z-R Function		THRESHOLD (mm/h)	$R_{0.01}$ (mm/h)	$Z_{0.01}$ (dBZ)
		LAT	LONG	A	b			
AFRICA	S. AFRICA (Durban)	29.88°S	31.05°E	157.76	1.52	11.34	60	48.99
	RWANDA (Butare)	2.6°S	29.75°E	265.6	1.45	8.84	71	51.06
	NIGERIA (Ile-Ife)	7.47°N	4.567°E	396.24	1.32	8.18	68	50.12
	EQUITORIAL Congo	2.88°S	23.66°E	364	1.36	8.15	71	50.79
	NIGER (Niamey)	13.52°N	2.11°E	508	1.28	7.16	42	47.84
	SENEGAL (Dakar)	14.69°N	17.45°W	368	1.24	9.89	62	47.89
	BENIN	8.83°N	2.18°E	433	1.33	7.5	55	49.51
ASIA	INDIA (Calcutta)	22.57°N	88.37°E	106.68	1.67	11.56	100	53.62
	INDIA (Ahmedabad)	23.03°N	72.58°E	195.29	1.42	11.50	54	47.55
	INDIA (Hassan)	13.06°N	76.10°E	169.15	1.44	12.38	85	50.04
	SINGAPORE	1.30°N	103.80°E	285.83	1.33	10.24	102	51.28
AMERICAS	USA (Oregon)	44.00°N	120.50°W	295	1.59	6.86	22	46.04
	USA (Marshall Is.)	7.07°N	171.27°E	226	1.46	9.78	85	51.71
	USA (Florida)	28.10°N	81.60°W	322	1.33	9.37	80	50.39
	CANADA (Ottawa)	45.42°N	75.7°W	220	1.60	8.15	38	48.71
OCEANIA	MICRONESIA (Kapingamarangi)	1.07°N	154.78°E	315	1.20	12.15	102	49.09
	AUSTRALIA (Darwin)	12.45°S	130.83°E	170	1.47	11.69	82	50.44

Calcutta, Hassan and Ahmedabad because of the aforementioned reason. The results containing *Z-R* parameters, R_{th} and $Z_{0.01}$ from the computations are presented in Table 3-7. The values of $R_{0.01}$ for regions are obtained directly from the ITU-R estimates from the global designation for different climatic in ITU-R P.837-6 [*ITU-R Rec. P.837-6*, 2012]. The S-C rain rate transition threshold, R_{th}, tend to converge at 10 mm/h (or closer to 38 dBZ) as confirmed by previous studies [*Gamache and Houze*, 1982; *Tokay and Short*, 1996; *Nzekou et al.*, 2004]. However, we find that the transition rain rates at other locations have a deviation of ±3 mm/h from this convergent value, as influenced by their geographical and climatic factors. As seen in Table 3-7, the mean radar reflectivities at 0.01% of the exceeded rain rate, $Z_{0.01}$, computed for all the global locations also seem converge closer to 50 dBZ with a deviation of ±4 dBZ. From these comparisons, it is obvious that a positive correlation exists between the R_{th} and their corresponding $R_{0.01}$ as seen in Figure 3-7. A power-law relationship is seen to exist between these two parameters based on Figure 3-7. This relationship is given as:

$$R_{th} = 2.31R_{0.01}^{0.34} \quad [mm/h] \tag{3.10}$$
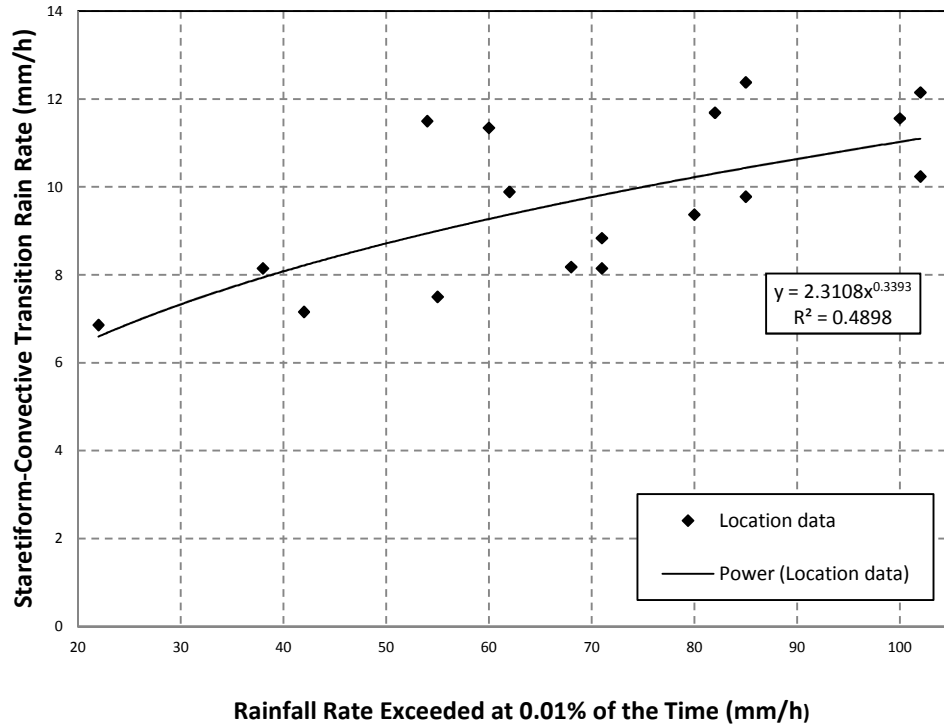
Figure 3-7: Comparison of $R_{0.01}$ and S-C thresholds at different locations around the world

It is obvious from (3.10) that these two parameters are positively correlated across the examined locations. This implies that areas with higher $R_{0.01}$ have a corresponding higher R_{th}, and vice-versa.

3.7 Chapter Summary

The microphysical analysis of rainfall undertaken in this study has revealed the variation in subtropical and equatorial locations. The structures of the compared microphysical parameters i.e. rain rate, rain DSD and reflectivity in Durban and Butare, are much different under stratiform regimes. However, these set of parameters are similar at both locations under convective conditions. This implies that showers and thunderstorm rainfalls have the same characteristics at the compared locations. This characteristic does not suffice for predicted specific attenuation as there are substantial disparities in the DSD structures for rain droplets with sizes less than 2.5 mm. These disparities noticed at Butare result in a progressive decline of specific attenuation as carrier frequency is scaled, irrespective of the rain rate. Indeed, this is purely based on geographic and climatic differences resulting in dearth of small rain droplets ($\leq$ 3 mm). Based on this study, it is predicted that Butare is an ideal location for earth-space communication, especially for design frequencies above 40 GHz. This study has also found a correlation between the S-C transition rain rate (R_{th}) and $R_{0.01}$, where the former varies over a

range of 6 mm/h $\leq R_{th} \leq$ 13 mm/h over the compared locations. However, the shorter measurement period at Butare is a limitation that could influence the overall cyclical rainfall patterns. Therefore, it is suggested that longer measurement period of rainfall statistics at both sites, will greatly improve the knowledge of rainfall microphysics for radio link design. In conclusion, the results derived from this study will be beneficial to the knowledge of rain microphysics in radio and microwave engineering around the world.

CHAPTER FOUR

Queueing Theory of Rain Spikes over Radio Links

4.1 Introduction

In the previous chapter, the variation of rainfall microstructures at two African locations with subtropical and equatorial climatic characteristics was investigated. The S-C threshold divide employed revealed that spatial variation of rain microstructures is indeed more similar as rainfall rate exceeds at least 10 mm/h (convective conditions). Judging from the results of the probability characteristics, it is obvious that rainfall attenuation at both sites is more dependent on the DSDs at high microwave bands. In this chapter, the temporal effects of precipitation over radio links is investigated by employing the queueing theory approach. The approach is an extension of the Markov chain technique, which deals with traffic-like random instances of events, with stochastic probabilities of progression in the time domain. Rainfall rate is a unique case of progressive random generation with an apparent traffic-like behaviour, which can aptly be described with a tool such as queueing theory. Therefore, the contents of this chapter are mainly concerned with the theoretical and empirical investigations of the rainfall queue characteristics in Durban, South Africa. The determination of queue parameters and the appropriate queue disciplines, alongside the development of other related indices are discussed in this chapter.

4.2 Background and Inspiration of the Queueing Theory Approach

Apart from the contemporary multiple power problems arising from algorithmic routines at base stations due to radio resource allocation, the static provisions for power demands in link budget, are mainly attributed to radio propagation and rain fade losses. The inclusion of static fade margin for rain fade loss in link budgets is accommodated throughout the annual life-cycle of a base station, to cater indiscriminately for non-periodic cycles of wet and dry spell periods [*ITU-R Rec. P.530-15*, 2013]. In practice, dry spells are known to have a higher probability of occurrence than wet spells; hence, this questions the rationale behind the static countermeasure proposed by the ITU-R. This current ITU approach questions the need to continually adopt dynamic countermeasure techniques for optimization of radio resources. Broadly speaking, the definition of rain fades is valid when rainfall rates exceed a particular level, corresponding to the designed threshold of the link performance [*Mämmela and Kolteba*, 2011]. This threshold could be transformed to performance parameters like Bit Error Rate (BER) and Signal-to-Noise Ratio (SNR) via knowledge of fade depth. Since all rain-fade events during rainfall are embedded within an underlying rainfall event, they are assumed as instances within specified rainfall duration. Typical rain fade duration have been found to be distributed in a log-normal

manner, with deep fades lasting no more than 30 minutes and shallow fades not less than 24 hours [*Acosta*, 1997]. The study of rainfall duration life-cycles, it seems, play an important role in understanding the effects of rain fades and their occurrences. A way of achieving this is by studying the underlying dynamics of the rainfall process such as rainfall event duration, duration cycles (or arrival cycle) and waiting periods.

The dynamics of the rainfall process is mainly reliant on the mechanics of its occurrence. Rainfall occurrences are random events which are strongly dependent on the geographical and climatic variability of a location [*Ajayi et al.*, 1996]. Usually, rainfall is dynamic within its defined time frame, also known as *rainfall duration*. Analysis of rainfall duration is important as it reveals the information of the service time, coinciding with outage period of communication networks. By observation, a rainfall event consists of a visible train of rain rate spikes which appear in a random manner – they are identifiable by the maximum rainfall rate attained by spike with successive overlapping patterns. In some special cases of longer rainfall events, there exist a large number of such rainfall spikes; continually overlapping each other in succession with each attaining a maximum rain rate. By inspection, the rise and fall of rainfall spikes during a rain event, is strongly related to the motional physics of clouds during rainfall. Therefore, the random generation of rain spikes in succession, may imply the arrival and departure of rain-clouds when viewed from a reference point. As a simple rule, these sequences of rainfall patterns evidently qualify as a *birth-death* (BD) process. This is similar to traffic analysis of dynamic objects from a static point of reference as applied in telecommunication traffic analysis, factory line processes, processor design optimization e.t.c. [*Kleinrock*, 1975; *Bolch et al.*, 1998; *Gross and Harris*, 1998; *Hillier and Lieberman*, 2001; *Gautam and Ravindra*, 2006; *Fiandrino and Piavanelli*, 2010]. The BD process is not an entirely new concept applied in the understanding of queueing problems, since a wide array of diverse black-box problems related to random queue behaviours can be explained by this process. The systematic and consecutive birth (arrival) and death (departure) of objects in a system can be processed in a First Come, First Served (FCFS) traffic-like behaviour, if served by one or more clearance points, known as *servers* usually designated as *s*.

In this chapter, rainfall traffic is explored with queueing characteristics such as rainfall service time and rainfall inter-arrival time. Therefore, we examine rainfall spike generation cycle as an infinite queue, multiple server FCFS traffic (M/E_k/s/FCFS/∞), described by exponential arrival time and Erlang-*k* service time distributions with multiple servers. This approach itself is novel and two important reasons suffice for undertaking this approach. Firstly, the rainfall spike traffic statistics can provide us with a better understanding of the bounds of spike service time

(or outage times), and hence, describing rain cell sizes and their life-cycles. Also, this knowledge is a good foundation for the development of a new paradigm for rainfall time series prediction and rain rate tracking, and hence, more robust understanding of rain fades.

4.3 The Mathematics of Queueing Theory of Rainfall Process

The application of queueing theory to the understanding of the rainfall process requires basic definition of certain parameters and quantities to ease the knowledge been discussed. In lieu of this, a number of propositions related to the work to be undertaken are hereby discussed as follows:

Proposition 1: The rainfall event process is a stochastic process where the instances of rainfall rates are generated randomly over a time parameter. Rainfall rate is a typical random variable that can be designated as R_t with a time parameter ($t \in T$). Then, the mathematical process of the rainfall is completely described by $\{R_t : t \in T\}$ for $T \subseteq \mathbb{R}_+ = [0, \infty)$. The time-varying characteristics of R_t is the point of focus. Thus, if the time parameter is conceptualized as a countable finite process, then the overall process can be defined as a single "chain" with discretised state spaces [*Bolch et al.*, 1998].

Proposition 2: If proposition (1) holds true, then it follows that a rainfall process is a unique process of the order of the Markov chain process. Evidently, the present state of such a system is independent of the past state. Thus, a Discrete-Time Markov Chain (DTMC) is sufficient to describe the entire process.

Proposition 3: Following propositions (1) and (2), the countable states in a rainfall process is assigned a variable, *Q*, with a 'discrete' time parameter of *T*. If the total number of countable states is given as K_o, then the number of observation points is so characterized as $k \in K_o$.

Proposition 4: The Probability Distribution Function (PDF) of the random variable, R_t, contains the complete information of its characteristics. Thus, the future states of a rainfall process can be described as thus [*Bolch et al.*, 1998]:

$$P(R_{n+1} = q_{n+1} | R_n = q_n, R_{n-1} = q_{n-1}, \dots, R_o = q_o) = P(R_{n+1} = q_{n+1} | R_n = q_n) \quad (4.1)$$

The RHS of (4.1) is equivalent to the probability dependency of the future state of the rainfall process (R_{n+1}) on the current state (R_n). Markov chains can transit from one state to another

and as a result, can attain any state probability influenced by time steps of *n*. If we assume for a given time, *n*, a state transits from state *j* to *k*. This is given from [*Bolch et al.*, 1998] as:

$$p^{(1)}{}_{jk}(n) = (R_{n+1} = q_{n+1} = j \mid R_n = q_n = k) \qquad \forall n \in T \qquad (4.2)$$

This represents a one-step transition which can otherwise be re-written as:

$$p^{(1)}{}_{jk} = (R_{n+1} = j \mid R_n = k) \qquad (4.2b)$$

Bolch et al. [1998] suggested that a one-step process can be represented as singular transition matrix given by:

$$\mathbf{P}^{(1)} = \mathbf{P} = [p_{jk}] = \begin{bmatrix} p_{00} & p_{01} & \cdots & p_{1k} \\ p_{10} & p_{11} & \cdots & \vdots \\ \vdots & \vdots & \ddots & \vdots \\ p_{j0} & \cdots & \cdots & p_{kk} \end{bmatrix} \qquad (4.3)$$

For an *n*-step process, the resulting state probability is dependent on the initial state probability so that:

$$\mathbf{P}^{(n)} = \mathbf{P}\mathbf{P}^{(n-1)} = \mathbf{P}^n \qquad (4.4)$$

This forms the basis for further estimation of probabilities until n→∞, where steady state is attained by the system if the transition probability, **P**, is a regular matrix.

4.3.1 The Markovian Framework of Queues in Rainfall

In the context of describing rainfall as a queueing process, the following assumptions are applied throughout the development of the queue theory in this chapter:

- Rainfall rate is a stochastic and countable phenomenon described by R_t where $t \in T$ for $\forall t \subset \mathbb{R}$. The rainfall event, which by definition is the generation process for rainfall rate samples is governed and self-regulated, by natural climatic and geographical laws.

- The queueing process of a rainfall event can be completely described by three queue parameters namely: service time (t_s), inter-arrival time (t_a) and overlap time (t_o).

- The rainfall spike generation process can be represented as a self-regulated infinite queue, whose probability of occurrence is determined by Markov parameters, at time instances so that: $t_s \in (0, \infty)$, $t_a \in (0, \infty)$ and $t_o \in (0, \infty)$.

- The rainfall spike queue mechanism can be completely specified by non-negative service, inter-arrival and overlap times so that $t_s \subset T$, $t_a \subset T$ and $t_o \subset T$. Where T is the total duration of the event. It follows that, $T = \sum_{k=1}^{n} k t_{s,k}$, where n is the total number of visible spikes.

- The queueing sequence described by cyclical and stochastic arrays of independent appearances of spikes/clouds, is a combination of service and inter-arrival times viewed as a DTMC process, with n-available states related to the BD process.

- Each of n-states corresponds to singular instances of time entities related to the points along a known Markovian or non-Markovian processes (service or inter-arrival times). Their outputs are equivalent to states probabilities, $\{\mathbf{Q}_o, \dots < \mathbf{Q}_{n-1}\}$, defined by arrival and departure of spikes/clouds in a possible BD process

Based on the assumptions above, it would suffice that the arrival and departure times of two spikes are such that no overlap time exists between the two spikes. However, there are very few cases where succeeding spike trains have zero overlap from theory. Thus, when there is no separation between two consecutive spikes, then an overlap, or perhaps, a form of congested queue is said to exist. Therefore, the overlap time statistics being added to the Markov parameters is an indication of the congested 'queue' encountered by spikes within a rain event.

4.3.2 The Birth-Death Scenario of Rain Spikes

Many random systems are known to exhibit exponential behaviours in the generation of their instances in the time domain. Usually, when random systems with Markovian queueing properties invoke instances that are exponentially generated, the Markovian queue system can be easily adopted [*Bolch et al.*, 1998]. The Kendall-notated M/M/s/∞/FCFS queues simply implies a system where the inter-arrival and service times have probabilities which are exponentially distributed, with a fixed number of servers and infinite queues, scheduled in a FCFS manner [*Bolch*, 1998; *Hillier and Lieberman*, 2001]. For the inter-arrival and service times, the probability density function can be approximated as a Poisson and/or exponential distribution. The Poisson distribution and exponential distribution are classic cases of memoryless processes *i.e.* the current state is independent of the past states. For a typical Markov process with aperiodic and positive recurrence, the time averaged property of a

sampled population would the same as that of the total population. This property termed *ergodicity* is applied throughout this work.

It is imperative to understand the mathematics behind its underlying BD process. Firstly, we assume that the system is a Markov process; this is mathematically given in [*Bolch et al.*, 1998] and written as:

$$P_{ij}^{(1)}(n) = P(t_{n+1}|t_n) = P(t_n|t_{n-1}) = P(t_{n-1}|t_{n-2}), \quad \forall_n \in N, n \subset \mathbb{R} \quad (4.5)$$

This can be conveniently simplified for *n*-state Markov process, given by:

$$P_{ij}^{(n)} = P(t_{n+1} = j|t_n = i), \qquad \forall_n \in N, n \subset \mathbb{R} \quad (4.6)$$

for,

$$\sum_{\forall j} P_{ij} = 1 \qquad (4.7)$$

For a BD process as seen from Figure 4-1, we can see that this process can be described by [*Bolch et al.*, 1998] and is given as:

$$P(N_{t+1} = j|N_t = k) = \begin{cases} \lambda_k & j = k+1 \\ \mu_k & j = k-1 \quad j > 0, k > 0, n \subset \mathbb{R} \\ 0 & |j-k| > 1 \end{cases} \quad (4.8)$$
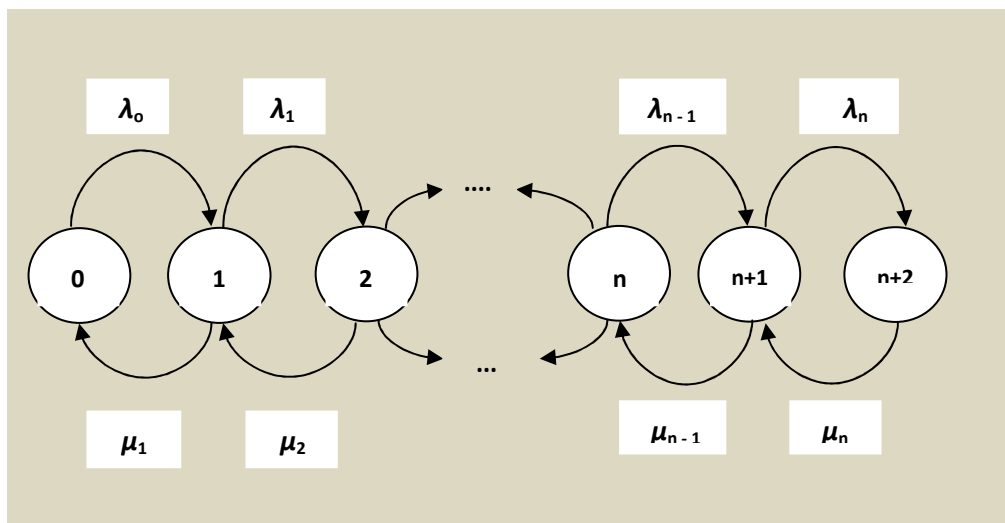
Figure 4-1: The Birth-Death Markovian Queue with Several Transitions State [*Hillier and Lieberman*, 2001].

In a heterogeneous M/M/s/∞/FCFS queue system, the service rates (μ) and arrival rate (λ) in the presence of a fixed number of servers, *s*, can be described as:

$$\lambda_n = \lambda, \qquad\qquad\qquad (4.9a)$$

$$\mu_n = \begin{cases} n\mu & 0 \leq n \leq s \\ s\mu & n \geq s \end{cases} \qquad\qquad (4.9b)$$

where *n* is an initialized counting parameter related to the number of server, *s*.

4.3.3 Queueing Modelling and Analysis of Rain Spike Traffic

A queueing system is described as arrival of instances or events into a designated queue for onward processing by one or more clearance points known as servers [*Hillier and Lieberman*, 2001]. As seen in Figure 4.2, a typical queueing system is made of four basic blocks: the input source, queue, server and served instances. The source of the arriving instances, though random, is governed by a definite probability distribution corresponding to known Markovian or non-Markovian process. The arrival pattern of the instances may follow two major designations: First (Last) Come, First (Last) Served (FCFS)/(LCLS) or First (Last) Come, Last (First) Served (FCLS)/(LCFS) [*Bolch et al.*, 1998]. The period spent by each arriving instances, also random, corresponds to a known probability process.
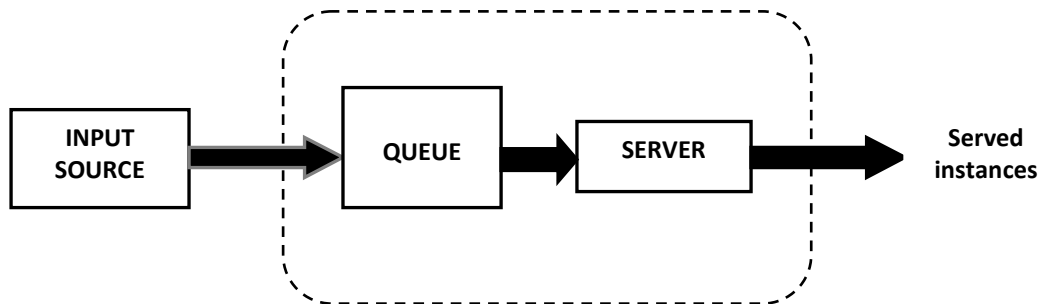
Figure 4-2: The basic framework of a queueing process [*Hillier and Lieberman*, 2001]

4.3.4 The Physical Manifestation of Spike Generation in Rain Traffic

The rainfall formation cycle involves the generation of rain clouds from the residues of the natural hydrological processes [*Rodriguez et al.*, 2012]. Over time within a rain event, this traffic process naturally results in a spontaneous and random variation of rainfall rates. Thus, the process itself is an infinite process which exists as a reaction of nature and environment to natural climatic-related variables.

This rain cloud generation process and consequent precipitation, when observed from a stationary point of view (or a reference time) can be seen as a natural and self-regulated traffic as seen in Fig. 4-3. Also, the arrival of rain clouds can be seen as FCFS traffic process with different rainfall 'services' being offered. These offered services being the remote cause of the variation in rain rates, can be seen as a train of rain spikes parallel to cloud motion. The cloud motion is sustained by a certain quantity called the *advection velocity*, which varies with different types of rainfall structure and cell sizes [*Pawlina*, 2002; *Begum et al.*, 2006]. It should be noted that rainfall clouds are dissipative as they travel along the direction of the prevailing advection velocity. This indicates that their area of influence and density diminishes as they travel due to the production of rain droplets; this is essentially a process of mobile energy transfer. It could therefore be assumed that the peak of a spike roughly coincides with the cloud portion of a rain cell at its highest density. On rain cell (or cloud) mobility, several authors have proposed different values of advection velocities for stratiform and convective rains [*Pawlina*, 2002; *Begum et al.*, 2006]. For example, *Pawlina* [2002] proposed that advection velocity values be lower for stratiform rains and, higher values for convective rains.

Usually, the appearance of an individual spike determines the temporal service being offered by the passing cloud. The period of service (or service time) in this case, roughly multiplied by the number of spike appearances determines the length of the rainfall duration. From Figs. 4-3 and 4-4, we can observe three major concepts describing the appearance of a spike (or the arrival of a cloud) - they are the inter-arrival, service and overlap times. The inter-arrival time, t_a, is defined as the time difference between the arrivals of two consecutive rain clouds/spikes at the reference point. The service time, t_s, may be defined as the actual duration of the spike. A third
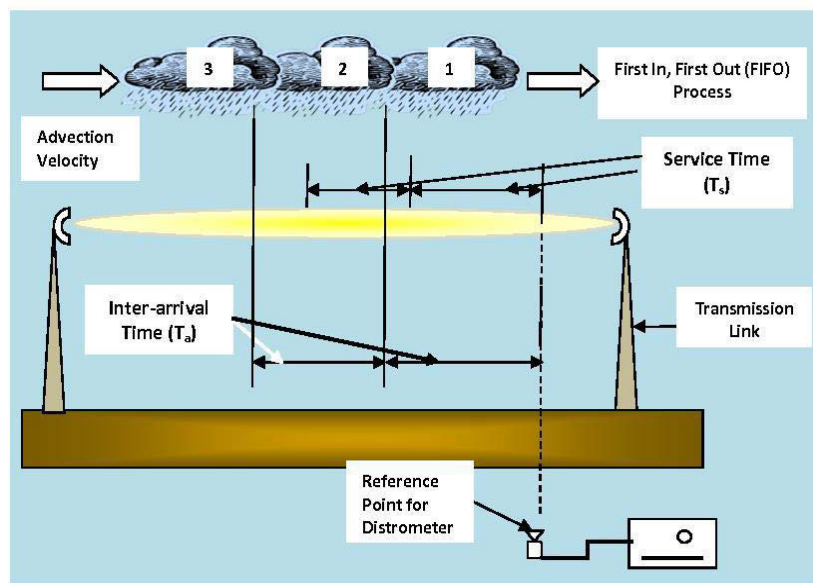
Figure 4-3: The concept of Rainfall Traffic Generation as a Queueing Model
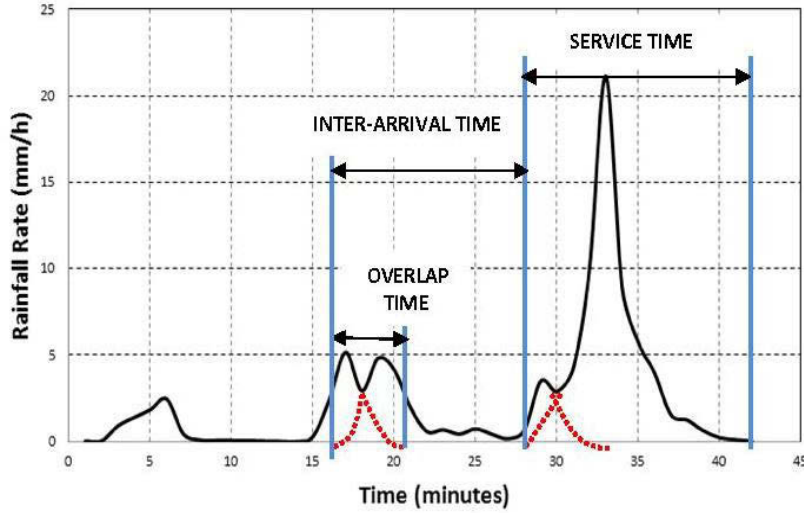
Figure 4-4: Identification of some queue parameters from rain spike profiles for a rainfall event on the 24th of January 2009 between 15:15 and 15:56 hrs.

parameter, t_o, known as the overlap time represents the intercept time between a 'dying' spike and arriving spike. Overlapping spikes can be seen as a major factor accommodating the regeneration of detectable rainfall rates between two clouds, with one arriving and the other departing. Also, regular overlaps in the successive arrival of spikes are evidences of queues in the system.

The approximate parameter estimates serving as probability density predictors to a Markovian queue distribution can be used to infer the behaviour(s) of such an array. For this study, the set of expressions for both the mean service time, $\overline{t_s}$, mean inter-arrival time, $\overline{t_a}$, and mean overlap time, $\overline{t_o}$, for successive instances of spikes in rainfall events of N sampled population may be given as [*Hillier and Lieberman*, 2001]:

$$\overline{t_s} = \frac{1}{N_s}\sum_{i=1}^{N_s}\Delta t_{s,i} = \frac{1}{\overline{\mu}} \qquad [minutes] \qquad \forall t_s \in \mathbb{R} \qquad (4.10)$$

$$\overline{t_a} = \frac{1}{N_a}\sum_{i=1}^{N_a} t_{a,i} = \frac{1}{\overline{\lambda}} \qquad [minutes] \qquad \forall t_a \in \mathbb{R} \qquad (4.11)$$

$$\overline{t_o} = \frac{1}{N_o}\sum_{i=1}^{N_a} t_{o,i} = \frac{1}{\overline{\sigma}} \qquad [minutes] \qquad \forall t_o \in \mathbb{R} \qquad (4.12)$$

where N_s, N_a and N_o are the maximum number of samples for the service time, inter-arrival time and overlap time respectively. Other notations representing the mean (or average) service, mean inter-arrival and mean overlap times are given as their reciprocals. They are: the mean service rate, $\bar{\mu}$, mean arrival rate, $\bar{\lambda}$, and mean overlap rate, $\bar{\sigma}$, respectively. Again, by inspection, if the service time has a maximum number of N sampled population, then the number of arrival samples will be lesser than N.

Broadly speaking, the overall number of arrived clouds represents the total sampled population of the rainfall queueing system under investigation. For easy understanding, this elaborate process of cloud/spike arrivals, as well as departures, is assumed to bear a similitude to the *Birth-Death* (BD) process. Firstly, for discrete systems, the inter-arrival process signifies the commencement (or birth) of a spike/cloud within a rainfall event. Then, the service time determines the generation, decomposition and the consequent death of the arriving spikes/clouds. Hence, rainfall spike queueing process can be regarded as a special case of the Discrete Markov Chain Process (DMCP). In this study, we will neglect the complicated derivations related to generic BD processes as they can be seen in related literature by *Kleinrock* [1975], *Bolch et. al.*[1998] and *Hillier and Lieberman* [2001]. We shall mainly apply the knowledge from the literature to acquire an understanding of rainfall queueing problems and its consequent application.

4.4 Determination of Service and Inter-Arrival Times of Queues

In this study, the queues of the collected data will be described by three queue parameters namely: the service rate, arrival rate and overlap rate. For this purpose, the service time, inter-arrival time and overlap time can be assumed as any known distribution ranging from exponential distribution to Erlang-*k* distribution.

The possible distributions describing any of the queue parameters earlier mentioned are hereby discussed. The Erlang-*k* distribution is a phase-like distribution useful in describing Markov queues, undergoing an exponential process, with *k* number of stages. It exists as a special case of the Generalized Gamma Distribution (GGD) [*Wingo*, 1987], where *k* exponential stages are encountered to generate different phases of the assumed queue. It was named after *Agner Krarup Erlang* (1878 – 1929), who first proposed its unique use in classical telephone networks as a distribution where each stage offers different services, so to say, depending on the value of *k*. This distribution is peculiar because it has the advantage of easily adjusting its shape profile based on the available number of *k* stages. It is most suitable for datasets with Coefficient of Variation (CV) less than 1. The Erlang distribution is given as [*Fiandrino*, 2010]:

$$f(t_s) = \frac{k\mu \, (k\mu t_s)^{k-1} \, exp \, (-k\mu t_s)}{\Gamma(k)} \quad \text{for } t_s \geq 0, \qquad \forall t_s \in \mathbb{R} \qquad (4.13)$$

where k is an integer value representing the shape parameter (and number of stages), t_s is the service time variable in minutes and μ is the service rate parameter.

The exponential distribution is the second proposed model as an appropriate fit for the collected random data with CV approximately equal to 1. An exponential system is a simplistic representation of a memoryless system *i.e.* random processes in which the present stage is generally independent of the previous stage. The exponential function is given as:

$$f(t_a) = \lambda \, exp \, (-\lambda t_a) \quad \text{for } t_a \geq 0, \qquad \forall t_a \in \mathbb{R} \qquad (4.14)$$

where t_a is the inter-arrival time variable in minutes and λ is the arrival rate.

To determine appropriate value of parameter, μ and λ in both cases of (4.13) and (4.14), the Maximum Likelihood (ML) parameter estimation technique is applied to obtain rate parameter of both the Erlang-k and exponential distributions. The ML method specifies that the mean of, t_i, and its reciprocal, the rate parameter, μ, is given from [*Kreyszig*, 2006] as:

$$\bar{t} = \frac{1}{n}\sum_{i=1}^{n} t_i \; ; \quad \bar{\mu} = \frac{1}{\bar{t}} \qquad (4.15)$$

The determination of rate parameters in (4.13) and (4.14) is entirely dependent on the randomness of the collected data, as we shall see in section 4.5. The computed value of CV will often give us a rough prognosis of the suitable distribution for the data.

4.5 Measurement and Data Processing

The measurements for this study were undertaken at the city of Durban, KwaZulu-Natal province, South Africa from electronic logs generated by the Joss Waldvogel (JW) distrometer RD-80 series, between January 2009 and December 2010. Details of this installed equipment in Durban have been discussed in subsection 3.3 of chapter 3.

The instrument has a rain rate sampling time of one minute (or 60 seconds) with a sampling error of ±5%. During the period of measurement, a few outages occurred but this is assumed to have little significance on the overall collected data for this work. As a precaution, only rainfall

events with a maximum rainfall rate greater than 3 mm/h were considered in this work. This is because the overall contributions of rain droplets to rain attenuation at this 3 mm/hr threshold are often minimal below 300 GHz operating frequency. Also, the effects of dead-time errors were assumed to be minimal in the data processing, as other rainfall microstructures such as rainfall drop and radar reflectivity, were of little concern.

For processing the measurements, a regime demarcation based on maximum rainfall rates observed per rain event is proposed for this study. This is based on the four rainfall regime classification already undertaken in a number of studies on Durban [*Afullo*, 2011; *Alonge and Afullo*, 2012c], and also other areas [*Adimula and Ajayi*, 1996; *Mandeep and Allnut*, 2007]. The bounds considered for each designated rainfall regime are drizzle ($R < 5$ mm/h), widespread (5 mm/h $\leq R < 10$ mm/h), shower (10 mm/h $\leq R < 40$ mm/h) and thunderstorm ($R > 40$ mm/h) [*Alonge and Afullo*, 2012c]. Firstly, it is important to examine the variation of the service times and inter-arrival times, based on the maximum rainfall rate observed in an event. This also provides statistics on the typical Markov metrics, as well as the frequencies of single event occurrences, for the examined events. We expect that these properties differ with different regimes, as are their rainfall microstructural properties.

Figures 4-5(a) – (d) depict the procedural steps taken to process the collected data. A three-stage method is applied on the data namely: isolation, segmentation and identification. Firstly, rain data series in a distinct and singular rain event A is isolated from its composite data of two independent rain events A and B as seen in Fig 4-5(a) and 4-5(b). Thereafter, event A is segmented into service time bounds distinguishable by rain spike peaks as seen in Fig 4-5(c). As observed, event A consists of a finite number of rain spikes with a total of five distinct segments from 1-5. Thus, at segmentation, the theory of the BD Markovian theory is applied to locate the possible points of a dying spike, which also coincides with re-emergence of another spike. In most cases, these points occur far above 1 mm/h as seen for segments 4 and 5 in Fig. 4-5d, which obviously indicates the existence of an overlap between the two spikes. Since two spikes are overlapping (see Fig 4-5d), there is need to determine the 'ground-zero' threshold for the commencement and end tails. An extrapolation technique is undertaken to determine these thresholds (corresponding to 0.003 mm/h), for which the Newton's Divided Difference (NDD) interpolation function is adopted. The NDD function with rain rate, *r* in mm/h, and time, *t,* in minutes, is given from [*Abramowitz and Stegun*, 1972] as:

$$\emptyset_n(r) = \prod_{k=0}^{n} (r - r_k), \tag{4.16a}$$
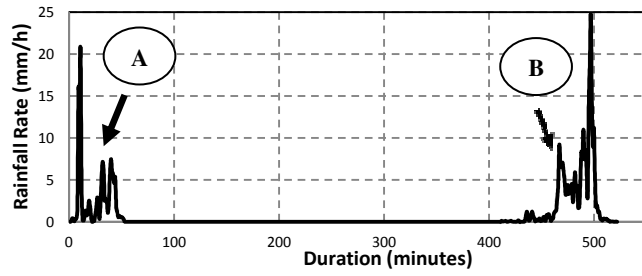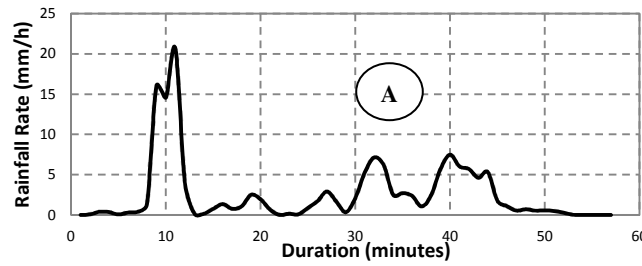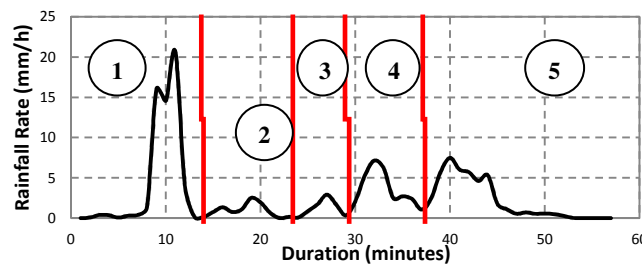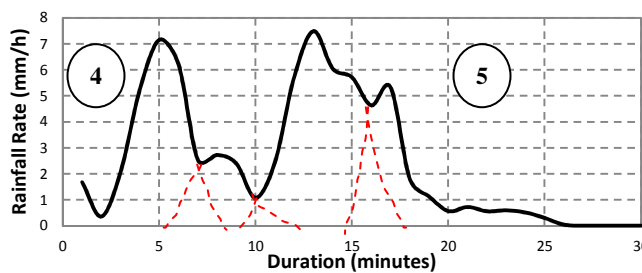
Figure 4-5: The three-stage procedure for processing rainfall time series data from RD-80 Distrometer

(*a*) Composite Rain Events

(*b*) Isolation of Single Events

(*c*) Segmentation of Segment A into Fractal Spikes

(*d*) Identifying some points of Event Overlaps (in red dotted line)

$$t(r) = t_o + \sum_{k=1}^{n} \emptyset_{k-1}(r)[r_o, r_1, \dots, r_k] + H_n \qquad (4.16b)$$

for which the remainder H_n of (7b) is given as,

$$H_n(r) = \emptyset_n(r)\frac{t^{(n+1)}(\xi)}{(n+1)!} \qquad (4.17)$$

where r_k is the rainfall rate index from data and t refers to the indices of time along the time series axis. A MATLAB$^{©}$ code was written to separately calculate these thresholds from our data samples with an assumption of 0.003 mm/h as near-zero rain rate threshold. A depiction of the identified predicted terminal points for each spike as shown in Fig 4.5(d), with the trails for each spike, in red dotted line.

Table 4-1: Summary of BD parameters obtained from measurement for different rainfall regimes in Durban

REGIME/CLASS	TIME BOUNDS (minutes)	OCCURRENCE NUMBER		
		SERVICE TIME	INTER-ARRIVAL TIME	OVERLAPPING TIME
DRIZZLE	$0 < t \le 10$	61	108	124
	$10 < t \le 20$	66	17	3
	$20 < t \le 30$	15	2	0
	$30 < t \le 40$	5	0	0
	TOTAL	**147**	**127**	**127**
WIDESPREAD	$0 < t \le 10$	56	125	145
	$10 < t \le 20$	91	31	11
	$20 < t \le 30$	26	2	1
	$30 < t \le 40$	2	0	0
	$40 < t \le 50$	1	0	0
	TOTAL	**176**	**158**	**157**
SHOWER	$0 < t \le 10$	35	101	108
	$10 < t \le 20$	61	20	13
	$20 < t \le 30$	22	2	3
	$30 < t \le 40$	4	0	1
	$40 < t \le 50$	5	2	0
	TOTAL	**127**	**125**	**125**
THUNDERSTORM	$0 < t \le 10$	21	58	79
	$10 < t \le 20$	40	19	8
	$20 < t \le 30$	20	7	3
	$30 < t \le 40$	11	2	0
	$40 < t \le 50$	10	4	0
	TOTAL	**102**	**90**	**90**

The summary of the data processed from the distrometer measurements are provided in Table 4-1. For the service time, over 90% of the available data for all regimes have spike service times less than 30 minutes. However, thunderstorm spikes have less than 22% of its service times longer than 30 minutes. For the inter-arrival time and overlap time, we observe that over 90% of the data is within the 30 minutes domain. Although, we can see that thunderstorm spikes have some samples with inter-arrival times greater than 30 minutes. Generally, it is seen that all the queueing parameters appear to have uniform periods of 30 minutes, with about 90% data conformity. Also, it is observed that the queueing parameters for all regimes tend to decrease as the time bounds increases. For the service time data, we observe that the data peaks at time bounds between 10 minutes $\leq t \leq$ 20 minutes for each regime.

4.6 Results and Discussions

The results obtained from the modeling and simulation of measured data are categorized into modelling of queue parameters, error analysis of proposed models, server composition, steady state performances and the investigation of other related parameters. These are discussed in the following sub-sections as follows.

4.6.1 Modelling of Queueing Parameters for Different Rain Regimes in Durban

The results obtained from comparison of the proposed model and actual measurements for service time and inter-arrival time distributions are shown in Figures 4-6(a) – (d), Figures 4-7(a) – (d) and Figures 4-8(a) – (d). The most suitable fitting function for each of the categories of data was mainly determined by the values of their respective CVs. The service time and overlap time distributions were fitted with exponential and Erlang-k distributions. Conversely, the inter-arrival time distribution was fitted with the exponential function for all regimes since their CVs were closer to one by observation. It should be noted that an attempt to fit the inter-arrival data with Erlang distribution will result in the first case of an Erlang stage for which k is approximately *unity*. This is ultimately the same as the exponential distribution from theory. Generally from the results, we note that the mean values of the service time, inter-arrival and overlap times all seem to increase as the bounds of rain regime increase. Based on this observation, it is found that the average service rate reduces with increasing rain regime bounds (from drizzle to thunderstorm), and so also is the average overlap rate. The number of Erlang stages, k, adopted is determined by the minimum error statistics, relative to the measurements and are also seen to vary with rain regimes. The value of k, representing the number of Erlang stages, is obtained from statistical calculus and regression analysis with minimal error as derived rigorously in Appendix E. In this study, this parameter, k_{opt}, can be obtained given that a

prior knowledge of measured PDF, $f(t_i; k, \tau)$, is known. Firstly, the first derivative of the Erlang distribution is undertaken such that:

$$\frac{df(t_i; k, \tau)}{dt} = 0 \tag{4.18}$$

Results for the solution of (4.18) can be further simplified, as seen in the full derivation in Appendix E, to obtain the eventual function representing the number of stages. Thus, the best fit for k_{opt} comparative to the measured PDF, from this method is given as thus:

$$k_{opt} = round(5.417\tau^{-2.11}\{max[f(t_i; k, \tau)]\}^{2.11}) \text{ for } k = k_{opt} \tag{4.19}$$

(a)

(c)

(b)

(d)
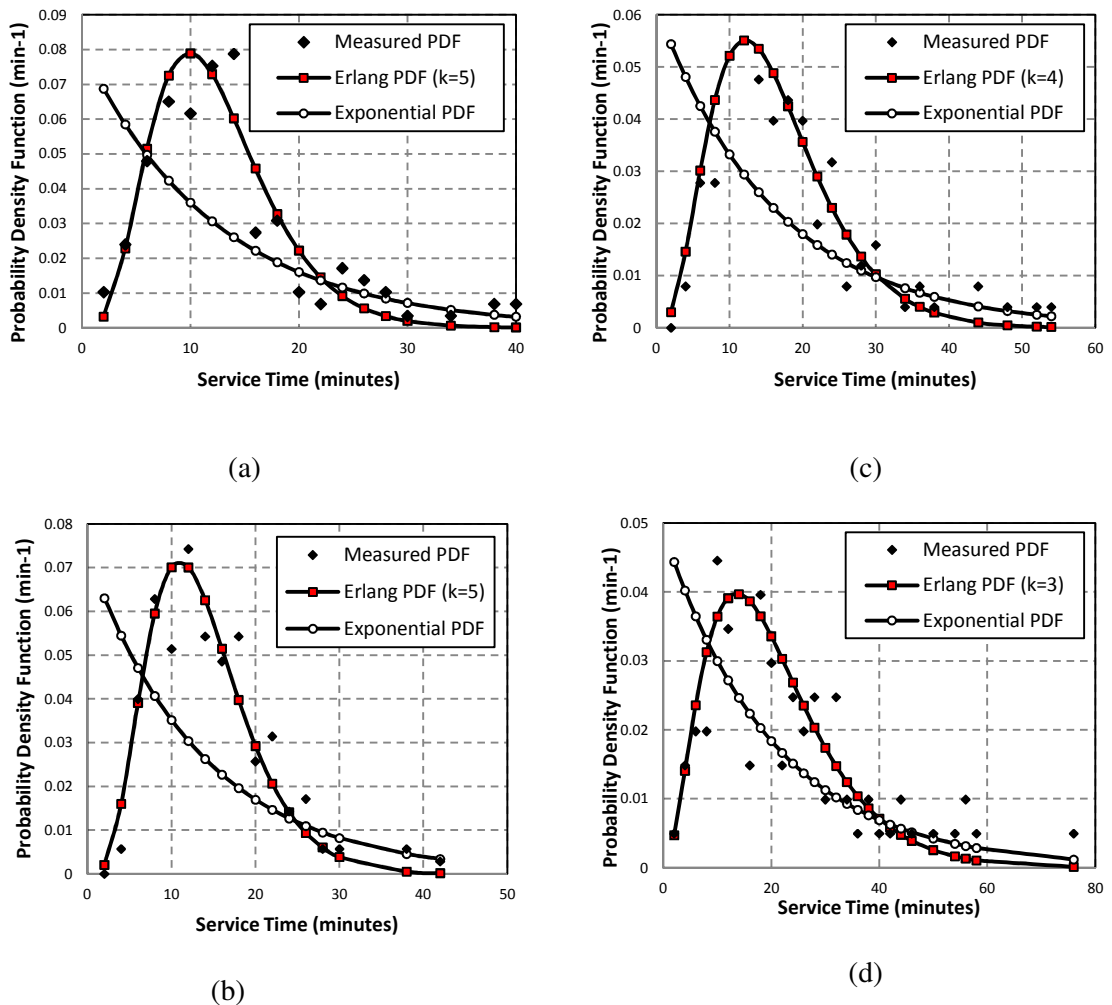
Figure 4-6: Proposed Erlang-k Service Time Distributions for different rainfall regimes in Durban, KwaZulu-Natal Province:
(a) Drizzle ($\bar{\mu} = 0.0808$)
(b) Widespread ($\bar{\mu} = 0.0729$)
(c) Shower ($\bar{\mu} = 0.0615$)
(d) Thunderstorm ($\bar{\mu} = 0.0489$)
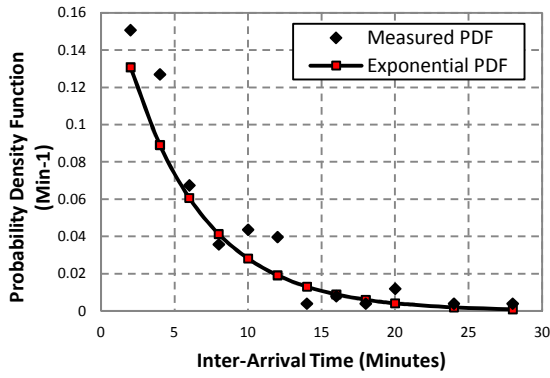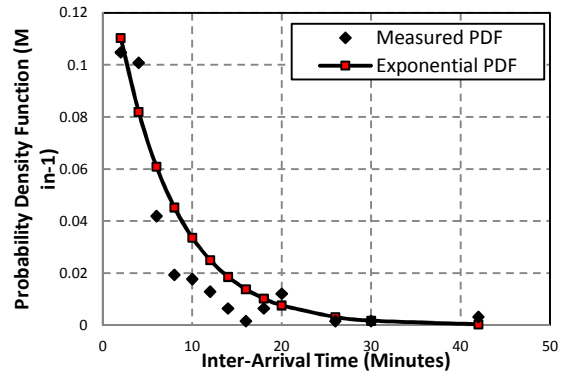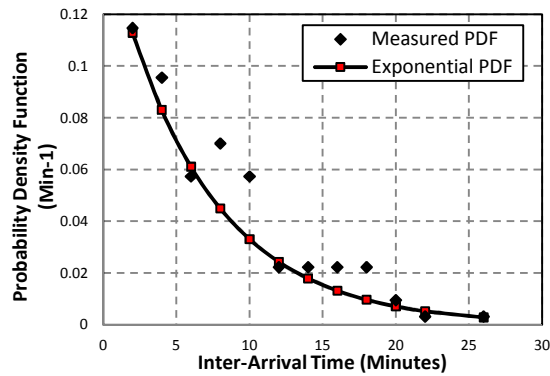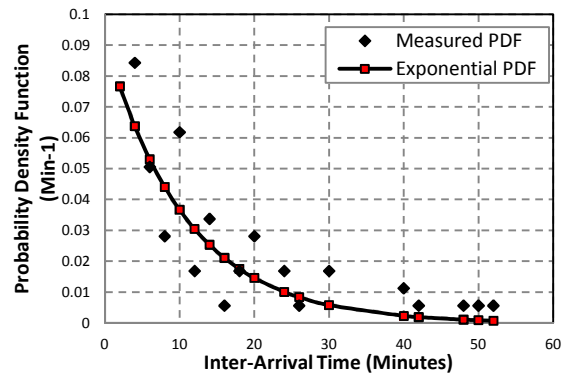
Figure 4-7: Proposed exponential inter-arrival time distribution for different rainfall regimes in Durban, KwaZulu-Natal Province:
(a) Drizzle ($\bar{\lambda} = 0.1921$)
(b) Widespread ($\bar{\lambda} = 0.1533$)
(c) Shower ($\bar{\lambda} = 0.1486$)
(d) Thunderstorm ($\bar{\lambda} = 0.0922$)

where τ is the computed mean (or expectation) of the data from measurement.

From (4.19), different values of k are obtained for the different rain regimes according to the queue parameters. For the service time, the value of k is seen to vary between 3 and 5, with thunderstorm spikes having the lowest value and both drizzle and widespread having the highest. For the overlap time, all spike distributions except those observed during thunderstorm events have a value of $k = 3$. Similarly, the lowest observed value of k is that from thunderstorm spikes with a minimal value of 2.

The overall results from Table 4-2a, 4-2b and 4-2c for the trio parameters of service time, inter-arrival time and overlap time respectively tend to show an increase from drizzle to thunderstorm
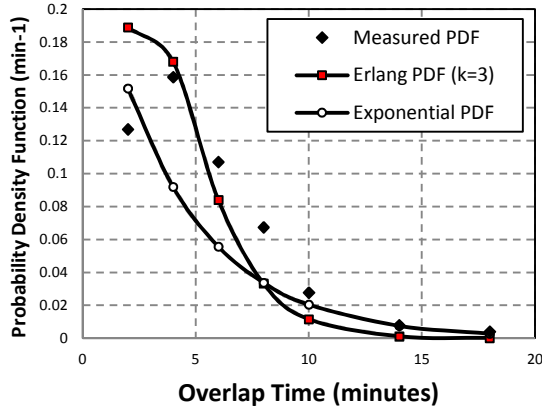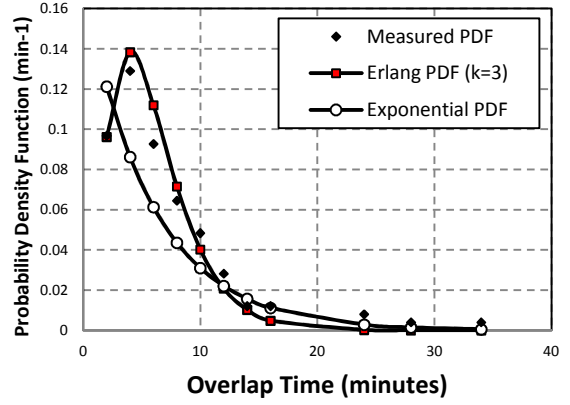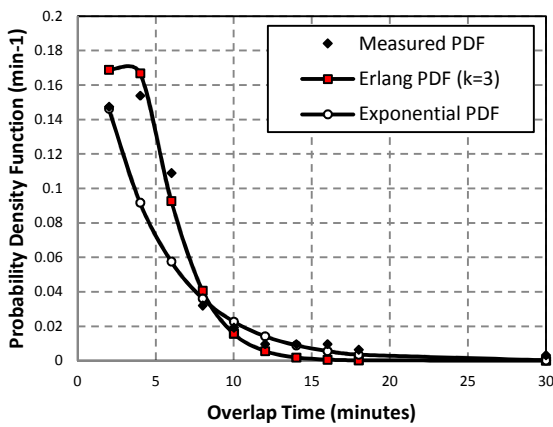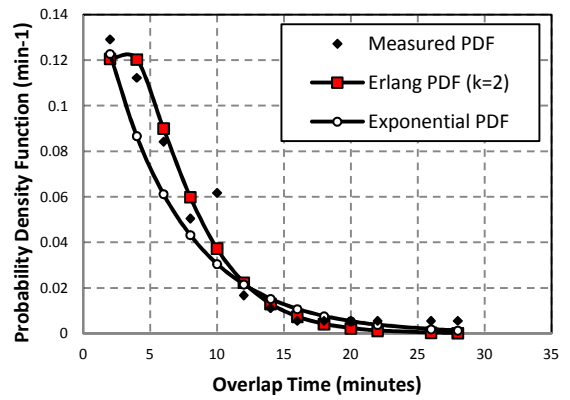
Figure 4-8: Proposed Erlang-*k* Overlap Time Distribution for different Rainfall Regimes in Durban, KwaZulu-Natal Province:
(a) Drizzle ($\bar{\mu} = 0.2506$)
(b) Widespread ($\bar{\mu} = 0.2331$)
(c) Shower ($\bar{\mu} = 0.1705$)
(d) Thunderstorm ($\bar{\mu} = 0.1739$)

events. The results from Tables 4-2a and 4-2c are typically applicable to the parameters of the Erlang and exponential distributions, while Table 4-2b is only applicable to the exponential distribution of the inter-arrival data. Concerning the generated queue parameters, some observations regarding spike generations during rain events are very glaring. Firstly, rainfall service time tend to increase as the maximum rain rate attained by a spike increases. This means that spikes/clouds attaining high rainfall rates are likely to have longer service time, and thus longer rain duration. Secondly, there is far a greater chance of overlap (or interrupt) as the maximum rain rate attained by spikes/clouds increases. These first two theories support the fact

Table 4-2a: Fitted parameters of Erlang-*k* and exponential probability distributions for spike service time in Durban

RAIN REGIME	CV	$\overline{T}_s\ (min)$	$\overline{\mu} = 1/\overline{t}_s$ (spikes/min)	k
Drizzle	0.6052	12.3755	0.0809	5
Widespread	0.4868	13.7095	0.0729	5
Shower	0.5866	16.2556	0.0615	4
Thunderstorm	0.6737	20.4409	0.0489	3

Table 4-2b: Fitted parameters of exponential probability distribution for spike inter-arrival time in Durban

RAIN REGIME	CV	$\overline{T}_a\ (min)$	$\overline{\lambda} = 1/\overline{t}_a$ (spikes/min)
Drizzle	0.9636	5.2065	0.1921
Widespread	0.8208	6.5242	0.1533
Shower	1.0260	6.7312	0.1486
Thunderstorm	1.0731	10.8475	0.0922

Table 4-2c: Fitted parameters of Erlang-*k* and Exponential probability distributions for Spike overlapping Time in Durban

RAIN REGIME	CV	$\overline{T}_o\ (min)$	$\overline{\sigma} = 1/\overline{t}_o$ (overlaps/min)	k
Drizzle	0.6986	3.9906	0.2506	3
Widespread	0.9212	4.2899	0.2331	3
Shower	0.8903	5.8667	0.1705	3
Thunderstorm	0.9142	5.7509	0.1739	2

that the inter-arrival time between two spikes (one arriving and another departing) also increases with the spike's maximum rainfall rate. To understand this observation, it will be important to note that rainfall spikes/clouds in the thunderstorm regime class must usually first pass through the drizzle, widespread and shower stages. This stage progression may be responsible for the longer service time and larger inter-arrival time, as seen in most thunderstorm events. From the results, we see that the average lifespan of a spike in Durban, irrespective of the rain regime bounds, is between 12 to 20 minutes. We expect the appearance of another spike, at most between 5 to 10 minute duration, prior to the end of an existing spike with an overlap time.

4.6.1.1 Error Analysis of Proposed Distributions

The error statistic tests used to examine the suitability of our proposed models are the Root Mean Square Error (RMSE) and Chi-square statistic (χ^2). The equations representing each of these statistic tools are given as:

$$\text{RMSE} = \left[\frac{1}{n} \sum_{i=1}^{n} (x_i - x'_i)^2 \right]^{\frac{1}{2}} \tag{4.20}$$

$$\chi^2 = \sum_{i=1}^{n} \frac{(x_i - x'_i)^2}{x_i} \tag{4.21}$$

where x_i is the actual dataset of measurement and x'_i is the proposed model dataset. The equations in (4.20) and (4.21) are valid for n sampled population.

The results from the error statistic analysis, using (4.20) and (4.21) are given in Table 4-3. For the χ^2 statistics, 5% threshold of significance level (SL) corresponding to the Degree-of-Freedom (DF) was chosen to determine the satisfaction of the model criteria. If null hypotheses are not rejected at this chosen significance level, then 95% of the predicted model values satisfy the actual measurements. The standard χ^2 table of values can be accessed in [6]. From these results, it is seen that the exponential model for the arrival process fits the actual data for all regimes, with RMS errors (in percent) ranging between 1.18% and 1.51%. The χ^2 estimates are also significant (less than the 0.05 threshold) relative to the data. For the service time and overlap time, the Erlang-k distribution gives a better performance, with lower RMSE and better χ^2 estimates, over exponential distribution as seen in Table 4-3 (see values with *). It is obvious that the rain spike queue behaviour of the measured data in Durban obvious mimics a phase-like distribution which is best most described by Erlang distribution. This is not surprising since from the data as the number of arriving rain spikes tend to have service time between 10 and 15 minutes. Since it is earlier assumed that the overlap time is a subset of the service time, it follows that a phase-like queue process sufficiently describes it.

From the service time modelling, it is observed that percentage RMS error for the best fitted model ranges between 0.8% and 1.04% irrespective of the rainfall regime. Also, the model results are significant to the actual distribution since their χ^2 are less than the 5% significance threshold. For the Erlang-k overlap rate, it is observed that the percent RMS ranges between 0.84% and 3.45%, which gives a good fit to the actual distribution for the different regimes r

Table 4-3: Error analysis of the Fitted Queue Distributions for Different Rain Regimes in Durban

QUEUE PARAMETER	REGIME	PROPOSED MODEL	RMSE	χ^2	DF	SL
SERVICE TIME	DRIZZLE	M	0.0246	0.3004	145	174.10
		E_k^*	**0.0094**	0.7226		
	WIDESPREAD	M	0.0268	0.3413	174	205.78
		E_k^*	**0.0077**	0.1224		
	SHOWER	M	0.0216	0.3188	125	152.09
		E_k^*	**0.0084**	0.2648		
	T/STORM	M	0.0159	0.2983	100	124.34
		E_k^*	**0.0104**	0.3470		
INTER-ARRIVAL TIME	DRIZZLE	M	0.0151	0.0860	125	152.09
	WIDESPREAD	M	0.0118	0.0594	156	186.15
	SHOWER	M	0.0129	0.0919	123	149.89
	T/STORM	M	0.0128	0.2118	88	110.89
OVERLAP TIME	DRIZZLE	M	0.0357	0.1368	125	152.09
		E_k^*	**0.0292**	0.2913		
	WIDESPREAD	M	0.1739	0.9053	155	185.05
		E_k^*	**0.0099**	0.0441		
	SHOWER	M	0.0197	0.0648	123	149.89
		E_k^*	**0.0084**	0.0204		
	T/STORM	M	0.0135	0.0768	88	110.89
		E_k^*	**0.0087**	0.0215		

[*]selected model with lowest error statistics for the queue parameter

considered. The χ^2 statistic for all regimes are also very significant to the model as seen in theivalues, since they have lower values than their 5% threshold level. Generally, it is seen that the percentage RMS error is less than 4% for all cases of queueing parameters which in turn, suggests that the models are good fits of the measurements.

A closer look at the error statistics show that two major queue disciplines are valid for the spike queue pattern in subtropical Durban, they are: M/M/s/∞/FCFS (or a single stage E_k/M/s/∞/FCFS i.e. at $k = 1$) and M/E_k/s/∞/FCFS/. Following the evidences from the error statistics, it is observed that the Erlang-k distribution is more suited for the service time model and exponential model is most suited for the inter-arrival time model. Since the service time process of rain spikes queues (and clouds) for rain events for different regimes is Erlang-k distributed and the inter-arrival time is inherently exponentially distributed, it therefore follows

that the overall queueing behavior of rain spikes in Durban is *semi-Markovian*. As understood from the Kendall designation, it is therefore conclusive that a M/E$_k$/s/∞/FCFS discipline is valid to describe the rainfall queueing process in Durban, irrespective of the rain regime encountered.

4.6.2 Determination of Server Number in Queue System

As seen from earlier results, the spikes generated during rainfall events in Durban follows a distinct queue pattern which is described by either M/M/s/∞/FCFS (Markovian) or M/E$_k$/s/∞/FCFS (semi-Markovian) queue discipline. Investigations from this current study have shown that latter discipline is the most acceptable since it has minimum fitting error statistics. In both cases of queue pattern, the actual number of servers operating in the system, irrespective of the rain regime, is unknown. To assess the performance indices of the proposed queue disciplines, the knowledge of the server activity in the system is required. Thus, it is necessary to verify that steady state stability criterion of the entire queue systems obeys the rule [*Kleinrock*, 1975; *Bolch et al.*, 1998; *Hillier and Lieberman*, 2001]:

$$\rho = \frac{\lambda}{\mu} < 1 \tag{4.22}$$

By applying (4.22), the estimated utilization factor (ρ) for drizzle, widespread, shower and thunderstorm rainfall regimes are found to be 2.37, 2.10, 2.41 and 1.89 respectively. Therefore, the designed queue system for all regimes cannot attain system stability. To attain steady state stability, the minimum number of servers, s_{min}, in the system must satisfy the given condition:

$$s_{min} \geq ceil\left(\frac{\lambda_a}{\mu_s}\right) \tag{4.23}$$

From (4.23), values of s_{min} of 3 are computed for the first three regimes with the exception of thunderstorm regime where it is given as 2. The results suggest that the queueing mechanism for rain spikes in rain events is inevitably unstable; hence, the earlier assumed source of the constant overlaps between spikes in this work is actually the queue instability. While this interpretation of server is naturally embedded within the framework of the rainfall process itself, it is suspected that the cloud velocity profile and other peripheral physics might be involved.

4.6.3 Performance of the Proposed Queue Disciplines

The performance of a queue system is governed by the steady state behaviour of its traffic which includes the assessment of queue characteristics and variations. The steady state

conditions are derived from the preliminary solution of global balance rate equations for a typical queue system. From literature, there are four major performance indices required to be investigated for any queue discipline. They are provided in literature and given as [*Kleinrock*, 1975; *Bolch et al.*, 1998; *Hillier and Lieberman*, 2001]:

(i)   The steady state number of instances in the queue designated as L_q

(ii)   The steady state waiting time in the queue designated as W_q

(iii)   The steady state number of instances in the system designated as L

(iv)   The steady state waiting time in the system designated as W

These indices are different as the queue disciplines changes and multiple servers exist in the system [*Kleinrock*, 1975]. Therefore, the performance metrics of any queue discipline changes with increment in number of servers and the changes in queue parameters. Because of this, the set of descriptors for computing these metrics are different for both M/M/s/∞/FCFS and M/E$_k$/s/∞/FCFS queue disciplines. In this investigation, the behaviour of both disciplines will be examined. It follows that for a typical M/M/s/∞/FCFS discipline, the set of performance descriptors are given by [*Hillier and Lieberman*, 2001]:

$$L_q = \frac{P_o \left(\frac{\lambda}{\mu}\right)^s \rho}{s! \ (1 - \rho)^2} \tag{4.24a}$$

where, $$P_O = \left[\sum_{n=0}^{s-1} \frac{\left(\frac{\lambda}{\mu}\right)^n}{n!} + \frac{\left(\frac{\lambda}{\mu}\right)^s}{s! \ (1 - \rho)}\right]^{-1} \tag{4.24b}$$

$$W_q = \frac{L_q}{\lambda} \quad [minutes] \tag{4.25}$$

$$L = L_q + \frac{\lambda}{\mu} \tag{4.26}$$

$$W = \frac{L}{\lambda} \tag{4.27}$$

And the descriptors of the M/E$_k$/s/∞/FCFS discipline are given as:

$$L_q = \frac{1 + k}{2k} \frac{\lambda^2}{s\mu(s\mu - \lambda)} \tag{4.28}$$

$$W_q = \frac{L_q}{\lambda} \; [minutes] \tag{4.29}$$

$$L = \lambda W \tag{4.30}$$

$$W = W_q + \frac{1}{s\mu} \; [minutes] \tag{4.31}$$

where L_q is the number of spikes in the queue, W_q is the waiting time of a spike in the queue in minutes, W is the overall waiting time of a spike in the queue system and L is the overall number of spikes in the system.

By applying equations (4.24a) - (4.31), the performance indices of the system (L_q, W_q, W and L) are computed via simulation using MATLAB® for servers between 3 and 20. The results generated show that the M/E$_k$/3/∞/FCFS queue discipline gives a better and convergent solution corresponding to increment in server number. Table 4-4 shows a summary of the performance metrics at $s = 3$ for the compared queue systems for different rain regimes. Observations from this table indicate that the computed metrics (in bolded) are generally lower for the semi-Markovian queue discipline than seen for the Markovian discipline. This is mainly due to the effects of the Erlang-k stages which are totally absent in the Markovian model. For instance, the values for the number of spikes and their corresponding waiting time in queue (L_q and W_q) in any rain regime are higher for a typical M/M/s. Since the default number of natural servers in the rain process is about 3, spike numbers (L) of 2.6, 1.68, 2.88 and 1.34 are obtained in M/E$_k$/s for drizzle, widespread, shower and thunderstorm regimes respectively. This is compared to 4.78, 3.26, 5.13 3.51 respectively for M/M/s. Similarly, for the same number of servers, the system waiting times (W) of 13.57, 11, 19.44 and 14 minutes are obtained respectively in M/E$_k$/s. Again, the respective figures of 24.87, 21.27, 34.53 and 24.65 minutes are obtained in M/M/s. This reveals that lower values of performance indices are indeed obtained for M/M/s disciplines across all rain regimes. To further understand their performances, the disciplines are examined as the servers in their systems are increased.

As seen from the compared results in Figures 4-9 and 4-10, there is an obvious difference in the performance 'curve' of the M/M/s discipline. In addition to the earlier observation, the step-wise zero-convergence of the Markovian discipline is rather slow for the L and W indices. It is also observed that constant values are attained for these performance pair when a minimum of 10 servers are active in the system. Beyond this, the addition of more servers to the system has zero effect on the convergence rate; this is atypical of proper queue system. The performance of the M/E$_k$/s queue discipline however shows that the zero-convergence of L and W is continuous as

Table 4-4: System performance of M/E$_k$/3/∞/FCFS and M/M/3//∞FCFS for different rainfall regimes in Durban

REGIME	DISCIPLINE	SERVICE TIME		INTERARRIVAL TIME	PERFORMANCE METRICS			
		μ	k	λ	L_q	W_q	L	W
DRIZZLE	M/E$_k$/3	0.0809	5	0.1921	**9.45**	**1.82**	**13.58**	**2.61**
	M/M/3	0.0809	X	0.1921	12.52	2.41	24.88	4.78
WIDESPREAD	M/E$_k$/3	0.0729	5	0.1533	**6.43**	**0.99**	**11.00**	**1.69**
	M/M/3	0.0729	X	0.1533	7.55	1.16	21.27	3.26
SHOWER	M/E$_k$/3	0.0615	4	0.1486	**14.02**	**2.08**	**19.44**	**2.89**
	M/M/3	0.0615	X	0.1486	18.27	2.72	34.53	5.13
T/STORM	M/E$_k$/3	0.0489	3	0.0922	**7.16**	**0.71**	**14.51**	**1.34**
	M/M/3	0.0489	X	0.0922	7.19	0.66	27.65	2.55

X means that this parameter has no equivalent value for exponential distribution
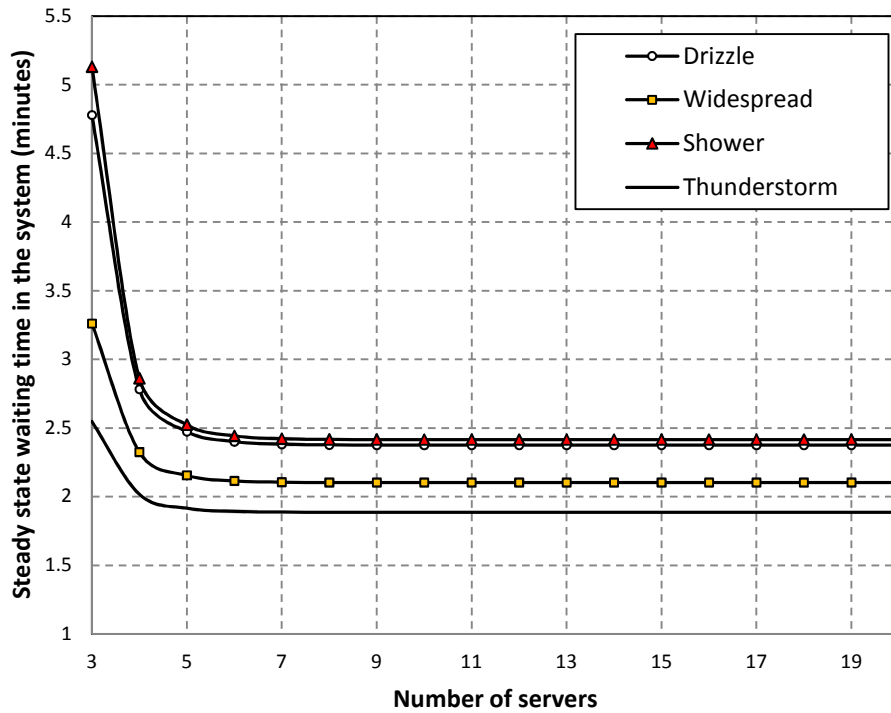
(a)
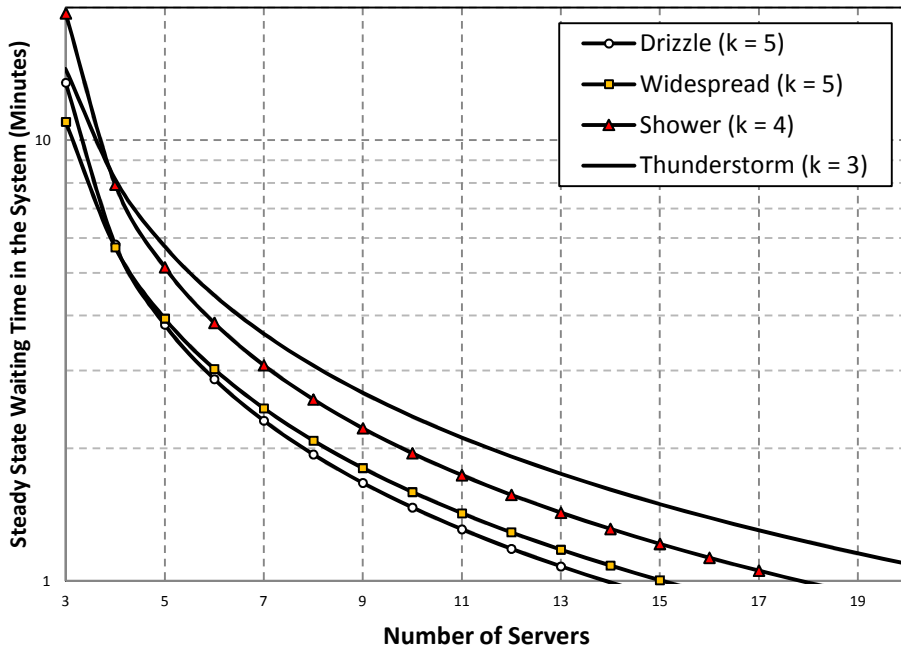
(b)

Figure 4-9: The effect of increasing the number of servers on the overall system waiting time (a) M/M/s/FCFS/∞ (b) M/E$_k$/s/FCFS/∞
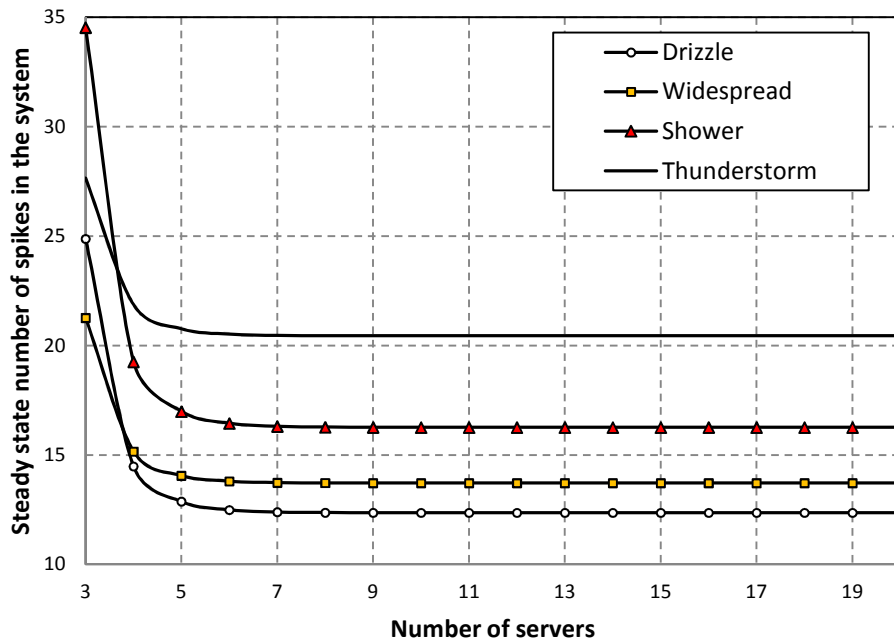
(a)
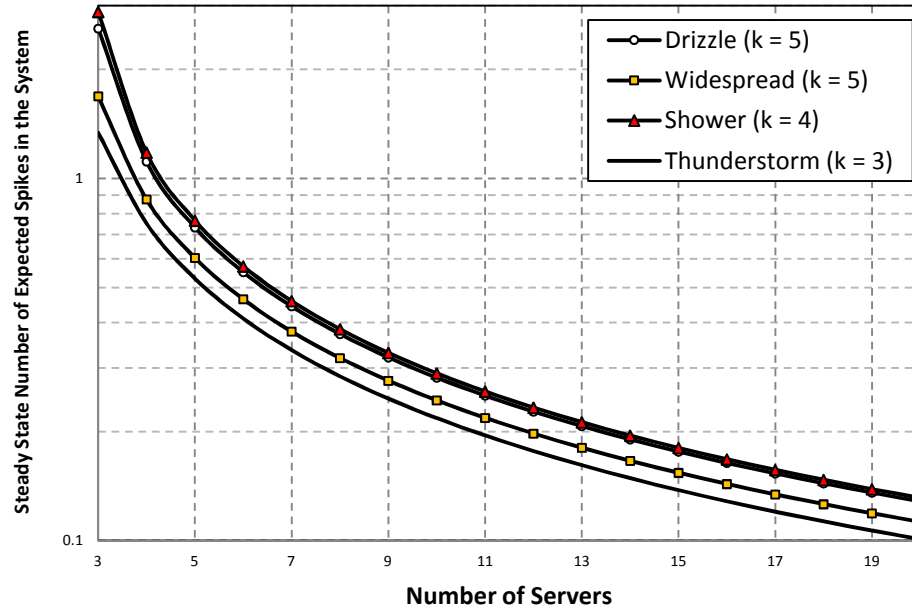
(b)

Figure 4-10: The effect of increasing the number of servers on the expected number of spikes for different rain regime (a) M/M/s/FCFS/∞ (b) M/E$_k$/s/FCFS/∞

more servers are added to the system. The effect of the stages for different rain regime also ensures that lower values of these performance indices are attained irrespective of the server numbers. An extensive summary of the simulated performance results for both queue disciplines are presented in the tables in Appendix F. As seen from the investigations and of the performance indices, it is conclusive that the M/E$_k$/s discipline is the most appropriate to describe the spike traffic in Durban. This is because it offers the advantages of lower system waiting times, shorter queue times and better zero-convergence of performance metrics. In addition, it can be seen from the *L* and *W* metrics for all regimes that the M/E$_k$/s queue applied in this study is twice as efficient as M/M/s queue.

4.6.4 Jump State Probabilities of Rainfall Spikes

The investigation of rain spike stochastic generation during rain events as undertaken in this study has confirmed the existence of queues in rainfall process. This knowledge has shown that the arrival (and departure) process of spike and clouds instances within a rain event are plainly governed according to a semi-Markovian discipline.

While the rain traffic analysis can evaluate the pattern of spike generation within an event context, it cannot identify and distinguish between the types and categories of spikes. The

identificueion of generated spike by their peak rain rates can be best distinguished by a known probability process. If the prevailing rain regime classification is applied (*i.e.* drizzle, widespread, shower and thunderstorm) to group the peak rain rates, it would be paramount to know, for example, the probability of a drizzle spike being succeeded by a thunderstorm spike and so on. This poses a genuine question as thus: *what is the probability that the regime state of a rain spike jumps (or changes) to another regime state on arrival of another spike in the queue?* Based on this question, it is expedient to develop state transition matrices to estimate the spike jump from one regime state to another. Since the rainfall process itself is of Markovian scheduling, it is logical to depict the probability of jumping from one current transition state, M_o to any state, M_n. This is described as:

$$P(M_n|M_o) = p_{ij} \qquad \text{for } i,j \in \mathbb{R} \, \forall n \tag{4.32}$$

where *n* is the number of possible states of system transitions as spikes are generated in the queue process. Invariably, (4.32) can be represented as a simple matrix as below:

$$P(M_n|M_o) = \begin{pmatrix} p_{i1} & \cdots & p_{in} \\ \vdots & \ddots & \vdots \\ p_{n1} & \cdots & p_{nn} \end{pmatrix} \tag{4.33}$$

By examining the processed rainfall queue data, it is observed that spikes from different rain regimes have a defined number of states for probability transition. Rain spikes generated in drizzle regime for instance have only one state because drizzle events are peak spike threshold of rain rates below 5 mm/h. For widespread events, generated spikes can only transit between two states, *i.e.* drizzle and widespread, with threshold below 10 mm/h. For shower events, generated spikes have a three-state transition probability of jumping randomly through drizzle, widespread and shower with threshold of 40 mm/h. Finally, thunderstorm storm events have four complete transition states where the spikes can transit randomly through drizzle, widespread, shower and thunderstorm.

By physically examining the processed data from rainfall measurements in Durban, it is possible to identify the transitions of a generated spike in one regime state to another. By following the state diagrams, it can be deduced that a two-state system for example has four possible or 2^2 transition states. A special case of steady state occurs in the system when the transition probability matrix, **P**, jumps continuously until it attains an infinite number of transitions [*Bolch et al.*, 1998]. This condition leads to a steady state problem which must satisfy the condition that follows:

$$qP = q \qquad \text{for} \quad q \neq 0 \qquad (4.34)$$

where q is the system vector at steady state such that its elements represent constant values of row elements of P under this condition. The solution of q can be solved by applying the *eigenvalue* approach so that:

$$(P^T - \lambda I)q^T = 0 \qquad (4.35)$$

where I is an n x n identity matrix dependent on the number of states.

Following this arrangement, q^T becomes the eigenvector of P and can be easily resolved. The results that follow hereafter present the state transitions matrices of transiting spikes in Durban for the rainfall regimes of widespread, shower and thunderstorm.

4.6.4.1 Jump State Transition Matrices for Rain Regimes

There jumping state transition matrices obtained in this subsection are so classified according to their rainfall event bound. Therefore, it is expected that the number of states increase from drizzle to thunderstorm events. A drizzle event can only generate drizzle spikes and hence, will continually maintain one state which is drizzle. Widespread events can generate drizzle and widespread spikes, hence, only two states are possible. Following this trend, it is obvious that shower and thunderstorm events can only transit spikes in three and four states respectively. Transition state diagrams are presented in Figures 4-11 to show the transition possibilities of between distinct spikes in similar events. Figures 4-11a, 4-11b and 4-11c show the state transition states available for widespread events, shower and thunderstorm events. Since the drizzle events are perpetually stuck in one state, the state diagram is excluded. The elements pertaining to each of these transitions are presented as transition matrices. For any widespread event, the state transition matrix is given as:

$$\mathbf{P}_{widespread} = \begin{bmatrix} p_{DD} & p_{DW} \\ p_{WD} & p_{WW} \end{bmatrix} \qquad (4.36)$$

where P_{DD}, P_{DW}, P_{WD} and P_{WW} are the transition probabilities of drizzle (D) and widespread (W) spikes.

The state transition matrix available for shower events is thus given:

$$\mathbf{P}_{shower} = \begin{bmatrix} p_{DD} & p_{DW} & p_{DS} \\ p_{WD} & p_{WW} & p_{WS} \\ p_{SD} & p_{SW} & p_{SS} \end{bmatrix} \qquad (4.37)$$

(a)

(b)

(c)
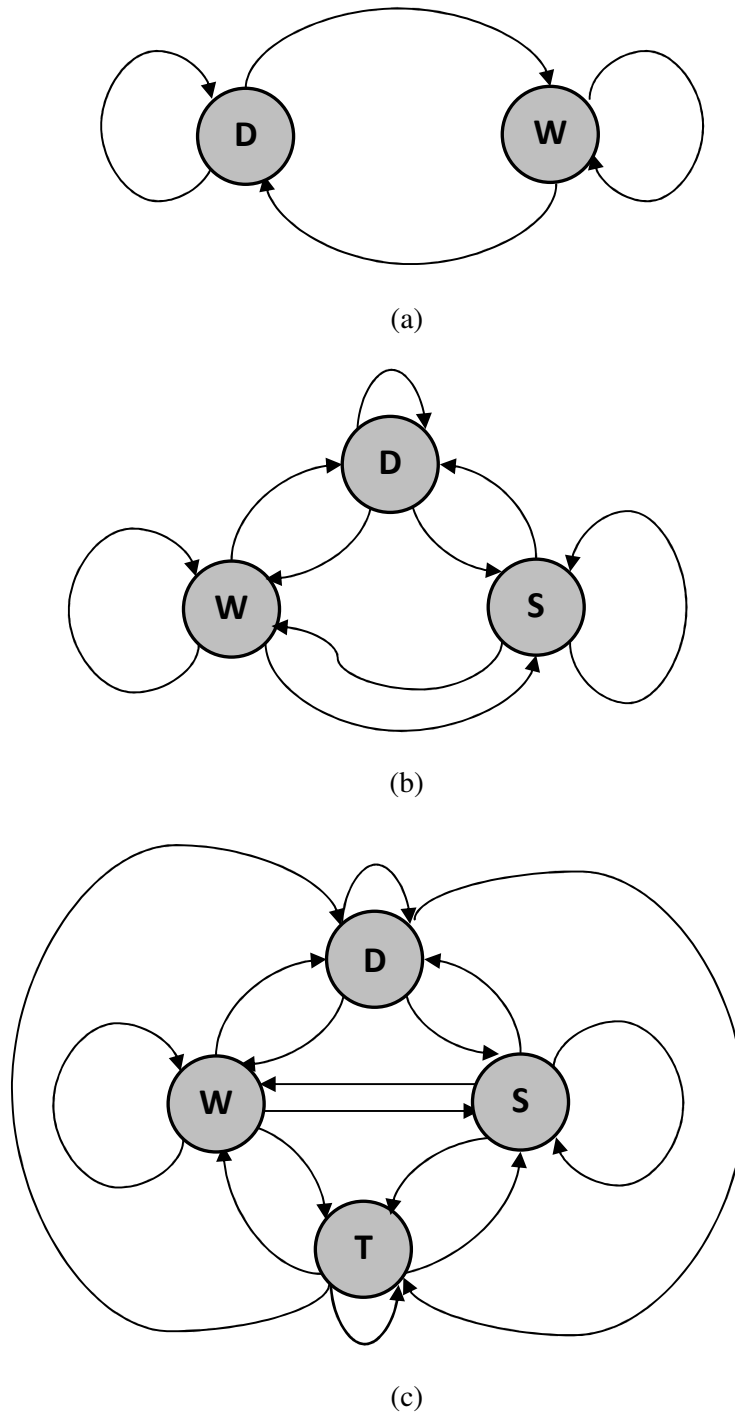
Figure 4-11: The state transition diagrams for spikes generated in different rainfall regimes (a) Widespread (b) Shower (c) Thunderstorm .

where P_{DD}, P_{DW}, P_{DS}, P_{WD}, P_{WW}, P_{WS}, P_{SD}, P_{SW}, P_{SS} are the transition probabilities of drizzle (D), widespread (W) and shower (S) spikes.

Finally, thunderstorm events have transitional matrix as follows:

$$\mathbf{P}_{thunderstorm} = \begin{bmatrix} p_{DD} & p_{DW} & p_{DS} & p_{DT} \\ p_{WD} & p_{WW} & p_{WS} & p_{WT} \\ p_{SD} & p_{SW} & p_{SS} & p_{ST} \\ p_{TD} & p_{TW} & p_{TS} & p_{TT} \end{bmatrix} \tag{4.38}$$

where P_{DD}, P_{DW}, P_{DS}, P_{DT}, P_{WD}, P_{WW}, P_{WS}, P_{WT}, P_{SD}, P_{SW}, P_{SS}, P_{ST}, P_{TD}, P_{TW}, P_{TS}, P_{TT} are the transition probabilities of drizzle (D), widespread (W), shower (S) and thunderstorm (T) spikes.

Table 4-5 presents the populated transition matrices for each of the rainfall events as given in (4.36), (4.37) and (4.38). The number of product operation or stages required to attain steady-state conditions, n, is also presented. The results from the steady state vector are hereby discussed in the context of probability, the vector itself being a stochastic vector. It is important to note that the sum of all the elements contained in this is approximately equal to one. Therefore, it follows at steady state that in a widespread event, there is 73.7% chance of drizzle spikes compared to 26.3% chance of widespread spikes. In shower events at steady state, the probabilities of drizzle, widespread and shower spikes are 51.5%, 19.5% and 29% respectively. Finally, for spikes under thunderstorm events, the occurrence probabilities of 42.7%, 9.9%, 21.4% and 25.8% are observed for drizzle, widespread, shower and thunderstorm spikes respectively. In all these regimes, drizzle spikes are all obviously dominant as seen from the discussion in comparison to other spike types.

Table 4-5: State Transition Matrix and Steady State Vectors for Spike Generation in Durban

REGIME	TRANSITION MATRIX	n	STEADY STATE VECTOR
DRIZZLE	[1]		[1]
WIDESPREAD	$\begin{bmatrix} 0.7528 & 0.2472 \\ 0.6935 & 0.3065 \end{bmatrix}$	4	[0.7372 0.2628]
SHOWER	$\begin{bmatrix} 0.6839 & 0.1782 & 0.1379 \\ 0.3621 & 0.2069 & 0.4310 \\ 0.3165 & 0.2152 & 0.4684 \end{bmatrix}$	12	[0.5146 0.1947 0.2913]
T/STORM	$\begin{bmatrix} 0.6071 & 0.0714 & 0.0714 & 0.2500 \\ 0.3750 & 0.2500 & 0.125 & 0.2500 \\ 0.3333 & 0.1111 & 0.3333 & 0.2222 \\ 0.2308 & 0.0769 & 0.3846 & 0.3077 \end{bmatrix}$	10	[0.4276 0.0989 0.2136 0.2587]

4.6.5 Relationship between Spike Peak Rainfall Rate and Service Time

In this study, it is seen that the arrival of a cloud may be synonymous with the generation of rainfall spike in the time domain. Following this assumption, it might be beneficial to establish the relationship between the maximum rainfall rate of a spike and its contemporary service time. It follows that for a given maximum rain rate attained by a spike, R_m, the arrived cloud has a lifespan equivalent to the spike service time. Thus, the probability of overlap, Pr(Overlap) occurring in a spike for a given maximum rain rate in its lifespan, is given as:

$$\Pr(overlap) = \frac{t_o}{t_s} \tag{4.39a}$$

$$\therefore \quad \Pr(No\ overlap) = 1 - \Pr(overlap) = 1 - \frac{t_o}{t_s} \tag{4.29b}$$

From the queueing studies undertaken in this paper, the Erlangian service times and overlap times for a single spike are both non-mutually exclusive event instances. From earlier results, the service time is observed to be always greater than the overlap time, since the latter is a subset of the former. This is true because the overlap period for a single spike occurs as a fractal of its service time. Therefore, the concept of an adjusted service time is conceived because of the occurrence of overlaps. The adjusted service time, t_s', which is the actual service time, is given as:

$$t_s' = \Pr(No\ overlap) \times t_s \quad [minutes] \tag{4.40}$$

From our data and initial results on spike queues, it is seen that the service times (both t_s and t_s') of any rain spike increases with increasing peak rain rate recorded. By using the complete dataset of 548 spike samples from Durban, without distinguishing between the regimes and considering only averaged rain rates, we find this relationship by regression technique as seen in Figure 4-12. Thus, we have:

$$t_s' = \eta_1 R_m^{\nu_1} \quad [minutes] \tag{4.41}$$

and, for service time occurrences with assumed overlaps,

$$t_s = \eta_2 R_m^{\nu_2} \quad [minutes] \tag{4.42}$$
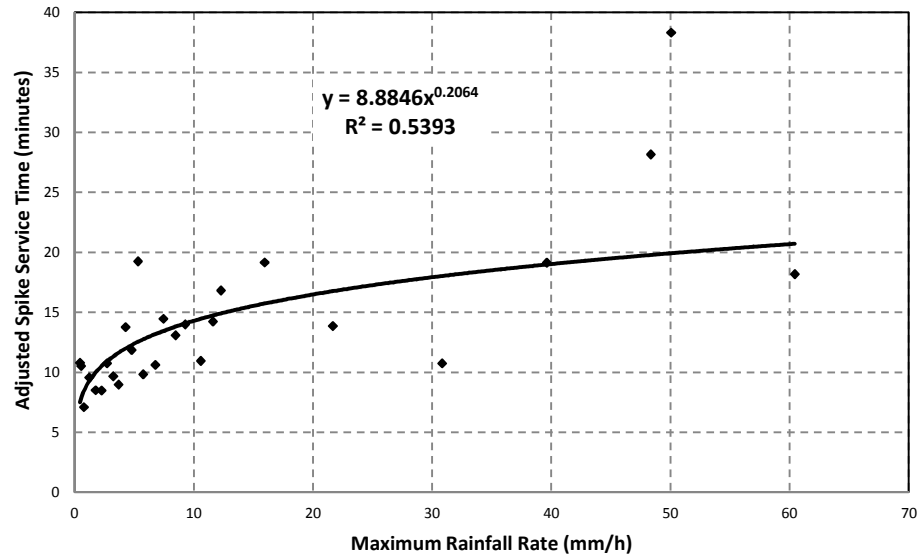
(a)
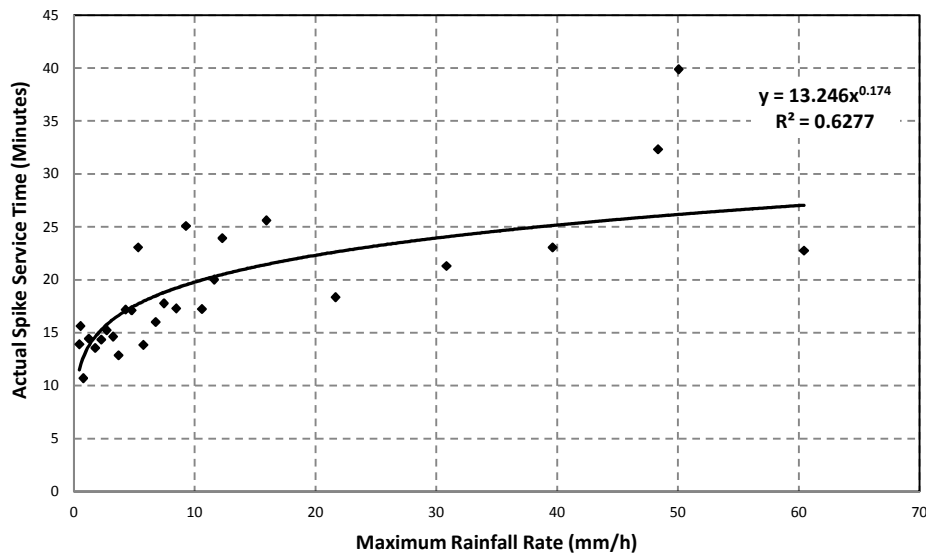
(b)

Figure 4-12: Scatter plots of spike service time versus maximum rainfall rate for the city of Durban (a) Adjusted service time versus maximum rainfall rate (b) Actual service time versus maximum rainfall rate

The paired coefficients of $\eta_1 = 8.8846$ and $v_1 = 0.2064$ and $\eta_2 = 13.246$ and $v_2 = 0.174$ were obtained respectively for (4.41) and (4.42) for the city of Durban located in KwaZulu-Natal province. The scatter-plots for these derived relationships are given in Fig. 4-12(a) and (b). The implication of the results in Fig. 4-12 affirms that the maximum rain rate of a single spike (or single rain cell) increases as the service time (or lifespan) increases at our location. This invariably means that cases such as thunderstorm events with higher rainfall rate components

tend to have spikes with higher lifespan. Although, it seems the accuracy of this method reduces time. In the same vein, about 28 minutes of rainfall duration is proportionate to a maximum rainfall rate of 60 mm/h based on the actual service time.

4.7 Chapter Summary

The interesting concept of rainfall spike queues as an $M/E_k/s/\infty/FCFS$ Semi-Markovian queue was investigated in this work. From our results, we have confirmed that the queue arrival pattern of rainfall spikes in a typical rainfall event in Durban is essentially exponentially distributed. The service time (or lifespan) of any arriving spike is found to follow, with minimal fitting errors, an Erlang-k distribution. Therefore, the overall rainfall processes over different rainfall regimes in Durban all seem to exhibit a default queue discipline of $M/E_k/3$. It is worthy to also note that the maximum peaks attained by each generated spikes are random and possess jumping state transitional probabilities which varies across different rainfall regimes. These maximum peaks are found to have a positive power-law relationship with its corresponding service times. These statistics are instrumental to the future (and alternative) development of dynamic techniques for implementing rain fade mitigation. At a latter stage of this thesis, these concepts are further developed to determine rain cell sizes, and hence, predict rain path attenuation. This is necessary since the analysis of single (and multiple) rain cells provide an avenue for the understanding of rain fade effects in communication networks. This gives us wider research options required to establish a sound relationship between rainfall attenuation, rain cells and queueing theory. In the next chapter, the queueing theory concept is also applied to the distrometer measurements at the equatorial location of Butare, Rwanda. A comparison of the queueing characteristics and performance metrics in Durban and Butare is further undertaken.

CHAPTER FIVE

Comparison of Rainfall Queue Characteristics in Tropical Africa

5.1 Introduction

Attenuation due to precipitation remains an important design factor in the future deployment of terrestrial and earth-space communication radio links at high frequency bands. Largely, there are concerted efforts to understand the dynamics of precipitation forms in attenuation occurrence in subtropical, tropical and equatorial region of Africa. The role of time-varying rainfall in the process of rain attenuation though overtly stochastic, is very important. Thus, the knowledge of queueing theory in rainfall offers new interpretations to the generation and transition process of rain attenuation. In the preceding chapter, it was established that the appearance of rain rates over radio links in Durban ($29^o52'$S, $30^o58'$E) invariably follows a First Come, First Served (FCFS), multi-server (s), infinite queue and semi-Markovian process, designated as a M/E_k/s/∞/FCFS discipline. In this chapter, the queueing theory approach is applied to distinct rain spike traffic over radio links in Butare ($2^o36'$S, $29^o44'$E) to firstly determine the locations' queueing characteristics. The queueing characteristics in Durban and Butare so obtained are comparatively analysed over four categorized rainfall event regimes of drizzle, widespread, shower and thunderstorm. Therefore, the contents of this chapter involve investigating the attributes and significant variations of rainfall queues at these African locations, over different regimes. In addition, other queue relationships and mathematical formulations describing other queue-related parameters are discussed.

5.2 Brief Review of the Queueing Theory Concept

Rainfall precipitation is a major source of attenuation to radio links, particularly at designated carrier bands transmitting at X-band frequencies and beyond [*Green*, 2004; *Ajayi et. al*, 1996]. Static and dynamic rain fade mitigation techniques have been suggested by researchers as stop-gap measures required to correct this phenomenon [*Acosta*, 1997; *Castanet et. al*, 2003; *ITU-R P.530-15*, 2013]. For instance, the International Telecommunication Union (ITU) radio group recommendations in [*ITU-R P.530-15*, 2013; *ITU-R P.837-6*, 2012; *ITU-R P.838-3*, 2005)] employ static technique to address rain fade mitigation.

Rain attenuation over a radio link, as research has shown from previous studies varies randomly and inhomogeneously over the entire life span of a rain event, in space and time [*Ajayi*, 1990;

Ajayi et. al, 1996]. This is possible because the measurable quantity of rainfall rate varies randomly during a rain event. During a rain event, distinct peaks are attained by rainfall rates corresponding to their allocated time series. Thus, a stationary observer positioned at a reference point over a radio link may detect this variation of rainfall rate, as the arrival and departure of objects at a position parallel to the reference. Simply, the collection of rainfall rate measurements at a point during a rainfall event over time is actually a time-series record of moving clouds (objects) – delivering bulk rain rates over the radio link. This scenario is akin to a production line process where empty bottles are queued and aligned to pass through a nozzle filling point. Evidently, it can be proven that the rainfall rate delivery process over radio links is a queue in which the arrival (and departure) of rainfall spikes follow a basic queueing pattern. If this process is properly understood, then this queue could be described as a Birth-Death (BD) process which is a special case of general Discrete-Time Markov Chain (DTMC) process [*Bolch*, 1998]. There have been a number of attempts to model the rainfall process using general Markov chain procedure and its derivatives [*Alasseur et. al*, 2004; *Héder and Bitòs*, 2008; *Maruddani et. al*, 2010]. The drawback of these Markov models are often linked to their unique transition state matrices, as they are dependent on the geography and climate of the region of study. In this current work, the BD process firstly assumes that the departure of a rain cloud over a radio link, is succeeded by the arrival of another rain cloud, until the rain event duration is completed. To understand this process, a distinct rainfall spike with a peak rainfall rate is assumed as a single object (or cloud) in rain event queue. Using this technique, it can be demonstrated by queueing theory that a queue discipline is most appropriate to describe the queue pattern pertaining to any rain spikes traffic. Basic queue parameters such as the service time and arrival time are intrinsic to describing this queue system [*Kleinrock*, 1975; *Hillier and Lieberman*, 2001]. Another parameter defined as the overlap time is needed to ascertain the period for which two spikes (one at birth and the other dying) intercept one another during rainfall.

Therefore, this chapter firstly seeks to extend and compare the queueing characteristics as earlier proposed in chapter three from RD-80 distrometer measurements obtained at two African locations with distinct climates: Durban (subtropical) and Butare (Equatorial). These two locations are areas of intense rainfall and are particularly prone to the effects of rainfall attenuation for terrestrial and Earth-space communication at microwave frequencies [*Ajayi et. al*, 1996]. A survey into the annual climatic influences in Durban reveals a larger frequency of drizzle and widespread rainfalls, with few cases of thunderstorm events [*Afullo*, 2011; *Alonge and Afullo*, 2012]. Whereas, Butare is characterized by larger spectrum of shower and

thunderstorm rainfalls; infact, it exhibits a super-tropical climatic pattern. Therefore, these locations are climatically modulated by two extreme cases of tropical rainfall - where Durban is subtropical and Butare, equatorial. Thus, the objectives of this paper entail investigating the comparison of the underlying queue pattern of rain spike traffic, queue characteristics and its variations at the two proposed sites..

5.3 The M/E$_k$/s/∞/FCFS Queue for Rainfall Queueing Theory Analysis

The M/E_k/s/∞/FCFS represents a semi-Markovian queue discipline in which queued instances (or objects) undergo a queue pattern where its service times is Erlang-k distributed (E_k) and their inter-arrival times is exponentially distributed (M) [*Hillier and Lieberman*, 2001]. In this discipline, the maximum length of the approaching instances (*L*) are assumed infinite (∞) and processed by servers (*s*) according to a First Come, First Served (FCFS) schedule [*Kleinrock*, 1975]. This overall discipline depicts queues, where the instances are scheduled in an orderly manner, based on the probabilities of their intrinsic distributions. In the context of this study, the major components of any queue system are: the service time, inter-arrival time and servers.

The rainfall spike service time shall be defined as the total lifespan of a spike in a rain event. The *service time distribution* is represented as an Erlang-k distribution with a service rate of μ_s. Therefore, the queue service distribution is defined from *Hillier and Lieberman* [2001]:

$$s(t; k, \mu_s) = \frac{(k\mu_S)^k t^{k-1} exp\,(-k\mu_S t)}{\Gamma(k)} \quad [min^{-1}] \; for\, k, t > 0; \; t\,\forall\,\mathbb{R} \quad (5.1)$$

where k is an integer related to the number of stages and μ_s is the service rate of the spike distribution with the unit of spike/min.

The *inter-arrival time distribution* describes a Markovian process related to the exponential distribution with an arrival rate, λ_a. The queue arrival distribution is defined from *Walck* [2007] as:

$$a(t; \lambda_a) = \lambda_a\, exp(-\lambda_a t) \quad [min^{-1}] \quad for\, t > 0; \; t\,\forall\,\mathbb{R} \quad (5.2)$$

where λ_a is the arrival rate of the inter-arrival distribution with the unit of spike/min.

The service and arrival rates are the reciprocal of the mean service time and mean inter-arrival time respectively. The equivalent expressions related to their respective mean queue characteristics are given as:

$$\overline{\mu_s} = \left(\frac{1}{N_s} \sum_{k=1}^{N_s} t_k \right)^{-1} \quad [min^{-1}] \tag{5.3}$$

$$\overline{\lambda_a} = \left(\frac{1}{N_a} \sum_{i=1}^{N_a} t_i \right)^{-1} \quad [min^{-1}] \tag{5.4}$$

where t_k and t_i are arrays representing the service time and inter-arrival time of the queue discipline, with queue lengths (or sampled data) of N_s and N_a respectively.

For the purpose of the system modeling, we shall assume that our instances are distinct rainfall spikes generated during rain events – each with its distinct queue parameters. During a rainfall event, the subsequent arrivals of rainfall spikes over a radio link generate a well-defined offered traffic. For a stable queue, the server is expected to process any spike arriving within its designated service time. To achieve system stability, the overall multi-server queue system is required to satisfy the steady-state criterion [*Bolch et. al*, 1998; *Hillier and Lieberman*, 2001]:

$$\rho = \frac{\lambda_a}{s\mu_a} \leq 1 \tag{5.5}$$

where, ρ, is a dimensionless unit called the *utilization factor* which determines the reliability and stability by the system. In many natural and real-life systems like rainfall processes, it is most likely to find defined values of *s* for which ρ > 1. This condition may result in the occurrence of excess queues and rain spike delays. Usually, this queue problem is more complicated when the system is served by a single server.

It follows from the previous chapter that the queue paradigms and assumptions applied in Durban is also applicable in Butare. They are thus reviewed and summarised as follows:
  i.   A rain event is defined as the entire length of a physical process, specifying the commencement and end of rainfall, defined by a bounded period, *T*.
  ii. Network outages during rainfall are directly related to rainfall attenuation, as specified by ITU-R P.530-15. All outage durations are assumed to occur within the bounded

period of a rain event: where the outage duration, a subset of the rain event, is lognormally distributed (*ITU-R P.530-15*, 2013).

iii.   All rain events comprises of sub-events with a period, t_i, which are individual subsets, the total sum of which equals the rain event T. Therefore, $T = \sum_i t_i$.

iv.   A sub-event is identified by a distinct rain spike within a rain event and is independently specified by its lifespan known as the service time, t_s, which is inversely related to the queue service rate, μ_s. Mathematically, $t_s \subset T$.

v.   Within a rain event, the inter-arrival and inter-departure of sub-events occurs in a random pattern related to the queueing parameters of arrival time and departure time. The inter-arrival time, t_a, is inversely related to the queue arrival rate, λ_a.

vi.   The existence of two conjoined sub-events may result in truncated inter-departure process resulting in spike overlap with period, t_o, where $t_o \subset t_s$. The overlap rate, defined as σ_o, is a probabilistic property – inversely related to the overlap time.

vii.   All specified properties of a distinct rainfall sub-event (or rainfall spike) are governed by a Markovian (or semi-Markovian) process. This process can be completely understood by a suitable queue discipline aptly embedded in a Kendall notation [*Kendall*, 1953; *Bolch et. al*, 1998].

Following the description from assumption (vi), it therefore follows that the Erlang-k distribution is also sufficient to describe its distribution. For this reason, the overlap rate is described as:

$$\overline{\sigma_o} = \left(\frac{1}{N_o} \sum_{j=1}^{N_o} t_j \right)^{-1} \quad [min^{-1}] \tag{5.6}$$

where N_o is the number of overlap samples in the overlap time array, t_j

5.4 Measurement and Data Processing

Datasets which form the basis for the queue modelling in this work are obtained from raw rainfall measurements via the Joss-Waldvogel RD-80 distrometer. These measurements are obtained from locations in Butare, Rwanda ($2^o36'$S, $29^o44'$E) and Durban, South Africa ($29^o52'$S, $30^o58'$E). The installed RD-80 distrometer undertakes the sampling and archiving of rainfall measurements from the outdoor unit at one minute interval, with accuracy of ±5% [*Bartholomew*, 2009]. The installation in Durban operated for total of two years (January 2009-December 2010), albeit with few cases of outages. In Butare, a total of one year measurement was undertaken between March 2012 and February 2013.

Retrieved rainfall data are classified into event classes as thus: drizzle (1 mm/h $\leq R <$ 5 mm/h), widespread (5 mm/h $\leq R <$ 10 mm/h), shower (10 mm/h $\leq R <$ 40 mm/h) and thunderstorm ($R \geq$ 40 mm/h) as initially undertaken in Chapter Four. This categorization is followed by the isolation of rain events, by identifying points at the edges of their times series, where the events are seen to completely diminish. Thereafter, the identification of spikes within rain events is realized by observing distinct spikes and isolating them. The recovery of a distinct spike from conjoined spikes is pertinent as the BD process may occur prematurely between spikes. To resolve this, the Newton divided-difference extrapolation algorithm [*Kreyzig*, 2006] is applied to recover the truncated portions of such conjoined rain spikes. To eliminate errors associated with dead times and false events, rainfall events with maximum rain rates less than 3 mm/h are excluded from the processed data. By applying the ergodic properties of queues, it can be deduced that only fractional queue samples from the rainfall data are required to establish and generalize the behaviour of the entire dataset. A summary of the processed samples of the rainfall data at both locations is shown in Table 5-1 with drizzle (DR), widespread (WS), shower (SH) and thunderstorm (TS) regimes.

From Table 5-1, it is observed that over 75% of spike samples at both sites have service times less than 40 minutes. For thunderstorm events, the percentages of samples less than 40 minutes are 60.3% and 86% respectively in Durban and Butare. For the inter-arrival time, however, more than 90% of the spikes arrive within 40 minutes of the initial spike, at both sites. More than 95% of the samples undergo overlaps within a maximum period of 20 minutes. From these results, we find similarity in the time domain structures of rain spikes at both sites.

Table 5-1: Distribution of the sampled measurements of queue parameters over time bounds for different regimes in Durban and Butare

SERVICE TIME (minutes)								
TIME BOUNDS (minutes)	*Durban*				*Butare*			
	DR	**WS**	**SH**	**TS**	**DR**	**WS**	**SH**	**TS**
$0 \le t < 20$	126	146	95	61	53	92	117	91
$20 \le t < 40$	20	28	26	30	10	17	43	12
$40 \le t < 60$	0	1	5	9	1	2	6	1
$t \ge 60$	0	0	0	1	0	0	0	1
$\sum$	**146**	**175**	**126**	**101**	**64**	**111**	**166**	**105**
INTER-ARRIVAL TIME (minutes)								
TIME BOUNDS (minutes)	*Durban*				*Butare*			
	DR	**WS**	**SH**	**TS**	**DR**	**WS**	**SH**	**TS**
$0 \le t < 20$	124	155	120	76	50	102	126	90
$20 \le t < 40$	2	2	2	9	3	0	9	6
$40 \le t < 60$	0	1	2	4	0	0	0	0
$\sum$	**126**	**158**	**124**	**89**	**53**	**102**	**135**	**96**
OVERLAP TIME (minutes)								
TIME BOUNDS (minutes)	*Durban*				*Butare*			
	DR	**WS**	**SH**	**TS**	**DR**	**WS**	**SH**	**TS**
$0 \le t < 20$	126	155	120	86	54	102	133	96
$20 \le t < 40$	0	1	4	3	0	0	0	0
$\sum$	**126**	**156**	**124**	**89**	**54**	**102**	**133**	**96**

5.5 Rain Spike Queue Modelling Comparison in Durban and Butare

The modelling of queue parameters for the service time, inter-arrival time and overlap time distributions are computed by applying the Method of Maximum Likelihood (ML) parameter estimation technique. To determine the error deviation and model suitability, the Root-Mean-Square Error (RMSE) and Chi-Square (χ^2) error statistics are applied. These two expressions are given by:

$$RMSE = \left[\frac{1}{N} \sum_{i=1}^{N} (O_i - P_i)^2 \right]^{1/2} \tag{5.7}$$

$$\chi^2 = \sum_{i=1}^{N} \frac{(O_i - P_i)^2}{O_i} \tag{5.8}$$

where O_i and P_i are the observed data and modelled data related to the applied distribution respectively.

5.5.1 Service Time Queue Distribution

Since the service time distribution is assumed as an Erlang-k distribution, the values of the integer k are selected by varying the function until minimum RMSE and χ^2 are obtained. The Probability Density Functions (PDFs) from the service time distribution modeling for both Durban and Butare are shown in Figure 5-1. The PDF shapes are observed to be similar for drizzle regime and as observed as on Table 5-2, the average service time in Durban is higher than seen in Butare. For the widespread regime, a similarity in the queue distribution is seen in Fig. 5-1b with the mean service times observed in Durban (13.71 minutes) and Butare (15.3 minutes). For the shower regime, the mean service time (t_s) are also observed as close to one

(a)

(c)

(b)

(d)
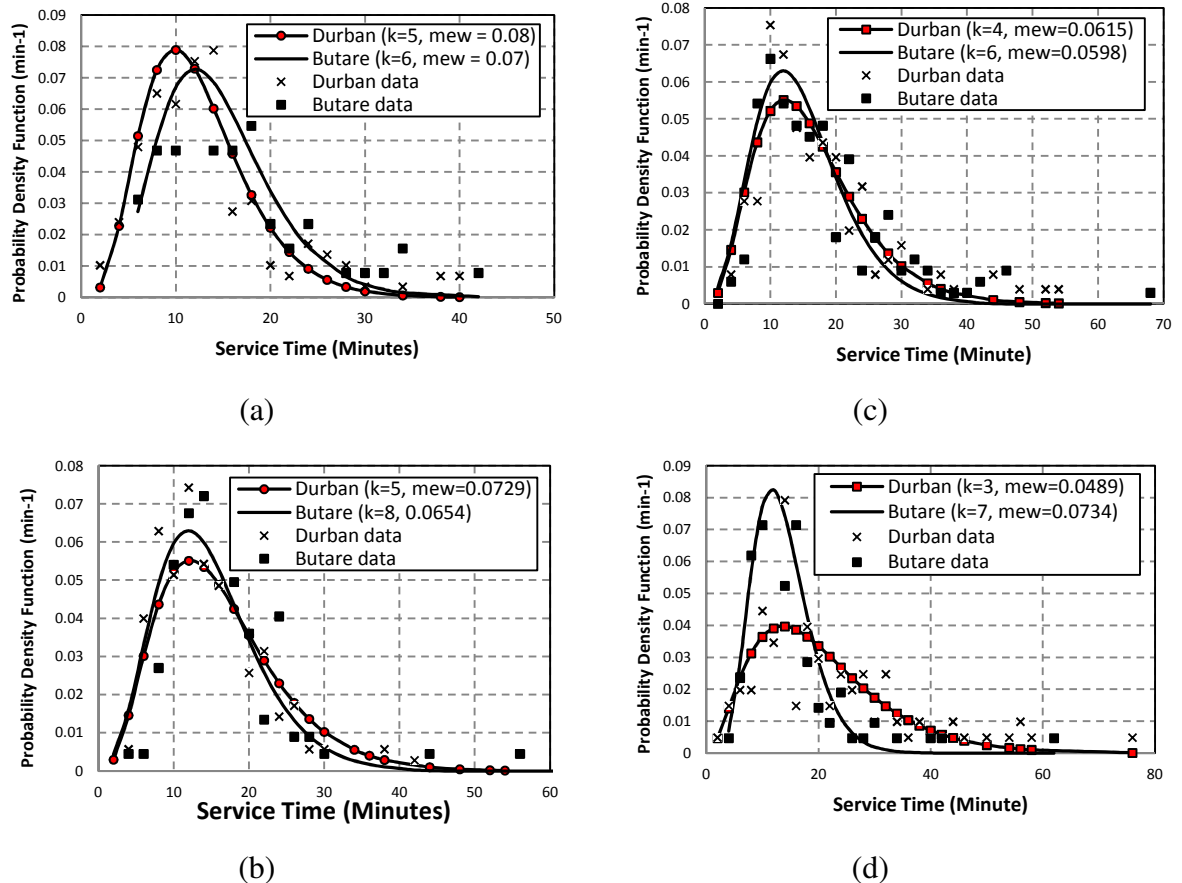
Figure 5-1: PDF plots of Service Time Distribution of Rainfall Spikes for Different Regimes in Durban and Butare: (a) Drizzle (b) Widespread (c) Shower (d) Thunderstorm

Table 5-2: Comparison of Service Time Parameters in Durban and Butare

Location	Regime	μ_S	t_S	k	RMSE	χ^2	DF	SL
DURBAN	Drizzle	0.0808	12.3755	5	0.0094	0.7226	145	174.10
	Widespread	0.0729	13.7095	5	0.0077	0.1224	174	205.78
	Shower	0.0615	16.2556	4	0.0083	0.2648	125	152.09
	Thunderstorm	0.0489	20.4409	3	0.0104	0.3469	100	124.34
BUTARE	Drizzle	0.0691	14.4786	6	0.0156	0.5925	63	82.53
	Widespread	0.0654	15.2942	8	0.0133	0.5567	111	136.59
	Shower	0.0598	16.7265	6	0.0092	0.0929	165	195.97
	Thunderstorm	0.0734	13.6167	7	0.0103	0.0103	104	128.80

another at both sites (please, see Fig. 5-1c). This is confirmed in Table 5-2 where the 16.26 minutes and 16.72 minutes are recorded as the average service times. Finally, the thunderstorm queue results as observed in Fig. 5-1d reveal divergence in the queue patterns, at both sites. The average t_s in Durban is about 20.44 minutes, whereas, this value is about 13.62 minutes in Butare. Broadly speaking, a gradual increase in the mean spike service time is observed in Durban from drizzle regime to thunderstorm regime. On the other hand, the service time seem to gradually decline for the same set of regimes in Butare.

For the purpose of radio planning especially at high carrier frequencies, it may be noted that rain spikes generated during thunderstorm regimes have a higher probability of causing network outages. For this, it is observed from Table 5-2 that spikes in Durban tend to have longer service times than Butare for thunderstorm spikes. The disparity of the spike service at both sites might be a result of geographical effects governing the rainfall process. The implication of this is that - longer outage times may be experienced in Durban - than observed in Butare during severe thunderstorm rains. Also interesting, is the observation of the k-stages for the modeled distribution, for which the variations at both sites are observed. Values of k in Durban tend to decrease from drizzle regime to thunderstorm regimes. However, in Butare these values tend to increase for the same set of regimes. This implies that the spike generation process in Butare tend to pass through more k-stages during rainfall.

The RMSE and χ^2 for the Erlang-k models for each of the regimes are well within acceptable limits (see Table 5-2). The Degree-of-Freedom (DF) and Significant Level (SL) for each of the fitted models are also included. As a general remark, the RMSE at both sites do not exceed a percentage RMSE of 2%. Also, χ^2 values for all regimes at both sites are satisfied since the

computed values do not exceed their significant levels at 5% according to their specified Degrees-of-Freedom.

5.5.2 Inter-arrival Time Queue Distribution

The spike inter-arrival distribution modelled in Durban and Butare are presented in Figure 5-2. The mean inter-arrival times, t_a, in Durban for drizzle, widespread, shower and thunderstorm regimes are 5.21, 6.52, 6.73 and 10.85 minutes (please, see Table 5-3). In Durban, we see a progressive increase in the average t_a in an ascending order from drizzle to thunderstorm regimes. In Butare, the set of mean inter-arrival time for the same regimes are 7.41, 5.33, 7.81 and 6.50 minutes. It appears there is no trend indicating an increase or decrease of arrival time at this site. For drizzle and shower regimes, the mean inter-arrival times are found to be higher in Durban. This is not the case for spikes arrivals in Durban for widespread and shower regimes, as observations tend to favour the conditions in Butare. For the purpose of radio planning, it is. observed that the arrival rate of spikes in Butare is higher for thunderstorm

(a)   (c)

(b)   (d)
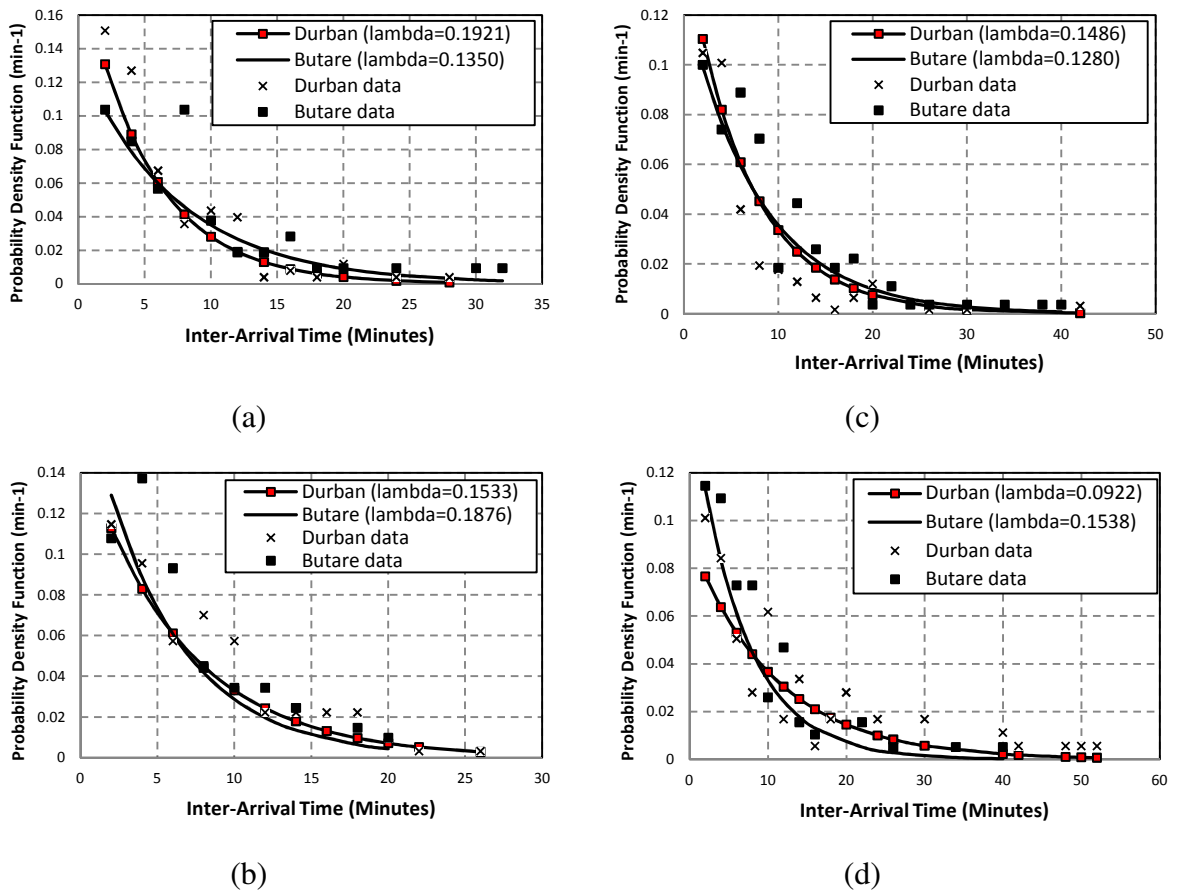
Figure 5-2: PDF plots of Inter-Arrival Time Distribution of Rainfall Spikes for Different Regimes in Durban and Butare (a) Drizzle (b) Widespread (c) Shower, and (d) Thunderstorm

Table 5-3: Comparison of Inter-Arrival Time Parameters in Durban and Butare

LOCATION	REGIME	λ_a	t_a	RMSE	χ^2	DF	SL
DURBAN	Drizzle	0.1921	5.2065	0.0151	0.0860	125	152.09
	Widespread	0.1533	6.5242	0.0118	0.0594	156	186.15
	Shower	0.1486	6.7312	0.0129	0.0919	123	149.89
	Thunderstorm	0.0922	10.8475	0.0128	0.2118	88	110.89
BUTARE	Drizzle	0.1350	7.4077	0.0165	0.1363	52	69.83
	Widespread	0.1876	5.3317	0.0232	0.0854	101	125.46
	Shower	0.1280	7.8122	0.0115	0.0713	134	162.02
	Thunderstorm	0.1538	6.5024	0.0190	0.0505	101	125.46

regime i.e. > 40 mm/h. This implies that in a typical spike queue in Durban, a spike arrives later than observed in Butare. This observation may imply that the service rebound time for a wireless network may be longer in Durban during thunderstorm events. For the exponential (Markovian) model at both sites, the RMSE and χ^2 inter-arrival process in Durban are within acceptable limits. In Durban, the percentage RMSEs for all regimes are well below 1.5% with χ^2 satisfying 5% significance level. In Butare, the computed percentage RMSE for all regimes does not exceed 2.5% with satisfactory χ^2.

5.5.3 Overlap Time Queue Distribution

The overlap time is seen as a subset of the spike service time, and therefore exhibits the same probability characteristics as the service time. Therefore, Erlang-*k* distribution is also sufficient for the modelling of overlap distribution. The results from the two sites are presented in Table 5-4 and Figure 5-3. We observe from the results that the overlap time patterns for drizzle regime are similar at both locations *i.e.* 4 minutes. However, the mean overlap times are seen to be

Table 5-4: Comparison of Overlap Time Parameters in Durban and Butare

LOCATION	REGIME	σ_o	t_o	k	RMSE	χ^2	DF	SL
DURBAN	Drizzle	0.2506	3.9906	3	0.0292	0.2913	125	152.09
	Widespread	0.2331	4.2899	3	0.0099	0.0441	155	185.05
	Shower	0.1705	5.8667	3	0.0084	0.0204	123	149.89
	Thunderstorm	0.1739	5.7509	2	0.0164	0.0488	88	110.89
BUTARE	Drizzle	0.2431	4.1112	4	0.0459	0.2309	53	70.99
	Widespread	0.1888	5.2962	4	0.0391	0.1444	101	125.46
	Shower	0.2323	4.3047	4	0.0335	0.1673	132	159.81
	Thunderstorm	0.2647	3.7781	7	0.0373	0.0084	95	118.75
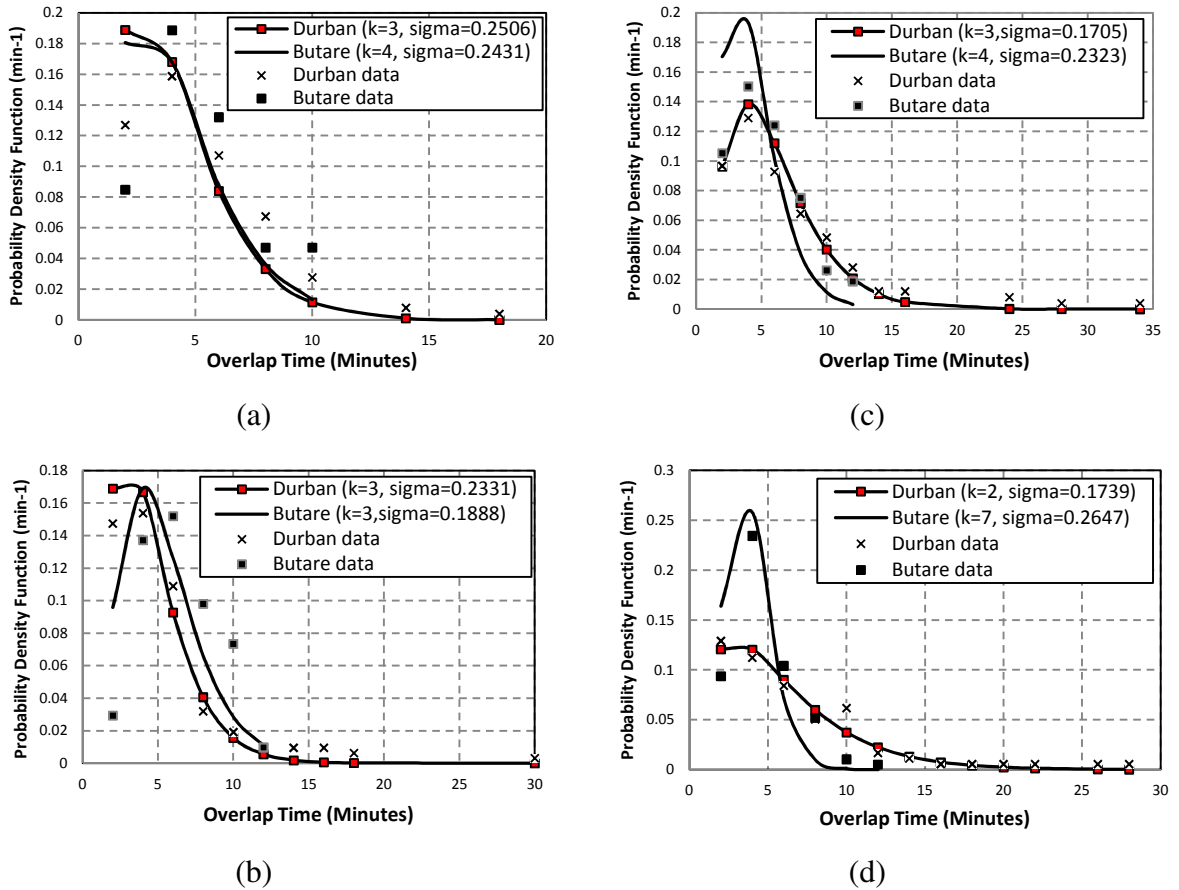
Figure 5-3: PDF plots of Overlap Time Distribution of Rainfall Spikes for Different Regimes in Durban and Butare (a) Drizzle (b) Widespread (c) Shower, and (d) Thunderstorm

higher in Durban for shower and thunderstorm regimes. The value of k for Durban and Butare appear to remain constant at 3 and 4 respectively for the first three regimes *i.e.* drizzle, widespread and shower regimes. However, k values estimated for thunderstorm regimes (see Table 5-4) are different in Durban and Butare with their respective values being 2 and 7. For theerror statistics, the maximum RMSE at maximal error for all regimes is pegged at 4.6%, while the maximum χ^2 at 0.2913 satisfy the significance level criteria. In general, we expect higher overlaps in Butare for drizzle and widespread spikes compared to Durban with the reverse scenario for shower and thunderstorm spikes.

5.5.4 Variation of Queue Servers in Durban and Butare

The generation of rainfall spike queues is regulated by multiple servers, which determine the service time and inter-arrival times. Thus, the understanding of the $M/E_k/s/\infty/FCFS$ queue discipline is incomplete without computing the actual number of multiple servers in the system.

By applying (5.5), it can be found that the steady-state criterion ($\rho < 1$) is unsatisfied across all regimes at both locations. Therefore, it is important to compute the minimum number of servers, s_{min}, at both locations. It follows that the minimum number of servers required to sustain the spike traffic is unique to each rainfall regime in this study. To estimate this number, (5.5) is modified so that the minimum number of servers to satisfy the queue stability criterion. This is given as:

$$s_{min} \geq ceil\left(\frac{\lambda_a}{\mu_s}\right) \tag{5.9}$$

where *ceil* denotes the upper bound of the computed minimum number of servers, s_{min}. λ_a and μ_s are the arrival rate and service rate respectively.

By applying (5.9), s_{min} was computed from the queue parameters obtained for the different regimes in Durban and Butare. The results computed for both locations are presented in Table 5-5. As seen from this table, s_{min} computed in Durban has a constant value of 3 for all regimes except for the lower value for thunderstorm where, $s_{min} = 2$. With the exception of drizzle regime in Butare, where $s_{min} = 2$, the minimum servers observed for other regimes are constant with a value of 3. It is important to note that s_{min} is reliant on the microphysics of the rainfall processes at both locations. At both locations, regime with lower value of s_{min} is suspected to be influenced by varied service and inter-arrival times. There is a huge possibility that number of servers could be related to the air motion and advection velocities of the rain clouds. However, further investigations from ground and space-borne data are required to understand this relationship.

Table 5-5: Minimum Number of Queue Servers in Durban and Butare for Different Regimes

MINIMUM NUMBER OF QUEUE SERVERS				
LOCATION	Drizzle	Widespread	Shower	Thunderstorm
DURBAN	3	3	3	2
BUTARE	2	3	3	3

5.6 Overall Queueing Results in Durban and Butare

The overall results obtained from the two sites, irrespective of the rain regime, show that the general queueing parameters are very similar. These can be seen in Table 5-6 and Table 5-7. For instance, the service times in Durban and Butare are both seen to be 15.2 minutes and 15.3 minutes respectively. For the inter-arrival time, Durban and Butare are seen to have average

values of 7.02 minutes and 6.78 minutes respectively. Lastly, overlap times of 4.87 minutes and 4.41 minutes are observed in Durban and Butare respectively. Generally, the only distinguishable difference at the two locations can be seen in the values of k for the service time and overlap time distributions. This suggests that the number of stages vary at the two locations. From the result, Butare is always seen to possess k stages of one unit higher than those in

Table 5-6: General Comparison of Queueing Parameters in Durban and Butare

SERVICE TIME							
LOCATION	μ_s	t_s	k	**RMSE**	χ^2	**DF**	**SL**
Durban	0.0659	15.1801	5	0.0033	1.218	547	605.52
Butare	0.0653	15.3152	6	0.0053	0.3578	445	495.17
INTER-ARRIVAL TIME							
LOCATION	λ_a	t_a		**RMSE**	χ^2	**DF**	**SL**
Durban	0.1425	7.0169		0.0076	0.0095	495	547.86
Butare	0.1476	6.7754		0.0788	0.0521	385	431.73
OVERLAP TIME							
LOCATION	σ_o	t_o	k	**RMSE**	χ^2	**DF**	**SL**
Durban	0.2053	4.8714	3	0.0065	0.0168	494	546.81
Butare	0.2267	4.4097	4	0.2278	0.1209	383	429.61

Table 5-7: Comparison of Time Exceedences for the Queueing Parameters in Durban and Butare

Percentage of Time for which Service Time is Exceeded (%)											
LOCATION	**10**	**5**	**1**	**0.5**	**0.2**	**0.1**	**0.05**	**0.02**	**0.01**	**0.005**	**0.002**	**0.001**
Durban	26.5	32.1	52	55	57.8	58.2	58.9	59.2	59.8	60.1	60.8	61.6
Butare	26	31.2	44.6	51.9	62	62.3	62.5	62.8	63	63.2	63.4	63.6
Percentage of Time for which Inter-Arrival Time is Exceeded (%)											
LOCATION	**10**	**5**	**1**	**0.5**	**0.2**	**0.1**	**0.05**	**0.02**	**0.01**	**0.005**	**0.002**	**0.001**
Durban	16.2	19.1	41	41.7	50	50.1	50.2	50.22	50.3	50.35	50.46	50.5
Butare	14.5	19	33	37.8	38.13	38.2	38.4	38.5	38.6	38.65	38.8	38.9
Percentage of Time for which Overlap Time is Exceeded (%)											
LOCATION	**10**	**5**	**1**	**0.5**	**0.2**	**0.1**	**0.05**	**0.02**	**0.01**	**0.005**	**0.002**	**0.001**
Durban	9.6	13.1	24	27.5	29.8	30	30.11	30.21	30.5	30.62	30.77	30.8
Butare	8	9.3	10.2	10.3	10.5	10.65	10.9	11	11.2	11.23	11.3	11.5

Durban. In Table 5-6, the time exceedences for each of these queueing parameters are presented for each location. From the available results, the profile in Durban is roughly seen as a scaled version of the Butare distribution. For design purposes, exceedence values at 0.01% may be critical to the viability of radio links during rainfall. From observations at 0.01% availability, the service times in Durban and Butare are 56.3 and 62.3 minutes respectively (see Table 5-7). Also, the observed inter-arrival times at these same locations are found to be 50.1 and 38.2 minutes respectively. The overlap times are also respectively found to be 30.5 and 10.3 minutes at these locations. It is suspected that the spike generation mechanisms during thunderstorm rainfalls, as well as other climatic differences, may be responsible for this variation. As earlier seen in the regime analysis, thunderstorms tend to have higher average values for both service time and overlap times. This trend, as seen in the regime analysis, is also observed under the behaviour of the overall data.

5.7 Significant Relationships from the Queue Analysis

5.7.1 Overall Peak Rain Rate Distribution

The peak rainfall rate observed for each spike in a queue is an important parameter, as it contributes to the definition of the queue behavior. The modelling of these peak rainfall rates clearly show that their generation mechanism is exponentially distributed. This is true most especially for processes occurring during drizzle, widespread and shower regimes. For these regimes, it is observed that the slope parameter, Λ_p, is sufficient to parameterize their exponential models. In Butare, we find the slope parameter for drizzle, widespread and shower as 0.57, 0.48 and 0.33 respectively. in Durban, the slope parameters for this set of regimes are 0.61, 0.35 and 0.14 respectively. These regimes are generally found to satisfy the criteria for which the Coefficient of Variation (CV) is equal to unity. However, the thunderstorm regions at both locations are found to possess CV greater than unity, hence, exponential models are not sufficient to model the queue distributions. For this reason, we propose the two-phase hyper-exponential distribution as an appropriate model to describe the peak rain rate queues. This distribution is given by *Walck* (2007) as:

$$f(r_{pk}) = \Lambda_{p1}p_1 \exp(-\Lambda_{p1}r) + \Lambda_{p2}p_2 \exp(-\Lambda_{p2}r) \qquad (5.10)$$

where r is the rain rate in mm/h, Λ_{p1} and Λ_{p2} are the slope parameters for the first and second stages of the hyper-exponential distribution respectively. Similarly, p_1 and p_2 are the probabilities attributed to each phase such that $p_1 + p_2 = 1$.
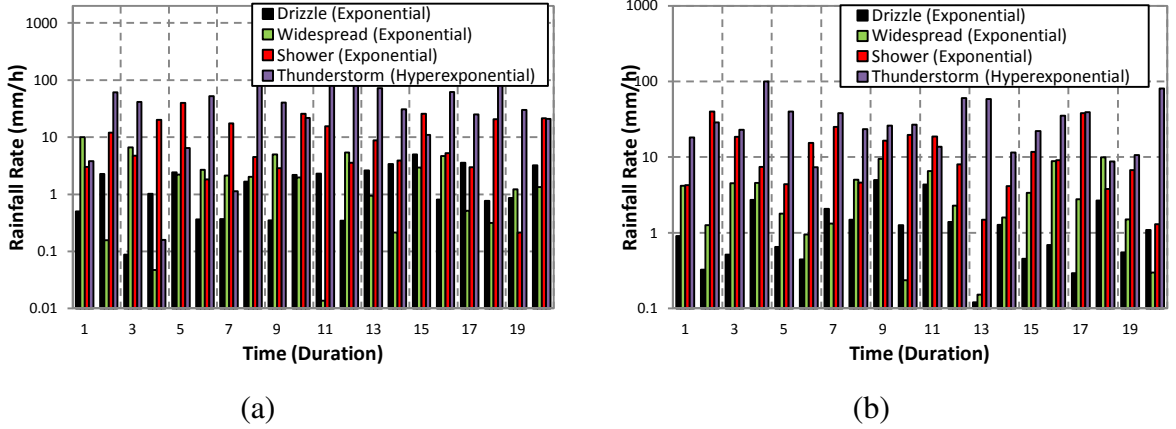
Figure 5-4: Generation of rain spike peaks for Different rain regimes (a) Durban (b) Butare

In Durban, the following parameters of the two-phase model model are: $\Lambda_{p1} = 0.11$, $\Lambda_{p2} = 0.03$, $p_1 = 0.79$ and $p_2 = 0.21$. While in Butare, the parameters are given accordingly as: $\Lambda_{p1} = 0.091$, $\Lambda_{p2} = 0.032$, $p_1 = 0.74$ and $p_2 = 0.26$. In Figure 5-4, the peak appearances of spikes under drizzle, widespread, shower and thunderstorm are generated over hypothetical event durations of 20 minutes. These appearances are randomly generated by applying the equivalent random exponential distribution for spike peaks at both sites.

5.7.2 Relationship between Mean Peak Rainfall Rate and Mean Service Time

The mean power-law relationship between the peak rainfall rate (R_m) and their corresponding mean service time (s_m) for any rain spike without overlap is given by:

$$S_m = \alpha R_m{}^\beta \qquad [minutes] \qquad (5.11)$$

where α and β are the coefficients of the power-law relationship.

By applying regression analysis, the relationships at both locations were observed have different trend as seen in Fig. 5-5. In Durban, the regression coefficients obtained are $\alpha = 12.17$ and $\beta = 0.21$; while in Butare, $\alpha = 19.01$ and $\beta = -0.21$. From Fig. 5-5, it is found that a positive exponent exists for Durban, while, a negative exponent exists for Butare. This confirms the earlier observation that shower and thunderstorm rain events in Butare occur for a relatively shorter time, compared to observations in Durban. The models show that the spike service times at both sites, are close for peak rainfall rates at 3.5 mm/h, while a huge disparity occurs

for peak rainfall rates other than this value. For instance, at 15 mm/h, an averaged spike service of roughly 21.5 minutes and 11.6 minutes are observed in Durban and Butare respectively. Whereas, at say 70 mm/h, spikes generated in Durban could have a life span as much as 30 minutes, while, those in Butare last for roughly 8 minutes. Since the length in spike service time is evidently related to sub-event outage duration in radio links, it is predicted that Durban may
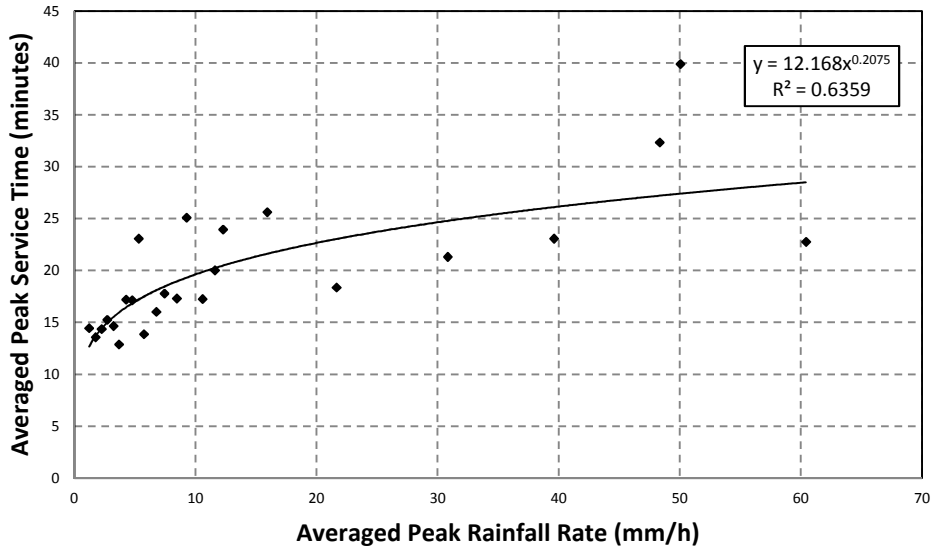
(a)
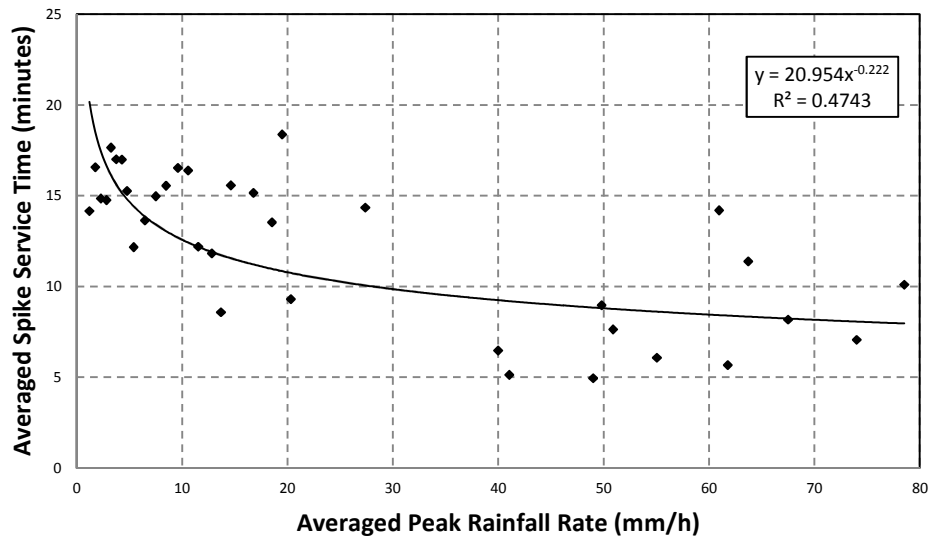
(b)

Figure 5-5: Comparison of spike service time versus peak rainfall rate observed at (a) Durban, South Africa (b) Butare, Rwanda.

witness longer outage periods than Butare. In addition, the rebound time for network recovery (as earlier stated) from rain attenuation effects is predicted to be shorter in Butare than Durban.

5.7.3 Spike Jump Transition Probabilities

The comparison of the spike transition in this subsection follows the earlier discussion in subsection 4.6.4. Table 5-8 presents a summary of results of transition matrices and steady state vector, **q**, obtained from Durban and Butare over three rainfall regimes: widespread (WDS), shower (SHW) and thunderstorm (TST). The transition state matrices are seen at both locations tend to be slightly similar in elemental make-up for each regime. Our interest, however, lies in the steady state vector at each location under different regime. It is observed that the values of *n* are higher in Butare than Durban; this might be an implication of geographical characteristics. This suggests that it takes longer probability *jumps* to attain steady state in Butare. At steady

Table 5-8: Transition Matrices and Steady State vectors in Durban and Butare for rain regimes

REGIME	PLACE	TRANSITION MATRIX	n	q
WDS	DURBAN	$\begin{bmatrix} 0.7528 & 0.2472 \\ 0.6935 & 0.3065 \end{bmatrix}$	4	$[0.7372 \quad 0.2628]$
	BUTARE	$\begin{bmatrix} 0.8286 & 0.1714 \\ 0.4808 & 0.5192 \end{bmatrix}$	10	$[0.7372 \quad 0.2628]$
SHW	DURBAN	$\begin{bmatrix} 0.6839 & 0.1782 & 0.1379 \\ 0.3621 & 0.2069 & 0.4310 \\ 0.3165 & 0.2152 & 0.4684 \end{bmatrix}$	12	$[0.5146 \quad 0.1947 \quad 0.2913]$
	BUTARE	$\begin{bmatrix} 0.6875 & 0.125 & 0.1875 \\ 0.3387 & 0.3871 & 0.2742 \\ 0.2747 & 0.2087 & 0.5165 \end{bmatrix}$	12	$[0.4899 \quad 0.2040 \quad 0.3057]$
TST	DURBAN	$\begin{bmatrix} 0.6071 & 0.0714 & 0.0714 & 0.2500 \\ 0.3750 & 0.2500 & 0.125 & 0.2500 \\ 0.3333 & 0.1111 & 0.3333 & 0.2222 \\ 0.2308 & 0.0769 & 0.3846 & 0.3077 \end{bmatrix}$	10	$[0.4276 \quad 0.0989 \quad 0.2136 \quad 0.2587]$
	BUTARE	$\begin{bmatrix} 0.7273 & 0.0455 & 0.1136 & 0.1136 \\ 0.1000 & 0.2000 & 0.4000 & 0.3000 \\ 0.2250 & 0.1000 & 0.475 & 0.2000 \\ 0.1290 & 0.1290 & 0.4516 & 0.2903 \end{bmatrix}$	14	$[0.3912 \quad 0.0936 \quad 0.3219 \quad 0.1929]$

Table 5-9: Overall Transition Matrices and Steady State vectors in Durban and Butare from overall Data

LOCATION	TRANSITION MATRIX	n	q
DURBAN	$\begin{bmatrix} 0.7105 & 0.2026 & 0.0684 & 0.0184 \\ 0.5234 & 0.2578 & 0.2031 & 0.0156 \\ 0.3182 & 0.2045 & 0.4516 & 0.0227 \\ 0.2308 & 0.0769 & 0.3846 & 0.3077 \end{bmatrix}$	10	$[0.5907 \quad 0.2111 \quad 0.1711 \quad 0.0261]$
BUTARE	$\begin{bmatrix} 0.7473 & 0.1299 & 0.1047 & 0.0181 \\ 0.3790 & 0.4274 & 0.1694 & 0.0242 \\ 0.2595 & 0.1756 & 0.5038 & 0.0611 \\ 0.1290 & 0.1290 & 0.4516 & 0.3077 \end{bmatrix}$	13	$[0.5430 \quad 0.1991 \quad 0.2184 \quad 0.0394]$

state, occurrence probabilities of drizzle and widespread spikes are found to be 73.7% and 26.3% respectively at both locations under widespread events. For shower events, the occurrence probabilities in Durban are 51.5%, 19.5% and 29% are observed for drizzle, widespread and shower spikes compared to 49%, 20.4% and 30.6% respectively in Butare. Thunderstorm events in Durban have occurrence probabilities of 42.8%, 9.9%, 21.4% and 25.9% for drizzle, widespread, shower and thunderstorm spikes respectively. In Butare, the steady state probabilities are 39.1%, 9.4%, 32.2% and 19.3% respectively for the same regimes. The steady state results at both sites comparably appear similar although it is clear that the number of stages required to attain this state varies. From the overall data, the transition matrices and steady state vectors are presented in Table 5-9.

The jumping state transition matrix at both sites under this condition shows that not much difference exists between their characteristics. As for the number of stages required to attain steady state, Butare is observed to have a higher values. During steady, the occurrence probabilities of having drizzle, widespread, shower and thunderstorm spikes are 59.1%, 21.1%, 17.1% and 2.6% respectively. This is compared to 54.3%, 19.9%, 21.8% and 3.94% respectively in Butare. This shows that similarities do exist in the appearance patterns at both locations.

5.8 Rainfall Synthesis from Queueing Approach

The shape of a spike around its peak, generally appears as asymmetrically normal (or Gaussian distribution), with the power spectrum gradually decreasing along its left and right lobes [*Alonge and Afullo*, 2013]. The right and left lobes are side lobes, which can be ignored within the time domain, as they are embedded with noisy components. Rainfall growth patterns are

often probabilistic and each growth point is reliant on the state information of the previous point. Rain growth modelling for rain queues is not a subject within the scope of this study. However, an approximate function to this generate each of this spikes is undertaken using discretized step values representing each spike. This results in an overall queue system of rectangular spikes, with flat peaks. For each of these step values, the rainfall rate is assigned as:

$$R(t) = U_n \quad [mm/h] \text{ for } t_s \in T \qquad (5.12)$$

where T is event period during which n step levels with rainfall rates with values, U_n, are assigned to rain spikes generated within a queue discipline.

The queue disciplines representing each regime are simulated for both locations using MATLAB®. The rain rate peaks from simulations are normalized from their FCFS generation process, according to the bounds of their regime. The simulated plots for each of the regimes are presented in Figure 5-6. Each of the plots consists of 100 spike arrivals, with different queue parameters describing the queue patterns for different regimes at both locations. The rain peak probability process is used to generate the service times, for which arrival times are designated, according to the time domain.

One of the important parameters in this study is the relationship between the number of spikes and their corresponding event duration. The number of spike arrival, γ, whose aggregate sum equals the averaged event duration, T_{ave}, in minutes tends to be highly correlated. This is found to be simply described by a power-law relationship given by:

.

$$T_{ave} = \eta_1 \gamma^{\eta_2} \quad [minutes] \qquad 1 \leq \gamma \leq 100 \qquad (5.13)$$

where the coefficients η_1 and η_2 are values corresponding to spikes generated during a rain event.

The simulated values of the power-law coefficients in (5.13) are obtained by averaging the event duration over 100 iterations, while increasing the number of spike arrivals per simulated event. The coefficients (η_1, η_2) obtained under drizzle regimes in Durban and Butare are (12.37, 0.78) and (13.22, 0.86) respectively. For widespread rains, (14.59, 0.79) and (10.91, 0.83) are also obtained respectively. Under shower conditions, these coefficients are given as (18.43, 0.78) and (8.57, 0.89) at each location, accordingly. Finally, the set of coefficients computed for
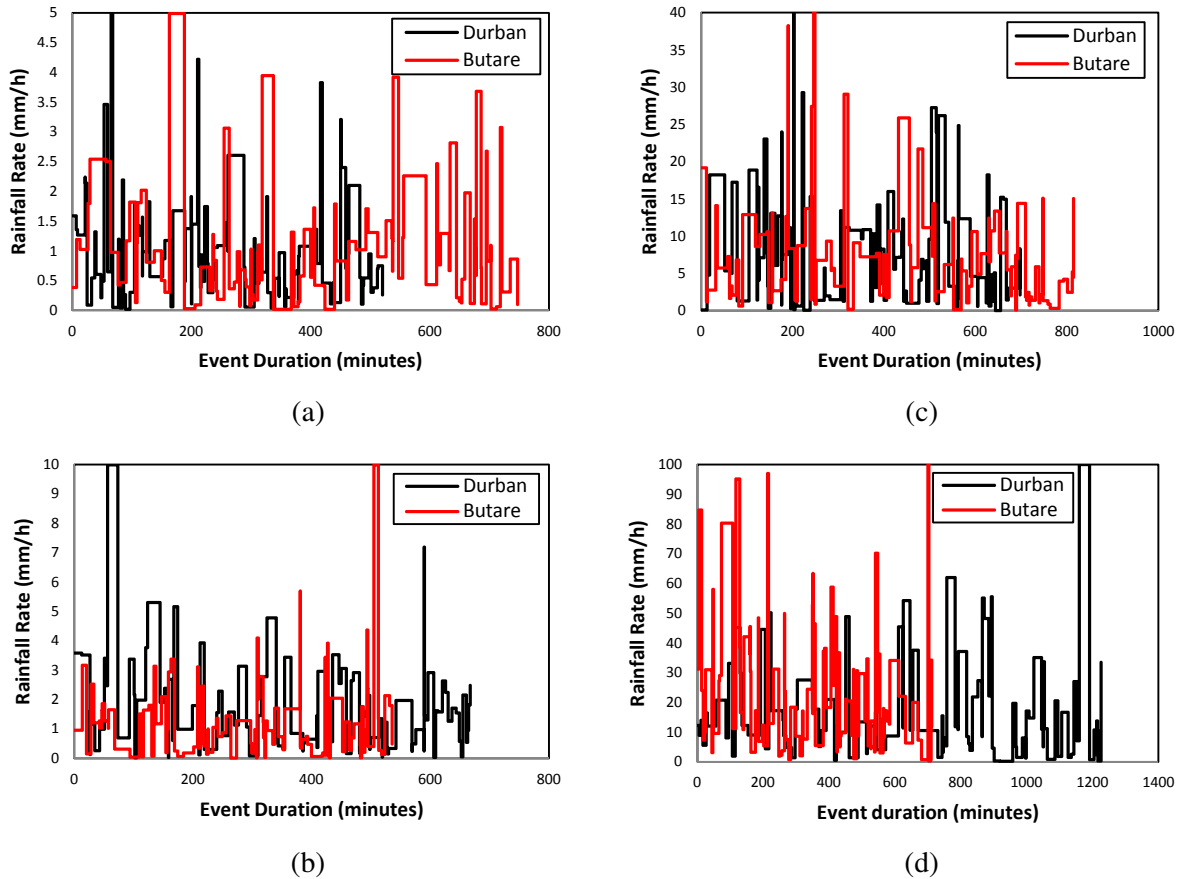
Figure 5-6: Simulated rain events from queue parameters for different rain regimes in Durban and Butare (a) Drizzle (b) Widespread (c) Shower (d) Thunderstorm

thunderstorm rains are (23.37, 0.8) and (7.55, 0.78) respectively. The results from the simulation confirm that event durations at both locations, under different rain regimes, are obviously different. Invariably, we find that for an equivalent number of spikes, drizzle events in Butare tend to last longer compared to the scenario in Durban (see Figure 5-6a). Conversely, thunderstorm events in Durban last longer than seen in Butare, for the same number of spikes (see Figure 5-6d).

5.9 Chapter Summary

In this chapter, it was earlier demonstrated that the rainfall event process over a radio link at equatorial Butare also follow a well-defined queuing pattern which is essentially a semi-Markovian queue discipline. Therefore, rain spike traffic as a single queue entity of rainfall process is found to be generated aperiodically, according to the nature of the rain regime at both investigated sites. More importantly, the distribution of the queue parameters for different proposed regimes in subtropical and equatorial climates tends to vary significantly. While

climatic and geographical factors cannot be completely ruled out in these variations, the overall data tend to exhibit similar queue characteristics. Broadly speaking, it is conclusive to note that the service time for a single spike in Durban increases with attained maximum rain rate. This is in contrast to the observations at Butare, where the spikes at high rain rates tend to have shorter service times. The implication is that rainfall attenuation growth processes in Durban is slower with a high possibility of larger network outage window, especially at severe rainfall conditions with high rain rate. However, the periodic extent to which radio links are affected within a generated spike is dependent on further study of the rain spike growth process. The transition matrices and steady state vectors comparison also indicate that the jump transitions from one state to another are quite similar at the two locations. However, the time required to attain steady state varies irrespective of the regime being considered at both sites. The knowledge of rainfall queue theory over radio links is a prerequisite for the future development of countermeasure paradigm for dynamic rain fade mitigation as this will complement the current ITU-R approach. In the chapter that follows, the queueing theory technique in rainfall is applied to provide knowledge and understanding of rainfall growth processes and rain cell statistics at these two tropical African sites.

CHAPTER SIX

Queueing Theory Application in Rain Cell Estimation

6.1 Introduction

The previous chapter focused on the investigation of rainfall queueing characteristics at equatorial Butare and further comparison with results obtained from subtropical Durban. So far, this thesis has developed and established a queue discipline for rainfall processes which essentially describes rain traffic generated from single unit of rain spikes. However, the proposed queueing approach only provides a template for the natural scheduling of these queue-generated spikes. The queueing theory is however silent on the physical characteristics, representation and appearance of queue-generated rain spikes. Therefore, this chapter will foray into the probability theory and descriptive mathematics of each rain spike as they undergo queueing processes in Durban and Butare. The relationship between rain spikes and rain cell metrics will also be investigated as they both play an important role in the estimation of path attenuation over radio links. The frequency bands under consideration are the microwave and millimeter bands deployed under LOS radio systems. Therefore, the chapter will conclude by comparing the proposed results with link measurements from Durban.

6.2 Sinc Function Descriptions of Rain Spikes

The proposed description of a rain spike in this thesis is essentially an entity governed by a BD process as explained in the queue approach introduction in Chapter four. Thus, standard rain spikes are expected to have an initial time with rainfall rate usually closer to zero. This time gradually peaks up until a maximum rainfall is reached and then gradually slopes down to its initial zero position. As seen in Fig. 6-1, a typical rain spike (also an event) is seen as an initially progressing phenomenon and then later regresses once it attains its peak. The shape of rainfall service time around its peak generally appears asymmetrically normal (or Gaussian distribution) with the power spectrum gradually decreasing along its left and right lobes. Broadly speaking, the representation assumed for generic rainfall duration requires an envelope-like function to understand the shape of time-varying rainfall spike. To this end, *Alonge and Afullo* [2013a] initially proposed a sinc mathematical function, modified as an envelope, in early studies of rain spike. The function is an *n*th-powered sinc model mimicking the shape profile of a typical rain spike and is given by:

$$R(t) = \varphi\,[sinc\,(\beta t)]^n \qquad for\ \varphi \approx 1, \beta > 0\ and\ n > 0;\ \forall t \in \mathbb{Z} \qquad (6.1)$$
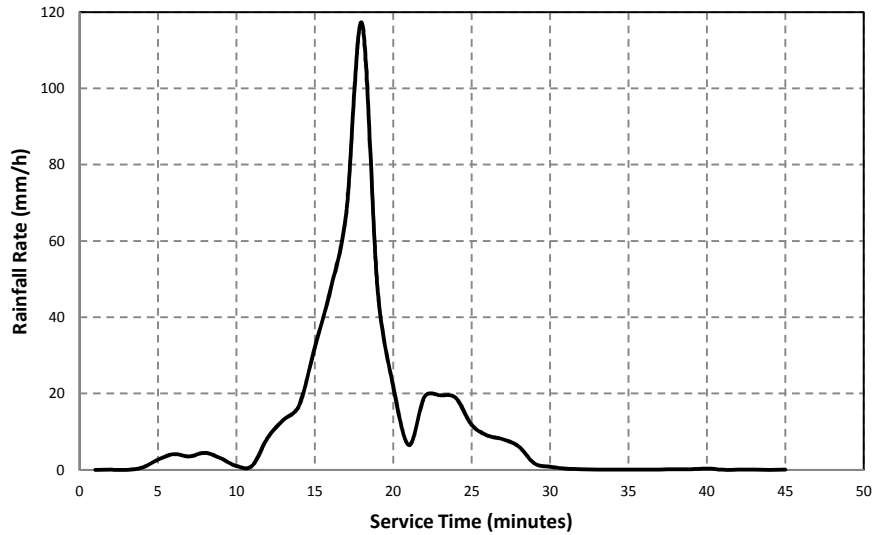
Figure 6-1: Rainfall event at University of KwaZulu-Natal campus on 25th of April, 2009 between 16:34 hrs and 17:19 hrs
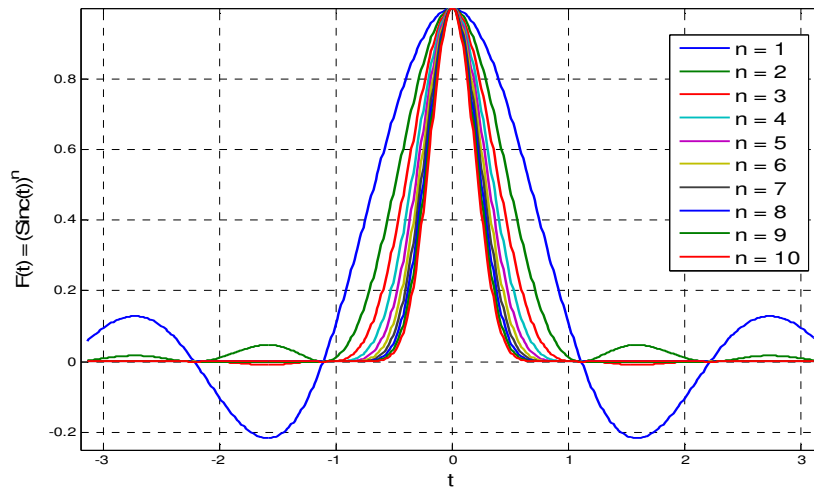
Figure 6-2: Plots of different values of *n* for the *nth*-powered sinc function for $\beta = 0.9$.

where *t* is a random independent variable corresponding to the time progression in minutes. Here, we assume that the random variable varies as the time progresses in the time domain. The constant, φ, is the maximum rainfall rate in the dataset but set to unity for relative rainfall rate. The value, *n*, is the power of the overall sinc function.

The power, *n*, is a very important parameter in determining appropriately, the sinc envelope function. Fig. 6-2 shows the different plots of integer values, *n*, with the sinc function. The idea is to develop the simplest shape profile with a main lobe and side-lobes to approximate the

rainfall process. As seen in the figure, the values of $n = 1$ and 2 both have main lobe and side-lobes. However, the values for which $n \geq 3$ produces flattened out side lobes. These values will increase the side-lobe errors in the model when applied. Therefore, the values of 1 and 2 appear to be the appropriate choices. However, the nth-powered sinc function for the value of $n = 1$ generates some negative values of side lobe components. On the other hand, $n = 2$ generates only positive values of the side-lobes. Therefore, the most ideal value of n for nth-powered sinc function from our observation is 2. It should be noted that the inner product of (6-1) is actually applied in the case of $n = 2$.

6.2.1 Classification of Rain Spike by Sinc Templates

A close observation of rain events in Durban show several sub-events, which are observable spikes, all which follow the typical birth and death processes. Therefore, when rainfall durations are examined, the spike's main lobe which is of primary interest to rainfall attenuation peaks becomes significant. However, the position of the main lobe can be centrally-skewed (with or without side lobes), right-skewed or left-skewed. The main lobes when skewed have side-lobes at adjacent positions. Therefore, four possible templates are assumed for any spike according to (6.1). These templates are described in Table 6-1 by time-bounds imposed on the proposed function. The frequency domain obtained from Fast Fourier Transform (FFT) routine and Welch PSD for these templates are also depicted on Table 6-1. They are described accordingly:

(a) Template A

This template describes a rainfall spike completely specified by a main lobe with left and right side lobes. This template imitates the rainfall for a normal duration with proper rain cell formation. The bounds of the time, t, are defined as $-\pi \leq t \leq \pi$.
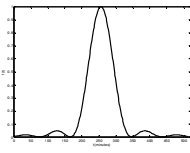
(b) Template B

This template describes a rainfall spike characterized by a right-skewed main lobe with left side lobes. This template represents a spike with a sudden peak towards the end of its life time. The duration bounds are specified by $-\pi \leq t \leq a_2\pi$

(c) Template C

This template represents a rainfall spike for which the spike begins with a sudden peak and some few rainfall rate samples at the end. In this case, the interval for which t exists is given by $-a_1\pi \leq t \leq \pi$.

Table 6-1: Normalized *n*th-powered Sinc function templates for rainfall rate

TEMPLATE	TIME BOUNDS	TIME DOMAIN	FREQUENCY DOMAIN	SPECTRAL DENSITY (PSD)
1. Rainfall duration with a Main lobe accompanied by right and left side-lobes.	$-\pi \leq t \leq \pi$			
2. Left-Skewed rainfall duration with right side-lobes.	$-\pi \leq t \leq a_2\pi$			
3. Right-Skewed rainfall duration with left side-lobes.	$-a_1\pi \leq t \leq \pi$			
3. Rainfall duration with main lobe and no side-lobes.	$-a_1\pi \leq t \leq a_2\pi$			
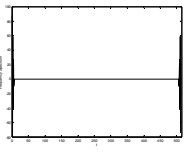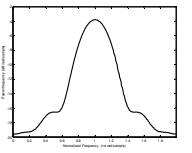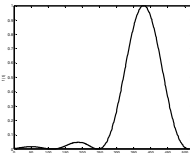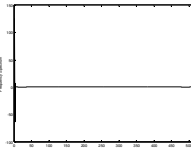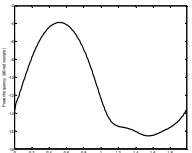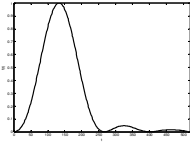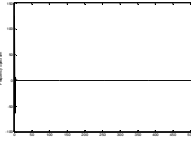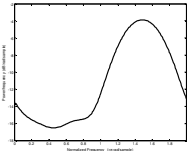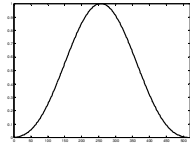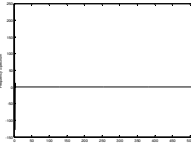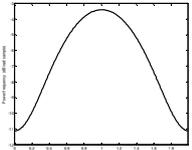
(d) Template D

Sometimes, a rainfall spike can be characterized by a progressive increase (and eventual decrease) in the rainfall rate during its service time. This template can work as an appropriate envelope with bounds of *t* defined by $-a_1\pi \leq t \leq a_2\pi$. In most case, the assumption $a_1 \approx a_2$ may hold for equal side lobes.

The sinc classification is useful for profiling the characteristics shape of rain spikes. The function, however, fails to explain the probability properties involved in its birth and death. This approach therefore fails to highlight the importance of probability theory hypothesis in rainfall queueing process. The next section will discuss the subject of probability analysis of rain spikes.

6.3 Probability Analysis of Rain Spike Characteristics in Queues

As seen in the previous chapters, the queue service time distribution from the datasets obtained in Durban and Butare have been demonstrated to be Erlang-k distributed irrespective of the spike traffic during rainfall. From earlier investigations, the service time defines the lifespan of rain spike generated in the queue process, according to a known queue discipline. It is imperative to understand the probability characteristics of rain spikes as they are the closest representation of the random manifestation of time-varying rain fades. Since rainfall fade is potentially deleterious to satisfactory network performance at microwave and millimeter bands, it is rewarding to investigate its closest representation. By definition, the basic unit of a rainfall event is a single rainfall spike which is generated as an 'unstable' traffic according to certain queue patterns. The manifestation of this queue results in the presence of finite number of spikes in any prevailing rain event with random rainfall rate appearances.

The mathematical approach employed in the understanding of rain spikes in this study, is partly semi-empirical. as it applies knowledge from the empirical results seen in the previous chapter to relevant probability theories. Firstly, a rainfall spike which is an independent entity of a rainfall event follows a BD process is represented as shown in Figure 6-3. Discrete points along the spike $R_n, R_{n+1}, R_k, R_{k+1}$ are identified according to the *birth* and *death* phases. This spike is assumed to follow a symmetrical geometry such that the period required to attain R_m from birth
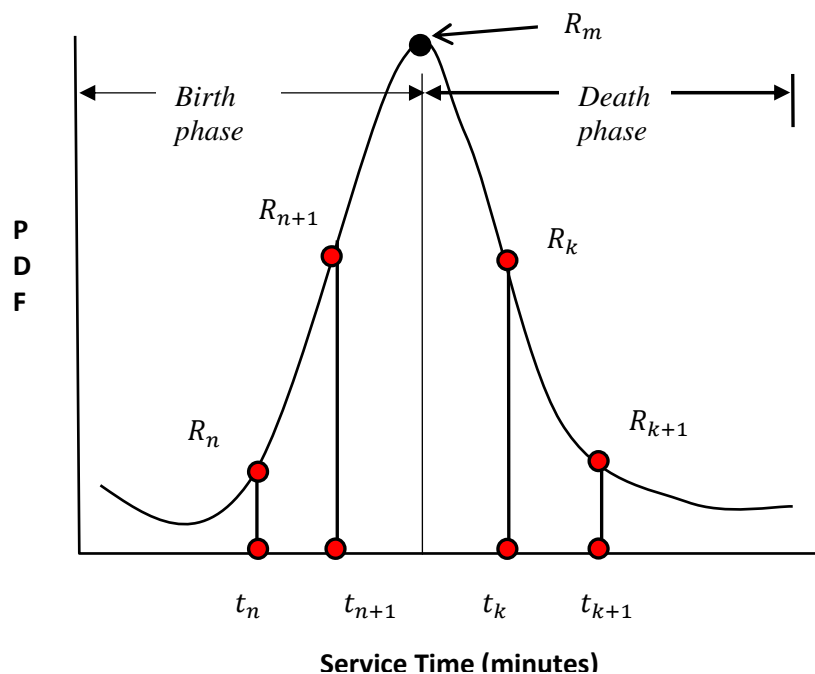
Figure 6-3: Rain spike characteristics in the time domain as obtained in a queue

(growth) is approximately equal to the period required to attain death from R_m. Therefore, the concept of growth rate and death rate is embedded within the characteristics of a rain spike. Mathematically, it follows that the *growth rate* from Fig. 6-3 is defined as:

$$r_g = \frac{1}{\tau_g} = 60 \times \frac{R_{n+1} - R_n}{t_{n+1} - t_n} = \frac{60 \, \Delta R_g}{\Delta t_g} \quad [mm/min^2] \qquad (6.2)$$

,and the *death rate*, is also given as:

$$r_d = \frac{1}{\tau_d} = 60 \times \frac{R_{k+1} - R_k}{t_{k+1} - t_k} = \frac{60 \, \Delta R_d}{\Delta t_d} \quad [mm/min^2] \qquad (6.3)$$

where 60 is time constant required to convert the time base of rainfall rate units in (6.2) and (6.3). So, it turns out that the growth and death rate of any spike attaining a maximum rain rate, R_m, may be related to the second derivative of rainfall accumulation within the same time differential as the unit suggests.

It can be seen that the time instances along a rain spike, $t_n, t_{n+1}, t_k, t_{k+1} \subset t_s$ are such that $t_s = nt_n$. This assumption remains valid if the sampling interval is uniform throughout the rainfall period as obtainable in any measurement process. For any queue process, each rainfall spike is generated according to a M/E$_k$/s/∞/FCFS discipline as seen in previous chapters. Thus, for the service time of any rain spike, the distribution tends to follow a well-defined Erlang-k distribution. From this, it is established that:

$$t_s \sim Erlang(k, \mu_s) \qquad (6.4)$$

where k and μ_s are the Erlang distribution parameters as already defined in this thesis.

Let the individual rain rate points along a rain spike follow a probability process based on a unknown PDF represented by $m(t)$. Along the rain spike, the points tend to follow a growth process, which is strictly a BD process as earlier proposed. During the *birth* process, a rain probabilistic growth process is initiated leading to the successive generation of rain rates in an increasing manner. The growth process reaches its equilibrium at the maximum rainfall rate, R_m, as seen in Fig. 6-3. Thereafter, the generated rain rates start to decline in a probabilistic manner at a certain rate as it approaches its *death*. This is the summary of the lifespan of a

typical spike generated during a queue process. In all, two typical questions suffice: what is the most suitable probability process responsible to describe the BD process of rain rates within a rain spike? What is the relationship of the probability process to the maximum rain rate attained by the spike? According to (6.4), it can be deduced that the probability process of individual rain rates within a rain spike is an extension of the service time distribution. Therefore, it is assumed that for *n* number of rain rate points within a rain spike at birth phase (likewise the death phase):

$$t_n \sim Erlang\left(k_v, \frac{\mu_s}{w}\right) \tag{6.5}$$

where *w* is a fractal constant related to the service rate. It is expected that mean of the distribution given in (6.4) may be approximately equal to the fractal mean of *n*-points linked to the proposed Erlang probability process in (6.5). Therefore, it is proper to conclude that:

$$\frac{\mu_s}{w} \approx v \quad \text{and} \quad k \rightarrow k_v \tag{6.6}$$

So that, the proposed process will follow the service time distribution with parameters advertently related to Erlang distribution such that:

$$m(t; k, v) \cong Erlang(k_v, v) \tag{6.7}$$

Therefore, it follows that the entire array of rain rates within a rain spike follows an Erlang-*k* probability process. This assumption simply implies that the birth and death of an arriving rain spike is masked by a probabilistic function with each generated rain rate points essentially being equal to the product of this function and a constant. Thus, the time-varying rain rate function describing a rain spike characteristics is mathematically given as:

$$R(t) = m(t; k_v, v) \times \Upsilon \qquad [mm/h] \tag{6.8}$$

where Υ is a dimensionless constant related to rainfall rate as will be later explained.

6.3.1 First Approximations of Rain Spike Parameters from Probability Analysis

It has been shown that the Erlang-*k* PDF is a function that offers the descriptive shape of data generated from a random process. In other words, the PDF describing the shape appearance of

a single and queue-generated spike during a rain event can be described by the following statistical relationship:

$$m(t; k_v, v) = \frac{(k_v v)^{k_v} t^{k_v-1} \exp(-k_v v t)}{\Gamma(k_v)} \; [min^{-1}] \quad \text{for } t > 0 \qquad (6.9)$$

where the mean of the PDF in (6.9) is given by:

$$v = \frac{\xi(R_m)}{\psi(R_m)} \qquad (6.10a)$$

The parameter, $\xi(R_m)$, is related to the product of the time index and the corresponding rainfall rates, all within the spike service time. This function is directly fitted to the maximum rain rate of the spike so that:

$$\xi(R_m) = \sum_{n=1}^{t_s} nR_n \approx x_1 R_m{}^{y_1} \qquad (6.10b)$$

where R_n is the rainfall rate at the nth time of the spike growth process.

The parameter, $\psi(R_m)$, is the sum of the rain rates within a single spike instance within the spike service time. Again, this function is fitted to the data by regression so that:

$$\psi(R_m) = \sum_{n=1}^{t_s} R_n \approx x_2 R_m{}^{y_2} \qquad (6.10c)$$

The integer value of k_v is modified from the optimized result for the Erlang-k number of stages as already derived in Appendix E. Therefore, the number of stages is given by:

$$k_v = round\left(\frac{R_m}{0.4488\,\xi\,v}\right)^{2.11} \qquad (6.10d)$$

where all the parameters as seen in (6.10d) have been earlier described.

The approximation of the constants and regression relationships for rainfall spikes as proposed in (6.10a) – (6.10d) are done according to the following procedure:

- The available spike datasets as processed in Durban and Butare as seen in Chapter five is utilized here. As noticed, the datasets for each location are classified according to the four rainfall regimes: drizzle, widespread, shower and thunderstorm.

- The processed data are categorised according to their time series ranges with a time slot header. This is to ensure that time slots allocated to emerging rainfall rates within a spike are matched to their time variations. With this arrangement, the time series, n, becomes the random variable and the rainfall rate, R_n, represents the number of appearances.

- The parameter, $\xi(R_m)$, for each data series is computed by applying the formulation in 6.10b and later fitted by regression to the maximum rainfall rate within the spike.

- The parameter, $\psi(R_m)$, is computed by applying the formulation in 6.10c and also fitted by regression analysis.

- The ratio of $\xi(R_m)$ and $\psi(R_m)$ from data are applied to compute the mean time of each of the spikes according to their time series in different regimes.

Regression analysis is employed in obtaining the required functions and their relationships. The power-law constants, x_1 and y_1, for $\xi(R_m)$, as well as, x_2 and y_2 for $\psi(R_m)$ estimated for different regimes in Durban and Butare are given in Table 6-2. The computed approximate constants are not seen to follow any particular trend for any rain regime as seen on the table. It is however

Table 6-2: Power-law constants for $\xi(R_m)$ and $\psi(R_m)$ for the prediction of rain growth

REGIME	LOCATION	$\xi(R_m)$		$\psi(R_m)$	
		x_1	y_1	x_2	y_2
DRIZZLE	DURBAN	4.84	0.88	25.53	1.21
	BUTARE	4.76	1.03	25.78	0.80
WIDESPREAD	DURBAN	6.41	0.77	36.31	0.87
	BUTARE	5.93	0.92	26.53	1.09
SHOWER	DURBAN	6.11	0.86	32.56	0.92
	BUTARE	5.94	0.88	34.31	0.94
THUNDERSTORM	DURBAN	5.83	0.89	40.46	0.97
	BUTARE	5.09	0.92	18.01	1.09

observed that the $\xi(R_m)$ parameters obtained for widespread and shower rainfalls at both sites are similar. These results seem to suggest that the delineation between these two regimes might be unimportant when comparing their spike characteristics at two locations. For the parameters of $\psi(R_m)$, the x_2 constants tend to be higher in Durban than Butare. This is however not true for the corresponding constants of y_2.

6.3.1.1 Error Statistics of the Proposed Approximation

The error statistics computed to support these approximations are derived from the computed and expected means of the data. The RMSE and χ^2 are the basic error tools applied to describe the deviations of the proposed model from the actual estimation. They are given by:

$$\text{RMSE} = \left[\frac{1}{n}\sum_{i=1}^{n}(v_i - v'_i)^2\right]^{\frac{1}{2}} \tag{4.20}$$

$$\chi^2 = \sum_{i=1}^{n}\frac{(v_i - v'_i)^2}{v_i} \tag{4.21}$$

where v and v' represent the mean from actual data and proposed approximation respectively.

The summary of the error statistics for each rainfall regime at both locations of tropical Africa are presented in Table 6-3. As seen from the statistics, the worst case scenarios of percent RMSE (under thunderstorm regime) is about 14% and 16% in Durban and Butare respectively.

Table 6-3: Error statistics of estimated mean for different rain regimes in Durban and Butare

REGIME	LOCATION	RMSE	χ^2	DF	SL*
DRIZZLE	DURBAN	0.1389	14.5536	203	237.34
	BUTARE	0.1035	2.8444	34	48.60
WIDESPREAD	DURBAN	0.1120	8.6057	180	212.30
	BUTARE	0.1031	5.7070	131	158.71
SHOWER	DURBAN	0.1319	11.3097	195	228.58
	BUTARE	0.1234	9.9795	180	212.30
THUNDERSTORM	DURBAN	0.1422	7.4856	101	125.46
	BUTARE	0.1604	6.9768	77	98.49

*Estimations at 5% significant level of χ^2 statistic

The RMSE in Durban for different regimes are higher compared to the results obtained at Butare except for the case of thunderstorm regime. Each of the compared regimes has different Degree-of-Freedom (DF), hence, different χ^2 statistics are observed at both locations. The approximations are also found to satisfy the data at 5% significant levels (SL) of χ^2 statistic at both locations over different regimes.

6.3.1.2 Variation of Rain Spike PDFs in Durban and Butare over Rain Regimes

Following the proposed distribution to describe the probability of rain rate within a spike as given in (6.9), the variation of these spikes over different regimes is expected to also vary accordingly. Figures 6-4 and 6.5 show the expected PDFs for queue-generated spikes each with different maximum rain rate of different regimes. It is expected that the mean and shape of rain spikes with similar maximum rainfall rates will be different across the regimes at both sites. This is so because the climatic conditions responsible for the queueing characteristics in each regimes is slightly different, even in the presence of similar cloud advection velocities.

(a)

(c)

(b)

(d)
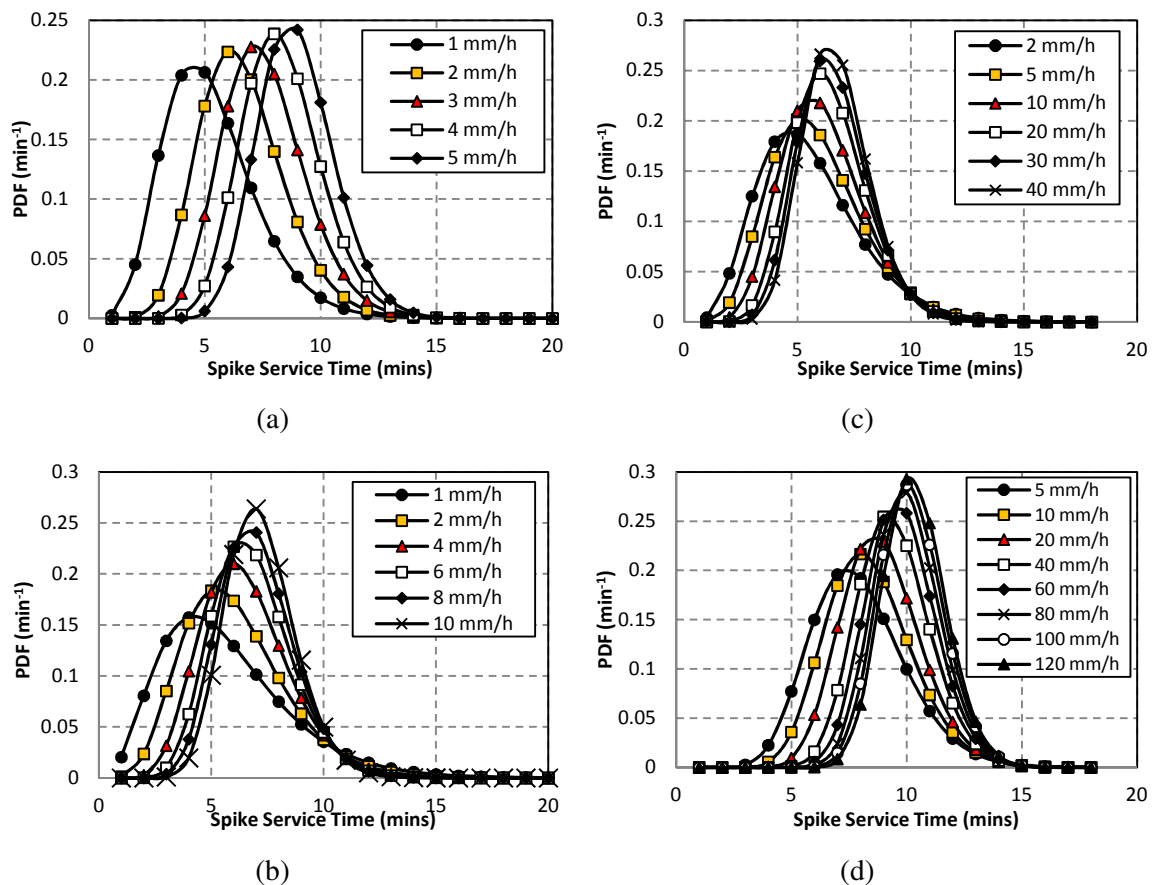
Figure 6-4: The PDF of rain spike growth for four regimes in a queue-generated process in Durban: (a) drizzle (b) widespread (c) shower (d) thunderstorm
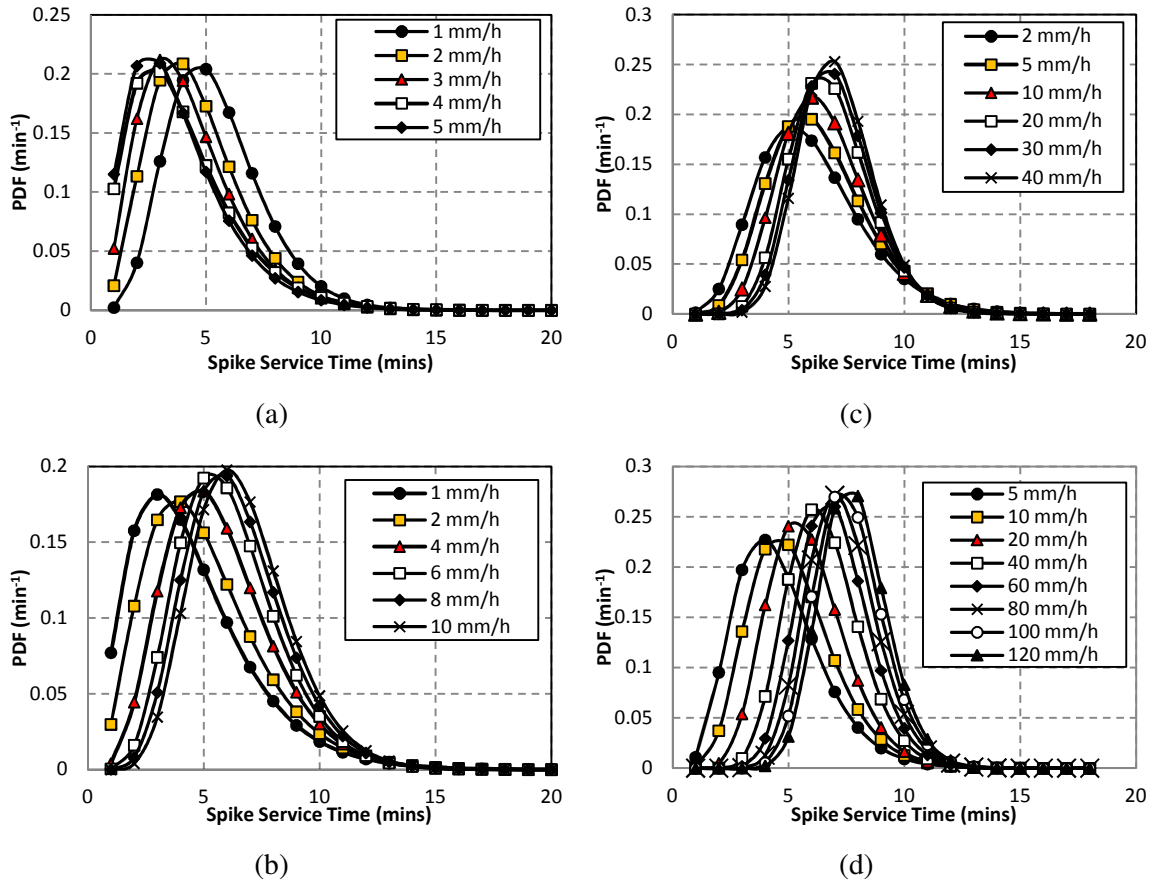
Figure 6-5: The PDF of rain spike growth for four regimes in a queue-generated process in Butare (a) drizzle (b) widespread (c) shower (d) thunderstorm

For the PDFs of generated spikes in Durban as seen in Fig. 6-4(a)-(d), the mean of the spikes are observed to shift rightwards from drizzle to thunderstorm regime for the same rain rate. The skewness of the PDFs is therefore increasingly rightward for the same rainfall in different regimes. For example, for a rainfall rate of 5 mm/h, the PDF mean are given as 5.6, 5.9, 6.3, 7.8 minutes for drizzle, widespread, shower and thunderstorm regimes respectively. As expected, the peaks of each PDF increases for each regime as the rain rate increases. This is valid as peaks attained by each spike increases with rainfall rate. Finally, it is seen that the spike mean could be as high as 10 minutes for PDFs of 120 mm/h indicating longer service time as earlier proposed.

At Butare, the PDF of the generated spikes plots are seen in Figure 6-5. At Butare, the PDFs for similar rain rates do not follow any trend as observed for the results in Durban. However, the PDFs are right-skewed as observed in Durban with their mean time mainly shifting rightwards also. At 120 mm/h, the mean of the PDF at Butare may not be 8 minutes in comparison to 10

minutes in Durban. The PDF peaks are seen to increase with rainfall rate for all regimes except in the case of drizzle rainfall where the peaks are similar for rainrates < 5 mm/h. Broadly speaking, the rightward shift of the mean of the service time at both sites simply confirms that the mean service time increases with rainfall rate.

6.3.2 Rain Growth Function in Durban and Butare

The actual rainfall time series for each spike can be generated from (6.9) once the Erlang-k PDFs are normalized so that the maximum value within the PDF at any time is always exactly *unity*. This is equivalent to scaling the PDF function by a particular constant to obtain the required shape function. Therefore, the expression in (6.9) when scaled is modified, yielding:

$$R(t) = \frac{m(t; k_v, v)}{max\{m(t; k_v, v)\}} R_m \quad [mm/h] \tag{6.11}$$

From (6.11), the constant, Υ, is given as the ratio of the maximum rain rate, R_m, and the maximum value of the PDF, $max\{m(t; k, v)\}$. Thus, we have:

$$\Upsilon = \frac{R_m}{max\{m(t; k_v, v)\}} \tag{6.12}$$

Therefore, the functional relationship describing the rainfall rate time series of any constituent rain spike in a rain event is a modified Erlang-k distribution, given by:

$$R(t) = \frac{\Upsilon(k_v v)^{k_v} t^{k_v - 1} \exp(-k_v vt)}{\Gamma(k_v)} \quad [mm/h] \tag{6.13}$$

where all parameters and variables in (6.13) have been previously defined.

6.3.3 The M/E$_k$/s Queue Scheduling and Rainfall Synthesis Revisited

In Chapter five, rainfall synthesis is simulated using rectangular spikes since the knowledge of the spike shape characteristics was unknown. In this sub-section, however, the synthesis is undertaken by applying the proposed function in (6.13) to replace the rectangular spikes. The constants for each of the parameters are already provided in the relationships in Table 6-2. The block diagram in Figure 6-6 highlights the procedure required to successfully generate M/E$_k$/s queues for rainfall synthesis. To schedule the queues according to their queue discipline at both

locations, the queueing results from Chapter four are also applied for the four rainfall regimes considered. Figure 6-7 shows the graphs for the simulated queue scheduling of 10 spikes in Durban and Butare. This scheduling leads to different event durations for the same number of spikes as seen in Chapter five. Again, rainfall duration for the same number of spikes is seemingly longer in Durban for thunderstorm events and shorter for drizzle events (Figs. 6-7a
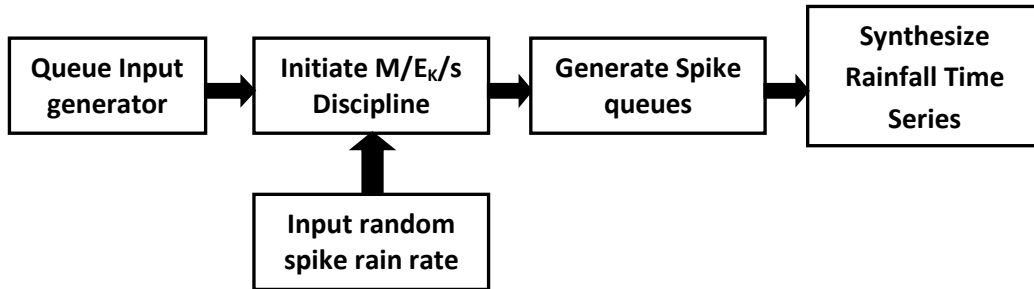
Figure 6-6: Queue scheduling procedure for rainfall synthesis of M/E$_k$/s queue discipline
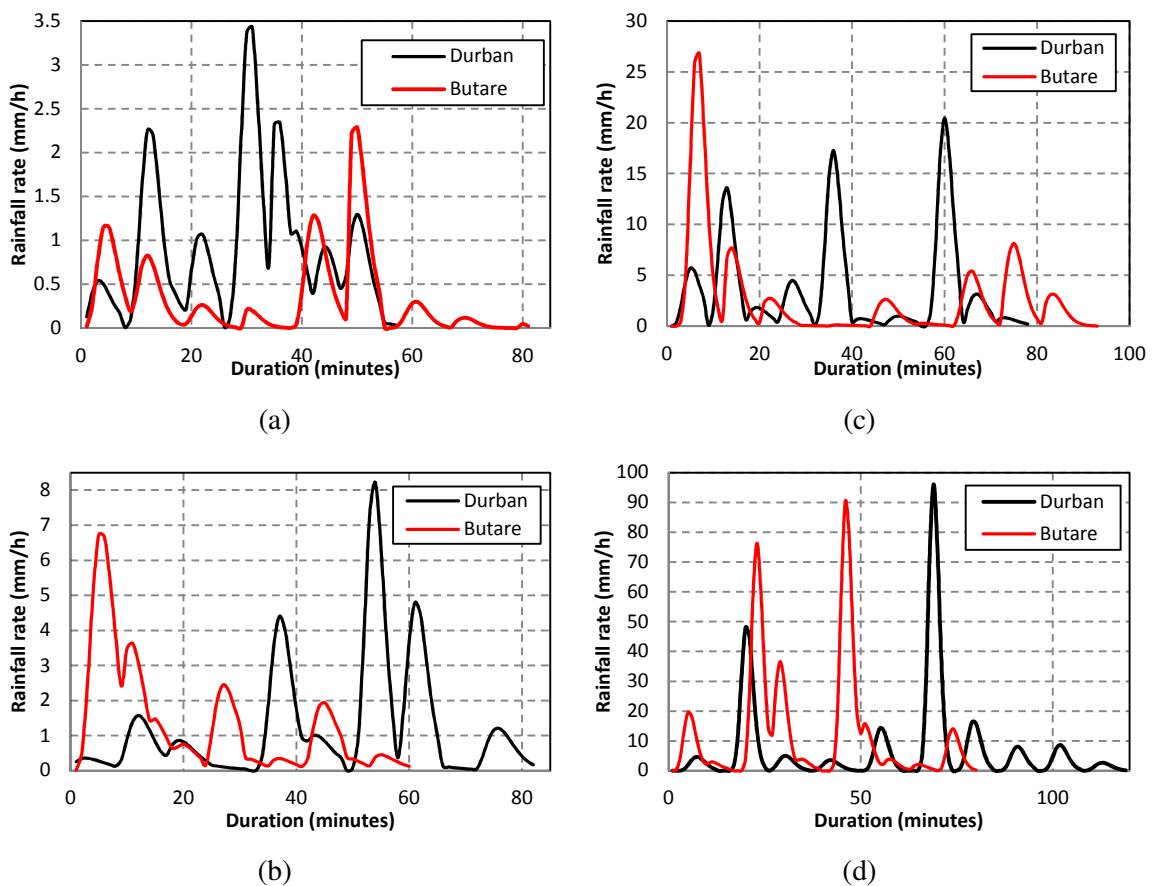
Figure 6-7: Rainfall synthesis with Erlang-k generated rain spike parameters in Durban and Butare (a) Drizzle (b) Widespread (c) Shower (d) Thunderstorm

and 6-7d), compared to observations at Butare.

The knowledge of rainfall synthesis through the queueing approach will be particularly useful in heuristic channel modelling of wireless networks, a subject beyond the scope of this thesis. However, it can also be utilized in the solving of multiple rain cell scenarios in radio links.

6.4 Estimation of Rain Cell Sizes from Queueing Theory
6.4.1 Introduction to Circular Rain Cell Theory

An important aspect of rainfall attenuation studies is the presence of rain cells over radio links. Rain cell is a generic term describing the horizontal and vertical planar area occupied by rain droplets, within the transmission path of a radio link. The determination of rain cells have been researched in a number of studies [*Bryant et al.*, 2001; *Melsheimer et al.*, 2001; *Feral et al.*, 2003; *Akuon and Afullo*, 2011a; *Akuon and Afullo*, 2011b]. In this current approach, a simplistic approach involving Birth-Death (BD) technique of rainfall spikes is applied. For simplicity, the arrival and departure of rain spikes are associated with rain cell motion over a radio link.

In a typical rain event, rain cells are propelled by advection velocities which allow them to move from one point to another within a communication link. When seen from space borne radar images, rain cells usually appear as shadowed circular patterns defining radar signatures. As explained by [*Melsheimer et al.*, 2001] different signatures and resolutions of rain cells symmetry can be obtained by using different target frequency bands. The general consensus of rain cell shape approximation as being circular is noticeable when viewed from the radar, and is accepted by a number of researchers [*Feral et al.*, 2003; *Karlinsky and Morin*, 2006; *Pontes et al.*, 2007]. Equally, researchers have proposed other complex shape approximations with improved rain cell geometries, such as EXCELL and HYCELL [*Capsoni et al.*, 1987; *Feral et al.*, 2003]. Interestingly, the HYCELL method has proposed Gaussian approximations for convective rain cells and exponential approximations for stratiform rain cells [*Feral et al.*, 2003]. It is a common knowledge that horizontal rain cells are formed as passing rain clouds produce rainfall which often intercept radio links [*Bryant et al.*, 2001; *Melsheimer et al.*, 2001; *Feral et al.*, 2003; *Akuon and Afullo*, 2011a; *Akuon and Afullo*, 2011b]. When a communication link is intercepted, especially at microwave and millimeter wave, there is always an outage probability due to rainfall attenuation [*Bryant et al.*, 2001]. Hence, rain cells play a significant role in the determination and understanding of rain attenuation.

The circular approximation for rain cell shapes, unlike the elliptical shape proposed in HYCELL is the simplest and most easily implemented shape. This shape assumes equal axial dimensions everywhere in the rain cell such that the diameter is equivalent to the Rain Cell Diameter (RCD). Investigation on RCDs have found that they inversely related to the rainfall rate [*Bryant et al.*, 2001; *Akuon and Afullo*, 2011a] Mathematically, the circular RCD, D_c, at any given location is represented by a negative power-law function given by:

$$D_c = \varphi R^{-\beta} \ [km] \quad \text{for} \quad \alpha, \beta > 0 \tag{6.14}$$

where value φ and β are power-law coefficients related to the (6.14) with rainfall rate of R.

From (6.14), it follows that the Rain Cell Area (RCA) is defined as the coverage area of the rain cell and mathematically follows a circular geometry given by:

$$D_a = 0.25\pi\varphi^2 R^{-2\beta} \quad [km^2] \tag{6.15}$$

On measurement, space-bourne radar often provides good image correlation, while the use of ground rainfall data may be useful in ascertaining time constraints and progression associated with moving rainfall cells [*Ajayi et al.*, 1996]. In this case, a rain gauge, distrometer or ground radar may be required [*Karlinsky and Morin*, 2006; *Begum et al.*, 2006]. Radars can also be space borne as an embedded part of a satellite framework; this scenario allows for better correlation of the underlying shapes from space.

6.5 Determination of Horizontal Rain Cell Sizes in Durban and Butare

The use of rainfall time series data to estimate rain cell distances was first proposed in the work of *Drufuca* [1974] in the conceptualization of the Synthetic Storm Technique (SST). The SST is a method of converting rainfall rate time series data into rain attenuation data over terrestrial links at any transmission frequency. This technique was later developed for rain attenuation estimation over Earth-space link in a series of published works by *Matricciani* [1996], *Matricciani and Riva* [2005] and *Matricciani* [2008]. Of particular interest to rain cell estimation is the concept of transforming the time elements, corresponding to values of rainfall in the time domain, into Rain Cell Diameter (RCD). To achieve this, the concept of *translation velocity*, also known as *advection velocity* is employed in the generation of RCDs. The implementation of SST requires ground measuring equipments capable of measuring rainfall

rate at a practical sampling interval. In this current study, the ground instrument applied is the JW RD-80 impact distrometer in Durban and Butare.

The distance gained by arriving rain rates, within the travelling rain clouds, towards the observation point is equivalent to the RCD. This diameter, D_c, is estimated from the advection velocity, V_a, assigned to the moving cell (or cloud) by translation as applied in the studies of *Drufuca* [1974], *Matricciani* [1996], *Begum et al.* [2006] and *Akuon and Afullo* [2011a]. This gives the mathematical relationship given by:

$$D_c = \sum_{i=0}^{N-1} 0.06 V_a t_{N-i} \; [km] \quad \text{for } t \in T \qquad (6.16)$$

where t_{N-i} is the reverse successive point along each spike as they appear in the time series and N is the total number of discrete rain rates within the spike.

The eventual RCDs corresponding to the rainfall rate in the time domain is estimated as a *reverse cumulative sum* i.e. based on a last come, first sum approach (see (6.16)). This is undertaken by adding the translated distances (or RCDs) of a cell (spike) starting from the moment a maximum rainfall rate, R_m, is attained to the point of its birth (or conception) . The advection velocity, V_a, is assigned in (6.16) based on the Stratiform-Convective (S-C) rain rate bound, R_{th}, identified in Durban and Butare:

$$V_a = \begin{cases} 6 \, m/s & \text{for } R \leq R_{th} \\ 10 \, m/s & \text{for } R > R_{th} \end{cases} \qquad (6.17)$$

The typical values of R_{th} can be found using radar reflectivity algorithm of *Gamache and Houze* [1982]. This algorithm ensures that the S-C bound at any region, from rainfall measurements, is exactly at 38 dBZ. This algorithm was applied earlier in Chapter three where R_{th} in Durban is found to correspond to 11.34 mm/h and that at Butare, 8.84 mm/h, over the entire rainfall measurement period.

6.5.1 Influence of Rain Cell Arrival Angles over Horizontal Planes

The arrival angle of the circular rain cell is also very important in estimating the optimal length factor of the link required for rain attenuation prediction. The queue-generated circular cell

propelled by the advection velocity can approach the terrestrial link in different ways, each presenting a unique problem. Let the transmitter (A) and receiver (B) be bounded by a logical circle whose diameter is equivalent to their path length. Then, an approaching queue-generated rain cell can appear anywhere within the wireless network from any direction as seen in Figure 6-8. In this figure, the red circular line signifies the transmission area and the black dotted circular lines indicate the arriving rain cells. These possible scenarios are categorized into three scenarios will be briefly discussed:

(a) CASE I: Rain cell queues approaching the radio link as a parallel traffic

This case presents the propelling of circular cell queues in direction parallel to the circular transmission area. In this scenario, it is envisaged that the rain cells moves along the entire path length of the transmission area, hereby leaving trails of rainfall droplets along the link. The reference angle of arrival is *zero* in this case.

CASE I
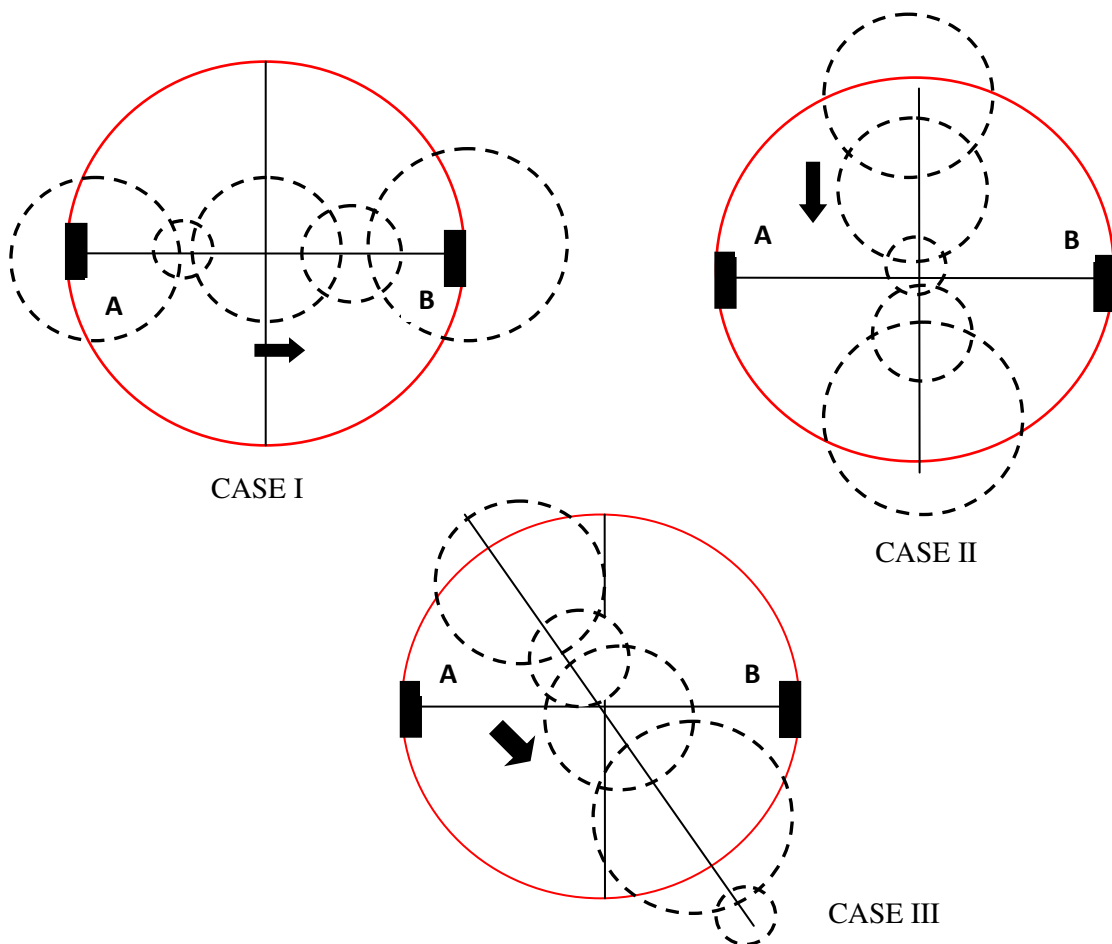
CASE II

CASE III

Figure 6-8: Scenarios of queue-generated rain cells moving over wireless radio link

(b) CASE II: Rain cell queues approaching the radio link as a perpendicular traffic

When the rain cells approach the transmission area in a direction perpendicular to the actual diameter of the transmission area, the reference angle of arrival is approximately 0.5π *rad* or $90°$ to the horizontal. In this scenario, a fractional part of the transmission area is affected.

However, this is dependent on the radio link path length (transmission diameter) and the rainfall type. If the rain type tends to be increasingly convective (shower or thunderstorm) and the path length is long enough, only part of the link may be affected. If the rain type is however stratiform in formation, the influence of the path length range may be neglected as the entire radio link may eventually be affected over time.

(c) CASE III: Rain cell queues approaching the radio link at an angle

This scenario is similar to the perpendicular case except that the angle of arrival of rain cell queues may be $< 90°$ or $> 90°$. The same conditions are present as seen in Case II with fractional affected transmission area dependent on the path length and rain types.

Evidently, Case I appear to be the worst case scenario as the cell queues or moves along the radio link in a parallel manner. This simply means that the entire path length may mostly be covered by rainfall. Path attenuation due to rainfall is expected to be higher in this scenario as all the generated rainfall cells are actively mobile along the radio link. This parallel case is therefore assumed throughout the study of rain cell estimation in this study.

6.5.2 Empirical Determination of Single Rain Cell Sizes

The measurements from the distrometer rainfall database are used to generate the RCDs corresponding to each rain spike. By applying the equations given in (6.16) and (6.17), the RCD in Durban for shower and thunderstorm regimes are estimated. On computing the RCDs, data sorting is undertaken in a descending order according to their rainfall rates. The grouped data is averaged over similar rain rates, and the mean RCD is obtained from the data. In this way, similar mean rain rates and related RCDs are retrieved from the data. This procedure is repeated for samples according to the proposed rainfall rate classes. A relationship between rainfall rate and the RCD is established for data categories by applying regression technique at both sites as shown in Figures 6-9 and 6-10. From the plots in these figures, it is deduced that slightly different relationships exist for the RCD relationships under these two scenarios. These relationships for different regimes are further discussed.
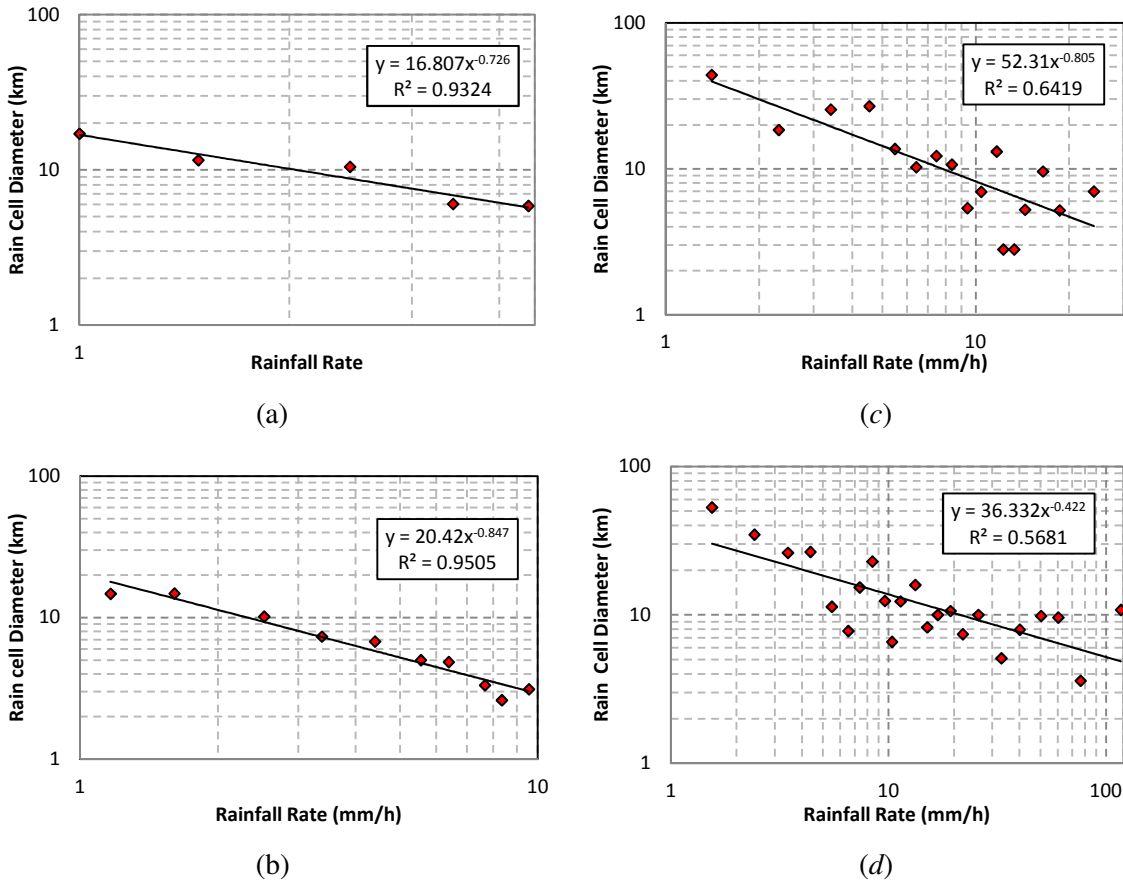
Figure 6-9: Regression fitting technique of collected samples for RCD dependence on rainfall rate in Durban: (a) Drizzle (b) Widespread (c) Shower (b) Thunderstorm
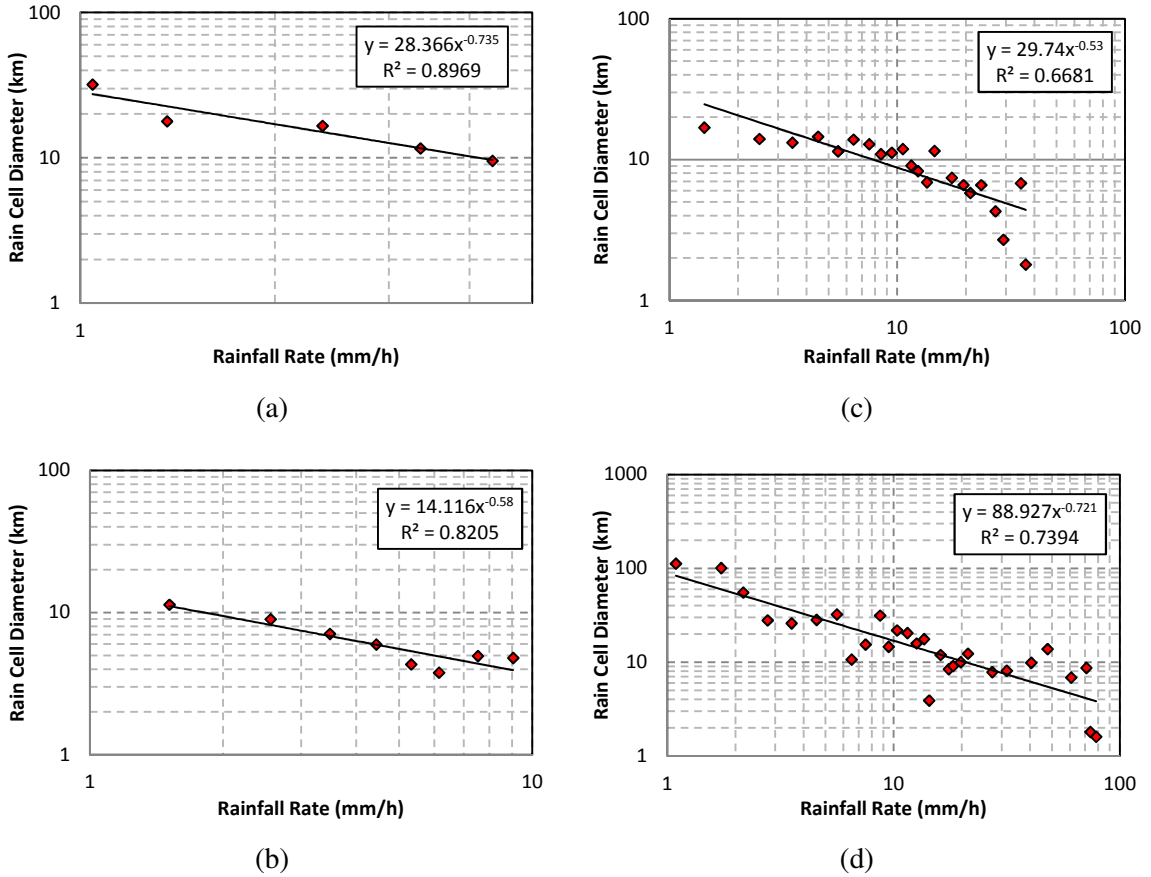
(a) DRIZZLE

The regression fitting results from Figure 6-9 show that drizzle rains in Durban tend to have smaller RCDs compared to those at Butare. The RCDs estimated from data are given as:

$$\text{Durban:} \quad D_c = 16.81R^{-0.726} \; [km] \quad \text{for } R < 5 \; mm/h \quad (6.18a)$$

$$\text{Butare:} \quad D_c = 22.87R^{-0.55} \; [km] \quad \text{for } R < 5 \; mm/h \quad (6.18b)$$

From the previous queue results, the mean service times for drizzle spikes in Durban and Butare may not exceed 12.38 and 13.71 minutes respectively. These values suggest similarities in their lifecycles which is also reflected in their estimated RCDs at Butare which is seen to be larger by about 4 km compared to Durban. Using (6.18a) and (6.18b), it is estimated that spikes with peak rain rates at 5 mm/h have diameters of about 5.23 and 9 km in Durban and Butare respectively. Drizzle cells generated within drizzle events are particularly noted to have shorter diameters

Figure 6-10: Regression fitting technique of collected samples for RCD dependence on rainfall rate at Butare: (a) Drizzle (b) Widespread (c) Shower (b) Thunderstorm

partly because they have shorter durations. A drizzle event has quite a number of such spikes – larger in population in comparison with thunderstorm events. A large population of these small drizzle cells, succeeding one another according to a queue discipline, tends to make drizzle events to generally last for a longer period.

(b) WIDESPREAD

For widespread rain regimes, the regression (6.9b) and (6.10b) from measurements gives RCDs as follows:

$$\text{Durban:} \quad D_c = 20.42R^{-0.85} \ [km] \quad \text{for } 5 \leq R < 10 \text{ mm/h} \quad (6.19a)$$
$$\text{Butare:} \quad D_c = 14.12R^{-0.58} \ [km] \quad \text{for } 5 \leq R < 10 \text{ mm/h} \quad (6.19b)$$

These results show that the RCDs at both sites have about 1 km difference with Butare having larger values with respect to the rainfall rate. In Durban, not much difference is observed in the

RCDs computed for drizzle and widespread rainfalls less than 5 mm/h. At 10 mm/h, RCD in Durban is about 3 km, compared to almost 4 km, at Butare. Queue results show that the mean service time of spikes (cells) at both locations are very close at roughly 16 minutes. This could explain the minute difference in their computed RCDs at all rain rates.

(c) SHOWER

For rain events where the maximum rain rate is 40 mm/h, rain cells are expected to possess characteristics between stratiform and highly-convective rainfalls. Results from regression analysis in (6.9c) and (6.10c) are given as:

$$\text{Durban:} \quad D_c = 52.31R^{-0.8} \ [km] \qquad \text{for } 10 \leq R < 40 \text{ mm/h} \qquad (6.20a)$$
$$\text{Butare:} \quad D_c = 29.74R^{-0.53} \ [km] \qquad \text{for } 10 \leq R < 40 \text{ mm/h} \qquad (6.20b)$$

Therefore, RCDs at Butare are shown to be about 2 km larger at low rain rates (< 5 km) and 2 km smaller at high rain rates (> 25 km).

(d) THUNDERSTORM

Cells generated within thunderstorm regimes have the widest range of rainfall rates and represents the typical scenario of a complete cell. From the processed data, the RCDs obtained are thus given:

$$\text{Durban:} \qquad D_c = 36.33R^{-0.42} \ [km] \qquad \text{for } R \geq 40 \qquad (6.21a)$$
$$\text{Butare:} \qquad D_c = 88.93R^{-0.72} \ [km] \qquad \text{for } R \geq 40 \qquad (6.21b)$$

From the functions at (6.21a) and (6.21b), it is observed that at about 2 mm/h, the RCD in Durban is about 27 km compared to 54 km at Butare. However, at 100 mm/h, the RCD in Durban is roughly 5.25 km compared to 3.23 km at Butare. This suggests that rain cells with smaller peak rainfall rates under thunderstorm regime tend to have a larger diameter and hence, cell areas. As rainfall rate increases, the rain cells at Butare tend to become smaller compared to observations in Durban. An intersection of the functions at both sites is seen to occur at 20 mm/h. It is conclusive to note that rain cells in thunderstorm events tend to give the best representation of RCDs at both sites, and hence, is more suitable to be applied as the general model.

6.5.2.1 Consistency of Proposed Rain Cell Models

To verify the consistency of the proposed thunderstorm RCD models in Durban and Butare are compared with the *Bryant et. al* [2001] model for tropical regions. The *Bryant et al.* model was developed with measurements from Lae, Papua New Guinea (6°44'S, 147°E), a highly tropical location. The precipitation rate at this location is very significant such that the annual $R_{0.01}$ often exceeds 100 mm/h. From the rainfall research carried out on this location, it is observed that shower and thunderstorm rainfall will be much more intense. The proposed thunderstorm models for the two African sites are compared with this location as seen in Table 6-4. In addition, the initial results of circular RCDs obtained from Durban by *Akuon and Afullo* [2011a] are also compared. The comparison undertaken shows that current results obtained in Durban using the single cell approach compare well with the initial results of *Akuon and Afullo* [2011a]. In comparison with the results of rapid decaying RCD results from Lae, current results show a slowly decaying rain cell in Durban and Butare instead. In addition, it can be seen that more tropical locations at Butare and Lae have larger RCDs at lower rain rate, higher rain rates have smaller RCDs compared to two Durban estimations on Table 6-4.

It is conclusive to deduce from these results that tropical and equatorial locations, when compared to subtropical locations, have larger RCDs at low rain rates and smaller RCDs at high rate. The overall climatic characteristics at these locations, coupled with proximity to the equator are advantages at these locations. In addition, geographical features cannot be ruled as a factor.

Table 6-4: Comparison of proposed thunderstorm RCD with existing models

RAINFALL RATE (mm/h)	PROPOSED RCD ESTIMATES [km]		OTHER RCD MODELS [km]	
	DURBAN	BUTARE	Akuon & Afullo [2011a]	Bryant et al. [2001]
5	18.48	27.91	24.33	49.29
10	13.81	16.95	17.68	21.45
20	10.32	10.29	12.86	9.34
30	8.71	7.68	10.67	5.74
40	7.72	6.25	9.35	4.06
50	7.03	5.32	8.43	3.11
60	6.51	4.66	7.76	2.49
70	6.09	4.17	7.23	2.08
80	5.77	3.79	6.79	1.77
90	5.49	3.48	6.44	1.54
100	5.25	3.23	6.13	1.35
110	5.05	3.02	5.87	1.21
120	4.86	2.83	5.64	1.09

6.6 Computation of Length Factor For Single Spikes over Radio Links

The *reduction factor*, now known as the *length factor,* in the ITU recommendation is an important parameter utilized for estimating path attenuation due to rain [*ITU-R P.530-15*, 2013]. In this recent recommendation of ITU, the length factor is dependent on four parameters namely: frequency, rainfall rate, radio link distance and specific attenuation coefficient. This function is given by:

$$r = \left[0.477 d^{0.633} R_{0.01}{}^{0.073\alpha} f^{0.123} - 10.579(1 - exp(-0.024d))\right]^{-1} \qquad (6.22)$$

where d is the radio link distance, $R_{0.01}$ is the rain rate exceeded at 0.01% of the time, f is the transmission frequency of the link and α is the exponent of the specific attenuation function.

In link budget planning, distance limitations are often encountered in the microwave link systems for line-of-sight designs. Thus, it is usual to put into cognizance, the degrading Fresnel conditions, in the estimation of the length factor. It follows from the derivation of rain cell sizes that the length factor can be implemented. Based on this study, the empirical length factor is dependent on the rain cell size and link distance. This is given by:

$$r = \frac{\eta D_c}{L + D_c} \qquad (6.23a)$$

where,

$$\eta = \xi_1 L^{-\xi_2} \quad for \quad L < 50\ km \qquad (6.23b)$$

$$\xi_1 = a_1 R^{-b_2} \quad and \quad \xi_2 = a_2 R^{-b_2} \qquad (6.23c)$$

where L and R are the link path length and rainfall rate respectively.

Unlike the current ITU-R length factor function in (6.22), the proposed length factor from our study is independent of transmission frequency. These results were fitted for link distances up to 50 km (for an assumed height of 150m above sea level), since this is the upper bound distance required for optimal microwave link performance, in the Fresnel region. The obtained results for each classified regimes in Durban fitted for rain rates above 2 mm/h and link distances greater than 5 km are presented in Table 6-5.

Table 6-5: Parameters of length factor from rain cell sizes in Durban and Butare

RAIN REGIMES	$r = \xi_1 L^{-\xi_2}$ for 5 km $\leq L \leq$ 50 km	
DURBAN	$\xi_1 = 10.89R^{-0.49}$	$\xi_2 = 0.59R^{-0.33}$
BUTARE	$\xi_1 = 14.89R^{-0.354}$	$\xi_2 = 0.80R^{-0.229}$

6.7 Prediction of Path Attenuation due to Rain in Durban

For this study, the specific attenuation is computed using the modified gamma DSD model already given cited in (2.17) with annual parameters from the data from Durban and Butare. The μ in this expression is set to 3 and the other parameters of this model (N_m and Λ) obtained for the two sites are provided in Table 6-6.

The specific attenuation due to precipitation, over the entire diametric spectrum of rain drops is provided in given in [*Ajayi et al.*, 1996] as:

$$\gamma = 4.343 \times 10^{-3} \sum_{i=1}^{20} N(D_I)Q_{ext}(D_i)\Delta D_i \quad [dB/km] \qquad [6.24]$$

where $N(D_i)$ is the rain DSD, $Q_{ext}(D_i)$ is the extinction cross section in mm^2 and ΔD_i is the diameter interval in mm. The Mie technique is dependent on the ambient temperature in Durban which is assumed as 20°C in this study as discussed in sub-section 2.5.1. The parameters for Mie coefficients from regression analysis in Durban are given in Appendix C at 20°C in Durban. This same temperature is assumed at Butare since the annual temperature is roughly about 20°C.

The path attenuation over a radio link is computed by referring to *ITU-R P.530-15* [2009] conditions where:

$$A_p = r\gamma L \quad [dB] \qquad (6.25)$$

where the parameter γ is the specific attenuation due to rain in dB/km and r is the length factor already provided in (6.23a).

The predictions are compared with the closest terrestrial link measurements undertaken in Durban in 2004. The link transmits over a path length of 6.73 km, while operating at a transmission frequency of 19.5 GHz. The link details and other related information pertaining to

Table 6-6: Parameters of the modified gamma DSD model in Durban and Butare

| LOCATION	μ	N_m	Λ
DURBAN	3	$3.08 \times 10^5 R^{-0.984}$	$7.6154 \times R^{-0.256}$
BUTARE	3	$3.606 \times 10^4 R^{-0.567}$	$5.8035 \times R^{-0.205}$

equipment set-up can be found in *Naicker and Mneney* [2004]. Table 6-7a and 6-7b gives a summary of the path attenuation prediction in Durban and Butare over 19.5 GHz. The plots for the results on this table are also available on Figure 6-11a and 6.11b. Predictions from the proposed model are found to majorly approximate rainfall path attenuation over the average value of the link measurements. In addition, it is observed from the predictions in Durban that path attenuations are slightly higher than figures from the ITU model by almost 2 dB when rainfall rate > 10 mm/h. At Butare, it is observed that the figures are only higher than the ITU model as long as rain rate < 30 mm/h. At 79 mm/h, the margin between ITU model and the proposed prediction at Butare is almost 7 dB. This is also noticed in the length factor values where the Butare experiences diminishing length factor at rain rates > 20 mm/h, compared to Durban. The geographical terrain at Butare has been earlier identified in Chapter three as a major factor influencing the attenuation characteristics. From the comparison, it is shown that the rain attenuation predictions in Durban using the proposed model compares well with the terrestrial measurements. The predictions at Butare, are however not expected to compare well, since the site is not within the climatic region of the terrestrial measurements.

Table 6-7a: Comparison of Predicted Attenuation with 6.73 km terrestrial Link Measurements in Durban at 19.5 GHz.

RAINFALL RATE (mm/h)	LENGTH FACTOR (proposed)	LENGTH FACTOR (ITU-R)	PREDICTED ATTENUATION (dB)	ITU-R VALUES(dB)	DURBAN LINK MEASUREMENT (dB)		
					Min	Ave	Max
1.00	2.04	1.39	0.87	0.81	0.38	1.20	3.40
2.60	1.80	1.11	2.17	1.79	0.80	2.50	5.40
3.00	1.76	1.08	2.48	2.02	0.90	2.80	5.60
4.20	1.67	1.01	3.38	2.69	1.40	4.00	6.10
5.80	1.58	0.95	4.53	3.56	2.50	5.10	6.30
10.00	1.42	0.86	7.34	5.74	4.90	8.60	16.30
15.00	1.29	0.80	10.39	8.21	5.90	13.00	23.00
21.00	1.19	0.75	13.75	11.08	6.80	16.20	27.20
30.00	1.09	0.71	18.37	15.26	7.00	16.40	28.50
51.00	0.93	0.65	27.79	24.63	7.10	19.20	32.00
79.00	0.81	0.61	38.46	36.65	12.00	20.00	34.00

Table 6-7b: Comparison of Predicted Attenuation at Butare over 6.73 km terrestrial Link Measurements at 19.5 GHz.

RAINFALL RATE (mm/h)	LENGTH FACTOR (proposed)	LENGTH FACTOR (ITU-R)	PREDICTED ATTENUATION (dB)	ITU-R VALUES (dB)	DURBAN LINK MEASUREMENT (dB)		
					Min	Ave	Max
1.00	2.19	1.39	0.83	0.81	0.38	1.20	3.40
2.60	2.08	1.11	2.31	1.79	0.80	2.50	5.40
3.00	2.05	1.08	2.67	2.02	0.90	2.80	5.60
4.20	1.95	1.01	3.70	2.69	1.40	4.00	6.10
5.80	1.84	0.95	4.99	3.56	2.50	5.10	6.30
10.00	1.60	0.86	7.97	5.74	4.90	8.60	16.30
15.00	1.40	0.80	10.97	8.21	5.90	13.00	23.00
21.00	1.23	0.75	13.99	11.08	6.80	16.20	27.20
30.00	1.05	0.71	17.72	15.26	7.00	16.40	28.50
51.00	0.80	0.65	23.99	24.63	7.10	19.20	32.00
79.00	0.62	0.61	29.41	36.65	12.00	20.00	34.00
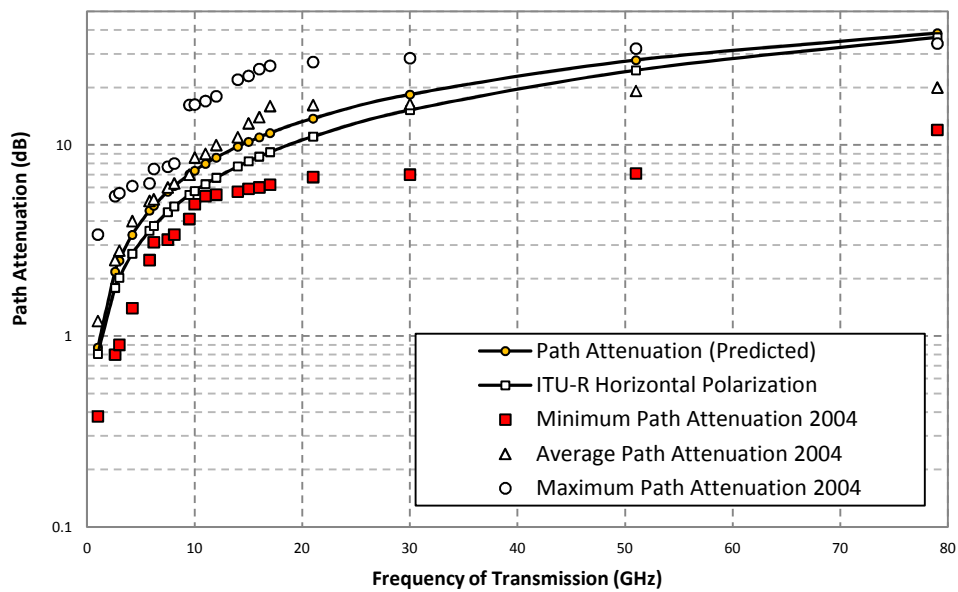
Figure 6-11a: Comparison of predicted attenuation in Durban with measurements at 19.5 GHz over a 6.73 km horizontally-polarised terrestrial microwave link.
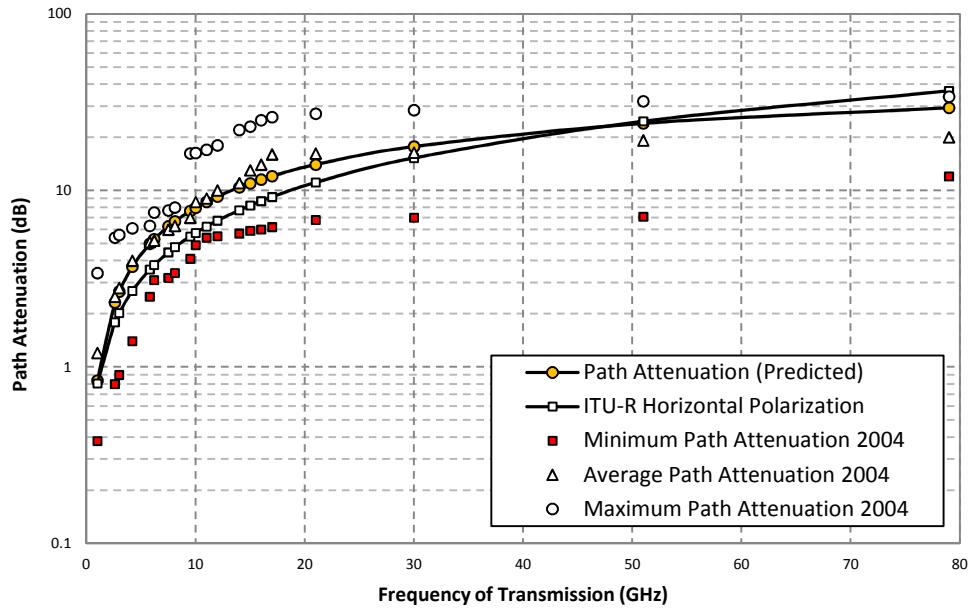
Figure 6-11b: Comparison of predicted attenuation in Butare with measurements at 19.5 GHz over a 6.73 km horizontally-polarised terrestrial microwave link.

Broadly speaking, the proposed length factors are projected to increase as the parameters of the radio link are increased *i.e.* higher microwave frequencies and larger path length. The assumption of single horizontal rain cell is only strictly valid for the data at both sites at all frequencies, as long as the path length does not exceed 10 km threshold. For path lengths exceeding 10 km, the proposed model shows a rapid decline in the actual rain attenuation experienced along the path. An increase in the path length of radio links without consideration for the existence of multiple cells result in the under-estimation of path attenuation due to rain. The presence of intense rainfall rates in tropical African locations, as seen from the computed RCDs, results in smaller rain cell sizes at high rain rates along any hypothetical microwave link. The multiple cell problems for different path lengths can be resolved by applying the queueing theory approach since the cell appearances are probabilistic. This way, the maximum factor required to compensate for the actual number of multiple rain cells existing within a typical link can be determined.

Chapter Summary

In this chapter, the shape of rain spikes in the time domain is investigated at the two sites and an Erlang-*k* distribution was developed for the modelling. This follows the theory that individual

time slots allotted to rain rates within a spike are subsets of the overall service time. From results, the parameters of this proposed distribution describing rain spike shape are found to vary across different regimes at both locations. The PDF of spike shape function essentially leads to development of a rain rate function for different rainfall regimes, applicable in rainfall synthesis and rain cell estimation. This implies that each arriving rain spike in a queue-generated rain event has an underlying approximate PDF describing its dynamics. Investigation of horizontal rain cells from ground data at both sites is considered using the SST approach to compute rain cell distances. Results from this investigation in Durban and Butare have shown that circular RCDs vary over different regimes. However, rain cells from thunderstorm regimes have been shown to give the best representation of the prevailing RCDs at the equatorial and subtropical sites as it gives a realistic spectrum of rain rate. Computed RCDs at both locations are used to determine approximate length factors for single rain cells occurring in thunderstorm regimes. It is shown that the predicted rainfall attenuation from length factors gives a good estimation of link measurements over a terrestrial link of 19.5 GHz at 6.73 km. Although, there are potential limitations due to the presence of multiple cells, it is obvious that the proposed circular approximation is encouraging. This study will assist in the planning of radio links, more so, as the demand for higher frequency bands continues due to prevailing proliferation of wireless services requiring high data-rate efficiencies.

CHAPTER SEVEN

Conclusions and Recommendations

7.1   Introduction

Among the requirements to be satisfied by any future wireless link is the intelligent implementation and management of scarce base station radio resources throughout the year. Usually, the topmost parameters of channel bandwidth, power level and modulation scheme are necessary trade-offs considered by network providers in system design [*Foty et al.*, 2011]. With constraints from the Shannon capacity theorem for emerging digital wireless networks, allocating permanent rain fade margin to counter time-varying rain attenuation, is a possible liability in Radio Resource Management (RRM). The application of this fade margin is actually the traditional SRFM proposed by ITU-R in their series of recommendations [*ITU-R P.838-3*, 2005; *ITU-R P.837-6*, 2012; *ITU-R P.530-15*, 2013]. As rightly said in the review, the SRFM is disadvantagaeous to modern wireless networks in the deployment of higher microwave and millimeter bands because of precipitation effects. Thus, it is envisaged that the method of SRFM as a countermeasure to rainfall attenuation may not be around for a very long time. However, the need to make FMTs more adaptive to time-domain variation has encouraged the development of DRFM from different researchers. DRFM can be made more robust and effective if the knowledge of the characteristics of rainfall processes are understood mathematically. Thus, the objective of this thesis has been geared towards demystifying the underlying characteristics of rainfall. This has initiated the development of a novel concept for the understanding rainfall process through the Queueing Theory Technique (QTT). This is an indirect approach of understanding the time-variation of rainfall attenuation over the time domain – where time series data bank may be largely insufficient. The QTT approach has shown that rain spikes all act as a single unit of queue instances vis-à-vis their natural traffic scheduling. The results from this study has majorly demonstrated and proven that the theory of rain queues is valid – and has likewise shown that – a semi-Markovian queue discipline is the most appropriate to describe such rainfall rate queues at the subtropical and equatorial Africa. From the novel studies in this thesis, a number of notable conclusions and future suggestions can therefore be drawn from the queueing theory approach.

7.2 Conclusions

This section hereby discusses the conclusions drawn from chapters three, four, five and six of this thesis.

7.2.1 Chapter Three – Comparison and Analysis of Rainfall Microstructures in Tropical Africa

The variation of rainfall microstructures over Stratiform-Convective (SC) bounds is an important indices to investigate rainfall at different climatic regions. Over tropical Africa, the location of Durban (subtropical) and Butare (equatorial) have shown that the delineation of SC bounds is separated by at least 2.5 mm/h. Considering that $R_{0.01}$ at both locations varies, then this is very much expected. From the results, Butare will experience early transition into convective rainfall types as an equatorial location quickly than Durban, a subtropical location. equatorial locations are noted to have significant occurrence of showers and thunderstorm rainfalls compared to subtropical locations. For stratiform rainfalls, there is an obvious difference in the probability distribution profiles of rainfall microstructres at both climatic locations. The rainfall rate, rainfall DSD and radar reflectivity distributions all seem to have different profiles at both locations over stratiform rain regime. This is mainly due to the significantly higher percentage of drizzle rainfalls in Durban, resulting in the preponderance of smaller rain droplets in this category. Thus, rainfall rates below 10 mm/h, during rain events, have been reported to follow temperate characteristics [*Fashuyi et al.*, 2006]. However, convective rainfalls at both location have the closer probability profiles for the same category of rain microstructures. This is further proven by the close model parameters of both rainfall DSD and radar distributions as seen in the results. Also, the proponderance of small droplets at both locations is clearly opposite to what is obtained under convective. This suggests that shower and thunderstorm characteristics of rainfall are a little similar under convective conditions. One deviation to this, is however in the monthly variation of radar reflectivities, which is clearly dependent on seasonal cycles. An investigation of SC thresholds at other global locations also shows that a rainfall rate of roughly about 10 mm/h, as suggested by literatures, is the valid transition parameter.

7.2.2 Chapter Four - Queueing Theory of Rain Spikes over Radio Links

The Markov theory of rainfall queues was developed empirically from the rainfall time series data in Durban. The appearances of rainfall spikes, which are linked to rain cell movement over a radio link, tend to appear randomly during rain events. Their service and inter-arrival times follow a Birth-Death scenario which qualifies them as instances of rainfall traffic. The service time distribution clearly exhibited exponential or Erlang-k characteristics, while inter-arrival time distribution is strictly an exponential process. Therefore, results from the data showed that the typical distribution may either follow a *Markovian* (M/M/s/∞/ FCFS) or *semi-Markovian*

($M/E_k/s/\infty/$ FCFS) queue discipline. However, the semi-Markovian discipline showed better error fitting results and realistic convergence under steady state conditions. The natural server number present in rainfall processes was found to be closer to three (3) for most rain regimes. Therefore, it is concluded that the rainfall process in Durban is naturally derived from a $M/E_k/3/\infty/$ FCFS queue discipline. Further results also show that the 'jump' probability from one spike to another within a rainfall time series can be represented by a $(n \times n)$ matrix with different steady state vectors for each regime. The service times of rainfall spike within the queue are also found to be positively correlated and dependent on the maximum rainfall rates attained by the spike. This shows that spikes in Durban with high rainfall rates tend to spend more time in any typical rain event suggesting higher outage periods.

7.2.3 Chapter Five - Comparison of Rainfall Queue Characteristics in Tropical Africa

The semi-Markovian queue description is extended to Butare, an equatorial location in this chapter. Rainfall queues in subtropical and equatorial Africa tend to exhibit similar queue characteristics when examined over annual cycles. However, this is not the case when both locations are compared on the basis of rainfall regimes. Compared to Durban, Butare is found to have increasing service times (with increasing *k*) as the maximum rain rate of spike increases. However, there is no distinct trend observed for the inter-arrival times in relation to any spike's maximum rain rate. Clearly, the queue dynamics of spikes generated at shower and thunderstorm events at Butare are obviously different from observations in Durban. These results have clear implications for rain attenuation analysis as this could lead to significant differences in outage frequencies due to rainfall. The geography and climatic characteristics are factors that might influence this. The *jump* probabilities at both locations are similar for different regimes and even for the overall data at steady state conditions. This suggests that dynamics of Markov jump probability at both locations, have similar meteorological characteristics, as present at both locations. Queue generated spikes can be applied in the simulation of rainfall conditions, provided the queue parameters are known. From this, it is conclusive to know that rainfall event durations tend to be different given an equivalent random number of spikes generated as a queue at any regime. Thus, it is possible to simulate different rainfall conditions at both locations and apply this to radio propagation studies in the future.

7.2.4 Chapter Six - Queueing Theory Application in Rain Cell Estimation

An extension of the queueing theory approach is employed in the development of standard probability functions representing rain spikes. The spike instances of the semi-Markovian queue

are investigated by considering them as a time-varying PDF entity with distribution parameters strongly dependent on the maximum rain rate attained by the spike. The Erlang-k distribution was found useful in the description of rainfall PDFs for different rainfall regimes in subtropical and equatorial Africa. It was observed that individual spikes generated during rain events are unique and have varying mean service times over different regimes. An approximate rain rate function, obtained from the underlying characteristics of spikes, is found to exist as a scaled version of the PDF. The rain rate function is representative of circular rain cells, under queue-generated conditions. These queued cells are assumed to move over radio links, propelled by an advection velocity, required to translate its time series to distance. The results of RCDs for different rain regimes in Durban and Butare show spatial variation of cell areas at the two sites. Butare, being closer to the equator, is expected to experience more convective rainfalls resulting in smaller rain cells. This is confirmed in the results obtained under thunderstorm regimes for scenarios where rainfall rates are greater than 40 mm/h. While computations of length factors from single units of circular rain cells may be valid for terrestrial links with path lengths less than 10 km. Further computations beyond 10 km, show rapid decline of length factors as a result of absent multiple rain cells. Finally, it is seen that the the path attenuation due to rain at 19.5 GHz at Butare tend to give higher figures for rain rates < 30 mm/h compared to Durban. The DSD formation process and geographical factors as mentioned in Chapter three is a major influence on the predicted rain attenuation at Butare.

7.3 Suggestions for Future Research

Based on the pilot studes of rainfall queueing theory investigated in this thesis, a number of future research areas have been suggested as below:

- The underlying rainfall characteristics undertaken in this study has only been investigated at two tropical African locations. This concept can be applied to rainfall data from different climatic regions of the world to determine their respective queueing characteristics. This may be necessary to determine the global uniformity of queueing parameters, and hence, establish their queueing characteristics.

- The existence of natural multiple servers in the scheduling of rainfall queues as implied by the proposed semi-Markovian queue discipline requires further investigations. The actual role of advection velocities and rain cell statistics in rain queues should be

investigated to obtain an interpretation for the presence of servers. This knowledge can enhance the understanding rain queues and rain cells.

- The estimation of rainfall attenuation over radio links with longer path lengths, by the utilization of multiple cells in rain queues, requires further research. Radio links with longer path lengths have a higher occurrence probability of multiple cells, especially under severe thunderstorm conditions. A rigorous study of this scenario using rainfall queueing theory is required to be undertaken to optimize radio link performance in real time.

- The development of a queueing discipline for a given location suggests that rainfall time series can be 'recreated' even on a long term basis. Therefore, the determination of network outage statistics at satisfactory rain attenuation thresholds can be resolved. In this case, the research questions are as thus: what are the effects and statistics of network outages at the investigated tropical locations ? What type of distributions are required to describe these queue-generated outages?

- Channel modelling is a topical area of research in rainfall attenuation studies. The concept of queueing theory of rainfall can be harnessed to develop sound and logical channels over different attenuation bounds. This research can be achieved by considering different digital modulation schemes such as Rayleigh, Rician and Nakagami faded-channels in tandem with rainfall queues.

REFERENCES

Abramowitz, M. and I.A. Stegun (Ed.): <u>Handbook of Mathematical Functions with Formulars, Graphs and Mathematical Tables</u>, Dover, New York, 9th printing, p.880

Acosta, R.J. (1997): 'Rain Fade Compensation Alternatives for Ka-Band Communication Studies,' *3rd Ka-Band Utilization Conference*, Sorrento, Italy, September, pp. 15-18.

Adetan, O.E. and T.J. Afullo (2013): 'The Critical Diameters for Rainfall Attenuation in Southern Africa,' *Progress in Electromagnetic Research B*, Vol. 46, pp. 275 - 297.

Adetan, O.E. and T.J. Afullo (2014): 'Raindrop Size Distribution and Rainfall Attenuation Modeling in Equatorial Subtropical Africa: Critical Diameters,' *Annals des Telecommunication*, 10.1007/s12243-013-0418-z, pp. 1-13.

Adimula, I.A and G.O. Ajayi (1996): 'Variation in raindrop size distribution and specific attenuation due to rain in Nigeria,' *Ann. Telecom*, vol.51, No. 1-2, pp. 87–93.

Afullo, T. J. O. (2011): 'Raindrop size Distribution Modeling for Radio Link Design along the Eastern Coast of South Africa,' *Progress in Electromagnetic Research B*, Vol. 34, pp. 345-366.

Ajayi, G.O. (1990): 'Some aspects of tropical rainfall and their effect on microwave propagation,' *Int. J. Satell Commun.*, 8(3), 163–172, doi:10.1002/sat.4600080308.

Ajayi, G.O. and R.L. Olsen (1985): 'Modeling of a tropical raindrop size distribution for microwave and millimeter wave applications,' *Radio Science*, Vol. 20, number 2, pp. 193–202, April

Ajayi, G.O., Feng, S., Radicella, S.M. and Reddy, B.M. (Ed) (1996): <u>Handbook on Radiopropagation Related to Satellite Communications in Tropical and Subtropical Countries</u>, Trieste: ICTP, pp. 7–14.

Akuon, P.O. and T.J. Afullo (2011b): 'Path Reduction Factor Modelling for Terrestrial Links based on Rain Cell Growth,' *Proc. IEEE AFRICON 2011 conf.,* Livingstone, Zambia, ISBN 978-1-61284-991-1, September, pp. 1-5.

Akuon, P.O. and T.J.O Afullo (2011a): 'Rain Cell Sizing for the Design of High Capacity Radio Link Systems in South Africa,' *Progress in Electromagnetic Research B*, Vol. 35, pp. 263 - 285.

Alasseur, C., L. Husson and F. Perez-Fontan (2004): 'Simulation of rain events time series with Markov model,' 15th IEEE International Symposium on Personal, Indoor and Mobile Radio Communications, PIMRC 2004, 4, 2801-2805, doi: 10.1109/PIMRC.2004.1368831.

Alonge, A.A. (2011): <u>Correlation of Raindrop Size Distribution with Rain Rate Derived from Disdrometers and Rain Gauge Networks in Southern Africa</u>, Dissertation submitted to the University of KwaZulu-Natal, Durban.

Alonge, A.A. and Afullo, T.J. (2014): 'Rainfall Microstructural Analysis for Microwave Networks: Comparison at Equatorial and Subtropical Africa,' *Progress in Electromagnetic Research B*, Vol. 59, pp. 279-303.

Alonge, A.A. and T.J. Afullo (2012a): 'Rainfall Drop-Size Estimators for Weibull Probability Distribution using Method of Moments Technique,' *African Research Journal of SAIEE*, Vol. 103, No. 2, pp. 83-93.

Alonge, A.A. and T.J. Afullo (2012c): 'Regime Analysis of Rainfall Drop-size Distribution Models for Microwave Terrestrial Network,' *IET Microwave Antennas Propag.*, Vol. 6, issue 4, pp. 393-403.

Alonge, A.A. and T.J. Afullo (2013a): 'Temporal characterization of rainfall time series for wireless networks,' presented at 3rd International Conference on Wireless Communications, Vehicular Technology, Information Theory and Aerospace & Electronic Systems (Wireless VITAE), New Jersey, USA, doi: 10.1109/VITAE.2013.6617078.

Alonge, A.A. and T.J. Afullo (2013b): 'Rainfall Microstructures for Microwave and Millimeter Wave Link Budget at Tropical and Subtropical Sites,' Presented at 2013 IEEE Africon Conference, Le Meridien ile Maurice, Mauritius, September.

Alonge, A.A. and T.J.O. Afullo (2012b): 'Seasonal Analysis and Prediction of Rainfall Effects in Eastern Southern Africa at Microwave Frequencies,' *Progress in Electromagnetic Research B*, Vol. 40, pp. 279-303.

Anagnostou, E.N. (2004): 'A convective/stratiform precipitation classification algorithm fro volume scanning weather radar observations,' *Meteorol. Appl.*, Vol. 11, pp. 291-300.

Atlas, D. and C.W. Ulbrich (1974): 'The physical basis for attenuation-rainfall relationships and the measurement of rainfall parameters by combined attenuation and radar methods,' *J. Rech. Atmos.*, 8, pp. 275–298.

Atlas, D. and Ulbrich, C.W. (1977): 'Path- and aero-integrated rainfall measurements by microwave attenuation in the 1-3-cm band,' *Journal of Applied Meteorology*, 16, 1322-1331.

Atlas, D., R.C. Srivastava and R.S. Sekhon (1973): 'Doppler Radar Characteristics of Precipitation at Vertical Incidence,' *Rev. Geophys. Space Phys.*, Vol. 11, pp. 1-35.

Awaka, J., T. Iguchi, H. Kumagai and K. Okamoto (1997): 'Rain Type Classification Algorithm for TRMM Precipitation radar,' *Proceedings of the IEEE 1997 International Geosci. Remote Sen. Sym*, pp. 1636-1638.

Awang M.A. and J. Din (2004): 'Comparison of the Rain Drop Size Distribution Model in Tropical Nigeria,' 2004 RF and Microwave Conference, Selanghor, Malaysia.

Aydin, K. and S.E.A. Daisley (2002): 'Relationships between rainfall rate and 35-GHz attenuation and differential attenuation: modeling the effects of raindrop size distribution, canting and oscillation,' *IEEE Trans. Geosci. Remote Sens.*, Vol. 40, No. 11, pp. 2343-2352.

Banjo, O.P. and E, Vilar (1986): 'Measurement and Modelling of Amplitude Scintillation on Low Elevation Earth-Space paths and Impact on Communication Systems,' *IEEE Trans. Commun.*, Vol. COM-34, pp 774-780.

Bartholomew, M.J. (2009): 'Disdrometer and tipping bucket rain gauge handbook,' DOE/SC-ARM/TR-079, ARM Climate Research Facility, Upton, New York.

Battan, L.J. (1973): Radar Observations of the Atmosphere, Univ. of Chicago Press, 323.

Beard, K.V. (1976): 'Terminal velocity and shape of cloud and precipitation drops aloft,' *Journal of the Atmospheric Sciences*, 33, 851-864.

Begum, S., C. Nagaraja and I. Otung (2006): 'Analysis of Rain Cell Size Distribution for Application in site Diversity,' First European Conference on Antennas and Propag. (EuCAP 2006), pp. 1-5.

Bhattacharyya S., M. Dan and A.K. Sen (2000): 'Modelling of drop size distribution of rain from rain rate and attenuation measurements at millimeter and optical wavelengths,' International Journal of Infrared and Millimeter Waves, Vol. 21, No. 12, pp. 2065-2075.

Bolch, G., Greiner, S., de Meer, H. and K.S Trivedi (1998): Queueing Networks and Markov Chains: Modelling and Performance with Computer Science Application, John Wiley and Sons, Chapter 6, 209-233.

Bryant, G.H, I. Adimula, C. Riva and G. Brussard (2001): 'Rain Attenuation Statistics from Rain Cell Diameters and Heights,' *Int. J. Sat Commun.*, Vol. 19, pp. 263-283.

Capsoni, C., L. Luini and C. Riva (2006): 'Stratiform and convective rain discrimination starting from the site P(R),' *IEEE Trans. Propag.*, Vol. 54(11), pp. 3566-3569, November.

Capsoni, C., F. Fedi, C. Magistroni, A. Paraboni and A. Pawlina (1987): 'Data and theory for a new model of the horizontal structure of rain cells for propagation applications,' *Radio Sci.*, Vol. 22, No 3, pp. 395-404.

Castanet, L., A. Bolea-Almanac and M. Bousquet (2003): 'Interference and Fade Mitigation Techniques for Ka and Q/V Band Satellite Communication Systems,' COST 272-280 International Workshop on Satellite communication from Fade Mitigation to Service Provision, Noordwijk, Netherlands.

Chen, K.S., C.Y. Chu and Y.C. Tseng (2011): 'A semi-empirical model of rain attenuation at Ka-band in Northern Taiwan,' *Progress in Electromagnetic Research M*, Vol. 16, pp. 213–223.

Crane, R.K., (1980): 'Prediction of Attenuation by Rain,' *IEEE Trans. On Comm.*, Vol. 28(9), pp 1717-1733.

Crane, R.K., (1996): <u>Electromagnetic Wave Propagation Through Rain</u>, John Wiley and Sons Inc., New York. pp 1-4, 39-40.

Crane, R.K., (2003): <u>Propagation Handbook for Wireless Communication System Design</u>, CRC Press LLC, Florida. pp. 1-3, 66-67.

Das, D. and A. Maitra (2012): 'Time Series Predictor of Ku Band Rain Attenuation over an Earth-Space Path at a Tropical Location,' *Int. J. Satell. Commun.*, Vol. 30, pp. 19-28.

Das, S., A. Maitra and A.K. Shukla (2010): 'Rain attenuation modeling in the 10-100 GHz frequency using drop size distributions for different climatic zones in tropical India,' *Progress in Electromagnetics Research B,* Vol. 25, pp. 211–224.

Drufuca, G. (1974): 'Rain attenuation statistics for frequencies above 10 GHz from rain gauge observations,' *J. Reach. Atmos.*, Vol. 8, pp. 399-411.

Dymarski, P. (2011): <u>Hidden Markov Models, Theory and Applications</u>, Intech Publishers, Croatia.

Fashuyi, M .O., P. A. Owolawi and T. O. Afullo (2006): 'Rainfall rate modelling for LoS radio systems in South Africa,' *Trans. of South African Inst. of Elect. Engineers (SAIEE)*, Vol. 97, pp. 74-81.

Feingold, G. and Z. Levin (1986): 'The Lognormal Fit to Raindrop Spectra from Frontal Convective Clouds in Israel,' *J. Climate Appl. Meteor.*, 25, pp.1346-1363.

Féral, F., H. Sauvageot, L. Castanet and J. Lemorton (2003): 'HYCELL—A new hybrid model of the rain horizontal distribution for propagation studies: 1. Modeling of the rain cell,' *Radio Sci.*, Vol 38, No 3, pp.1056.

Fiandrino, C. and E. Pievanelli (2010): <u>Network Modelling Formulary</u>, Politecnico di Torino.

Foty, D., B. Smith, S. Sinha and M. Schröter (2011): 'The Wireless Bandwidth Crisis and the Need for Power-Efficient Bandwidth,' IEEE AFRICON conference, Livingstone, Zambia, September, pp. 1-6.

Freeman, R.L. (2007): <u>Radio System Design for Telecommunications</u>, 3rd edition, A Wiley Interscience Publication, John Wiley and Sons Inc.

Fukuchi, H. and T. Saito (2007): 'Spatial Correlation Analysis of Rainfall Rates for Advanced Attenuation Mitigation Technologies,' Presented at EuCAP conference, pp. 1-6.

Gamache J.F. and R.A. Houze (1982): 'Mesocale Air Motions associated with Tropical Squall Line', *Monthly Weather Review*, 110, pp. 118-135, 1982.

Gautam and A.R. Ravindra (Ed.) (2006): <u>Operation Research and Management Science</u> Handbook.

Green, H.E. (2004): 'Propagation Impairment on Ka-Band SATCOM in Tropical and Equatorial Regions,' *IEEE Antennas Propag. Magazine*, Vol. 46, No. 2, pp. 31-44.

Gross, D. and C.M. Harris (1998): <u>Fundamentals of Queueing Theory</u>, 3rd ed., John Wiley and Sons Inc., New York.

Gunn, R. and K.D. Kinzer (1949): 'The terminal velocity of fall for water droplets in stagnant air,' *J. Meteor.*, 6(4), pp. 243-248.

Hall, M.P.H., L.W. Barclay and M.T. Hewitt (1996): <u>Propagation of Radiowaves</u>, IEEE press, London

Héder, B. and J. Bitòs (2008): 'General N-State Markov model for rain attenuation times series generation,' *Wireless Personal Communication*, Vol. 46, 99-113.

Hillier, S.F. and J.G. Lieberman (2001): <u>Introduction to Operations Research</u>, McGraw-Hill, 7th edition).

Houze, R., B.F. Smull and P. Dodge (1990): 'Mesoscale Organization of Springtime Rainstorms in Oklahoma,' *Monthly Weather Review*, Vol. 118, pp. 613-654.

Houze, R.A. (1973): 'A Climatological Study of Vertical Transports by Cumulus-scale Convection,' *J. Atmos. Sci.*, 30, pp. 1112-1113.

Houze, R.A. (1997): 'Stratiform Precipitation in Regions of Convection: A meteorological Paradox?,' *Bulletin of the American Meteorological Society*, Vol. 78, No. 10.

IEEE 521-2002 (2009): 'IEEE Standard Letter Description for Radar-Frequency Bands,' *686 WG – Terminology Working Group*, New York.

Ippolito, L.J.: 'Radio propagation for space communication systems,' *Proceedings of IEE*, vol. 69, pp. 697-727, 1981.

Islam, M.R., J. Chebil and T.A. Rahman (1997): 'Review of Rain Attenuation Studies for Communication Systems operating in Tropical region,' Proc. IEEE Malaysia International Conference on Communications, S15.9.1-4.

ITU-R (2000): 'Nomenclature of the Frequency and Wavelength Bands used in Telecommunication,' *ITU-R V.431-7*, Geneva.

ITU-R (2005): 'Specific Attenuation Model for Rain for use in Prediction Methods,' *ITU-R P.838-3*, Geneva.

ITU-R (2012): 'Characteristics of Precipitation for Propagation Modelling,' *ITU-R Rec. P.837-6*, Geneva.

ITU-R (2013): 'Propagation Data and Prediction Methods for the Design of Terrestrial Line-of-Sight Systems,' *ITU-R Rec. P.530-15*, Geneva.

Karklinsky, M. and E. Morin (2006): 'Spatial characteristics of radar-derived convective rain cells over Southern Israel,' *Meteorologische Zeitschrift*, Vol. 15, No. 5, pp. 513 – 520, October.

Kendall, D.G. (1953): 'Stochastic processes occurring in the theory of queues and their analysis by the method of imbedded Markov chain,' *The Annals of Mathematical Statistics*, 24(3), 338-354, doi:10.1214/aoms/1177728975.

Kleinrock, L. (1975): Queueing Systems Volume I, Theory, John Wiley and Sons, New York..

Kotek, M., Grieser, J., Beck, C., Rudolf, B. and F. Rubel (2006): 'World Map of the Koppen-Geiger Climate Classification Updated,' Meteorol. Z., Vol.15, pp. 259-263.

Kozu, T. and K. Nakamura (1991): 'Rainfall parameter estimation from dual-radar measurements combining reflectivity profile and path-integrated attenuation', *J. of Atmos. and Oceanic tech.*, pp. 259–270.

Kreyszig, E. (2006): Engineering Mathematics, 9th edition, John Wiley and sons Inc., New York, 802-807.

Kumar, L.S., Y.H. Lee, J.X. Yeo and J.T. Ong (2011): 'Tropical Rain Classification and Estimation of Rain from Z-R (Reflectivity-Rain Rate) Relationships,' *Progress in Electromagnetic Research B*, Vol. 32, pp. 107-127.

Lam, H.Y., L. Luini, J. Din, C. Capsoni and A.D. Panagopoulos (2010): 'Stratiform and convective rain discrimination for equatorial region,' 2010 IEEE Student conference on Research and Development (SCORed), pp. 112-116, December.

Laws, J.O. and D.A. Parsons (1943): 'The Relation of raindrop-size to intensity,' *Trans. Amer. Geophys. Union,* 24, pp 452-460.

Li, L., P. Kooi, M. Leong and T. Yeo (1995): 'Microwave attenuation by realistically distorted raindrops: part I–theory,' *IEEE Trans. Antennas*, Vol. 43, no. 8, pp. 811–822, Aug.

Li, L., T. Yeo, P. Kooi and M. Leong (2000): 'An efficient calculation approach to evaluation of microwave specific attenuation,' *IEEE Trans. Antennas*, 48(8), pp. 1220–1229.

Liebe, H.J. (1981): 'Modeling attenuation and phase of radio waves in air at frequencies below 1000 GHz,' *Radio Sci.*, 16(6), pp. 1183-1199.

Liebe, H.J. (1983): 'An Atmospheric Millimeter wave propagation model.' NTIA Report 83-187, National Telecommunications and Information Administration, December.

Liebe, H.J. and G.A. Hufford (1989): 'Modelling millimeter wave propagation effects in the atmosphere,' AGARD, CP-454, October.

Maitra, A. (2004): 'Rain Attenuation Modelling From Measurements of Rain Drop Size Distribution in the Indian Region,' *IEEE Antennas Wireless Propag. Lett*, Vol. 3, pp 180-181.

Malinga, S.J., P.A. Owolawi and T.J.O. Afullo (2014): 'Determination of Specific Rain Attenuation using Different Total Cross Section Models for Southern Africa,' *African Research Journal of SAIEE*, Vol. 105, No. 1, pp. 20-30, March.

Mämmela, A. and A. Kolteba (2011): 'Link Budgets: How much Energy is Really Received,' *Vehicular Technologies: Increasing Connectivity*, April, pp. 433- 448.

Mandeep J.S. and J.E. Allnut (2007): 'Rain Attenuation Predictions at KU-Band in South East Asia Countries,' *Progress in Electromagnetic Research*, PIER 76, PP. 65 – 74.

Marayuma, T., Y. Shirato, M. Akimoto and M. Nakatsugawa (2008): 'Service area expansion of Quasi-Millimeter FWA systems through site diversity based on detailed rainfall intensity data,' *IEEE Trans. On Antennas and Propagation*, Vol. 56, No. 10, 3285-3292, doi: 10.1109/TAP.2008.929432.

Marshall J.S. and W.M. Palmer (1974): 'The distribution of Raondrops with size,' *J. of Meteorology*, Vol. 5, pp. 955-1019.

Marshall, J.S. and W.M. Palmer (1948): 'The Distribution of Raindrops with Size,' *J. of Atmos. Sci.*, 5, pp. 165-166.

Maruddani, B., A. Kurniawan, Sugihartono and A. Munir (2010): 'Rain Fade modelling using hidden Markov model for tropical area,' PIERS Symposium proceedings, Cambridge, USA.

Matricciani E. and C. Riva (2005): 'The Search for the Most Reliable Long Term Rain Attenuation CDF of a Slant Path and the Impact on Prediction Models,' *IEEE Transactions On Antennas and Propagation*, Vol. 53, No. 9, pp. 3075-3079, September

Matricciani, E. (1996): 'Physical mathematical model of the dynamics of rain attenuation based on rain rate time series and two layer vertical structure of precipitation,' *Radio Science*, 31, pp. 281-295.

Matricciani, E. (2008): 'Global formulation of the Synthetic Storm Technique to calculate rain attenuation only from rain rate probability distributions,' presented at 2008 IEEE International Symposium on Antennas and Propagation, San Diego, July 5-11.

Mätzler, C. (2002a): 'Drop-size distributions and Mie computation,' *IAP Res. Rep. 2002-16*, Univ. of Bern, Bern, Nov.

Mätzler, C. (2002b): 'MATLAB functions for Mie scattering and absorption,' *IAP Res. Rep. 2002-08*, Univ. of Bern, Bern, Jun.

Melsheimer, C., W. Alpers and M. Gade (2001): 'Simultaeneous Observation of Rain Cells over the Ocean by the Synthetic Aperture Radar aboard the ERS Satellites and by Surface-based Weather Radars,' *J. of Geophysical Research*, Vol. 106, No C3, pp. 4665 – 4677, March.

Meng, Y. S., Y. H. Lee and B. C. Ng (2009): 'Empirical near ground path loss modeling in a forest at VHF and UHF bands,' *IEEE Trans. Antennas Propag.*, Vol. 57, No. 5, pp. 1461–1468.

Mie, G. (1908): 'Beiträge zur optik trüber medien, speziell kolldaler metallösungen,' *Ann. Phys.*, 25, pp. 377–445, doi:10np.19083300302.

Morrison, J.A. and M.J. Cross (1974): 'Scattering of a plane electromagnetic wave by axisymmetric raindrops,' *Bell Syst. Tech, J*., Vol. 53, pp. 955-1019, July-August.

Moumouni, S., M. Gosset and E. (2008): 'Main features of rain drop size distributions observed in Benin, West Africa, with optical disdrometers,' *Geophysical Research Letters*, Vol. 35, L23807.

Moupfouma, F and Dereffye, J. (1982): 'Empirical model for Rainfall rate distribution,' *Electronics Letters*, Vol.18, No. 11, pp.460-461.

Moupfouma, F. (1985): 'Model of rainfall-rate distribution for radio system design,' *IEE Proceedings*, Vol.132, Pt. H, No. 1, pp.460-461.

Moupfouma, F. (1987): 'More about rainfall rates and their prediction for radio systems engineering,' *IEE Proc*., Vol. 134, No. 6, pp. 527-537, Dec.

Moupfouma, F. and L. Martin (1993): 'Point Rainfall Rate Cumulative Distribution Function valid at various Locations,' *Electron. Letters*, Vol. 29, pp. 1503-1505.

Naicker, K. and S.H. Mneney (2004): 'Propagation measurements and modeling for terrestrial line-of-sight links at 19.5 GHz,' *Proc. of IEEE AFRICON conference*, vol. 01, pp. 95−100, September.

Nakazawa, S., M. Nagasaka, S. Tanaka and K. Shogen (2010): 'A method to control phased array for rain fading mitigation of 21-GHz band broadcasting satellite,' 2010 Proceedings of the Fourth European Conference on Antennas and Propagation (EuCAP), pp. 1-5.

Nzekou, A., H. Sauvageot, A.D. Ochou and C.M.F. Kebe (2004): 'Raindrop size distribution and radar parameters at Cape Verde,' *J. Appl. Meteorol.*, Vol. 43, pp. 90-105.

Ochou, A. D., A. Nzekou and H. Sauvageot (2007): 'Parameterization of drop size distribution with rain rate,' *Atmos. Res.*, 84, 58–66.

Odedina, M.O. and T.J. Afullo (2008): 'Characteristics of seasonal attenuation and fading for line-of-sight links in South Africa,' *Proc. of SATNAC*, pp. 203–208, 2008.

Odedina, M.O. and T.J. Afullo (2010): 'Determination of rain attenuation from electromagnetic scattering by spherical raindrops: Theory and experiment,' *Radio Sci.*, vol. 45.

Ong J.T. and Y.Y. Shan (1997): 'Rain Drop Size Distribution Models for Singapore – Comparison with Results from different Regions,' *Tenth International Conference on Antennas and Propagation*, Vol. 2, pp. 281-285.

Owolawi, P. (2011): 'Rainfall Rate Probability Density Evaluation and Mapping for the Estimation of Rain Attenuation in South Africa and Surrounding Island,' *Progress in Electromagnetics Research B*, vol. 112, pp. 155-181.

Owolawi, P.A. (2010): Characteristics of Rain at Microwave and Millimetric Bands for Terrestrial and Satellite Links Attenuation in South Africa and Surrounding Islands, Ph.D thesis, Uni. of KwaZulu-Natal, Durban, July.

Owolawi, P.A. and T.J. Afullo (2007): 'Rainfall rate modelling and worst month statistics for millimetric line-of–sight radio links in South Africa,' *Radio Sci.*, Vol. 42.

Pawlina, A. (2002): 'No rain intervals within rain events: some statistics based on Milano radar and rain-gauge data', COST Action 280, 1st International Workshop, July.

Pontes, M.S., L.A.R. Da Silva Mello and R.S.L. de Souza (2007): 'Modelling of Effective Rainfall Rate and Rain Attenuation in Terrestrial Links in the Tropics,' *6th International Conference on Information, Communication and Signal Processing*, Singapore, December, pp. 1 – 4.

Pruppacher, H.R. and R.L. Pitter (1971): 'A semi-empirical determination of shape of cloud and raindrops,' *J. Atmos. Science,* Vol. 28, pp. 86-94.

Rodriguez, R.I.F., G.A.C. Prez, M. Werner, A.G. Castaño and A.M. Cano (2012): 'Rainfall Estimation by a Signal Attenuation Analysis in Mobile Systems,' *XV Symposium SELPER*, November.

Sabapathy, T., S.W. Tan and T.C. Chuah (2011): 'Fuzzy Weight Controller based Cell-Site Diversity for Rain Fading Mitigation in LMDS Networks in the Tropics,' *Progress in Electromagnetics Research B*, Vol. 28, pp. 234-251.

Sadiku, M.N.O. (2000): Numerical Techniques in Electromagnetics, 2nd edition, CRC press, pp. 96–103.

Sauvageot, H. and J.P. Lacaux (1995): 'The Shape of Averaged Drop Size Distributions,' *J. Atmos Sci,* Vol.52, pp. 1070-1083.

Seybold, J.S. (2005): Introduction to RF Propagation, John Wiley and Sons, New York, pp 218-245.

Shin, S.K., K. Lim, K. Choi and K. Kang (2002): 'Rain Attenuation and Doppler Shift Compensation for Satellite Compensation,' ETRI Journal, Vol. 24, (1), pp. 31-42.

Short, D. A., T. Kozu, and K. Nakamura (1990): 'Rain rate and raindrop size distribution observations in Darwin,' *Australia. Proc. Open Symp. on Regional Factors in Predicting Radiowave Attenuation due to Rain*, URSI, pp. 35–40.

Sinka C. and J. Bitó (2003): 'Site Diversity against Rain Fading in LMDS Systems,' IEEE Microwave and Wireless Comp. Letters, Vol. 13, No. 8, August.

Stout, G.E. and E.A. Mueller (1968): 'Survey of relationships between rainfall rate and radar reflectivity in the measurement of precipitation,' *J. of Appl. Meteor.*, 7, pp. 165-174.

Sweeney, D.G. and C.W. Bostian (1999): 'Implementing Adaptive Power Control as a 30/20 GHz Fade Countermeasure,' *IEEE Trans. Antennas Propagat.*, Vol. 47, (1), pp. 40-46, January.

Tenório, R.S., M.C. Da Silva Moraes and B.H. Kwon (2010): 'Raindrop Distribution in the Eastern Coast of Northeastern Brazil using Disdrometer Data,' *Revista Brasileira de Meterologia*, Vol. 25, No. 4, 415-426.

Tharek, A.R. and J. Din (1992): 'Rainfall Drop Size Distribution Measurements in Malaysia,' URSI, Ravenscar, North Yorkshire, UK, June.

Timothy, K.I., J.T. Ong and E.B.L. Choo (2002): 'Raindrop size distribution using method of moments for terrestrial and satellite communication applications in Singapore,' *IEEE Antennas Propag.*, Vol. 50, pp. 1420–1424, Oct.

Tokay, A., D.A. Short, C.R. Williams, W.L. Ecklund and K.S. Gage (1999): 'Tropical rainfall associated with convective and stratiform clouds: intercomparison of disdrometer and profiler measurements,' *J. Appl. Metor.*, Vol. 38, No. 3, pp. 302-320.

Tokay, D and A. Short (1996): 'Evidence from tropical raindrop spectra of the origin of rain from stratiform versus convective clouds,' *J. Appl. Meteor.*, Vol. 35, No. 3, pp. 355-371.

Ulbrich, C.W. (1983): 'Natural variation in the analytical form of the raindrop size distribution,' *J. of Climate and Applied Meteor.*, vol. 23, pp. 1764–1775.

Umebayashi, K., R.H. Morelos-Zaragoza and R. Kohno (2005): 'Modulation identification and carrier recovery system for Adaptive modulation in satellite communication,' *Proceedings of IEEE 61st Vehicular Technology Conference*, VTC-spring 2005, 2697-2701, doi: 10.1109/VETECS.2005.1543825.

Van de Kamp, M. (2003): 'Rain attenuation as a Markov process: How to make an event,' presented at COST 280, Second International Workshop, Eur. Coop. in the field of Sci and Technol., Noordwijk, Netherlands, May.

Van der Hulst, H.C. (1957): Light scattering by small particles, John Wiley and Sons Inc., New York.

Van Mook, F.J.R. (2002): Driving rain on building envelopes, PhD. Thesis, Building Physics and Systems, Technische Universiteit Eindhoven University Press, Eindhoven, The Netherlands.

Walck, C. (2007): Hand-book on Statistical Distribution for Experimentalists, Particle Physics book, Fysikum, University of Stockholm, Chapters 14, 17 and 20, 54-56, 77-78.

Wilson, C.L. and Tan, J. (2001): 'The characteristics of rainfall and melting layer in Singapore: Experimental results from radar and ground instruments,' *11th International Conference on Antennas and Propagation*, 480, pp. 852 – 856.

Wingo, D.R. (1987): 'Computing Maximum-Likelihood Parameter Estimates of the Generalized Gamma Distribution by Numerical Root Isolation,' *IEEE Trans. Reliability*, Vol. R-36, No. 5, pp. 586-590.

INTERNET REFERENCES

[1] Durban weather details accessed at http://www.worldweatheronline.com/Durban-weather-averages

[2] Specifications of Distrometer RD-80 accessed at http://www.distromet.com/98.

[3] Maps accessed at www.classroomclipart.com

[4] www.worldtravelguide.net/Rwanda/weather-climate-geography

[5] www.natinsencyclopedia.com/Africa/Rwanda-CLIMATE.html

[6] Chi-Square tables accessed at http://www.medcalc.org/manual/chi-square-table.php

APPENDICES

Appendix A: ITU-R Global Climatic Values for $R_{0.01}$ [*ITU-R P.837-6*, 2012]
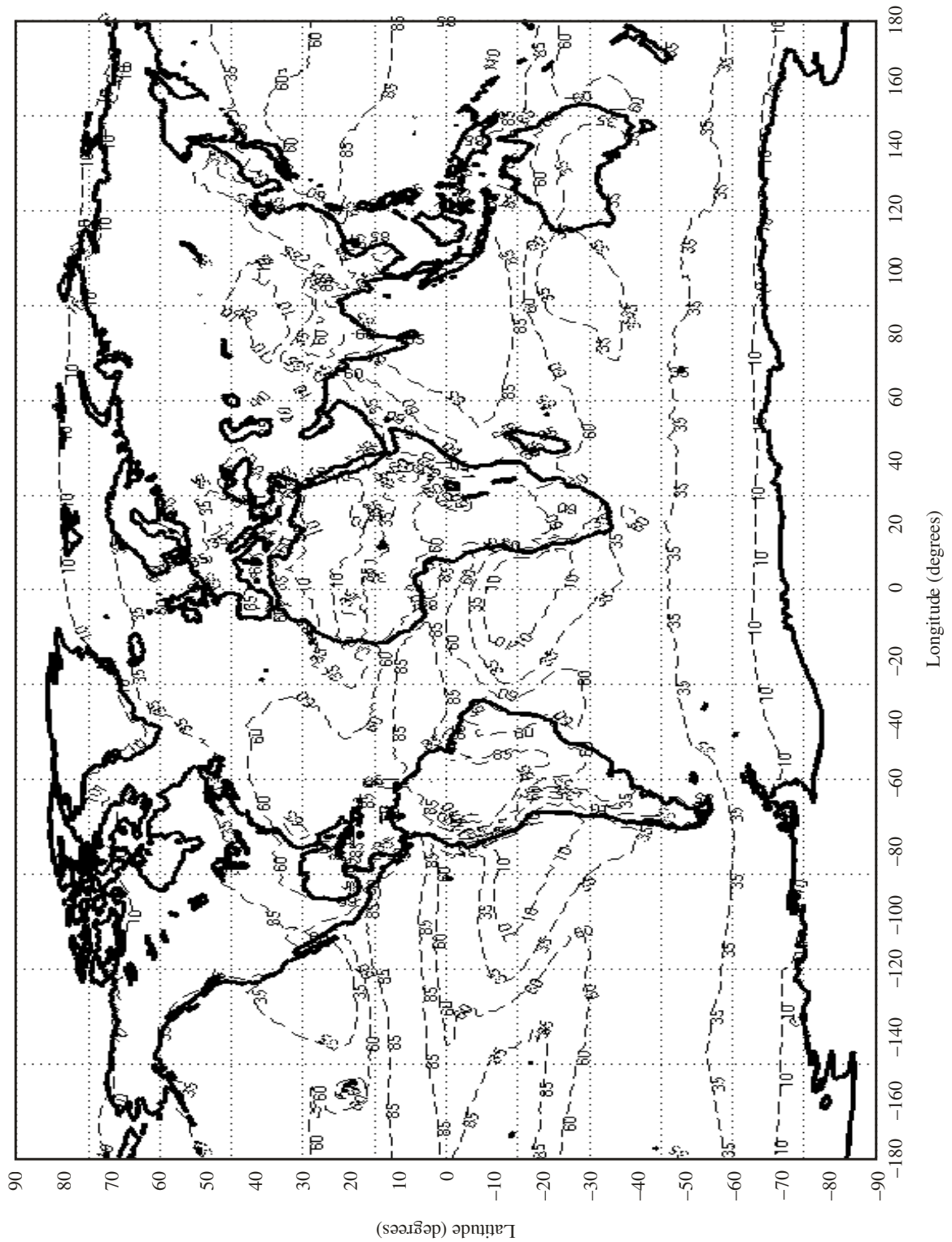
Appendix B: ITU-R Parameters for the Estimation of Specific Attenuation

[*ITU-R P.838-3*, 2005]

The ITU-R recommendation P. 838-3 document gives the procedure for estimating the specific attenuation at different frequencies by applying two power-law coefficients, k and α. The independent parameter is given as the rainfall rate at 0.01% of the time, R0.01, which is regional dependent. Thus, The specific attenuation is given by:

$$A_s = kR_{0.01}{}^{\alpha} \qquad\qquad (B.1)$$

The published values of k and α for horizontal and vertical polarization systems are thus presented:

Frequency (GHz)	k_H	α_H	k_V	α_V
1	0.0000259	0.9691	0.0000308	0.8592
1.5	0.0000443	1.0185	0.0000574	0.8957
2	0.0000847	1.0664	0.0000998	0.9490
2.5	0.0001321	1.1209	0.0001464	1.0085
3	0.0001390	1.2322	0.0001942	1.0688
3.5	0.0001155	1.4189	0.0002346	1.1387
4	0.0001071	1.6009	0.0002461	1.2476
4.5	0.0001340	1.6948	0.0002347	1.3987
5	0.0002162	1.6969	0.0002428	1.5317
5.5	0.0003909	1.6499	0.0003115	1.5882
6	0.0007056	1.5900	0.0004878	1.5728
7	0.001915	1.4810	0.001425	1.4745
8	0.004115	1.3905	0.003450	1.3797
9	0.007535	1.3155	0.006691	1.2895
10	0.01217	1.2571	0.01129	1.2156
11	0.01772	1.2140	0.01731	1.1617
12	0.02386	1.1825	0.02455	1.1216
13	0.03041	1.1586	0.03266	1.0901
14	0.03738	1.1396	0.04126	1.0646
15	0.04481	1.1233	0.05008	1.0440
16	0.05282	1.1086	0.05899	1.0273
17	0.06146	1.0949	0.06797	1.0137
18	0.07078	1.0818	0.07708	1.0025
19	0.08084	1.0691	0.08642	0.9930

Frequency (GHz)	k_H	α_H	k_V	α_V
20	0.09164	1.0568	0.09611	0.9847
21	0.1032	1.0447	0.1063	0.9771
22	0.1155	1.0329	0.1170	0.9700
23	0.1286	1.0214	0.1284	0.9630
24	0.1425	1.0101	0.1404	0.9561
25	0.1571	0.9991	0.1533	0.9491
26	0.1724	0.9884	0.1669	0.9421
27	0.1884	0.9780	0.1813	0.9349
28	0.2051	0.9679	0.1964	0.9277
29	0.2224	0.9580	0.2124	0.9203
30	0.2403	0.9485	0.2291	0.9129
31	0.2588	0.9392	0.2465	0.9055
32	0.2778	0.9302	0.2646	0.8981
33	0.2972	0.9214	0.2833	0.8907
34	0.3171	0.9129	0.3026	0.8834
35	0.3374	0.9047	0.3224	0.8761
36	0.3580	0.8967	0.3427	0.8690
37	0.3789	0.8890	0.3633	0.8621
38	0.4001	0.8816	0.3844	0.8552
39	0.4215	0.8743	0.4058	0.8486
40	0.4431	0.8673	0.4274	0.8421
41	0.4647	0.8605	0.4492	0.8357
42	0.4865	0.8539	0.4712	0.8296
43	0.5084	0.8476	0.4932	0.8236
44	0.5302	0.8414	0.5153	0.8179
45	0.5521	0.8355	0.5375	0.8123
46	0.5738	0.8297	0.5596	0.8069
47	0.5956	0.8241	0.5817	0.8017
48	0.6172	0.8187	0.6037	0.7967
49	0.6386	0.8134	0.6255	0.7918
50	0.6600	0.8084	0.6472	0.7871
51	0.6811	0.8034	0.6687	0.7826
52	0.7020	0.7987	0.6901	0.7783
53	0.7228	0.7941	0.7112	0.7741
54	0.7433	0.7896	0.7321	0.7700
55	0.7635	0.7853	0.7527	0.7661
56	0.7835	0.7811	0.7730	0.7623

Frequency (GHz)	k_H	α_H	k_V	α_V
57	0.8032	0.7771	0.7931	0.7587
58	0.8226	0.7731	0.8129	0.7552
59	0.8418	0.7693	0.8324	0.7518
60	0.8606	0.7656	0.8515	0.7486
61	0.8791	0.7621	0.8704	0.7454
62	0.8974	0.7586	0.8889	0.7424
63	0.9153	0.7552	0.9071	0.7395
64	0.9328	0.7520	0.9250	0.7366
65	0.9501	0.7488	0.9425	0.7339
66	0.9670	0.7458	0.9598	0.7313
67	0.9836	0.7428	0.9767	0.7287
68	0.9999	0.7400	0.9932	0.7262
69	1.0159	0.7372	1.0094	0.7238
70	1.0315	0.7345	1.0253	0.7215
71	1.0468	0.7318	1.0409	0.7193
72	1.0618	0.7293	1.0561	0.7171
73	1.0764	0.7268	1.0711	0.7150
74	1.0908	0.7244	1.0857	0.7130
75	1.1048	0.7221	1.1000	0.7110
76	1.1185	0.7199	1.1139	0.7091
77	1.1320	0.7177	1.1276	0.7073
78	1.1451	0.7156	1.1410	0.7055
79	1.1579	0.7135	1.1541	0.7038
80	1.1704	0.7115	1.1668	0.7021
81	1.1827	0.7096	1.1793	0.7004
82	1.1946	0.7077	1.1915	0.6988
83	1.2063	0.7058	1.2034	0.6973
84	1.2177	0.7040	1.2151	0.6958
85	1.2289	0.7023	1.2265	0.6943
86	1.2398	0.7006	1.2376	0.6929
87	1.2504	0.6990	1.2484	0.6915
88	1.2607	0.6974	1.2590	0.6902
89	1.2708	0.6959	1.2694	0.6889
90	1.2807	0.6944	1.2795	0.6876
91	1.2903	0.6929	1.2893	0.6864
92	1.2997	0.6915	1.2989	0.6852
93	1.3089	0.6901	1.3083	0.6840

Frequency (GHz)	k_H	α_H	k_V	α_V
94	1.3179	0.6888	1.3175	0.6828
95	1.3266	0.6875	1.3265	0.6817
96	1.3351	0.6862	1.3352	0.6806
97	1.3434	0.6850	1.3437	0.6796
98	1.3515	0.6838	1.3520	0.6785
99	1.3594	0.6826	1.3601	0.6775
100	1.3671	0.6815	1.3680	0.6765
120	1.4866	0.6640	1.4911	0.6609
150	1.5823	0.6494	1.5896	0.6466
200	1.6378	0.6382	1.6443	0.6343
300	1.6286	0.6296	1.6286	0.6262
400	1.5860	0.6262	1.5820	0.6256
500	1.5418	0.6253	1.5366	0.6272
600	1.5013	0.6262	1.4967	0.6293
700	1.4654	0.6284	1.4622	0.6315
800	1.4335	0.6315	1.4321	0.6334
900	1.4050	0.6353	1.4056	0.6351
1 000	1.3795	0.6396	1.3822	0.6365

Appendix C: Power-law coefficients for Durban at 20°C for a frequency range of 2 GHz to 1000 GHz using Mie technique [*Alonge*, 2011]

The Mie scattering technique has been simplified such that the ECS is defined as:

$$Q_{ext}(R) = k_{ext}\bar{a}^{\varsigma_{ext}} \quad [mm^2] \qquad (C.1)$$

where $\bar{a}$ is the radius of the rain drops. The power-law coefficients in Durban at 20°C are hereby presented in the following table.

FREQUENCY (GHz)	COMPLEX REFRACTIVE INDEX	k_{ext}	ς_{ext}
2	8.9014 + 0.4843i	0.0027	3.2737
4	8.7763 + 0.9442i	0.0191	3.7875
6	8.5830 + 1.3599i	0.0851	4.3988
8	8.3396 + 1.7196i	0.217	4.5805
10	8.0649 + 2.0188i	0.3857	4.5272
12	7.7755 + 2.2594i	0.5866	4.4443
15	7.3405 + 2.5234i	0.955	4.3453
16	7.1994 + 2.5892i	1.0939	4.3164
18	6.9272 + 2.6934i	1.3883	4.2576
19.5	6.7332 + 2.7509i	1.6169	4.2104
20	6.6705 + 2.7667i	1.6936	4.194
23	6.3171 + 2.8321i	2.1474	4.0885
25	6.1026 + 2.8532i	2.4567	4.0186
28	5.8107 + 2.8603i	2.8544	3.9035
30	5.6345 + 2.8530i	3.1204	3.8323
35	5.2500 + 2.8072i	3.7452	3.6639
40	4.9322 + 2.7383i	4.3106	3.5077
45	4.6668 + 2.6586i	4.8223	3.3646
50	4.4428 + 2.5752i	5.2855	3.2353
60	4.0869 + 2.4099i	6.0493	3.0094
70	3.8182 + 2.2560i	6.625	2.8209
90	3.4421 + 1.9907i	7.4097	2.5284
100	3.3061 + 1.8778i	7.6874	2.4156
150	2.9154 + 1.5083i	8.3061	2.0691
200	2.7103 + 1.2655i	8.3464	1.9293
250	2.5871 + 1.1051i	8.2291	1.8785
300	2.5029 + 0.9932i	8.0777	1.8672
350	2.4395 + 0.9115i	7.935	1.87
400	2.3882 + 0.8493i	7.8144	1.875
500	2.3067 + 0.7597i	7.6315	1.8812
600	2.2418 + 0.6958i	7.488	1.8919
700	2.1880 + 0.6455i	7.3793	1.899
750	2.1644 + 0.6235i	7.3338	1.9021
800	2.1426 + 0.6032i	7.2899	1.9055
850	2.1226 + 0.5841i	7.2585	1.9088
900	2.1042 + 0.5662i	7.2183	1.9104
1000	2.0715 + 0.5332i	7.1602	1.915

Queueing Theory Approach to Rain Fade Analysis at Microwave and Millimeter Bands in Tropical Africa

Appendix D: Distrometer Output Specification [*Bartholomew*, 2009]

The Joss-Waldvogel RD-80 impact distrometer is completely described by twenty independent diameter bins with different diameter classes, drop fall velocity and diameter interval. The Table below shows the corresponding values related to each bin and classes according to [*Bartholomew*, 2009; [2]].

Dropsize class in DISDRODATA program	Lower threshold of drop diameter (mm)	Average diameter of drops in class i D_i (mm)	Fall velocity of a drop with diameter $v(D_i)$ (m/s)	Diameter interval of drop size class i ΔD_i (mm)
1	0.313	0.359	1.435	0.092
2	0.405	0.455	1.862	0.1
3	0.505	0.551	2.267	0.091
4	0.596	0.656	2.692	0.119
5	0.715	0.771	3.154	0.112
6	0.827	0.913	3.717	0.172
7	0.999	1.116	4.382	0.233
8	1.232	1.331	4.986	0.197
9	1.429	1.506	5.423	0.153
10	1.582	1.665	5.793	0.166
11	1.748	1.912	6.315	0.329
12	2.077	2.259	7.009	0.364
13	2.442	2.584	7.546	0.286
14	2.727	2.869	7.903	0.284
15	3.011	3.198	8.258	0.374
16	3.385	3.544	8.556	0.319
17	3.704	3.916	8.784	0.423
18	4.127	4.35	8.965	0.446
19	4.573	4.859	9.076	0.572
20	5.145	5.373	9.137	0.455

Appendix E: Derivation of Optimal Number of Stages, k, for Erlang-k Distribution

The proposed function for Erlang-k distribution, described by three parameters t, k and τ, is given as:

$$f(t_i; k, \tau) = \frac{(k\tau)^k t_i^{k-1} \exp(-k\tau t_i)}{\Gamma(k)} \qquad \text{for} \quad k, t \ \forall \ \mathbb{Z} > 0 \quad \text{(E.1)}$$

where k is the number of stages and τ is the rate parameter (or mean of the data)

.

To optimize the value of k, the following steps are undertaken:

The first derivative of (E.1) is derived via the product rule as thus:

$$\frac{df(t_i; k, \tau)}{dt} = at^{k-1} \exp(-kt) - \frac{a(k-1)t^{k-2} \exp(-k\tau t)}{k\tau} \qquad \text{(E.2)}$$

Where,

$$a = \frac{(k\tau)^k}{\Gamma(k)} \qquad \text{(E.3)}$$

To satisfy the conditions of locating the minimum and maximum bounds of the Erlang-k distribution, (E.2) needs to be equated to zero at the Right-Hand Side (RHS). This ultimately yields the function of the independent variable, t, given as:

$$t = \frac{k-1}{k\tau} \qquad \text{(E.4)}$$

By substituting t into (E.2), the maximum value of $f(t_i)$ which is at unity is obtained given by:

$$max[f(t_i, k, \tau)] = \frac{k\tau(k-1)^{k-1} \exp(1-k)}{\Gamma(k)} \qquad \text{(E.5)}$$

This can be reduced to a simplified function with LHS dependent on k only. This results in:

$$\frac{max[f(t_i; k, \tau)]}{\tau} = \frac{k(k-1)^{k-1}\exp(1-k)}{\Gamma(k)} \tag{E.6}$$

It is found by regression technique that the RHS expression fitted over the range of $2 \leq k \leq 142$ is a power-law function, dependent on k only, with a RMS error of 3.26%. Therefore, the equivalent approximate expression for RHS is given by:

$$\frac{k(k-1)^{k-1}\exp(1-k)}{\Gamma(k)} \approx 0.4488k^{0.4742} \tag{E.7}$$

Invariably, the optimized integer value of Erlang-k stages for any Erlang distribution, k_{opt}, can be computed using the simple power-law function given as:

$$k_{opt} = round(5.417\tau^{-2.11}\{max[f(t_i; k, \tau)]\}^{2.11}) \tag{E.8}$$

Appendix F: Results of Simulated System Performance of M/E$_k$/∞ in Durban, South Africa

Table F-1: Computation of M/E$_k$/s Queue Performance Metrics for Drizzle Rain Regime

s	Utilization	W$_q$	L$_q$	W	L
3	0.7915	9.4532	1.816	13.5786	2.6084
4	0.5936	2.7202	0.5226	5.8143	1.1169
5	0.4749	1.3464	0.2586	3.8216	0.7341
6	0.3958	0.8123	0.156	2.875	0.5523
7	0.3392	0.5456	0.1048	2.3136	0.4445
8	0.2968	0.3925	0.0754	1.9395	0.3726
9	0.2638	0.2962	0.0569	1.6713	0.3211
10	0.2375	0.2316	0.0445	1.4692	0.2822
11	0.2159	0.1861	0.0358	1.3112	0.2519
12	0.1979	0.1529	0.0294	1.1842	0.2275
13	0.1827	0.1278	0.0246	1.0799	0.2074
14	0.1696	0.1085	0.0208	0.9925	0.1907
15	0.1583	0.0932	0.0179	0.9183	0.1764
16	0.1484	0.081	0.0156	0.8545	0.1642
17	0.1397	0.071	0.0136	0.799	0.1535
18	0.1319	0.0628	0.0121	0.7504	0.1441
19	0.125	0.0559	0.0107	0.7073	0.1359
20	0.1187	0.0501	0.0096	0.6689	0.1285

Table F-2: Computation of M/E$_k$/s Queue Performance Metrics for Widespread Rain Regime

s	Utilization	W$_q$	L$_q$	W	L
3	0.701	6.4308	0.9858	11.0033	1.6868
4	0.5257	2.2808	0.3496	5.7101	0.8754
5	0.4206	1.1948	0.1832	3.9383	0.6037
6	0.3505	0.7402	0.1135	3.0264	0.464
7	0.3004	0.5049	0.0774	2.4645	0.3778
8	0.2629	0.3669	0.0562	2.0815	0.3191
9	0.2337	0.2788	0.0427	1.803	0.2764
10	0.2103	0.2192	0.0336	1.5909	0.2439
11	0.1912	0.1768	0.0271	1.4239	0.2183
12	0.1752	0.1457	0.0223	1.2888	0.1976
13	0.1618	0.1222	0.0187	1.1774	0.1805
14	0.1502	0.1039	0.0159	1.0837	0.1661
15	0.1402	0.0895	0.0137	1.004	0.1539
16	0.1314	0.0778	0.0119	0.9352	0.1434
17	0.1237	0.0683	0.0105	0.8752	0.1342
18	0.1168	0.0605	0.0093	0.8226	0.1261
19	0.1107	0.0539	0.0083	0.7759	0.1189
20	0.1051	0.0484	0.0074	0.7342	0.1126

Table F-3: Computation of M/E$_k$/s Queue Performance Metrics for Shower Rain Regime

s	Utilization	W$_q$	L$_q$	W	L
3	0.8054	14.0219	2.0837	19.442	2.8891
4	0.6041	3.8762	0.576	7.9412	1.1801
5	0.4833	1.9008	0.2825	5.1528	0.7657
6	0.4027	1.142	0.1697	3.852	0.5724
7	0.3452	0.7653	0.1137	3.0882	0.4589
8	0.302	0.5497	0.0817	2.5822	0.3837
9	0.2685	0.4144	0.0616	2.2211	0.3301
10	0.2416	0.3238	0.0481	1.9498	0.2897
11	0.2197	0.2601	0.0386	1.7383	0.2583
12	0.2014	0.2135	0.0317	1.5685	0.2331
13	0.1859	0.1785	0.0265	1.4293	0.2124
14	0.1726	0.1514	0.0225	1.3129	0.1951
15	0.1611	0.1301	0.0193	1.2141	0.1804
16	0.151	0.113	0.0168	1.1292	0.1678
17	0.1421	0.099	0.0147	1.0555	0.1569
18	0.1342	0.0875	0.013	0.9909	0.1472
19	0.1272	0.0779	0.0116	0.9337	0.1388
20	0.1208	0.0698	0.0104	0.8828	0.1312

Table F-4: Computation of M/E$_k$/s Queue Performance Metrics for Thunderstorm Rain Regime

s	Utilization	W$_q$	L$_q$	W	L
3	0.6285	7.688	0.7088	14.5046	1.3373
4	0.4714	3.0391	0.2802	8.1516	0.7516
5	0.3771	1.6507	0.1522	5.7407	0.5293
6	0.3142	1.0412	0.096	4.4496	0.4102
7	0.2694	0.718	0.0662	3.6394	0.3356
8	0.2357	0.5255	0.0485	3.0817	0.2841
9	0.2095	0.4015	0.037	2.6737	0.2465
10	0.1885	0.3168	0.0292	2.3618	0.2178
11	0.1714	0.2564	0.0236	2.1155	0.195
12	0.1571	0.2118	0.0195	1.9159	0.1766
13	0.145	0.1779	0.0164	1.751	0.1614
14	0.1347	0.1516	0.014	1.6123	0.1487
15	0.1257	0.1307	0.012	1.494	0.1377
16	0.1178	0.1138	0.0105	1.3919	0.1283
17	0.1109	0.1	0.0092	1.303	0.1201
18	0.1047	0.0886	0.0082	1.2247	0.1129
19	0.0992	0.0791	0.0073	1.1554	0.1065
20	0.0943	0.071	0.0065	1.0934	0.1008